

Modulation of Mouse Corpus Cavernosum Smooth Muscle Contractility by EPAC-1 and K_V7 Channels

A thesis submitted to the

School of Health and Science

Dundalk Institute of Technology

For the degree of **Doctor of Philosophy**

By

Mitchell Mercer, M.Sc.

May 2026

Under the supervision of **Professor Keith Thornbury** and co-supervision of **Professor Gerard Sergeant**

Smooth Muscle Research Centre,

Dundalk Institute of Technology

Declaration

I hereby certify that this material, which I now submit for assessment on the programme of study leading to the award of Doctor of Philosophy is entirely my own work, and that I have exercised reasonable care to ensure that the work is original and have conformed to the regulations on the use of and declaration of Generative AI, and does not to the best of my knowledge breach any law of copyright, and has not been taken from the work of others save and to the extent that such work has been cited and acknowledged within the text of my work.

Signed: Mitchell Mercer

ID No.: D00262086

Date: 13/05/2026

Acknowledgement

First and foremost, I express my deepest gratitude to my supervisor, Prof. Keith Thornbury, for exceptional support from the outset of my PhD. His guidance, enthusiasm, and drive consistently motivated me to perform at my best. I also sincerely thank Prof. Gerard Sergeant and Prof. Mark Hollywood for their insightful discussions and valuable advice.

Special recognition goes to our laboratory technician, Billie McIlveen, whose tireless dedication and technical expertise were invaluable. I am particularly grateful for her early morning conversations that set a positive tone for each day.

I am deeply grateful to Dr Drumm, Dr Alkawadri, Dr Griffin, and Dr Rabab for their patience, guidance, and insight. In particular, I thank Dr Drumm for his mentorship, whose continued support was instrumental to my professional development. All deserve sincere recognition for their commitment to training students and imparting essential scientific skills and professional wisdom.

I thank my colleagues for their camaraderie and support, which made long days in the laboratory both productive and enjoyable. Special thanks go to Alina and Peixin for their consistent support. I also acknowledge Dr Lim for her invaluable guidance during my early weeks as a PhD student, which strongly influenced my scientific development. I extend special recognition to Srijit, whose dedicated collaboration alongside me during my final year in the electrophysiology laboratory was integral to this work, and to Neeraj for his daily wisdom and unforgettable humour. I further thank my lab partner and housemate, Alex, for his friendship and constant support.

I am profoundly grateful to my family, particularly my mum and grandparents, whose unwavering encouragement made this journey possible. I thank my sister, Emily, for her patience, and Aneurin for late-night conversations and FIFA evenings. My deepest thanks go to my partner, Elizabeth, whose extraordinary emotional support, patience, and encouragement were indispensable throughout the writing of this thesis. Finally, I thank my Belfast friends, Daniel, Conor, Jack, and Paddy, whose friendship and welcome weekend distractions provided essential balance during my PhD.

Table of Contents

Declaration 1
Acknowledgement 2
Table of Contents 3
Abstract 6
Research Dissemination 7
Glossary 9
1. Literature Review 15
1.1 Anatomy 16
1.1.1 Classical Human Penile Anatomy 16
1.1.2 Mouse Penile Anatomy 17
1.1.3 Penile Microanatomy 19
1.1.4 Arterial supply 20
1.1.5 Venous drainage 21
1.1.6 Somatic neural control 22
1.1.7 Autonomic neural control 22
1.2 Physiology of erectile activity 23
1.3 Corpus cavernosum smooth muscle (CCSM) 24
1.3.1 Ca^{2+} Signalling Cascade 25
1.3.2 Ca^{2+} Sensitisation by RhoA/Rho-kinase pathway 26
1.4 Erectile Dysfunction (ED) 27
1.4.1 Neurogenic ED 27
1.4.2 Vasculogenic ED 28
1.4.3 Psychogenic ED 29
1.4.4 Endocrinologic ED 30
1.4.5 Current treatment of ED 31
1.5 CCSM Relaxation mediated by cyclic nucleotides 32
1.5.1 Cyclic Guanosine Monophosphate (cGMP) Signalling 33
1.5.2 Cyclic Adenosine Monophosphate (cAMP) Signalling 36
1.5.2.1 Protein Kinase A (PKA) 37
1.5.2.2 Exchange Protein directly activated by cAMP (EPAC) 39
1.5.2.3 Cyclic nucleotide-gated channels (CNGCs) 41
1.6 Store-operated Ca^{2+} entry (SOCE) 41

1.7 Electrophysiology 43
1.7.1 L- and T-Type Ca^{2+} Channels 44
1.7.2 Ca^{2+}-activated Cl^- Channels - Anoctamin-1 (ANO1) 45
1.7.3 P2X receptor-mediated Cation Current 47
1.7.4 Voltage-dependent Na^+ (Na_v) Channels 48
1.7.5 Large-conductance Ca^{2+}-activated K^+ (BK_{Ca}) Channels 49
1.7.6 ATP-sensitive K^+ (K_{ATP}) Channels 50
1.7.7 Voltage-dependent K^+ (K_v) Channels 52
1.7.8 *KCNQ*-encoded Voltage-dependent Potassium (K_v7) Channels 52
1.7.8.1 $K_v7.1$ 53
1.7.8.2 $K_v7.2$ and $K_v7.3$ 56
1.7.8.3 $K_v7.4$ and $K_v7.5$ 56
1.8 Aims 58
2. Materials and methods 60
2.1 Tissue preparation 61
2.2 Isometric tension recording 61
2.3 Isolation of corpus cavernosum smooth muscle (CCSM) cells 62
2.4 Total RNA extraction 62
2.5 Complementary DNA (cDNA) synthesis 63
2.6 Reverse transcriptase-polymerase chain reaction (RT-PCR) 64
2.7 Agarose gel electrophoresis and imaging 66
2.8 Real time quantitative PCR (qPCR) 67
2.9 Single cell intracellular Ca^{2+} imaging 68
2.10 Cell culture 70
2.11 Transfection 70
2.12 Electrophysiology 71
2.12.1 Patch-clamp recordings 72
2.12.2 Pipette resistance 72
2.12.3 Series resistance 73
2.12.4 Voltage-clamp protocols 74
2.13 Immunocytochemistry 75
2.14 Statistical analysis 76
2.15 Solutions 77
2.16 Drugs 78

3. Results Chapter 1: Distinct Ca^{2+} signalling pathways underlie phasic and tonic contractions in corpus cavernosum smooth muscle 85
3.1 Introduction 86
3.2 Results 88
3.3 Discussion 106
4. Results Chapter 2: *KCNQ*-encoded voltage-dependent potassium (K_v7) alpha-subunits are expressed and form functional channels in corpus cavernosum smooth muscle 116
4.1 Introduction 117
4.2 Results 119
4.3 Discussion 146
5. Results Chapter 3: Activation of α_{1A}-adrenoceptors (α_{1A}Rs) inhibit *KCNQ*-encoded voltage-gated potassium isoform 5 ($K_v7.5$) channels 153
5.1 Introduction 154
5.2 Results 156
5.3 Discussion 166
6. Results Chapter 4: Modulation of contractions and cytosolic Ca^{2+} by cAMP and its downstream effector proteins, EPAC and PKA 176
6.1 Introduction 177
6.2 Results 180
6.3 Discussion 201
7. General Discussion, Future Directions and Conclusions 211
7.1 General discussion 212
7.2 Future directions 216
7.3 Conclusions 218
8. References 221

Abstract

'Modulation of Mouse Corpus Cavernosum Smooth Muscle Contractility by EPAC-1 and K_V7 Channels'

Mitchell Mercer

Penile erection is achieved through relaxation, via cyclic nucleotide signalling, of the corpus cavernosum smooth muscle (CCSM). Erectile dysfunction (ED) is commonly treated using phosphodiesterase-5 inhibitors (PDE5Is), such as Viagra™; however, many men are resistant to PDE5Is, underscoring the need for alternative targets. The exchange protein directly activated by cAMP (EPAC), previously unreported in mouse CCSM, is implicated in smooth muscle relaxation. Additionally, voltage-dependent K^+ (K_V) channels, particularly the K_V7 family, may influence CCSM cell membrane potential and contractility.

This study investigates the roles of EPAC and K_V7 channels in modulating mouse CCSM contractility. Isometric tension recordings were conducted on mouse CCSM crura, and Ca^{2+} imaging was performed on enzymatically-dispersed single cells loaded with Fluo-4-AM. EPAC-1 was identified as the predominant isoform, and its activation by 8-pCPT-2'-O-Me-cAMP (007-AM) markedly suppressed Ca^{2+} oscillations induced by 10μM phenylephrine (PE). In contrast, protein kinase A (PKA) activation had no effect but abolished oscillations induced by lower PE concentrations. Co-activation of EPAC and PKA attenuated contractile responses. Nifedipine (L-type Ca^{2+} channel blocker), retigabine ($K_V7.2$-5 activator), and Ani-9 (ANO1 blocker) abolished phasic PE-induced contractions, while tonic contractions were inhibited by blocking inositol 1,4,5-trisphosphate receptors (IP_3Rs) with 2-aminoethoxydiphenyl borate or STIM/Orai channels with GSK-7975A. *Kcnq5* emerged as the main K_V7 isoform. Retigabine and nifedipine suppressed spontaneous contractions and contractions and Ca^{2+} oscillations induced by low-concentration PE, whereas K_V7 inhibition with XE-991 enhanced these. Yet, Ca^{2+} oscillations induced by high-concentration PE persisted in the presence of nifedipine or retigabine. Whole-cell patch-clamp recordings in HEK-293 cells, expressing $K_V7.5$ and α_{1A}-adrenoceptors, revealed that PE inhibited $K_V7.5$ currents, and this effect was prevented by phentolamine in the bath or by PIP_2 in the pipette.

Our findings identify EPAC-1 and $K_V7.5$ as key modulators of CCSM contractility in mice, underscoring their potential as therapeutic targets in PDE5I-resistant ED.

Research Dissemination

Publications:

Mercer, M., Hollywood, M. A., Sergeant, G. P., & Thornbury, K. D. (2025). KV7 channels modulate tension and calcium signaling in mouse corpus cavernosum. *American journal of physiology. Cell physiology*, *328*(3), C729–C742.

Lim, X. R., Mercer, M., Harraz, O. F., Hollywood, M. A., Sergeant, G. P., & Thornbury, K. D. (2024). Evidence of an excitatory purinergic innervation in mouse corpus cavernosum smooth muscle. *The journal of sexual medicine*, *21*(11), 977–985.

Conference presentations:

DkIT Research Day 2023, Ireland

Poster communication

'Role of KCNQ-encoded voltage-gated potassium (K_V7) channels in erectile function'

2nd K_V7 Symposium 2023, Naples

Poster communication [awarded best poster prize]

'Role of KCNQ-encoded voltage-gated potassium (K_V7) channels in erectile function'

DkIT Research Day 2024, Ireland

Oral communication [awarded best oral communication prize]

'Role of KCNQ-encoded voltage-gated potassium (K_V7) channels in erectile function'

Command and Control: Unveiling the Regulation of Smooth Muscle Function, 2024, Ireland

Oral communication

'The role of membrane potential in corpus cavernosum smooth muscle contractility'

Poster communication [awarded joint runner-up poster prize]

'Role of KCNQ-encoded voltage-gated potassium (K_V7) channels in erectile function'

40th IUPS Congress, Frankfurt, Germany

Oral communication

'KCNQ-encoded voltage-gated potassium (K_V7) channels modulate corpus cavernosum smooth muscle contractility and display inhibition via activation of α_{1A} receptors'

Glossary

$\Delta F/F_0$	change in normalised fluorescence
007-AM	8-pCPT-2-O-Me'-cAMP
2-APB	2-aminoethoxydiphenyl borate
6-MB	N^6-monobutyryl-cyclic adenosine monophosphate
A9C	anthracene-9-carboxylic acid
AC	adenylyl cyclase
ADP	adenosine diphosphate
AKAP	A kinase anchoring protein
AMP	adenosine monophosphate
ANO1	anoctamin-1
ANOVA	analysis of variance
ASM	airway smooth muscle
ATP	adenosine triphosphate
BEST	bestrophin Ca^{2+}-activated Cl^- channel
BFNS	benign familial neonatal seizures
BK_{Ca}	large-conductance calcium-activated potassium channel
C-	carboxyl-
CAD	CRAC-activating domain
CaM	calmodulin
CaMKII	calmodulin kinase II
cAMP	cyclic adenosine monophosphate
CBD	cAMP-binding domain
CC	corpus cavernosum
CCG	corpus cavernosum glandis

CCSM	corpus cavernosum smooth muscle
CCU	corpus cavernosum urethra
cDNA	complementary deoxyribonucleic acid
cGMP	cyclic guanosine monophosphate
CNGC	cyclic nucleotide-gated channel
CNS	central nervous system
CO_2	carbon dioxide
CPA	cyclopiazonic acid
CRAC	calcium release-activated calcium
DAG	1,2-diacylglycerol
DM	diabetes mellitus
DMSO	dimethyl sulfoxide
DMT	Danish myo technology
DNA	deoxyribonucleic acid
DNase	deoxyribonuclease
dNTPs	deoxynucleotide triphosphates
DTT	dithiothreitol
ED	erectile dysfunction
EDTA	ethylenediaminetetraacetic acid
EFS	electrical field stimulation
EGTA	ethylene glycol-bis(β-aminoethyl ether)-N,N,N′,N′-tetraacetic acid
EMAS	European Male Aging Study
EMCCD	electron multiplying charge coupled device
eNOS	endothelial nitric oxide synthase
EPAC	exchange protein activated by cAMP

F	fluorescence
F/F_0	normalised fluorescence
F_0	null fluorescence
FK	forskolin
FPS	frames per second
GDP	guanosine diphosphate
GE	guanethidine
GMP	guanosine monophosphate
GPCR	g-protein coupled receptor
GTP	guanosine triphosphate
HCN	hyperpolarisation-activated and cyclic nucleotide-gated channel
HEK	human embryonic kidney
IbTx	iberiotoxin
IC_{50}	half-maximal inhibitory concentration
I_{ks}	slow delayed rectifier potassium current
IP_3	inositol-1,4,5- triphosphate
IP_3R	inositol-1,4,5- triphosphate receptor
IRAG	IP_3R-associated cGMP substrate
K_{ATP}	ATP-sensitive potassium channel
KCl	potassium chloride
KCNE	potassium voltage-gated channel subfamily E member
K_v	voltage-dependent potassium channel
K_v7	KCNQ-encoded voltage-dependent potassium channel
Li-ESWT	low-intensity extracorporeal shockwave therapy
L-NNA	N^{ω}-nitro-L-arginine hydrochloride

LTCC	long lasting-type calcium channel
MinK	minimal potassium channel subunit
MiRP2	minimal potassium channel subunit-related peptide 2
MLC_{17}	myosin light chain 17
MLC_{20}	myosin light chain 20
MLCK	myosin light chain kinase
MLCP	myosin light chain phosphatase
MMAS	Massachusetts Male Aging Study
mRNA	messenger ribonucleic acid
MUMP CC	male urogenital mating protuberance corpus cavernosum
MUMP	male urogenital mating protuberance
N-	amino-
N	animal number
n	sample number
Na_v	voltage-dependent sodium channel
NIF	nifedipine
nNOS	neuronal nitric oxide synthase
NO	nitric oxide
NSCC	non-selective cation current
NTC	non-template control
P1	adenosine-sensitive receptor
P2	ATP/ADP-sensitive receptor
P2X	ATP-gated ion channel
P2Y	purinergic g-protein coupled receptor
PCR	polymerase chain reaction

PDE	phosphodiesterase
PDE5I	phosphodiesterase-5 inhibitor
PE	phenylephrine hydrochloride
PGE_1	Prostaglandin E1
PGE_2	Prostaglandin E2
PIP_2	phosphatidylinositol 4,5-bisphosphate
PKA	protein kinase A
PKC	protein kinase C
PKG	protein kinase G
PLC	phosphoinositide-specific phospholipase C
PPi	pyrophosphate
qPCR	real-time quantitative-polymerase chain reaction
Rap1	ras-related protein 1
Rap2	ras-related protein 2
RhoA	ras homologous A
RhoGDI	RhoA-GDP dissociation inhibitor
RNA	ribonucleic acid
ROCK	rho-associated protein kinase
RPM	revolutions per minute
RTG	retigabine
RT-PCR	reverse transcriptase-polymerase chain reaction
RyR	ryanodine receptor
S	segment
S.E.M.	standard error of mean
SA	sino-atrial

SERCA	sarco/endoplasmic reticulum calcium-ATPase pump
sGC	soluble guanylate cyclase
SHHF	spontaneously hypertensive, heart failure-prone
siRNA	small interfering ribonucleic acid
SNP	sodium nitroprusside
SOAR	STIM/Orai-activating region
SOCE	store-operated calcium entry
SR	sarcoplasmic reticulum
STIC	spontaneous transient inward current
STIM	stromal interaction molecules
STOC	spontaneous transient outward current
SUR	sulfonylurea receptor
T	testosterone
T2DM	type 2 diabetes mellitus
TAE	Tris, acetic acid EDTA buffer
TIFF	tagged image file format
TMEM16A	transmembrane protein 16A
TOBS	tissue organ bath system
TTCC	transient-type calcium channel
TTX	tetrodotoxin
$V_{0.5}$	voltage of half-maximal activation
VDCC	voltage-dependent calcium channel
VED	vacuum erection device
VSD	voltage-sensing domain
VSM	vascular smooth muscle

1. Literature Review

1.1 Anatomy

The penis is the external male reproductive organ that enables copulation and sexual reproduction through ejaculation and also functions as the conduit for urination. It further contributes to female sexual stimulation and post-copulatory sexual selection, including mechanisms of rival sperm displacement (Simmons and Jones, 2007).

1.1.1 Classical Human Penile Anatomy

The classical human penile anatomy describes a proximal root, body, and distal glans. The penis comprises two dorsal corpora cavernosa, acting as the functional unit of erectile activity, running from the crural insertion onto the ischiopubic rami within the superficial perineal pouch (Fig1.1A) and covered in ischiocavernosus skeletal muscle (Fig1.1B). The ventral corpus spongiosum exists as the functional unit of urination and ejaculation, housing the spongy portion of the urethra and the distal expansion known as the glans, which contain the external urethral orifice (Fig1.1A). Corpus spongiosum is formed proximally from the median bulb of the penile root attached to the perineal membrane, covered by the bulbospongiosus muscle (Fig1.1B) (Sam and LaGrange, 2018). The paired corpora cavernosa are separated via a fenestrated tunica albuginea, allowing communication between the twin bodies and acting as a singular functional unit of erectile activity (Pretorius *et al*., 2001).

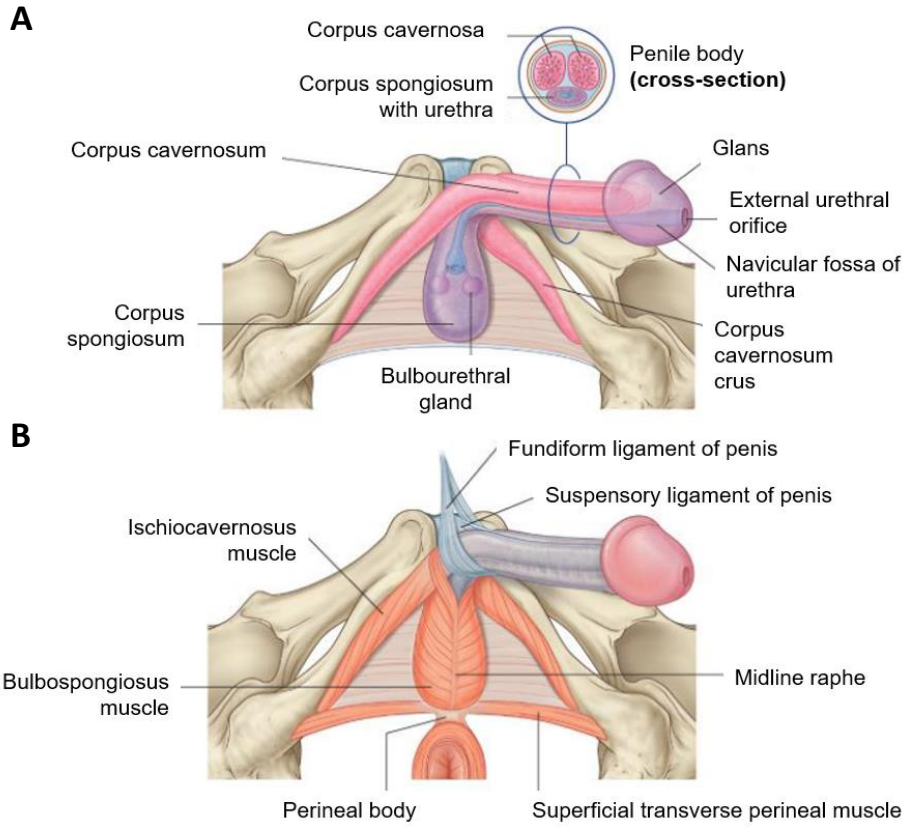


Figure 1.1. **A.** Illustration of the corpora cavernosa and corpus spongiosum forming the root, body, and glans of penis. **B.** Illustration of skeletal muscle and ligamentous support of the penile apparatus (Drake *et al*., 2015)

1.1.2 Mouse Penile Anatomy

The anatomy of the mouse penis consists of an internal proximal body and external distal glans connected by a right-angle bend of the urethra (Fig1.2A). The penile body consists of the penile corpus cavernosum and urethra. The corpora cavernosum of the penile body is similar to the human model in which the crura attaches to the ischiopubic rami, yet rather than forming two distinct corporal bodies via the tunica albuginea, the mouse corpus cavernosum fuses distally to the crura, forming a singular penile corpus cavernosum (CC; Fig1.2B/C; Cunha *et al*., 2020). Mouse penile anatomy lacks a corpus spongiosum, instead forming the corpus cavernosum urethra (CCU), harbouring the distal urethra, and the corpus cavernosum glandis (CCG; Fig1.3B; Hashimoto *et al*., 2021). The mouse penile glans extends from the right-angle bend of the penile body to the male urogenital mating protuberance (MUMP), a cartilaginous bifid distal expansion of the Os penis (Fig1.3A/B; Rodriguez *et al*., 2011). The Os penis is ossified bone harboured within the glans and covered with MUMP corpus cavernosum (MUMP CC) and encircled with CCG spongy tissue (Fig1.3B). Proximally, the MUMP forms the MUMP ridge at the fusion of MUMP tissue

with the glans (Fig1.3A; Rodriguez *et al*., 2011). The MUMP ridge is the distalmost invagination of the MUMP; proximal to the MUMP ridge is the internal prepuce, separated from the MUMP ridge by the MUMP ridge groove (Rodriguez *et al*., 2011). The mouse penis exhibits both internal and external prepuces, with external referring to the hair-covered penile covering and internal referring to the structure retracting over the glans (Fig1.3A; Blaschko *et al*., 2013).

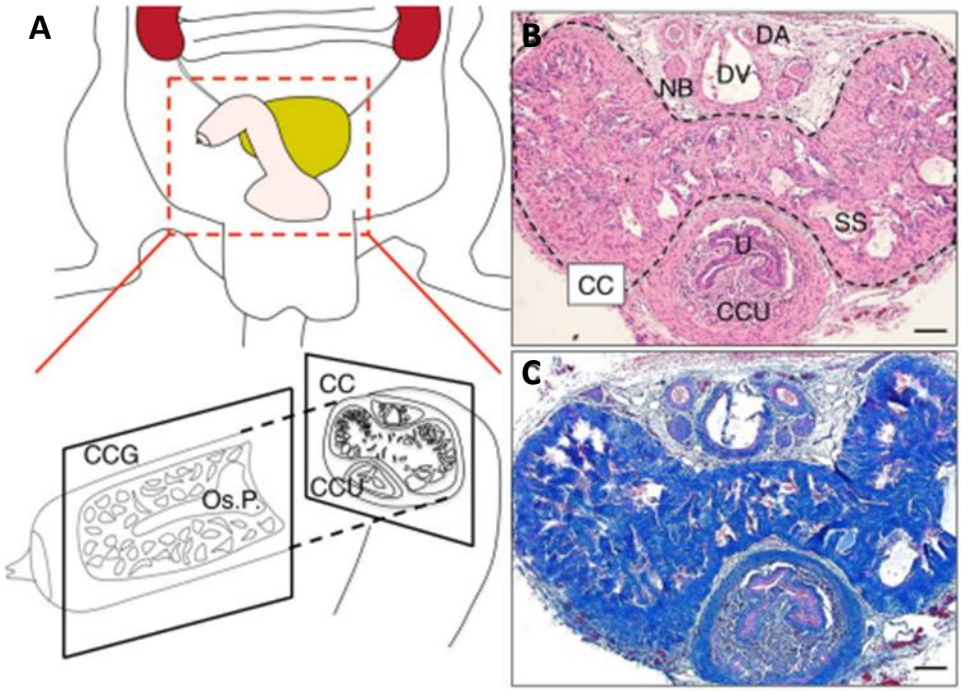


Figure 1.2. Structure of the mouse penis and corpus cavernosum. **A.** An illustration of mouse penis. Mouse penis possesses three corporal units (corpus cavernosum: CC, corpus cavernosum urethra: CCU, and corpus cavernosum glandis: CCG) and bone (Os penis: Os.P.). Lines indicate section orientation of penis. **B.** Image of hematoxylin-eosin staining of CC. Many sinusoidal spaces in CC are indicated by dotted line. Dorsal vein (DV), dorsal artery (DA), nerve bundle (NB), sinusoidal space (SS), and urethra (U). **C.** Image of Masson's trichrome staining of CC showing the collagen-rich regions. Sinusoidal spaces are separated by structures including collagen fibres (blue signal). (Hashimoto *et al*., 2021).

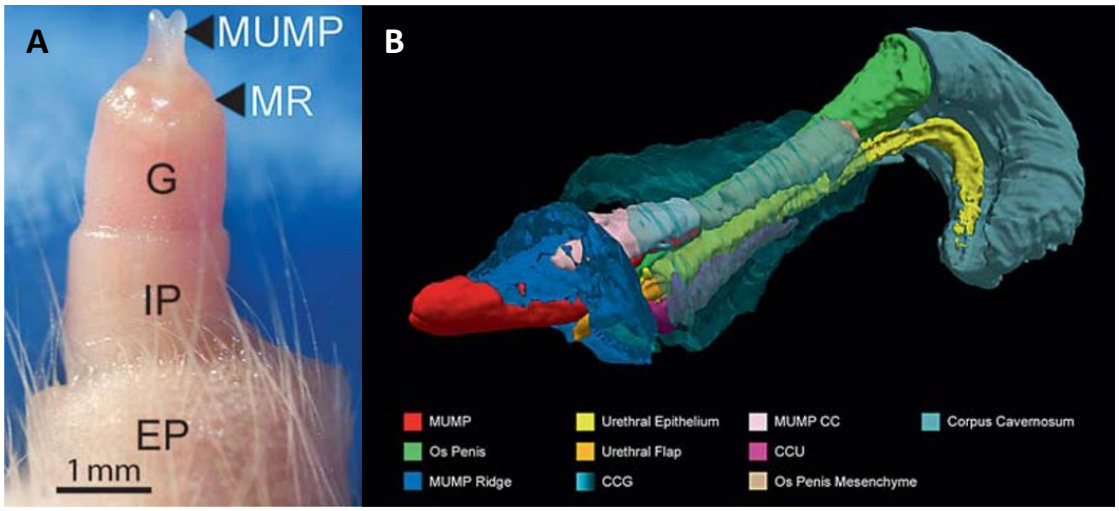


Figure 1.3. **A.** Gross morphology of the adult mouse penis: Glans (G), internal prepuce (IP), external prepuce (EP), male urogenital mating protuberance (MUMP), MUMP ridge (MR). **B.** 3D reconstruction of penile regions examined via MRI with IP protracted and EP excised. MUMP corpus cavernosum (MUMP CC), corpus cavernosum glandis (CCG), corpus cavernosum urethra (CCU). (Philips *et al*., 2015)

1.1.3 Penile Microanatomy

The corpus cavernosum (CC) is composed of numerous variable vascular spaces, termed vascular sinusoids, which are lined by an endothelial layer resting upon a basal membrane (Sathananthan *et al*., 1991). Interposed between the sinusoidal spaces are extensions of the fibrous tunica albuginea, consisting of undulating collagen fibres and longitudinally oriented elastin fibres. Owing to the substantial mechanical demands placed on penile tissue, this fibrous network facilitates distal tissue expansion and accommodates increases in intracavernosal pressure during erection, while elastin fibres may limit excessive stretching of the collagen framework (Bitsch *et al*., 1990). Elastin function declines with age, and reduced elastin integrity within the tunica albuginea is therefore implicated in age-related deterioration of erectile function (Luangkhot *et al*., 1992; Iacono *et al*., 1995; Costa *et al*., 2006).

Bundles of smooth muscle fibres, oriented in all directions, are present between sinusoids, with insertions into the tunica albuginea and its collagenous projections (Goldstein and Padma-Nathan, 1990). Multiple cell types co-habit the CC, encompassing smooth muscle cells (vascular and trabecular), fibroblasts, endothelial cells, pericytes, macrophages, and T lymphocytes (Fang *et al*., 2022; Zhao *et al*., 2022). Pericytes alter capillary-level vascular resistance via changes in pericyte tone

with processes running circumferentially around the capillary endothelium (Peppiatt *et al*., 2006; Hall *et al*., 2014). Yet, reports of pericyte presence appear to indicate increased prominence within the cavernosal periphery and the dorsal nerve bundle, rather than within the cavernous sinusoids (Yin *et al*., 2015).

Pericyte density is typically increased in tissues requiring tightly regulated endothelial permeability, with the highest expression found in the central nervous system (Díaz-Flores *et al*., 2009). In contrast, the CC transitions dynamically between collapsed sinusoidal states during detumescence and distended configurations during tumescence. Therefore, lower expression of cell-to-cell junction proteins in cavernous endothelium may serve to allow dynamic physical changes in the CC architecture (Wessells *et al*., 2004; Ryu *et al*., 2013). Consequently, extensive pericyte coverage may be unnecessary for the profound vascular changes typical of erectile ability. Nonetheless, pericytes likely contribute to vascular development, and experimental loss of pericytes has been shown to impair vessel formation and promote erectile dysfunction (ED; Yin *et al*., 2015).

ED pathogenesis involves several cellular correlates, including increased cavernosal vascular resistance, reduced smooth muscle content, impaired endothelium-dependent relaxation, and progressive fibrosis of the CC (Prieto, 2008; Musicki *et al*., 2015).

1.1.4 Arterial supply

The penis is supplied by the internal pudendal branch of the anterior division of the internal iliac artery. The internal pudendal artery exits the pelvis via the greater sciatic notch inferior to the piriformis, then enters the perineum via the pudendal canal (Moore *et al*., 2014). The internal pudendal artery has two branches, the bulbourethral artery and the cavernosal artery, before terminating as the dorsal artery of the penis (Fig1.4; Sam and LaGrange, 2018). The bulbourethral artery supplies the penile bulb, bulbourethral gland, and corpus spongiosum, while donating a branch to supply the urethra (Juskiewenski *et al*., 1982). The paired cavernosal arteries course through the corpus cavernosa, giving off numerous helicine branches to supply a network of intercommunicating vascular sinusoidal spaces (Fig1.5). The dorsal artery of the penis supplies the penile skin, glans, and fibrous tissue surrounding the corpora cavernosa, corpus spongiosum, and spongy portion of the urethra (Drake *et al*., 2005). Penile vasculature exhibits extensive anastomosis of the three distal branches of the internal

pudendal artery, ensuring comprehensive blood supply to penile structures (Drake *et al*., 2005).

Although the gross arterial anatomy of the penis is broadly conserved among mammals, the distribution of haemodynamic resistance within the penile circulation differs between species. In humans, the principal resistance to penile blood inflow occurs within the helicine arteries and trabecular smooth muscle of the corpora cavernosa, which regulate filling of the sinusoidal spaces during the transition from the flaccid to erect state (Lue *et al*., 1983). In contrast, rodent pelvic vasculature exhibits resistance more proximally, with the majority originating from the internal pudendal arteries (Hannan *et al.,* 2010; Hannan *et al*., 2011).

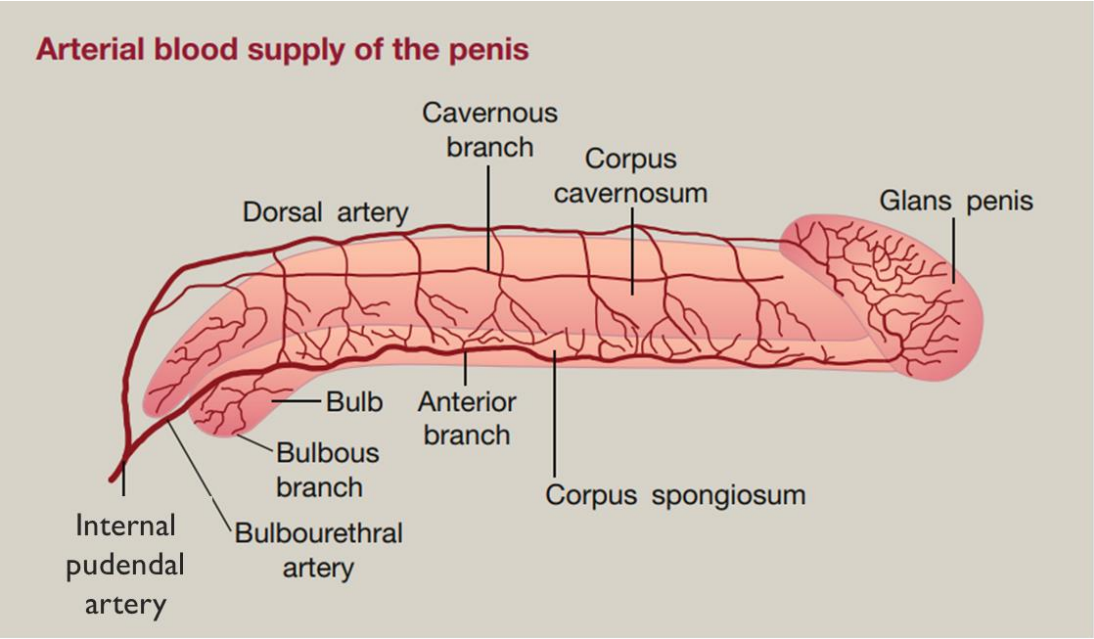


Figure 1.4. Longitudinal illustration of penis vasculature, with the internal pudendal (pudic) artery forming the bulbourethral, cavernosal and dorsal artery of the penis distally (Watkin and Patel, 2020).

1.1.5 Venous drainage

The superficial dorsal vein of the penis drains the skin and subcutaneous tissue of the penis to the superficial external pudendal vein (Drake *et al*., 2005). The deep dorsal vein of the penis lies deep to Buck's fascia, draining the glans and corpus spongiosum via circumflex veins, and distal corpus cavernosum via emissary veins that join the circumflex veins. The deep dorsal vein drains into the prostatic venous plexus (Fig1.5). Proximal corpus cavernosum is drained by emissary veins draining to

cavernosal veins, and penile root crura is drained by crural veins; cavernosal and crural veins drain to the internal pudendal veins (Hsu *et al*., 2003).

1.1.6 Somatic neural control

Sensory innervation of the penis is supplied by the pudendal nerve, which branches from the sacral plexus spinal nerve roots S2-S4, exiting the pelvis via the greater sciatic foramen running between the sacrospinous and sacrotuberous ligaments (Oelhafen *et al*., 2013). Re-entering the pelvis via the lesser sciatic foramen with the internal pudendal artery and vein, running via the pudendal canal, gives three branches: the inferior rectal nerve, the perineal nerve, and the dorsal nerve of the penis. The perineal nerve supplies somatic motor innervation to the bulbospongiosus and ischiocavernosus muscles, while the dorsal nerve of the penis runs deep to Buck's fascia lateral to the dorsal artery of the penis (Fig1.2).

Pudendal nerve block is a common procedure administered for treatment of pudendal neuralgia or during obstetric or urological procedures. A local anaesthetic solution is injected as the pudendal nerve enters through the lesser sciatic foramen, 1 cm inferomedial to the sacrospinous ligament attachment to the ischial spine. One common complication of pudendal neuralgia is sexual dysfunction. This could be a result of a lack of somatic sensation of the penis or motor innervation of the bulbospongiosus and ischiocavernosus (Abdi *et al*., 2004). The bulbospongiosus muscle compresses the penile bulb during urination or ejaculation, and the ischiocavernosus muscle maintains penile erection by compressing the penile crura, forcing blood into the corpora cavernosa (Sam and LaGrange, 2018; Vein, 2003).

1.1.7 Autonomic neural control

Autonomic innervation of the corpora cavernosa occurs via sympathetic and parasympathetic systems. Sympathetic preganglionic fibres from the lumbar splanchnic nerves to the superior hypogastric plexus are located at the level of the aortic bifurcation. Sympathetic fibres then traverse via the right and left hypogastric nerves medial to the internal iliac arteries to form the inferior hypogastric plexus. Parasympathetic preganglionic fibres from S2-S4 spinal segments ascend to join the inferior hypogastric plexus. Branches of the inferior hypogastric plexus then proceed to provide autonomic innervation to the penis via cavernosal nerves composed of sympathetic and parasympathetic nerves (Dean and Lue, 2005).

1.2 Physiology of erectile activity

Penile erection involves a sequence of arterial dilatation, smooth muscle sinusoid relaxation, and venous compression. Cavernosal arteries give rise to multiple branches referred to as helicine arteries, which supply cavernosal sinusoids. During penile flaccidity, helicine artery smooth muscle cells and sinusoidal smooth muscle cells remain in a tonic contraction state. Stimulation from the autonomic nervous system in response to sexual stimulus integrated from the CNS releases neurotransmitters, such as nitric oxide (NO) or acetylcholine (ACh) from parasympathetic fibres, initiating relaxation of the vascular smooth muscle (VSM) cells of the helicine arteries, causing arterial dilatation, and relaxation of sinusoidal smooth muscle cells. This allows increased blood flow into the corpora cavernosa; furthermore, vascular-induced expansion compresses the subalbugineal venous plexus, lying deep to the tunica albuginea and cavernosal sinusoids, a process referred to as tumescence (Fig1.5). In addition to direct venous compression, expansion of the corpora cavernosa also causes elongation and stretching of the emissary veins as they traverse the tunica albuginea, further increasing resistance to venous drainage and contributing to the veno-occlusive mechanism of erection (Udelson *et al*., 2000). Continued expansion of the cavernous body can completely occlude venous drainage via emissary veins, forming the full erection (Lue, 2000). The subsequent vasoconstriction and sinusoidal smooth muscle contraction are often mediated by sympathetic fibres of the cavernosal nerve and referred to as detumescence (Dean and Lue, 2005).

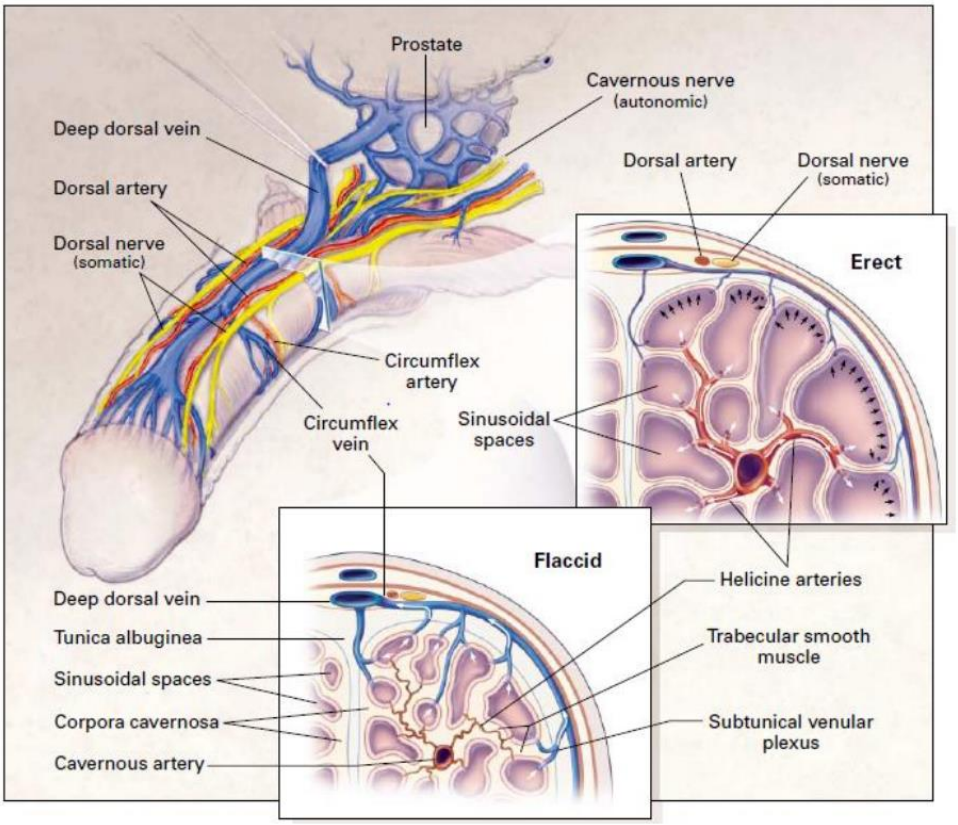


Figure 1.5. Illustration of penile neurovasculature and intracorporal circulation sequence during flaccid and erect penile states (Lue, 2000).

1.3 Corpus cavernosum smooth muscle (CCSM)

The corpus cavernosum smooth muscle (CCSM) is organised within a trabecular network surrounding the sinusoidal spaces. In contrast to visceral smooth muscle, CCSM does not form discrete longitudinal and circular layers. Instead, smooth muscle bundles are arranged in a three-dimensional “basket-weave” architecture, with fibres orientated in longitudinal, circular, and oblique directions (Goldstein and Padma-Nathan, 1990). This structural organisation facilitates coordinated, multidirectional expansion of the sinusoidal spaces and contributes to compression of subalbugineal venous plexus during tumescence.

Isolated mouse and rabbit CCSM strips form spontaneous phasic and/or tonic contractions (Hashitani *et al*., 2005; Hannigan *et al*., 2016; Thornbury *et al*., 2019). The ability of CCSM to synchronise relaxation and contraction implies that the tissue functions as a syncytium. This is supported by the presence of connexin-43-containing gap junctions, which permit intercellular communication via electrical access and secondary messengers (Campos de Carvalho *et al*., 1993; Moreno *et al*., 1993).

However, the cellular specificity of these gap junctions remains incompletely resolved. Although connexin-containing gap junctions have been identified within CCSM, existing studies primarily demonstrate coupling between smooth muscle cells and do not definitively establish whether communication occurs exclusively between these cells. Notably, connexin-43 expression has also been identified in c-Kit$^+$ interstitial cells located adjacent to smooth muscle (Uckert *et al.*, 2010). Consistent with this, c-Kit$^+$ interstitial cells have been reported in human and guinea pig corpus cavernosum, where they exhibit distinct morphology and are localised in close association with smooth muscle and vascular structures (Shafik *et al.*, 2007; Uckert *et al.*, 2010; Fu *et al.*, 2011). In other vascular beds, direct myoendothelial gap junctional coupling between endothelial and smooth muscle cells has been well established, facilitating intercellular communication across the internal elastic lamina (Chaytor *et al.*, 2005; Gairhe *et al.*, 2011). However, this myoendothelial coupling has not been directly demonstrated in corpus cavernosum.

The contractile state of CCSM is determined by Ca^{2+} signalling cascades and Ca^{2+} sensitivity from RhoA/Rho-kinase signalling pathways (Berridge *et al*., 2008). Spontaneous phasic contractility has been proposed to be initiated by localised Ca^{2+} release events involving ryanodine receptors (RyRs) and inositol-1,4,5-trisphosphate (IP_3) receptors (IP_3Rs). These Ca^{2+} release events propagate and induce depolarisation through activation of Ca^{2+}-activated Cl^- channels, which subsequently activate L-type Ca^{2+} channels (LTCCs), resulting in Ca^{2+} influx (Thornbury *et al*., 2019).

1.3.1 Ca^{2+} Signalling Cascade

Contractile agonists, such as noradrenaline released from adrenergic nerves, bind to plasmalemmal receptors and induce receptor conformational changes, leading to activation of phosphoinositide-specific phospholipase C (PLC) via $G_{q/11}$ coupling. PLC catalyses the hydrolysis of phosphatidylinositol-4,5-bisphosphate (PIP_2) to generate 1,2-diacylglycerol (DAG) and IP_3 (Andersson, 2011). IP_3 binds to IP_3Rs on the sarcoplasmic reticulum (SR), triggering Ca^{2+} release driven by a steep electrochemical gradient between the SR lumen (~0.1-1 mM Ca^{2+}) and the cytosol (~100 nM Ca^{2+} at rest), from which it can interact with contractile proteins (Andersson, 2011). Elevated cytoplasmic Ca^{2+} levels can further evoke Ca^{2+}-induced Ca^{2+} release from RyRs within the SR, propagating intracellular Ca^{2+} waves (Karaki *et al*., 1997).

Smooth muscle contraction occurs via the sliding filament mechanism, in which actin and myosin filaments slide past one another (Rice *et al*., 1970). Smooth muscle myosin is composed of two myosin heavy chains and two pairs of myosin light chains (MLC_{17} and MLC_{20}; Andersson, 2011). Two splice variants of the myosin heavy chain exist: SM-A, which is associated with tonic contractures, and SM-B, which predominates in phasic contractions. CCSM contains both SM-A and SM-B isoforms, indicating its capacity for both tonic and phasic activity (DiSanto *et al*., 1998).

Contraction is initiated by an increase in cytosolic Ca^{2+}, which binds to calmodulin to form a Ca^{2+}-calmodulin complex. This complex activates myosin light-chain kinase (MLCK), which phosphorylates MLC_{20}, thereby stimulating myosin ATPase activity and enabling cross-bridge cycling of myosin heads along actin filaments to increase smooth muscle contractility. Subsequent reductions in cytosolic Ca^{2+} promote dissociation of the Ca^{2+}-calmodulin-MLCK complex and dephosphorylation of MLC_{20} by myosin light-chain phosphatase (MLCP), resulting in smooth muscle relaxation (Andersson, 2011).

1.3.2 Ca^{2+} Sensitisation by RhoA/Rho-kinase pathway

In VSM, contractions induced by the α_1-agonist phenylephrine hydrochloride (PE) occur without sustained increases in cytosolic Ca^{2+} concentration; moreover, contractile tone persists after removal of the stimulus. (Collins *et al*., 1992) This phenomenon indicates Ca^{2+} sensitisation of the contractile apparatus and is mediated primarily via the RhoA/Rho-kinase pathway (DeFeo and Morgan, 1985). RhoA, a small monomeric GTPase, is activated through guanine exchange factor-mediated exchange of GDP for GTP, causing dissociation of RhoA-GTP complex from RhoA-GDP dissociation inhibitor (RhoGDI). Activated RhoA translocates to the plasma membrane, where it binds to and activates Rho-associated protein kinase (ROCK), a serine/threonine kinase. ROCK phosphorylates the myosin-binding subunit of MLCP, thereby inhibiting MLCP activity and sustaining contraction independently of cytosolic Ca^{2+} elevations (Sopko *et al*., 2014).

ROCK has therefore been investigated as a therapeutic target for ED. Overexpression of ROCK isoforms has been observed in experimental models of ED, with ROCK-1 elevated in diabetes-associated ED and ROCK-2 upregulated in cavernosal nerve-crush injury models (Sopko *et al*., 2014). Pharmacological inhibition of ROCK using SAR407899 induces erectile responses in both healthy and diabetic

rats (Guagnini *et al*., 2012). Similarly, the ROCK inhibitor Azaindole-1 improves erectile function in nerve-injured rats and demonstrates antihypertensive effects on VSM, highlighting the therapeutic potential of ROCK inhibition in ED management (Pankey *et al*., 2012; Lasker *et al*., 2013). However, the clinical translation of ROCK inhibitors is limited by safety concerns arising from their lack of penile selectivity and consequent systemic vasodilatory effects. The ROCK inhibitors Y-27632 and fasudil have been shown to produce significant reductions in systemic blood pressure in vivo (Masumoto et al., 2002; Doe et al., 2007). Consequently, strategies aimed at improving penile selectivity or enabling localised drug delivery have been proposed to mitigate these cardiovascular risks.

1.4 Erectile Dysfunction (ED)

ED is the failure to achieve or maintain a rigid penile erection for satisfactory sexual intercourse (Muneer *et al*., 2014). It is estimated that approximately 150 million men suffer from ED globally (Costa *et al*., 2006), with past epidemiological projections of approximately 322 million global cases by 2025 based on population ageing and disease prevalence trends (Ayta *et al*., 1999). The Massachusetts Male Ageing Study (MMAS) and European Male Ageing Study (EMAS) provided specific data on ED prevalence with respect to age. MMAS showed ED prevalence at 52% in men aged 40-70 years, whereas EMAS found an average prevalence of 30%. Increasing prevalence in age groups was also reported, with 40-49-year-old men showing 6% prevalence, ranging up to 64% in 70-79-year-old men (Corona *et al*., 2010; Feldman *et al*., 1994).

ED has been stratified into four systemic causes: neurologic, vasculogenic, psychogenic, and endocrinologic.

1.4.1 Neurogenic ED

Neurogenic ED results from impaired neural signalling within the cavernosal nerve and is commonly associated with CNS injury, Parkinson’s disease, and radical pelvic surgery. Lesions superior to the T10 spinal level do not directly alter corpora cavernosa structure but disrupt somatic control of erectile function. In contrast, sacral lesions (S2-S4) reduce parasympathetic innervation of the corpora cavernosa and are associated with loss of reflexogenic erectile responses (Brackett *et al*., 2010). Insufficient acetylcholine and NO release from sacral parasympathetic fibres of the cavernosal nerve maintains smooth muscle in a contracted state, resulting in sustained

vasoconstriction and sinusoidal collapse. Prolonged contractile tone promotes cavernosal structural remodelling, including smooth muscle fibrosis driven by apoptotic signalling, which can culminate in venous occlusive dysfunction. During attempted erection, venous leakage prevents maintenance of tumescence and coincides with impaired vasodilation and sinusoidal relaxation, leading to diminished erectile rigidity and reduced sexual satisfaction (Mulhall *et al*., 2008).

1.4.2 Vasculogenic ED

Vasculogenic ED arises from vascular pathology, including endothelial dysfunction, arterial disease, and iatrogenic vascular injury, leading to reduced penile blood flow, arterial insufficiency, and arterial stenosis. It is reported to account for approximately 75% of ED cases (Costa *et al*., 2006) and is commonly associated with co-morbid conditions such as hypertension, diabetes, and smoking. Resultant cavernosal hypoxia reduces levels of prostaglandin E1 (PGE_1), a metabolite that normally suppresses pro-fibrotic cytokine activity. Disinhibition of these cytokines promotes collagen deposition and fibrotic remodelling of the corpora cavernosa. Consistent with this mechanism, rat models demonstrate that increased collagen content and a reduced smooth muscle-to-collagen ratio impair corporal veno-occlusive function, thereby establishing venous leakage (Moreland, 1998; Nehra *et al*., 1996).

ED is particularly prevalent in men with type 2 diabetes mellitus (T2DM), with epidemiological estimates of 35-75% of men with T2DM developing ED, and often earlier, approximately 10-15 years, than age-matched controls (Kloner *et al.*, 2003; Maiorino *et al.*, 2014). The pathophysiology of diabetic ED is multifactorial and reflects the combined effects of endothelial dysfunction, neuropathy, and structural remodelling of the corpus cavernosum. Chronic hyperglycaemia promotes oxidative stress and the accumulation of advanced glycation end-products (AGEs), which impair endothelial NO synthase (eNOS) activity and reduce NO bioavailability (Cartledge *et al.*, 2001; Bivalacqua *et al.*, 2003). Reduced NO signalling limits cavernosal smooth muscle relaxation and compromises penile arterial inflow. In addition, diabetic autonomic neuropathy disrupts parasympathetic signalling to the cavernosal nerves, further diminishing NO release (Saenz de Tejada *et al.*, 1989b). Long-standing cavernosal hypoxia promotes apoptosis of smooth muscle cells and increased collagen deposition, reducing the smooth muscle-to-collagen ratio and impairing veno-occlusive function (Nehra *et al.*, 1996).

1.4.3 Psychogenic ED

Sexual behaviour in men is regulated by the hypothalamus, limbic system, and cerebral cortex, which transmit facilitatory or inhibitory signals to the spinal erection centres to modulate penile erection. Within these higher centres, the medial preoptic area (MPOA) and paraventricular nucleus (PVN) of the hypothalamus function as key integrative hubs, receiving sensory, cognitive, and emotional inputs and coordinating descending pathways that regulate autonomic outflow to the corpora cavernosa (Argiolas and Melis, 2005). Two principal mechanisms have been proposed to explain higher-centre control of erection: descending inhibitory input to the spinal erection centres and increased sympathetic outflow to the penis, resulting in local noradrenaline release from cavernosal nerves and, secondarily, elevated circulating catecholamines from the adrenal medulla (Steers, 1990). Animal studies demonstrate that sympathetic nerve stimulation induces detumescence (Diederichs *et al*., 1991a; Diederichs *et al*., 1991b). Clinically, patients diagnosed with psychogenic ED exhibit elevated circulating noradrenaline levels compared with healthy controls and patients with vasculogenic ED (Kim and Oh, 1992).

Psychogenic ED is most commonly associated with psychological factors such as performance anxiety, depressive symptoms, low mood, and interpersonal relationship difficulties, which can disrupt sexual arousal and activate inhibitory neural pathways regulating erectile function (Rajkumar and Kumaran, 2015). Anxiety-related performance concerns are particularly common in younger men, where fear of sexual failure activates central inhibitory pathways and increases sympathetic outflow, thereby suppressing erectile responses (Nguyen et al., 2017).

Psychogenic ED encompasses a multifactorial classification, reflecting diverse underlying pathophysiological pathways. The framework proposed by the International Society for Impotence Research is summarised in Figure 1.6 (Lizza and Rosen, 1999).

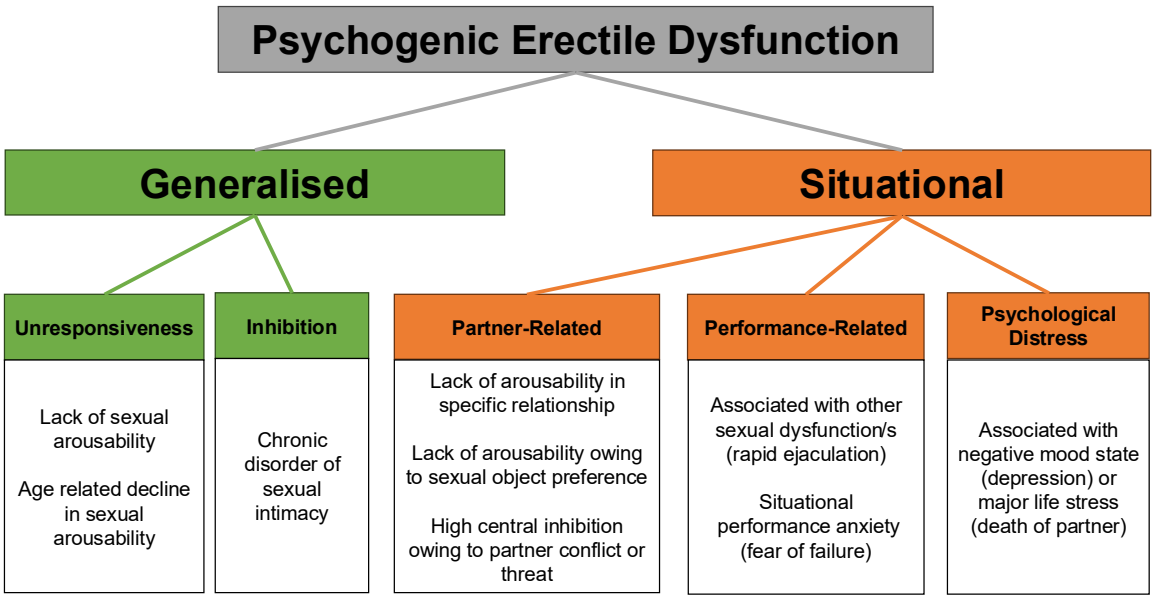


Figure 1.6. Psychogenic erectile dysfunction classification system outlined by International Society of Impotence Research (adapted from Lizza and Rosen, 1999).

1.4.4 Endocrinologic ED

Androgens, particularly testosterone, are essential for male reproductive development and the maintenance of sexual function. Testosterone enhances sexual desire, increases the frequency of sexual activity, and augments nocturnal erectile events (Mulligan and Schmitt, 1993). In animal models, castration reduces penile arterial inflow, increases venous leakage, and approximately halves cavernosal nerve-stimulated erectile responses; subsequent treatment with flutamide (androgen blocker), oestradiol, or gonadotropin-releasing hormone antagonists further exacerbates erectile impairment (Mills *et al*., 1994; Penson *et al*., 1996). Castration has also been shown to increase α-adrenergic responsiveness of penile smooth muscle, promote apoptosis, and reduce smooth muscle content within the corpus cavernosum (Shabsigh, 1997; Traish *et al*., 1999).

In men, hypogonadism results in decreased testosterone production and is frequently associated with dysfunction of the hypothalamic-pituitary axis (Dean and Lue, 2006). Hyperprolactinaemia, commonly secondary to pituitary adenomas or pharmacological agents, can produce symptoms including reduced libido, ED, galactorrhoea, gynaecomastia, and infertility. Elevated prolactin suppresses gonadotropin-releasing hormone secretion, thereby reducing circulating testosterone levels and further contributing to sexual dysfunction (Leonard *et al*., 1989).

1.4.5 Current treatment of ED

Treatments for ED can be broadly categorised as pharmacological, physical, and surgical. First-line pharmacological therapy consists of oral phosphodiesterase-5 inhibitors (PDE5Is), which act as competitive antagonists of the phosphodiesterase-5 enzyme to prolong cyclic guanosine monophosphate (cGMP) signalling and thereby enhance smooth muscle relaxation (Francis *et al*., 2008). Sildenafil was introduced by Pfizer in 1998 as the first oral PDE5I therapy for ED. Since then, additional agents have become widely used, including vardenafil (Levitra™), tadalafil (Cialis™) and avanafil (Stendra™), alongside sildenafil (Viagra™). Despite their clinical success, long-term compliance remains limited. Up to 70% of PDE5I-treated patients discontinue therapy within three years due to adverse effects such as headache, flushing, dyspepsia, and nasal congestion (Corona *et al*., 2011; Chen *et al*., 2015). Furthermore, approximately 30-40% of men with ED fail to respond to PDE5I treatment altogether (de Tejada, 2004). Multiple clinical trials have demonstrated reduced PDE5I efficacy in populations of men suffering from diabetes mellitus (DM; Fonseca *et al*., 2004; Cheng *et al*., 2007), likely associated with vascular complications, including endothelial dysfunction and peripheral neuropathy. These conditions impair NO bioavailability, limiting cellular cGMP formation required for PDE5I effectiveness and thereby reducing therapeutic responsiveness (de Tejada, 2004).

For patients unresponsive to oral PDE5Is, second-line pharmacological options include intracavernosal injection therapy using alprostadil. Alprostadil, a synthetic PGE_1 analogue, is self-administered directly into the corpus cavernosum where it activates EP receptors and promotes CCSM relaxation via adenylyl cyclase (AC)-mediated increases in cyclic adenosine monophosphate (cAMP; Porst, 1996). However, patient adherence to injection therapy is poor, with high early discontinuation rates driven by the discomfort of self-injection and adverse effects including penile pain, priapism, penile curvature, and bruising (Duncan *et al*., 2019; Bearelly *et al*., 2020). Repeated intracavernosal injection therapy may also lead to local structural complications including cavernosal fibrosis, corporal nodules, and penile plaques, which have been reported in a small cohort of patients receiving long-term therapy (Lea *et al*., 1996; Porst, 1996; Montague *et al.*, 2005). These structural alterations may contribute to reduced erectile responsiveness and treatment discontinuation during chronic use (Montague *et al.*, 2005).

Physical therapies represent non-pharmacological second-line interventions when PDE5I therapy fails. The most widely used modality is the vacuum erection device (VED), which has been shown to improve erectile function in approximately 84-95% of patients (Turner *et al*., 1991). A VED consists of a sealed plastic cylinder connected to a vacuum pump that generates negative pressure around the penis, drawing blood into the CC to induce erection (Hoyland *et al*., 2013). VEDs offer advantages including rapid efficacy, reliability, ease of use, and non-invasive application. Nonetheless, their use is associated with limitations, including impaired ejaculation due to urethral compression in 12-30% of users, as well as penile pain, discolouration, and petechiae resulting from capillary haemorrhage during device operation (Hoyland *et al*., 2013).

Low-intensity extracorporeal shockwave therapy (Li-ESWT) has recently emerged as a potential treatment for vasculogenic ED. The therapy delivers acoustic waves to penile tissue, promoting angiogenesis and improving penile haemodynamics through increased vascular growth factor release and recruitment of endothelial progenitor cells (Qiu *et al*., 2013). Early clinical trials demonstrated improvements in International Index of Erectile Function (IIEF) scores and penile haemodynamics in men with vasculogenic ED (Vardi *et al.*, 2010; 2012). Interest has expanded T2DM–associated ED because of the prominent vascular pathology underlying the condition. Randomised and prospective studies report improvements in IIEF scores and penile haemodynamic parameters following Li-ESWT in men with T2DM (Shendy *et al.*, 2021; Tao *et al.*, 2022), although efficacy appears reduced in severe diabetic ED (Ergün and Akyüz, 2022). Systematic reviews indicate that Li-ESWT is generally safe and may provide clinical benefit in men with well-controlled diabetes, but emphasise the need for larger, high-quality trials to determine long-term efficacy (Mason *et al.*, 2023).

1.5 CCSM relaxation mediated by cyclic nucleotides

Penile tumescence is determined by the relaxation of the CCSM in conjunction with the vasodilation of the penile arterial VSM. As previously discussed in this review, CCSM contractility is determined by Ca^{2+} signalling and Ca^{2+} sensitisation by the RhoA/ROCK pathway. Yet CCSM relaxation is primarily mediated by the secondary messenger action of cyclic nucleotides. Cyclic nucleotides include cGMP and cAMP. These induce CCSM relaxation via activation of intracellular signal transduction pathways or modulation of ion channels (Andersson and Wagner, 1995; Adams *et al*., 1997; Christ *et al*., 1997; Soderling and Beavo, 2000; Kim *et al*., 2000).

1.5.1 Cyclic guanosine monophosphate (cGMP) signalling

NO is a gaseous signalling molecule that functions as a neurotransmitter, modulates VSM tone, and regulates gene expression (O'Dell *et al*., 1991; Schuman and Madison, 1991; Rapoport *et al*., 1983; Förstermann *et al*., 1986; Pantopoulos and Hentze, 1995; Khan *et al*., 1996; Gudi *et al*., 1999; Liu *et al*., 2002). NO is synthesized by three NO synthase isoforms: neuronal (nNOS), endothelial (eNOS), and inducible (iNOS).

NO activates soluble guanylate cyclase (sGC) by binding to its heme moiety, stimulating conversion of guanosine triphosphate (GTP) to cGMP (Fig1.7; Prieto, 2008). In human corpus cavernosum, immunohistochemical studies have shown strong sGC expression in cavernosal smooth muscle, with additional immunoreactivity in sinusoidal endothelium, cavernosal arterial endothelium, and nerve fibres, whereas the cGMP-effector, protein kinase G (PKG) was most clearly localised to smooth muscle and is not clearly detected in endothelium (Klotz et al., 2000). These findings support cavernosal smooth muscle as the principal effector site of canonical NO-sGC-cGMP-PKG signalling in erection. In parallel, work in rat corpus cavernosum has suggested that endothelial sGC may be compartmentalised within caveolae, where it may contribute to NO-dependent signalling relevant to smooth muscle relaxation, although the precise functional significance of endothelial sGC in penile erection remains unclear (Linder et al., 2006).

In gastrointestinal smooth muscle, interstitial cells of Cajal (ICC) are established targets of nitrergic neurotransmission and express NO-sensitive sGC, thereby contributing to inhibition of intracellular Ca^{2+} signalling and regulation of motility (Iino et al., 2008; Iino et al., 2009; Lee et al., 2017; Drumm et al., 2019). C-Kit^{+} interstitial cells have also been described in corpus cavernosum, including human and guinea-pig tissue (Shafik et al., 2007; Uckert et al., 2010; Fu et al., 2011). Notably, in guinea-pig corpus cavernosum these interstitial cells were reported to co-express sGCα1 and sGCβ1, suggesting a potential role in NO-mediated cavernosal relaxation (Fu et al., 2011).

cGMP exerts its effects primarily through PKG, which exists as cytosolic PKG I (Iα/Iβ) and membrane-associated PKG II (Hedlund *et al*., 2000; Casteel *et al*., 2010). PKG activation relieves autoinhibition of the kinase domain and enables phosphorylation of downstream targets. In CCSM, NO-cGMP-PKG signalling

promotes relaxation through phosphorylation of phospholamban and disinhibition of the SR Ca^{2+}-ATPase (SERCA), facilitating Ca^{2+} uptake into the SR, subsequently reducing cytosolic Ca^{2+} concentration (Movsesian *et al.*, 1984; Raeymaekers *et al.*, 1988). PKG additionally modulates LTCCs and large-conductance Ca^{2+}-activated K^+ (BK_{Ca}) channels, resulting in membrane hyperpolarisation and reduced Ca^{2+} influx (Joshi *et al.*, 2012). Moreover, PKG I activation can suppress IP_3R-mediated Ca^{2+} release either through direct phosphorylation or indirectly via the IP_3R-associated cGMP substrate (IRAG). PKG has been shown to phosphorylate IP_3R_1 at serine-1755 *in vivo* in VSM cells (Komalavilas and Lincoln, 1994; Murthy and Zhou, 2003). However, PKG Iβ also forms a complex with IP_3R_1 and IRAG, suggesting that IRAG may function as an essential regulator of this inhibitory mechanism (Schlossmann et al., 2000). PKG Iβ phosphorylates IRAG at serine-696 in bovine models (Ammendola et al., 2001). Furthermore, this pathway appears to predominate in NO-mediated inhibition of colonic smooth muscle, as IRAG downregulation attenuated NO donor-induced relaxation responses (Fritsch et al., 2004)

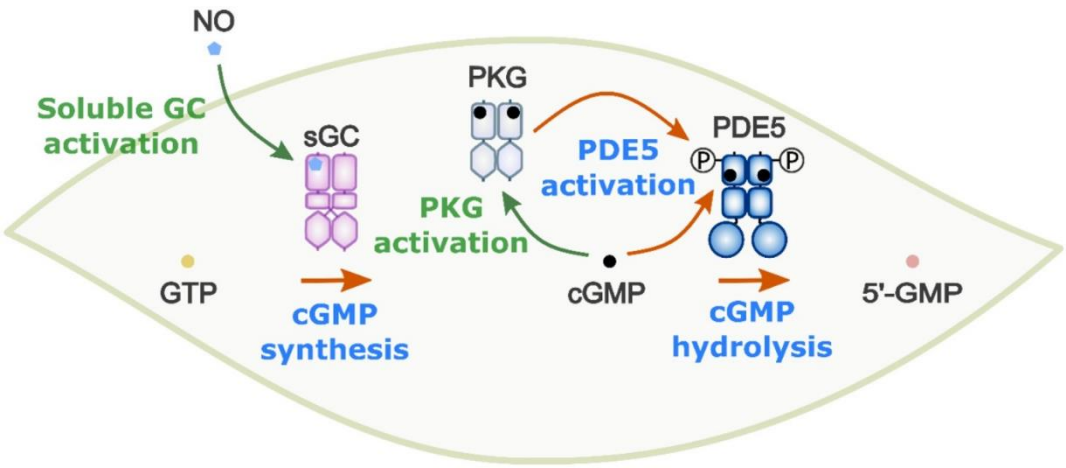


Figure 1.7. Role of phosphodiesterase 5 (PDE5) within the cyclic guanosine monophosphate (cGMP) signalling pathway. Nitric oxide (NO) enters cell and stimulates soluble guanylate cyclase (sGC), this enzyme catalyses the formation of a phosphodiester bond on guanosine triphosphate (GTP) to form cGMP. cGMP activates Protein Kinase G (PKG) by binding to GAFa domain. Activation of PKG activates PDE5 enhancing the cGMP binding to PDE5 and the subsequent hydrolysis of cGMP to guanosine monophosphate (5'-GMP) (Ahmed *et al.*, 2021).

In CCSM, NO-cGMP-PKG signalling is driven primarily by nNOS-derived NO released from parasympathetic cavernosal nerves with non-adrenergic non-cholinergic (NANC) neurotransmission innervating the CCSM and penile arteries (Hurt *et al*., 2002; 2012). The expression of nNOS has been confirmed in the pelvic plexus, cavernosal nerves, and periarterial nerve terminals in human and animal penile tissue via immunohistochemistry across numerous studies (Burnett *et al*., 1992; 1993; Domoto and Tsumori, 1994; Vizzard *et al*., 1994; Dail *et al*., 1995; Simonsen *et al*., 1995; 2001; Vanhatalo *et al*., 1996; 2000; Okamura *et al*., 1998; Hedlund *et al*., 2000). NOS inhibitors, namely L-NAME and N^G-nitro-L-arginine suppressed neurogenic and endothelium-independent relaxations of human CCSM (Rajfer *et al.*, 1992; Pickard *et al.*, 1991; Kirkeby *et al.*, 1993; Teixeira *et al.*, 2004). Moreover, NO release plays a significant role in the NANC component of inhibitory neurotransmission of the penile vasculature, with NOS and sGC inhibition suppressing vasodilatation (Simonsen *et al*., 1995; 1997; 2001; Segarra *et al*., 1998).

Neuronal-dependent NO release via nNOS appears to be crucial for the initial relaxation of CCSM and for triggering vasodilatation of the penile and helicine arteries, thereby facilitating penile vascular filling (Burnett, 2004). Subsequently, shear stress produced by vascular filling during early tumescence may stimulate eNOS and endothelial NO production, facilitating attainment and maintenance of the full erection (Burnett, 2004). Immunostaining for eNOS has been confirmed in CC endothelia (Hedlund *et al*., 1999, Burnett *et al*., 1996; Bloch *et al*., 1998), providing a firm basis for functional studies showing acetylcholine evoked endothelium-dependent relaxation of human CCSM, an effect reversible by NOS inhibition (Azadzoi *et al*., 1992; Simonsen *et al*., 1997). The transduction of vascular shear stress to NO release from endothelia is proposed to occur via activation of the phosphoinositide 3-kinase (PI3K)-protein kinase B (Akt) pathway (Burnett, 2004). The downstream activation of Akt can phosphorylate eNOS at serine-1177 and enhance sustained NO production, supported by Hurt *et al*. (2002) demonstrating cavernous nerve stimulation or papaverine increased phosphorylated Akt and eNOS, and subsequent inhibition of PI3K attenuated erections in vivo.

The significance of eNOS is highlighted by the pathophysiology of vasculogenic ED, with diabetes mellitus, ageing, hypercholesterolaemia and arterial insufficiency being associated with structural CC changes in response impaired endothelium-dependent erectile vasodilation and NO bioavailability (Christ *et al*., 1997; Azadzoi *et*

al., 1998; Traish *et al*., 2000; Sáenz de Tejada *et al*., 2005). The popular success and adoption of PDE5Is as a first-line therapy for ED, via enhancement of the actions of both nNOS- and eNOS-derived NO release by preventing cGMP breakdown, underscores the physiological importance of neurogenic and endothelial NO signalling in the CCSM. Burnett *et al*. (2002) demonstrated genetic deletion of nNOS showed minimal attenuation of erectile responses, yet eNOS knock-out displayed a clear impairment of erectile responses. Moreover, adenoviral delivery of eNOS gene to aged rats significantly enhanced erectile responses, similar to that of the younger controls (Champion *et al*., 1999).

1.5.2 Cyclic adenosine monophosphate (cAMP) signalling

cAMP is an intracellular second messenger essential for regulating cellular metabolism, growth, and differentiation (Halls and Cooper, 2017). In the cardiovascular system, cAMP modulates cardiac contractility by regulating ion channel activity in sympathetic fibres (Boularan and Gales, 2015). Within the central nervous system, cAMP contributes to synaptic plasticity and learning by mediating long-term potentiation at excitatory glutamatergic synapses (Frey *et al*., 1993; Weisskopf *et al*., 1994; Silva *et al*., 1998).

cAMP is synthesised from ATP (Fig1.8) by ACs, which exist as nine membrane-bound isoforms (AC1–9) and one soluble isoform (Halls and Cooper, 2017). ACs catalyse cAMP formation from a Mg^{2+}-ATP complex through generation of a cyclic phosphodiester bond at the ATP α-phosphate and release of pyrophosphate (PPi; Dessauer, 2002). Membrane-bound ACs are primarily regulated by G protein-coupled receptors (GPCRs). Extracellular ligand binding (e.g., noradrenaline, adrenaline, prostaglandin E1) induces a conformational change, activating heterotrimeric G proteins. Dissociation of the $G_{\alpha s}$ subunit stimulates AC activity and increases intracellular cAMP production, whereas $G_{\alpha i/o}$ signalling inhibits AC activity (Pierce *et al*., 2002).

The degradation of cAMP to adenosine monophosphate (AMP) by phosphodiesterases (PDEs) represents a major regulatory mechanism controlling cAMP signalling (Fig1.8; Houslay *et al*., 2007). Of the eleven PDE families expressed in mammalian cells, eight possess cAMP-hydrolysing capacity (Lugnier, 2006). Spatially restricted synthesis and degradation generate intracellular cAMP gradients that compartmentalise signalling. Pulsed isoprenaline stimulation demonstrated that

cAMP transients occur more rapidly at the plasma membrane than in the cytosol, indicating high local synthesis and degradation rates coupled with limited diffusion into intracellular compartments (Mongillo *et al*., 2004; Terrin *et al*., 2006).

PDE4 isoforms contribute significantly to this compartmentalisation. PDE4B predominantly regulates membrane-associated cAMP pools, whereas PDE4D controls cytosolic cAMP clearance (Fischmeister *et al*., 2006). This spatial segregation prevents indiscriminate activation of cAMP-dependent effectors while preserving targeted, compartment-specific signalling responses (Terrin *et al*., 2006).

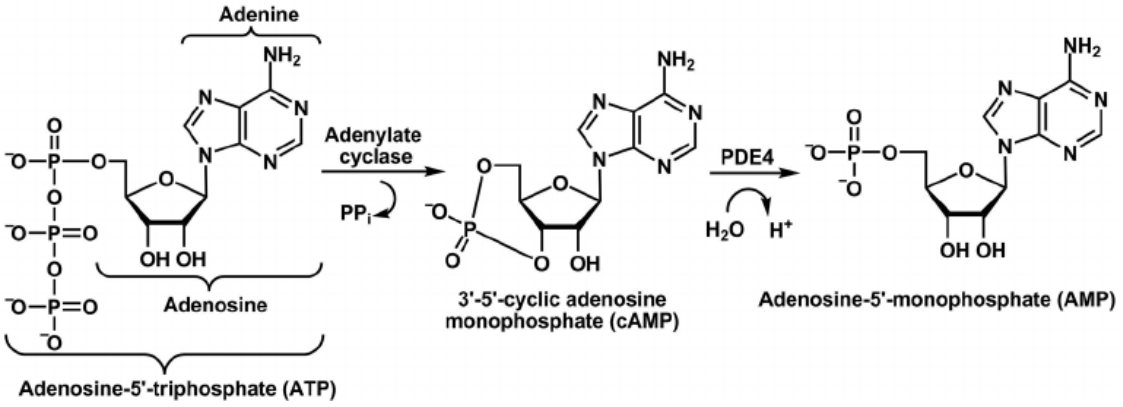


Figure 1.8. Formation of Cyclic Adenosine Monophosphate (cAMP) via Adenylyl Cyclase enzymatic formation of a cyclic phosphodiester bond. Subsequent break down of cAMP to Adenosine Monophosphate (AMP) via Phosphodieserase-4 (PDE4) (Barbossa *et al*., 2011).

1.5.2.1 Protein kinase A (PKA)

Protein kinase A (PKA), also termed cAMP-dependent protein kinase, is a ubiquitously expressed serine/threonine kinase belonging to the AGC kinase family, which also includes PKG and PKC. PKA is a principal effector of intracellular cAMP signalling and regulates a wide range of cellular processes, including ion channel function, metabolism, gene transcription, and smooth muscle contractility (Taylor *et al*., 2012). In its inactive state, PKA exists as a tetrameric holoenzyme composed of two regulatory (R) subunits and two catalytic (C) subunits (R_2C_2). Four R-subunit isoforms have been identified (RIα, RIβ, RIIα, and RIIβ), and three C-subunit isoforms (Cα, Cβ, and Cγ) contribute to holoenzyme diversity. Based on regulatory subunit composition,

PKA is broadly classified as type I (RI-containing) or type II (RII-containing; Kirschner *et al*., 2009).

Activation of PKA occurs following elevation of intracellular cAMP, whereby two cAMP molecules bind to each regulatory subunit, inducing a conformational change that promotes dissociation of the holoenzyme and release of active catalytic subunits. These free C subunits phosphorylate serine/threonine residues within consensus motifs on downstream substrates to modulate cellular signalling cascades (Welch *et al*., 2010). Signal specificity and spatiotemporal fidelity are achieved through subcellular compartmentalisation of PKA via A-kinase anchoring proteins (AKAPs). AKAPs constitute a structurally diverse family of scaffolding proteins that tether PKA holoenzymes to defined subcellular microdomains proximate to specific substrates and upstream signalling components (Ghigo *et al*., 2019). Selective AKAP binding to RI or RII subunits is mediated through isoform-dependent structural differences within the N-terminal docking domain of the R subunits (Huang *et al*., 1997; Gold *et al*., 2006). Most AKAPs display preferential affinity for RII-containing holoenzymes, although several demonstrate RI selectivity, and a limited number interact with both isoforms, albeit with reduced affinity for RI (Burns *et al*., 2003; Kinderman *et al*., 2006; Sarma *et al*., 2010).

AKAP-tethered PKA exerts highly localised modulatory effects on discrete subcellular targets, enabling tightly compartmentalised and physiologically precise responses (Ghigo *et al*., 2015). This spatial organisation is well characterised in VSM, particularly in the regulation of 'Ca^{2+} sparklets', which arise from clusters of LTCCs ($Ca_V1.2$) that exist in either low-activity or persistently active gating states (Amberg *et al*., 2007; Santana *et al*., 2008). Anchoring of PKA by AKAP7 at the plasma membrane promotes phosphorylation of $Ca_V1.2$ at Serine-1928, increasing channel open probability and shifting a greater proportion of channel clusters into the persistently active state, thereby enhancing localised Ca^{2+} influx through sparklet activity (Navedo *et al*., 2010).

In parallel, tethering of PKA to the SR enables coordinated regulation of Ca^{2+} refilling and release. AKAP7-anchored PKA phosphorylates the SERCA regulatory protein phospholamban at Serine-16, relieving its inhibitory constraint on the SERCA pump and enhancing Ca^{2+} reuptake into the SR, thereby increasing luminal Ca^{2+} load (Kranias and Hajjar, 2012). PKA also phosphorylates RyRs, increasing channel open probability and augmenting localised Ca^{2+} release events, including the generation of

'Ca^{2+} sparks' (Marx *et al*., 2000). In smooth muscle, these sparks can function as activators of adjacent BK_{Ca} channels, inducing membrane hyperpolarisation and inhibition of voltage-dependent Ca^{2+} influx (Nelson *et al*., 1995; Jaggar *et al*., 2000).

Beyond this indirect coupling, PKA directly enhances BK_{Ca} channel activity through phosphorylation of the pore-forming α-subunit at consensus serine residues within its C-terminal regulatory domain, including Serine-869. This phosphorylation increases Ca^{2+} sensitivity and shifts voltage dependence toward more negative membrane potentials, substantially elevating channel open probability and promoting membrane hyperpolarisation (Minami *et al*., 1993; Schubert and Nelson, 2001).

1.5.2.2 Exchange protein directly activated by cAMP (EPAC)

A PKA-independent pathway of cAMP signalling was identified with the discovery of the guanine nucleotide exchange factor Exchange Protein Directly Activated by cAMP (EPAC; de Rooij *et al*., 1998). EPAC contains a cyclic nucleotide-binding domain homologous to the regulatory subunits of PKA, enabling direct activation by cAMP. Upon cAMP binding, EPAC catalyses the exchange of GDP for GTP on the small GTPases Rap1 and Rap2, initiating downstream signalling cascades (Kawasaki *et al*., 1998; Cheng *et al*., 2008).

Two EPAC isoforms, EPAC-1 and EPAC-2, have been characterised. Although both share conserved Rap-GEF activity, they exhibit distinct physiological roles (Robichaux and Cheng, 2018). EPAC-1 contains a single cyclic nucleotide–binding domain and is ubiquitously expressed, where it regulates cell adhesion, endothelial barrier integrity, and cytoskeletal remodelling (de Rooij et al., 1998; Cullere et al., 2005; Robichaux and Cheng, 2018). In contrast, EPAC-2 possesses two low-affinity cyclic nucleotide–binding domains and is predominantly expressed in endocrine tissues and the central nervous system (Robichaux and Cheng, 2018). Functionally, EPAC-2 controls vesicle trafficking and exocytosis via Rap-dependent signalling, with key roles in insulin secretion and neurotransmitter release (Kang et al., 2001; Shibasaki et al., 2004; Gekel and Neher, 2008).

At the signalling level, EPAC-Rap activation regulates diverse cellular processes including cell adhesion, junctional organisation, secretion, differentiation, and cytoskeletal dynamics (Cheng *et al*., 2008). Several downstream transduction routes have been proposed, including Rap-dependent activation of phosphatidylinositol 4,5-bisphosphate (PIP_2)-specific phospholipase C-Ɛ (PLCƐ),

resulting in IP_3 formation and subsequent IP_3R-dependent Ca^{2+} release (Schmidt *et al*., 2001; Evellin *et al*., 2002). In cardiomyocytes, an EPAC-Rap1-PLCƐ signalling promotes SR Ca^{2+} release, with a PLCƐ knockdown significantly attenuating EPAC-induced Ca^{2+} release (Oestreich *et al*., 2007). Furthermore, EPAC-induced Ca^{2+} release has been implicated in β-adrenergic receptor-mediated cardiac hypertrophy. Cardiac tissue shows predominant expression of EPAC-1, which becomes upregulated under heart failure conditions, while the inverse EPAC-1 knockdown attenuates β-adrenergic-induced hypertrophy (Metrich *et al*., 2008).

Parallel mechanisms of EPAC-mediated effects on SR Ca^{2+} release exist within smooth muscle. EPAC activation increased 'Ca^{2+} sparks' and spontaneous transient outward currents (STOCs), an effect reversed by ryanodine, 2-aminoethoxydiphenyl borate (IP_3R inhibitor, 2-APB) and a Ca^{2+}-calmodulin-dependent kinase II (CaMKII) inhibitor, KN93 (Humphries *et al*., 2017). This mechanism was supported with evidence showing that EPAC activation phosphorylates γ-CaMKII isoforms, and additional findings that EPAC activation phosphorylates RyR_2 at serine 2814/2815 (Pereira *et al*., 2007; Gloerich and Bos, 2010). Consistent with this, EPAC activation has demonstrated contributions to smooth muscle relaxation across a range of tissues. Both EPAC and PKA activation: attenuated store-operated Ca^{2+} entry (SOCE) in rat aortic rings (Cuíñas *et al*., 2016); relaxed pre-contracted guinea pig and airway smooth muscle (Roscioni *et al*., 2011) and, lastly, promoted relaxation of human detrusor (Hayashi *et al*., 2016). EPAC-1 has been identified in rat CCSM and shown to be down-regulated under androgen-deficient conditions; however, its effects on CCSM contractility have not yet been investigated (Lin *et al*., 2023).

In addition to the numerous reports of EPAC-mediated Ca^{2+} signalling, the cAMP effector has demonstrated modulatory effects on ion channels. EPAC-dependent Ca^{2+} release inhibited ATP-sensitive K^+ (K_{ATP}) channels in rat aortic smooth muscle via Ca^{2+}-calmodulin-dependent phosphatase calcineurin-dependent dephosphorylation of $K_{ir}6.2$ or SUR1 subunits (Purves *et al*., 2009). This interaction is supported by co-immunoprecipitation of EPAC-1 and EPAC-2 with SUR1 (Kang *et al*., 2006). An EPAC activator enhanced *KCNQ*-encoded voltage-gated K^+ (K_v7) channel-blocker sensitive currents in VSM, demonstrated by increased co-localisation of the downstream effectors Rap1 and Rap2 with $K_v7.4$ α-subunits following isoprenaline stimulation (Stott *et al*., 2016).

1.5.2.3 Cyclic nucleotide-gated channels (CNGCs)

Cyclic-nucleotide-regulated cation channels belong to two related subfamilies, including classical ligand-gated CNG channels (CNGCs) and hyperpolarisation-activated and cyclic nucleotide-gated (HCN) channels. Both channels share a six-transmembrane structure with a pore and a C-terminal cyclic-nucleotide binding domain, which upon the binding of cyclic nucleotides inducing a conformational change permitting influx of extracellular cations (Ludwig *et al*., 1998; Santoro *et al*., 1998). Initially characterised in photoreceptors and olfactory sensory neurons, CNGCs are now known to be widely expressed, including in brain, kidney, endocrine tissues, and spermatozoa (Kaupp and Seifert, 2002).

In sperm cells, cyclic nucleotide signalling regulates key functions such as acrosomal exocytosis, motility, and chemotaxis. Activation of GC increases intracellular cGMP levels, correlating with elevated cytosolic Ca^{2+} through CNGC-mediated influx (Kaupp and Seifert, 2002). Similarly, in olfactory sensory neurons, odorant binding to G-protein-coupled receptors stimulates AC, increasing intracellular cAMP. This activates CNGCs, driving Ca^{2+} influx and membrane depolarisation that initiates action potential firing during olfaction (Kaupp and Seifert, 2002).

The expression of classical CNGC subunits and the functional effects of CNGC-selective pharmacological agents have not been investigated in CCSM. In contrast, direct molecular and functional evidence demonstrates the presence of HCN channels in human CCSM. Gur *et al.* (2020) demonstrated the presence of HCN_3 and HCN_4 isoforms in human corpus cavernosum tissue by western blot. Pharmacological blockade of HCN channels with ivabradine induced relaxation of pre-contracted CCSM strips and enhanced neurogenic relaxations; however, these effects were only observed at relatively high concentrations of ivabradine. HCN channels are best characterised in the cardiac sino-atrial node, where they mediate the ‘funny current’. Following membrane hyperpolarisation, after an action-potential-induced contraction, HCN channels open to permit influx of Na^+ and K^+, slowly depolarising the membrane and inducing a subsequent action potential (Larson, 2010).

1.6 Store-operated Ca^{2+} entry (SOCE)

Given the central role of Ca^{2+} as a second messenger in smooth muscle cells, SR Ca^{2+} content is tightly regulated to maintain cellular homeostasis. SOCE is mediated by Ca^{2+} release-activated Ca^{2+} (CRAC) channels, which are formed by Orai

pore-forming subunits and regulated by stromal interaction molecule (STIM) proteins (Hogan *et al.*, 2010). STIM proteins function as luminal Ca^{2+} sensors via their N-terminal EF-hand domains, which bind Ca^{2+} within the SR under resting conditions. Upon depletion of SR Ca^{2+} stores, Ca^{2+} dissociates from the EF-hand, triggering conformational changes that promote STIM oligomerisation and translocation to SR–plasma membrane junctions, where they engage Orai subunits (Liou *et al.*, 2005; Roos *et al.*, 2005). This interaction is mediated by the cytosolic C-terminal STIM/Orai-activating region (SOAR/CAD), which gates Orai channels to permit Ca^{2+} influx and subsequent SR refilling (Park *et al.*, 2009; Yuan *et al.*, 2009).

Two STIM isoforms, STIM-1 and STIM-2, share this core activation mechanism but exhibit distinct functional properties. STIM-1 has a higher Ca^{2+}-binding affinity and is therefore activated primarily following substantial SR Ca^{2+} depletion, driving robust Orai channel activation and rapid Ca^{2+} influx (Liou *et al.*, 2005; Roos *et al.*, 2005). In contrast, STIM-2 exhibits a lower Ca^{2+} affinity, allowing it to respond to more subtle reductions in SR Ca^{2+} concentration and thereby contribute to the maintenance of basal Ca^{2+} homeostasis (Brandman *et al.*, 2007). STIM-2 can also heterodimerise with STIM-1 via their cytosolic domains, lowering the threshold for STIM-1 activation and modulating the sensitivity of SOCE (Soboloff *et al.*, 2006; Subedi *et al.*, 2018). Functionally, this interaction influences SOCE kinetics, with STIM-2 promoting slower, sustained Ca^{2+} entry compared to the rapid, transient influx typically mediated by STIM-1.

Although Orai-1 was initially identified as the principal pore-forming subunit of CRAC channels, genetic and electrophysiological studies have demonstrated that native channels can exist as heteromeric assemblies of Orai-1, Orai-2 and Orai-3, with channel properties determined by their relative expression and stoichiometry (Emrich *et al.*, 2021). Orai-1 underlies the classical CRAC current, characterised by high Ca^{2+} selectivity and strong inward rectification (Prakriya *et al.*, 2006; Vig *et al.*, 2006), whereas Orai-2 appears to play a modulatory role, exhibiting reduced current amplitude and enhanced Ca^{2+}-dependent inactivation (Vaeth *et al.*, 2017). Orai-3 contributes additional functional diversity, displaying reduced sensitivity to oxidative stress and the ability to participate in store-independent channel complexes such as arachidonic acid–regulated Ca^{2+} (ARC) channels (Mignen *et al.*, 2008; Thompson *et al.*, 2010; Bogeski *et al.*, 2010).

In the human corpus cavernosum, expression of Orai-1, Orai-3 and STIM-1 has been demonstrated, with evidence of pathological upregulation of Orai-1 and particularly Orai-3 in tissue from aged individuals and patients with ED (Sevilleja-Ortiz *et al.*, 2020, 2021). Functional studies further support a role for SOCE in the CCSM, as increased adrenergic contractility observed in aged human and diabetic rat CCSM is attenuated by the Orai channel inhibitor YM-58483, indicating enhanced SOCE activity under these conditions. However, the expression and functional roles of Orai-2 and STIM-2 in this tissue remain poorly defined, and the precise contribution of isoform-specific STIM/Orai interactions to CCSM Ca^{2+} signalling requires further investigation.

1.7 Electrophysiology

The CCSM exhibits a relatively depolarised resting membrane potential typically ranging from approximately -41 to -60 mV in rabbit. In line with these findings, isolated CCSM cells display spontaneous transient depolarisations (STDs; Hashitani et al., 2005; Thornbury et al., 2019), indicating spontaneous changes in membrane excitability. The presence of connexin-43-containing gap junctions in CCSM indicates functional electrical coupling between smooth muscle cells, enabling the tissue to operate as a syncytium (De Carvalho et al., 1993). This coupling facilitates the spread of depolarisation and intracellular signals, supporting coordinated contractile activity across the trabecular network.

Consistent with this, CCSM exhibits rapidly propagating intracellular Ca^{2+} waves associated with inward currents, suggesting that synchronous activity is coordinated by membrane depolarisation (Sergeant et al., 2009). These Ca^{2+} waves precede phasic contractions of cavernosal trabeculae, indicating a close link between depolarisation-driven Ca^{2+} influx and phasic contractile activity. In contrast, tonic contraction is more likely to reflect sustained Ca^{2+} influx and/or SR Ca^{2+} release in conjunction with Ca^{2+} sensitisation mechanisms, rather than synchronised depolarisations. Collectively, these findings identify membrane excitability as a key determinant of CCSM contractility, governing the balance between phasic and tonic behaviours.

The CCSM has a plethora of ion channels that are able to modulate membrane potential, including: L- and T-type voltage-gated Ca^{2+} channels (Höppner *et al*., 1996, McCloskey *et al*., 2009), Ca^{2+} -activated Cl^- channels (Craven *et al*., 2004; Hannigan

et al., 2017; Lim *et al*., 2022a), P2X receptors (Doyle *et al*., 2014), voltage-dependent Na^+ (Na_v) channels (Lim *et al*., 2022b), large-conductance Ca^{2+}-activated K^+ (BK_{Ca}) channels (Werner *et al*., 2005; Hannigan *et al*., 2016), ATP-sensitive K^+ channels (Lee *et al*., 1999; Venkateswarlu *et al*., 2002; Insuk *et al*., 2003; Silva *et al*., 2005; Dalaklioglu and Ozbey, 2014), and voltage-dependent K^+ (K_v) channels (Malysz *et al*., 2001; Malysz *et al*., 2002; Jepps *et al*., 2016; Lee *et al*., 2020a).

1.7.1 L- and T-Type Ca^{2+} channels

Voltage-gated Ca^{2+} channels (VGCCs) comprise a family of pore-forming α_1 subunits encoded by the Ca_v gene superfamily and are classified based on electrophysiological and pharmacological properties into L-type (LTCC; $Ca_v1.1$-1.4), P/Q-type ($Ca_v2.1$), N-type ($Ca_v2.2$), R-type ($Ca_v2.3$) and T-type (TTCC; $Ca_v3.1$-3.3) channels. All VGCC α_1 subunits share a structure consisting of four homologous domains (DI-DIV), each containing six transmembrane segments (S1-S6), with the S4 helices acting as voltage sensors and the S5-S6 segments forming the Ca^{2+}-permeable pore (Catterall, 2000; Ertel *et al*., 2000). VGCC function is modulated via the expression of a variety of auxiliary β, $\alpha_2\delta$, and γ subunits, which regulate trafficking, gating kinetics, channel stability and sensitivity to pharmacological modulators (Dolphin, 2012).

McCloskey *et al*. (2009) confirmed the expression of LTCCs and TTCCs in rabbit CCSM cells, distinguished via their pharmacological sensitivity and biophysical properties. LTCCs are nifedipine (NIF)-sensitive and resistant to mibefradil and Ni^{2+} blockade, whereas TTCCs demonstrate mibefradil and Ni^{2+} sensitivity with relative NIF resistance (Perez-Reyes, 2003; McCloskey *et al*., 2009). Biophysically, TTCCs display more rapid activation and inactivation kinetics and activate at more hyperpolarised membrane potentials than LTCCs, consistent with their designation as low-voltage-activated channels (Perez-Reyes, 2003; McCloskey *et al*., 2009).

Channel activation and inactivation kinetics critically determine excitability in smooth muscle tissues. The overlap of steady-state activation and inactivation curves of LTCCs produces a prominent “window current” over a voltage range of approximately -45 to -10 mV, with maximal overlap near -30 mV, allowing steady, non-inactivating Ca^{2+} influx in rabbit CCSM cells (McCloskey *et al*., 2009). This sustained Ca^{2+} influx via the “window current” provides a mechanistic basis for the maintenance of myogenic VSM tone (Nelson *et al*., 1990; Smirnov and Aaronson, 1992; Jaggar *et*

al., 2000). Notably, in rabbit CCSM, the voltage corresponding to maximal LTCC window current closely approximates the E_{Cl} in smooth muscle (approximately -30 mV; Thornbury *et al*., 2019). Accordingly, activation of ANO1 in CCSM, which depolarizes membrane potential toward E_{Cl}, may effectively clamp the membrane potential within the LTCC "window current" range, thereby maximising Ca^{2+} influx (Thornbury *et al*., 2019), subsequently, sustaining CCSM tone (Christ, 1998).

TTCCs also generate a window current at more hyperpolarised potentials (-65 to -45 mV), overlapping with the reported resting membrane potential of CCSM (Hashitani *et al*., 2005; Kuo *et al*., 2011; Thornbury *et al*., 2019). Although the electrochemical driving force for Ca^{2+} influx is increased at these hyperpolarised potentials, the substantial overlap between activation and inactivation curves is limited for TTCCs, such that only a small fraction of channels remain open and available, thereby restricting the magnitude of sustained Ca^{2+} entry. This suggests that TTCCs may contribute to basal Ca^{2+} signalling, but the physiological impact of this current in CCSM remains unclear.

Finally, LTCCs play a fundamental role in the phasic contractile activity of CCSM. Contractile agonists such as PE and endothelin-1 evoke transmembrane Ca^{2+} influx primarily through LTCC activation (Andersson, 2011). Moreover, phasic contractions observed in human, rabbit, and rat CCSM closely correlate with rhythmic electrical activity, indicating the presence of oscillatory Ca^{2+} signalling events underpinning contractile responses (Hashitani *et al*., 2005).

1.7.2 Ca^{2+}-activated Cl^- channels - Anoctamin-1 (ANO1)

The CCSM of humans, rats, and rabbits expresses prominent Ca^{2+}-activated Cl^- currents (Karkanis *et al*., 2003; Craven *et al*., 2004; Williams *et al*., 2007; Sergeant *et al*., 2009; Doyle *et al*., 2012; Hannigan *et al*., 2017). Functional identification of these currents relied on three defining features: blockade by Cl^- channel antagonists niflumic acid and anthracene-9-carboxylic acid (A9C), activation by elevated intracellular Ca^{2+}, and shifts in reversal potential following Cl^- substitution, confirming anion selectivity (Karkanis *et al*., 2003; Craven *et al*., 2004; Hannigan *et al*., 2017). Molecular correlates of this current were subsequently identified as anoctamin-1 (ANO1), otherwise known as transmembrane member 16A (TMEM16A; Caputo et al., 2008; Schroeder et al., 2008; Yang et al., 2008), with expression validated in rabbit and mouse CCSM (Hannigan *et al*., 2017; Lim *et al*., 2022a). ANO1 exists as a homodimeric channel

complex, with each subunit comprising 10 transmembrane helices that form an individual ion-conducting pore. Channel gating is mediated by direct binding of intracellular Ca^{2+} to conserved regulatory sites within the cytoplasmic face of the protein, producing conformational rearrangements that permit Cl^- permeation (Paulino *et al*., 2017).

Electrical recordings from rabbit CCSM have reported resting membrane potentials between -50 and -41 mV (Hashitani *et al*., 2005) and -60 mV (Thornbury *et al*., 2019). The equilibrium potential for Cl^- (E_{Cl}) in smooth muscle is approximately -38 to -19 mV, due to elevated cytosolic Cl^- levels (32-44 mM; Chipperfield and Harper, 2000). Consequently, Ca^{2+}-dependent activation of ANO1 drives Cl^- efflux, generating an inward current and membrane depolarisation sufficient to activate LTCCs (Manoury *et al*., 2010).

Isolated CCSM cells exhibit spontaneous transient inward currents (STICs), under voltage clamp at -60 mV, reflecting activation of Ca^{2+}-activated Cl^- currents (Karkanis *et al*., 2003; Craven *et al*., 2004). In rabbit CCSM, STICs depend on SR Ca^{2+} release, being suppressed by the SERCA inhibitor cyclopiazonic acid (CPA) and the IP_3R inhibitor 2-APB (Craven *et al*., 2004). Similar mechanisms exist in mouse CCSM, in which blockade of SERCA, IP_3Rs, RyRs (using tetracaine, TC), and CRAC channels (using GSK-7975A) inhibited STICs and associated STDs (Lim *et al*., 2022a). These findings indicate that RyR- and IP_3R-dependent Ca^{2+} release, supported by Ca^{2+} influx via CRAC channels, provides the Ca^{2+} stimulation required for ANO1 opening and membrane depolarisation.

ANO1 activity is modulated by cGMP signalling. In rabbit CCSM, elevation of cGMP abolished STICs (Craven *et al*., 2004) and eliminated Ca^{2+} waves associated with Ca^{2+}-activated Cl^- currents (Sergeant *et al*., 2009). Given the dependence of these Ca^{2+} waves on SR Ca^{2+} release, cGMP likely suppresses ANO1 activity indirectly by inhibiting IP_3R- and/or RyR-mediated Ca^{2+} release. However, the functional effects of ANO1 appear to be species-dependent. In rabbit CCSM, inhibition of Ca^{2+}-activated Cl^- currents with A9C and niflumic acid abolishes spontaneous tone, consistent with a model in which ANO1-mediated Cl^- efflux depolarises the membrane into the LTCC 'window current' range, thereby sustaining Ca^{2+} influx (Nelson et al., 1990; Chu and Adaikan, 2008). In contrast, in mouse CCSM, selective ANO1 inhibition with Ani-9 suppresses phasic contractions without observable effects on tone (Lim et al., 2022a). In vivo, ANO1 inhibition increased intracavernosal pressure and prolonged electrically-

evoked erections in rats (Karkanis et al., 2003; Chung et al., 2009). Taken together, ANO1 is a key regulator of CCSM excitability, but its contribution to tone generation and Ca^{2+} influx mechanisms is species-specific, with important implications for its therapeutic targeting in ED

In addition to ANO1-mediated Ca^{2+}-activated Cl^- currents, bestrophin (BEST) channels have been proposed to mediate Ca^{2+}-activated Cl^- currents that are strongly regulated by cGMP signalling in VSM (Matchkov *et al.*, 2004). Moreover, small interfering RNA (siRNA)-knockdown of $BEST_3$ markedly reduced this current in rat mesenteric myocytes (Matchkov *et al.*, 2008). However, expression and functional roles of BEST channels in CCSM have not been clearly established.

1.7.3 P2X receptor-mediated cation currents

ATP is released from multiple cellular sources within the corpus cavernosum, including CCSM, nerve terminals, endothelial cells, erythrocytes, platelets, and other resident cell types (Gordon, 1986). Extracellular ATP activates purinergic receptors, which are classified into two principal families: adenosine-sensitive P1 receptors and ATP/ADP-sensitive P2 receptors. Mammalian P2 receptors are further divided into P2X receptors, which are ligand-gated non-selective cation channels, and P2Y receptors, which are G-protein-coupled receptors mediating metabotropic signalling pathways (Abbracchio *et al*., 2003; Burnstock, 2007). The physiological effects of ATP within CCSM are species-dependent and influenced by basal smooth muscle tone, with reported responses spanning both excitatory and inhibitory actions (Wu *et al*., 1993).

In VSM and the vas deferens, ATP functions as an excitatory co-transmitter with noradrenaline, eliciting contraction through stimulation of P2X purinoceptors, which permit inward flux of Na^+ and Ca^{2+} ions (Thornbury *et al*., 2019). Conversely, in arteries subjected to shear stress, endothelial ATP release activates P2Y receptors on endothelial cells, triggering NO production and subsequent elevation of cGMP within the VSM, resulting in vasodilatation (Shalev *et al*., 1999; Thornbury *et al*., 2019). In CCSM specifically, activation of P2X receptors using the stable agonist α,β-methylene ATP induced contraction of human CCSM in vitro, while exogenous ATP produced contractions in rabbit CCSM under low basal tension conditions (Wu *et al*., 1993; Filippi *et al*., 1999; Thornbury *et al*., 2019).

Electrophysiological analyses reveal that rabbit CCSM exhibits an ATP-evoked inward cation current, mediated in part by Na^+ influx, which is significantly attenuated following P2X-receptor desensitisation with α,β-methylene ATP and by application of NF449, a selective P2X1 antagonist (Doyle *et al*., 2014). Immunohistochemical studies in human CCSM demonstrate strong expression of P2X1 receptors and weaker expression of P2X2 receptors (Lee *et al*., 2000; Gur *et al*., 2009), supported with immunoreactivity for P2X1 in mouse CCSM cells (Lim *et al*., 2024). Recent evidence supports the presence of an excitatory purinergic innervation of the mouse CCSM as EFS-induced contractions persisted despite adrenergic and cholinergic blockade and were significantly reduced by NF449, confirming a functional role for P2X-mediated neurotransmission in CCSM contractility (Lim *et al*., 2024). In addition, ATP-evoked inward currents in mouse CCSM cells were blocked by α,β-methylene ATP and NF449.

Several studies further implicate P2X1 receptor upregulation in ED. Suadicani *et al*. (2009) reported that P2X1 expression in human CCSM was inversely correlated with erectile function, with higher receptor protein levels observed in tissue samples from patients with impaired erectile performance, supporting a pathological role for enhanced purinergic excitation in ED. Complementing these findings, Guo *et al*. (2020) demonstrated that androgen-deficiency via castration in rats significantly increased expression of P2X1, P2X2, and P2X3 receptors, alongside upregulation of key components of the RhoA/ROCK contractile signalling pathway (ROCK-1 and ROCK-2). These molecular changes were associated with reduced intracavernosal pressure responses to nerve stimulation and impaired erectile function, indicating that hypogonadism promotes a contractile phenotype characterised by upregulated purinergic signalling and Ca^{2+} sensitisation.

1.7.4 Voltage-dependent Na^+ (Na_V) channels

Voltage-gated Na^+ (Na_V) channels comprise nine α-subunit isoforms ($Na_V1.1$-1.9) encoded by the SCN1A-SCN11A gene family (Catterall *et al*., 2005). Na_V channels are classically associated with electrically excitable tissues, including neurons, cardiac myocytes, and skeletal muscle, where they drive action potential initiation and propagation. However, Na_V expression has also been documented in cell types not traditionally considered excitable, such as differentiated myofibroblasts, metastatic cancer cells, macrophages, and vascular endothelial cells, indicating broader functional roles beyond classical excitability (Andrikopoulos *et al*., 2011; Brackenbury, 2012; Chatelier *et al*., 2012; Sun *et al*., 2019).

Within smooth muscle, Na_v channels have been identified in tissues exhibiting spontaneous electrical activity, including the lymphatic vessels (Hollywood *et al*., 1997; Telinius *et al*., 2015), gastrointestinal tract (Holm *et al*., 2002; Neshatian *et al*., 2015), vas deferens (Teramoto *et al*., 2012), uterus (Sperelakis *et al*., 1992; Seda *et al*., 2007), and the portal vein (Saleh *et al*., 2005). Expression has also been reported in smooth muscle tissues not typically considered spontaneously active, notably the airways (Bradley *et al*., 2013) and pulmonary arteries (Okabe *et al*., 1988). Until recently, the presence of Na_v channels in CCSM had not been described.

Patch-clamp analyses subsequently demonstrated fast, voltage-dependent Na^+ currents in isolated mouse CCSM cells (Lim *et al*., 2022b). Two populations of currents were distinguished based on sensitivity to tetrodotoxin (TTX). The TTX-sensitive component was partially inhibited by selective blockers targeting $Na_v1.1$-1.3 (ICA-121431), $Na_v1.7$ (PF-05089771), and $Na_v1.6$ (4,9-anhydro-TTX), which produced an aggregate current blockade of approximately 48%. The remaining TTX-insensitive current was consistent with expression of $Na_v1.5$, $Na_v1.8$, and $Na_v1.9$ isoforms. Functionally, the Na_v channel activator veratridine reduced time-dependent inactivation of Na_v currents and prolonged action potential duration, effects that translated to induction of phasic contractions in mouse CCSM strips, which were abolished by TTX (Lim *et al*., 2022b). Supporting molecular evidence demonstrated the presence of mRNA transcripts for all $Na_v1.1$-1.9 isoforms in CCSM tissue, and immunocytochemical localisation of $Na_v1.4$ and $Na_v1.5$ proteins in isolated CCSM cells (Lim *et al*., 2022b).

1.7.5 Large-conductance Ca^{2+}-activated K^+ (BK_{Ca}) channels

BK_{Ca} channels are tetrameric channels composed of four pore-forming α-subunits encoded for by the KCNMA1 (Slo1) gene. Channel gating kinetics, sensitivity to voltage and Ca^{2+}, and pharmacological properties are modulated via accessory, β_{1-4}- and γ_{1-4}-, subunits, but also by the newly recognised leucine-rich repeat containing single transmembrane subunits, $LINGO_{1-4}$, forming substantial variety across tissues (Dudem *et al*., 2020; 2021; 2023; Al Kawadri et al., 2025). BK_{Ca} channels display increased open probability in response to elevations in sub-plasmalemmal Ca^{2+} and membrane depolarisation. Conformational changes opening the pore permit K^+ efflux down the electrochemical gradient, inducing membrane hyperpolarisation (Horrigan and Aldrich, 2002).

Expression of KCNMA1 mRNA and BK_{Ca} α-subunit protein has been demonstrated in human CCSM and cultured CCSM cells (Andersson, 2011). Functional evidence supports a pivotal role in erectile physiology, in which KCNMA1 knockout ($Slo^{-/-}$) mice exhibit heightened contractile responses to PE and reduced relaxations to EFS. In vivo, these animals also display significant oscillations in intracavernosal pressure and attenuated EFS-evoked rises in intracavernosal pressure, indicative of impaired CCSM relaxation (Werner *et al.*, 2005).

Pharmacological activation of BK_{Ca} by GoSlo-SR5-130 inhibited spontaneous activity in rabbit CCSM, an effect reversed by iberiotoxin (BK_{Ca} blocker; Hannigan *et al.*, 2015). This activation of BK_{Ca} was found to be reliant on the presence of regulatory β-subunits, indicating a cellular modulation of channel activity (Large *et al.*, 2015). BK_{Ca} channel activity can be altered via cyclic nucleotide signalling, with phosphorylation sites for PKA and PKG present within the C-terminus (Zhou *et al.*, 2001). BK_{Ca} channels can be indirectly modulated by cGMP, via PKG-mediated disinhibition of SERCA, increasing SR Ca^{2+} uptake in CCSM (Joshi *et al.*, 2012). The resulting elevation of intraluminal SR Ca^{2+} augments the frequency and amplitude of Ca^{2+} sparks, which locally activate BK_{Ca} channels to promote membrane hyperpolarisation and smooth muscle relaxation (Jaggar *et al.*, 1998; Porter *et al.*, 1998; Wellman *et al.*, 2001).

Despite strong genetic and pharmacological evidence supporting a role for BK_{Ca} channels in regulating CCSM excitability, these channels cannot be considered the sole determinants of membrane hyperpolarisation. Notably, substantial outward K^+ currents persist in the presence of BK_{Ca} inhibition or genetic ablation, with studies suggesting that approximately 40-80% of the total current is iberiotoxin-insensitive (Malysz et al., 2001; Werner et al., 2005). Furthermore, the preservation of erectile responses and continued breeding capacity in $Slo^{-/-}$ mice indicates that NO-cGMP-PKG-mediated relaxation remains largely functional in the absence of BK_{Ca} channels (Meredith et al., 2004; Werner et al., 2005; 2008). Together, these findings suggest that BK_{Ca} channels represent an important, but not exclusive, component of the hyperpolarising mechanisms governing CCSM excitability.

1.7.6 ATP-sensitive K^+ (K_{ATP}) channels

K_{ATP} channels are members of the inwardly rectifying potassium (K_{ir}) channel superfamily. The channel pore is formed by $K_{ir}6.1$ or $K_{ir}6.2$ subunits and is surrounded by sulfonylurea receptor (SUR) regulatory subunits, which exist as three isoforms:

SUR1, SUR2A, and SUR2B (Babenko *et al*., 1998). Each SUR contains 17 transmembrane domains and two intracellular nucleotide-binding domains that bind MgATP/MgADP. Binding of MgATP/MgADP to SUR promotes channel opening, whereas ATP directly binds to $K_{ir}6$ to inhibit channel activity (Foster and Coetzee, 2016). Consequently, reduced cytosolic ATP and increased MgADP favour K_{ATP} channel opening, leading to K^+ efflux and membrane hyperpolarisation (Martin *et al*., 2013).

K_{ATP} channels serve to tether intracellular energy metabolism to membrane excitability across a range of tissues. In pancreatic β-cells, glucose-metabolism-stimulated increase in the ATP/ADP ratio inhibits $K_{ir}6.2$-containing channels, inducing membrane depolarisation and the voltage-dependent Ca^{2+} influx required for insulin secretion (Ashcroft and Rorsman, 2012). In cardiac muscle, K_{ATP} channels serve a protective mechanism in instances of metabolic stress or ischaemia, when ATP production is limited, via shortening the cardiac action potential duration to limit Ca^{2+} influx and preserve cellular ATP levels (Nichols, 2006; Flagg and Nichols, 2011). Lastly, in VSM, SUR2B-containing K_{ATP} channels serve a critical role in metabolic autoregulation. Increased metabolic demand or ischemic stress reduces the intracellular ATP/ADP ratio, relieving ATP-dependent inhibition of $K_{ir}6$ subunits while enhancing MgADP-mediated activation of SUR2B. This regulatory mechanism promotes channel opening, leading to K^+ efflux-mediated hyperpolarisation and inhibition of voltage-dependent Ca^{2+} influx. Reduced intracellular Ca^{2+} promotes smooth muscle relaxation, inducing vasodilatation and thereby matching regional blood flow to the metabolic requirements of the tissue (Quayle and Standen, 1994; Foster and Coetzee, 2016).

Human CCSM cells express mRNA for $K_{ir}6.1$, $K_{ir}6.2$, and SUR2B (Insuk *et al*., 2003). Outward K^+ currents induced by the K_{ATP} openers pinacidil and SIN-1 were inhibited by the selective K_{ATP} blocker glibenclamide (Lee *et al*., 1999; Insuk *et al*., 2003). Additionally, resveratrol produced a concentration-dependent relaxation of PE-contracted rat CCSM, which was attenuated by glibenclamide, tetraethylammonium (broad-spectrum K^+ channel blocker), and barium chloride (a K_{ir} channel blocker; Venkateswarlu *et al*., 2002). However, the physiological contribution of K_{ATP} channels to CCSM membrane potential remains uncertain. Electrophysiological studies report that K_{ATP}-sensitive currents are detected only in a minority of excised patches

(approximately 1 in 10; Insuk et al., 2003), suggesting either a low functional channel density or heterogeneous distribution across CCSM cells.

1.7.7 Voltage-dependent K^+ (K_v) channels

Voltage-dependent K^+ (K_v) channels comprise a large superfamily grouped into K_v1-K_v12 subfamilies and play a central role in contributing to membrane potential and excitability in smooth muscle cells. In CCSM, voltage-dependent outward K^+ currents have been identified under conditions of pharmacological BK_{Ca} inhibition in rabbit CCSM cells and following genetic ablation of BK_{Ca} channels in $Slo^{-/-}$ mice, indicating the presence of additional K_v-mediated hyperpolarising mechanisms (Malysz *et al.*, 2001; Werner *et al.*, 2005).

Electrophysiological studies demonstrate that CCSM cells can be separated into two phenotypes based on the presence or absence of a delayed rectifier K^+ current. This delayed rectifier current exhibits time-dependent inactivation, sensitivity to tetraethylammonium (TEA), and an activation threshold between -50 and -40 mV. This activation threshold lies closely to the proposed membrane potential of rabbit CCSM cells (Hashitani *et al*., 2005; Thornbury *et al*., 2019), positing the delayed rectifier K^+ current as a key determinant of the resting membrane potential (Malysz *et al*., 2002).

Pharmacological profiling implicates K_v2 as a key molecular contributor to this delayed rectifier current. The current is inhibited by 4-aminopyridine and Hanatoxin-1, with the latter being a relatively selective blocker of K_v2 channels; yet the current remains unaffected by α-dendrotoxin, which selectively blocks K_v1 channels. These data support the interpretation that K_v2 channels predominantly underlie the delayed rectifier K^+ current in CCSM (Malysz *et al*., 2002).

1.7.8 *KCNQ*-encoded voltage-dependent K^+ (K_v7) channels

The K_v7 (*KCNQ*) family comprises five isoforms, $K_v7.1$-$K_v7.5$, encoded by the *KCNQ*1-5 genes (Robbins, 2001; Gutman *et al.*, 2005). Functional K_v7 channels assemble as tetramers of α-subunits, with each subunit containing six transmembrane segments (S1-S6). The voltage-sensing domain (VSD) is formed by segments S1-S4, conferring voltage sensitivity upon the channel, while S5-S6 constitute the pore-forming domain (Barros *et al.*, 2012). Membrane depolarisation induces conformational movement of the VSD that promotes exposure and stabilisation of PIP_2 binding sites,

a critical requirement for initiating and stabilising pore opening (Mandala and MacKinnon, 2023).

K_v7 channels assemble as homomeric or heteromeric complexes of α-subunits, enabling diversification of functional properties. Notably, $K_v7.2/K_v7.3$ heteromers generate the neuronal M-current, which stabilises membrane potential and limits repetitive firing by maintaining a relatively hyperpolarised resting state (Marrion, 1997; Jentsch, 2000). More broadly, K_v7 channels are considered important contributors to the resting membrane potential of smooth muscle cells, as their voltage-activation thresholds overlap closely with physiological resting membrane potentials (Greenwood and Ohya, 2009).

K_v7 isoforms are widely expressed across multiple tissues and mammalian species and frequently associate with single-pass transmembrane auxiliary subunits encoded by the *KCNE*1-5 genes (Abbott and Goldstein, 1998; McCrossan and Abbott, 2004; Abbott, 2016; Jepps, 2017). These KCNE subunits exert powerful modulatory effects on K_v7 channels, altering voltage dependence, activation and inactivation kinetics, current amplitude, and membrane trafficking (McCrossan and Abbott, 2004).

In addition to auxiliary subunits, K_v7 channels are regulated by intracellular signalling pathways through protein interactions involving their cytoplasmic domains. The C-terminal region of K_v7 α-subunits contains binding sites for calmodulin (CaM) and signalling molecules including PKC, PKA, and AKAPs, enabling modulation by Ca^{2+}- and cyclic nucleotide-dependent pathways (Baresse *et al.*, 2018).

1.7.8.1 $K_v7.1$

The $K_v7.1$ α-subunits have been recognised to co-assemble with the KCNE1-encoded minimal potassium channel subunit (MinK), to form the slow delayed rectifier K^+ current (I_{ks}; Fig1.9; Barhanin *et al*., 1996; Sanguinetti *et al*., 1996). I_{ks} current plays a critical role during the repolarisation phase of the ventricular cardiac action potential, contributing to action-potential termination and protection against excessive prolongation (Carmeliet, 1992). Loss-of-function mutations in *KCNQ1* or *KCNE1* can result in protein subunit misfolding, disruption in membrane trafficking, and early deconvolution of the channel complex (Maljevic *et al*., 2010). Structural alterations affecting PIP_2 binding have also been shown to modify $K_v7.1$ channel opening kinetics and stability (Loussouarn *et al.*, 2003). Dysfunction of the $K_v7.1$-MinK complex underlies Long QT Syndrome (LQTS), in which delayed cardiac repolarisation

predisposes patients to ventricular arrhythmias, including torsades de pointes and sudden cardiac death (Maljevic *et al.*, 2010).

Outside the heart, K_v7.1-MinK channels fulfil essential epithelial transport functions. In the marginal cells of the stria vascularis within the inner ear (Fig1.9), K_v7.1-MinK mediates K^+ efflux necessary for generation of the potassium-rich endolymph that maintains cochlear electrochemical gradients (Wangemann, 2002). In the kidney, *Kcne1* knockout mice develop hypokalaemia, salt wasting, and volume depletion, reflecting impaired K_v7.1-dependent K^+ recycling in proximal renal tubules (Arrighi *et al.*, 2001; Vallon *et al.*, 2001; Warth and Barhanin, 2002). In the gastrointestinal tract, K_v7.1 associates with KCNE3 (MiRP2) in colonic crypt epithelial cells (Fig1.9), where the complex localises to the basolateral membrane and provides sustained K^+ efflux that maintains hyperpolarisation to drive continuous Cl^- secretion, essential for mucosal fluid homeostasis (Schroeder *et al.*, 2000; Preston *et al.*, 2010).

Recent work has expanded the KCNE family with identification of a sixth member, KCNE6, which has been functionally characterised in lower vertebrates, where it co-assembles with K_v7.1 to generate slowly activating K^+ currents resembling delayed rectifier currents (Kasuya *et al.*, 2024). However, KCNE6 is absent or pseudogenised in most placental mammals, and its physiological relevance to human K_v7.1 channel complexes remains uncertain (Kasuya *et al.*, 2024).

K_v7.1-MinK channel activity is dynamically regulated by cAMP-dependent signalling. β-adrenergic stimulation elevates intracellular cAMP levels, leading to PKA-dependent phosphorylation that enhances I_{ks} amplitude and accelerates repolarisation (Yazawa and Kameyama, 1990). This modulation is enabled by the scaffolding protein AKAP9 (Yotiao), which anchors PKA to the C-terminal domain of K_v7.1, facilitating phosphorylation of Ser27 on the N-terminus of the α-subunit and coordinating channel regulation (Walsh *et al.*, 1988; Walsh and Kass, 1991; Potet *et al.*, 2001; Marx *et al.*, 2002).

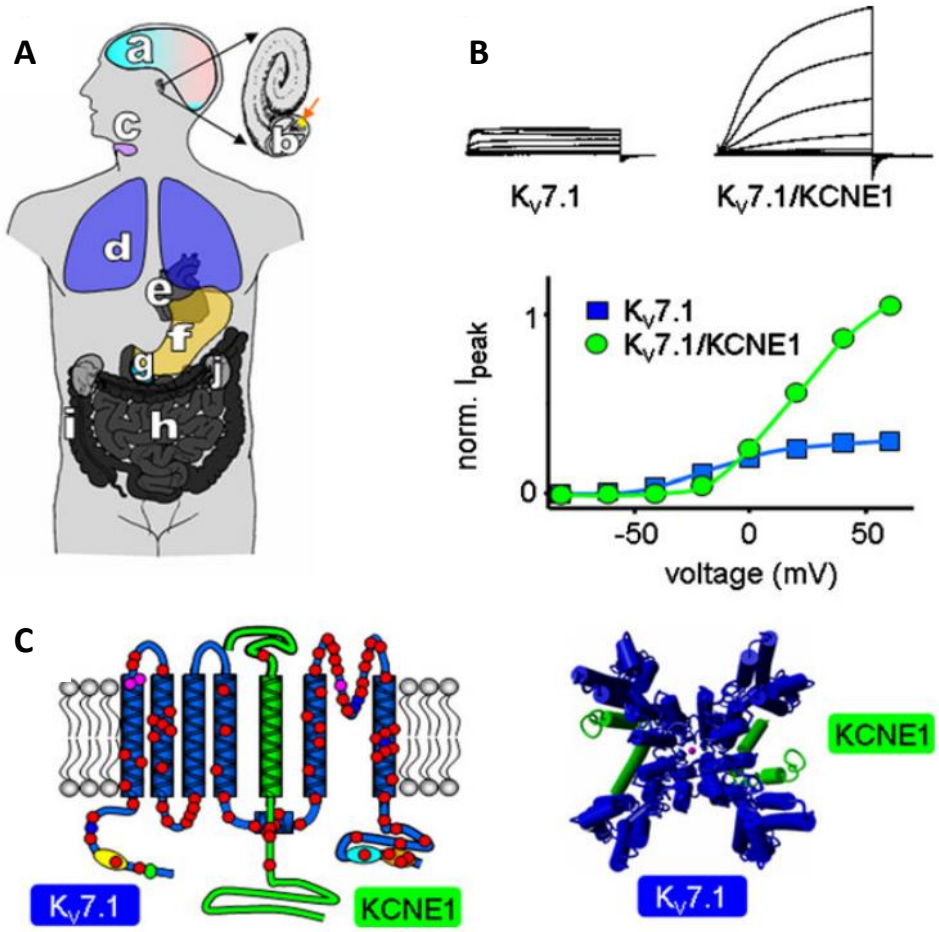


Figure 1.9. A. $K_V7.1$-MinK channels are expressed in the brain (a), stria vascularis (b), thyroid gland (c), lung (d), heart (e), stomach (f), pancreas (g), small intestine (h), colon (i), and kidney (j). **B.** $K_V7.1$ channels exert voltage-gated, rapidly activating, potassium-selective currents. Heteromeric $K_V7.1$-MinK channels activate much slower, show right-shifted activation curves, and have increased macroscopic currents compared with homomeric $K_V7.1$. **C.** $K_V7.1$ channels are formed by homo-tetrameric assemblies of $K_V7.1$ α-subunits which associate with possibly two KCNE β-subunits. The $K_V7.1$ N-terminus contains the PKA phosphorylation site Ser27 (green) and a basolateral targeting signal (yellow). The C terminus comprises the assembly domain (turquoise) and the AKAP binding site (leucine zipper motif, orange). Mutations in $K_V7.1$ and KCNE1 subunits can cause loss-of-function and long QT syndrome (red circle indicates positions of LQTS mutations). Top view on a hypothetical $K_V7.1$-MinK transmembrane region model (α-helical regions are shown as cylinders, $K_V7.1$ in blue, KCNE1 in green, potassium ion in magenta (Maljevic *et al*., 2010)

1.7.8.2 $K_v7.2$ and $K_v7.3$

$K_v7.2$ and $K_v7.3$ α-subunits are highly expressed throughout the nervous system and commonly co-assemble to generate the neuronal M-current, which stabilises the resting membrane potential and suppresses neuronal hyperexcitability (Brown and Adams, 1980; Wang *et al.*, 1998; Wickenden *et al.*, 2001; Roche *et al.*, 2002; Shah *et al.*, 2002). $K_v7.5$ can also heteromerise with $K_v7.3$, producing currents with biophysical properties closely resembling the classical M-current (Lerche *et al.*, 2000; Schroeder *et al.*, 2000; Tzingounis *et al.*, 2010).

Loss-of-function mutations in *Kcnq*2 or *Kcnq*3 reduce channel co-assembly and outward K^+ current density, resulting in membrane depolarisation and excessive neuronal firing that presents clinically as benign familial neonatal seizures (BFNS; Maljevic *et al.*, 2010). Pathogenic mutations in *Kcnq*2 alone have also been linked to peripheral nerve hyperexcitability syndromes, clinically manifesting as myokymia, fasciculations, and muscle cramps (Hart *et al.*, 2002). Mechanistically, some *Kcnq*2 mutations impair voltage sensing by shifting activation toward more positive membrane potentials, thereby off-setting the number of channels active at resting membrane potential (Wuttke *et al.*, 2007).

$K_v7.2/3$ channels are subject to dynamic regulation by cyclic nucleotide signalling. PKA activation enhances $K_v7.2$-containing channel activity via phosphorylation of Ser52 on the N-terminal domain, augmenting M-current amplitude (Schroeder *et al.*, 1998). In addition, AKAPs regulate channel modulation; specifically, AKAP79/150 is required for PKC-mediated phosphorylation of $K_v7.2$ and consequent current suppression (Hoshi *et al.*, 2003; Higashida *et al.*, 2005; Zhang and Shapiro, 2012). AKAP79/150 has been shown to bind directly to $K_v7.2$, although whether this scaffold also facilitates PKA-dependent phosphorylation remains unresolved (Hoshi *et al.*, 2003; Hoshi *et al.*, 2005; Zhang and Shapiro, 2012).

1.7.8.2 $K_v7.4$ and $K_v7.5$

*KCNQ*4 encodes the $K_v7.4$ α-subunit, which is prominently expressed in outer hair cells of the inner ear, where it forms homomeric channels or heteromers with $K_v7.3$ to generate an M-like current that stabilises membrane potential during sound amplification (Kubisch *et al.*, 1999). Pathogenic mutations in *Kcnq*4 are associated with progressive hearing loss, attributable to impaired K^+ efflux from outer hair cells leading to sustained depolarisation and defective mechanoelectrical amplification (Kharkovets

et al., 2006). K_v7.4 has also been implicated in skeletal muscle, where it contributes to regulation of proliferation and cellular differentiation and may influence drug metabolism within the sarcolemmal membrane (Iannotti *et al.*, 2010).

Collectively, K_v7.4 and K_v7.5 are the principal K_v7 isoforms expressed in smooth muscle cells (Barrese *et al.*, 2018). These subunits form functional homomeric or heteromeric channels, as demonstrated in multiple VSM preparations (Brueggemann *et al.*, 2011; Brueggemann *et al.*, 2014a; Chadha *et al.*, 2012; Jepps *et al.*, 2015). Functional studies employing siRNA-mediated knockdown of *Kcnq*4, morpholino suppression of K_v7 isoforms, and pharmacological inhibition using linopirdine have established that K_v7 channels contribute to β-adrenoceptor-mediated vasorelaxation, as inhibition markedly attenuates isoprenaline-induced relaxation of VSM (Chadha *et al.*, 2012). Furthermore, arterial relaxations triggered by cGMP-elevating agents, including atrial natriuretic peptide and sodium nitroprusside (SNP), are significantly reduced following K_v7 blockade (Stott *et al.*, 2015a).

Within the CCSM, transcriptional expression of *Kcnq*4/*KCNQ4* and *Kcnq*5/*KCNQ5* has been confirmed, and corresponding proteins detected via immunocytochemistry in both human and rat CCSM as well as rat penile arteries (Jepps *et al.*, 2016; Lee *et al.*, 2020a). Pharmacological activation of K_v7 channels with ML213 or BMS-204352 induced robust relaxation of pre-contracted CCSM preparations in an endothelium-independent fashion (Jepps *et al.*, 2016; Lee *et al.*, 2020a). Moreover, the relaxation mediated by cGMP-enhancing agents, including sildenafil and SNP, was reduced by the K_v7 inhibitor linopirdine, demonstrating a functional role for K_v7 channels downstream of cyclic nucleotide signalling (Jepps *et al.*, 2016). Reduced expression of *Kcnq*4/5 was observed in experimental models of ED, including spontaneously hypertensive heart-failure-prone rats and diabetic rats, supporting a pathogenic link between K_v7 channel downregulation and impaired erectile function (Jepps *et al.*, 2016; Lee *et al.*, 2020a).

K_v7 channels may act as downstream effectors of cAMP signalling in smooth muscle. Isoprenaline increases K_v7 currents in rat VSM and A7r5 cells (Chadha *et al.*, 2012; Stott *et al.*, 2015a; Mani *et al.*, 2016; Brueggemann *et al.*, 2018), and β-adrenoceptor-mediated relaxations in renal arteries are attenuated by PKA inhibition. Additionally, direct activation of EPAC enhances K_v7 currents in renal and mesenteric arteries, implicating both PKA- and EPAC-dependent pathways in K_v7 regulation (Stott *et al.*, 2016). In airway smooth muscle, β_2-adrenoceptor stimulation increases K_v7

activity, an effect attributed to PKA-mediated phosphorylation of Ser53 on the K_v7.5 N-terminus, which enhances PIP_2 affinity and channel opening (Brueggemann *et al.*, 2018; Brueggemann *et al.*, 2020).

The influence of KCNE auxiliary subunits on K_v7.4/5 channel complexes in smooth muscle remains poorly defined. In HEK-293 cells expressing K_v7.4/5, co-expression of KCNE4 attenuated responses to the K_v7.4-selective agonist URO-K10, suggesting a potential inhibitory regulatory interaction (Lee *et al.*, 2020b). On the contrary, *Kcne4* expression in diabetic rat tissue decreased, indicating a protective role of KCNE4 in erectile function (Lee *et al.*, 2020a).

Beyond auxiliary subunits, G-protein βγ subunits released during GPCR activation directly bind to K_v7.4 channels, increasing current amplitude in cultured cells and isolated rat renal artery smooth muscle (Stott *et al.*, 2015b). K_v7 channel trafficking also contributes to functional regulation, in which microtubule network-dependent delivery of K_v7.4/5 α-subunits to the plasma membrane enhances channel availability during cAMP-mediated relaxation. Disruption of the microtubule network increases surface expression of K_v7.4, leading to membrane hyperpolarisation and relaxation during isoprenaline or forskolin (FK) treatment, effects that are abolished by the K_v7 inhibitor XE-991 (Lindman *et al.*, 2018).

1.8 Aims

Despite extensive characterisation of the penile erection, the ionic mechanisms underlying CCSM relaxation remain unresolved. Despite the well-characterised nature of inward currents in rabbit CCSM, their contribution is more unclear in mouse CCSM. Furthermore, the relatively depolarised resting membrane potential of rabbit CCSM, suggests K_v7 channels, with their hyperpolarised voltage activation range may strongly contribute to the resting membrane potential of CCSM cells. Although studies in rat CCSM report modest functional effects of K_v7 modulators, evidence of *Kcnq*4/5 downregulation in pathological models ED supports their physiological relevance. However, the functional role of K_v7 channels in mouse CCSM remains undefined. In addition, the Ca^{2+} influx and intracellular Ca^{2+} release pathways that underlie phasic and tonic contractions in mouse CCSM, and their relationship to K_v7-dependent regulation of membrane excitability, have not been clearly established.

In parallel, the NO-cGMP-PKG pathway is well characterised and therapeutically exploited, the use of Alprostadil, to increase intracellular cAMP, as a second-line

therapy for PDE5I non-responders, suggests the conservation of cAMP pathways in severe ED. Historically, cAMP signalling in CCSM has been attributed almost exclusively to PKA, with little consideration of EPAC, despite its established role in regulating smooth muscle function in other tissues. Importantly, both PKA and EPAC have been shown to modulate ion channel activity, including K_v7 channels, yet cAMP-dependent regulation of K_v7 channels has not been explored in mouse CCSM.

Collectively, these gaps point to a missing mechanistic framework linking cyclic nucleotide signalling, membrane excitability and Ca^{2+} signalling in CCSM. Elucidating the contribution of K_v7 channels, and their potential regulation by PKA- and EPAC-dependent pathways, is therefore essential for understanding the control of CCSM contractility. Such insights may reveal novel therapeutic targets for ED that operate independently of the canonical NO-cGMP-PKG pathway.

The objectives of the present study were:

1. To define the Ca^{2+} influx and intracellular Ca^{2+} release pathways underlying phasic and tonic contractions.
2. To investigate the role of K_v7 channels in mouse CCSM.
3. To elucidate the effects of PKA- and EPAC-signalling in mouse CCSM, and whether they interact with K_v7 channels

2. Materials and Methods

2.1 Tissue preparation

C57BL/6 mice aged between 12 and 18 weeks old were euthanised via intraperitoneal injection of sodium pentobarbital. This was carried out in accordance with EU Directive 2010/63/EU and approved by the Dundalk Institute of Technology Animal Care and Use Committee.

The mouse pelvis was extracted by cutting the sacrum and lateral aspect of the ischia, then mounted in a Sylgard base petri dish (9 cm diameter) containing fresh Krebs' (Solution 1). Surrounding fat, connective tissues, penile bulb, and pelvic viscera were excised, allowing a finer dissection of the corpus cavernosum. The crura of the corpus cavernosum were dissected from the anterior aspect of the pubic rami. The excised crura were pinned down and washed with fresh Krebs' solution. The ischiocavernosus skeletal muscle was delicately trimmed away from the tunica albuginea. The proximal aspect of the crura (pubic insertion) were trimmed to expose the circumference of the tunica albuginea. The distal crura were dissected from the remainder of the mouse penis prior to the bifurcation (Fig2.1).

2.2 Isometric tension recording

CCSM crura were hooked at each opening; both the proximal (attachment to pubic ramus) and distal (connection to penis body) openings were hooked obliquely with an 'S-shaped' insect pin transversely through the tunica albuginea. The distal opening pin was attached to 20 cm of nylon string. The string was tied to the transducer mount, and the proximal pin was secured on the lower triangular hook of the tissue holder. CCSM crura were mounted between electrical field stimulation (EFS) electrodes in a 20 mL organ bath containing Krebs' solution and maintained at 37^{o}C using an electrically built-in heated air circulation while being bubbled with a 95% O_2 and 5% CO_2 gas mixture throughout the experiments (Fig2.2). CCSM crura were adjusted to 5 mN of tension and allowed to equilibrate for 40 minutes.

Drugs were added to the organ bath containing Krebs' solution (20 mL) from a stock solution to achieve the desired final concentration ($C_1V_1 = C_2V_2$). Krebs' solution was drained via a suction pump, and fresh Krebs' solution was washed in using pressurised suction bottles.

CCSM developed spontaneous and agonist-induced phasic contractions, defined as a transient increase and decline in amplitude (>0.1 mN), recorded using the Danish Myo Technology (DMT) Tissue Organ Bath System (TOBS) 750 model,

containing an integrated transducer calibrated daily with a 5 g weight and a force resolution of 0.1 mN. This transducer converts transducer force into an amplified analogue signal with a voltage proportional to the force applied to the transducer. This analogue signal was converted to a digital signal via a LabTrax 4/16 Channel Data Acquisition A/D converter (World Precision Instruments, Europe). Data recording utilised Data-Trax 2 software (World Precision Instruments, Europe) on a PC.

2.3 Isolation of corpus cavernosum smooth muscle (CCSM) cells

CCSM crura were chopped up into 1 mm^3 pieces and placed in a 5 mL test tube with an accompanying stir bar. The enzymatic dispersal was initiated with the addition of a 4 mL enzyme mix consisting of 15 mg collagenase (Sigma, Type 1A), 10 mg bovine serum albumin (Sigma, heat shock fraction), and 10 mg Trypsin inhibitor (Sigma, from Glycine max soybean), all dissolved in Ca^{2+} free Hanks' (Solution 2). The tube was incubated at 37 ^oC via a water bath, and enzymatic digestion proceeded for 3 minutes. Following this, 1 mL of 1 mg proteinase (Sigma, XXIV) was dissolved in Ca^{2+} free Hanks', and the combined 5 mL of enzyme mix and CCSM tissue was triturated with a glass Pasteur pipette. Incubation continued for a further 2 minutes (observed every 30 seconds under the microscope), before centrifugation for 30 seconds at 1000 RPM (Clifton 010 series). The CCSM tissue formed a white pellet, with a discoloured supernatant, this was discarded and washed carefully with room-temperature Ca^{2+} free Hanks' solution five times, taking care not to disturb the pellet. The tissue pieces were re-suspended in Ca^{2+} free Hanks' solution at 37^oC for 10 minutes. 1 mL of solution containing dispersed cells was placed on a 35 mm x 10 mm WillCo-dish® glass bottom dish with Ca^{2+} solution added to a concentration of 100 µM and stored in the fridge at 4^oC. Dishes were removed and placed at room temperature for 30 minutes prior to use.

2.4 Total RNA extraction

CCSM crura were placed in Eppendorf tubes containing 1 mL of TRIZOL reagent prior to extraction. During extraction, tissue was homogenised via flash freezing in liquid nitrogen and ground into a powder using a cold pestle and mortar. The tissue was transferred into a ribonuclease (RNase)-free Eppendorf tube containing 1 mL of TRIZOL reagent. The CCSM homogenate was triturated within TRIZOL reagent using 18- and 21-gauge needles to disrupt the cell membranes. The sample was incubated at room temperature for 5 minutes. Subsequently, 200 µL of chloroform

was added to initiate aqueous and organic liquid separation, and the sample was vortexed for 15 seconds before being left at room temperature for 3 minutes, prior to centrifugation at 14500 RPM for 15 minutes in a cold room. This separated the sample into three distinct layers: an upper clear aqueous layer (containing RNA), an occluded interlayer, and a lower red phenol-chloroform layer. The supernatant clear aqueous layer was transferred into a sterile Eppendorf tube using a micropipette, taking care not to disturb the interlayer. 500 µL of isopropanol was added to precipitate RNA, and the sample was vortexed for 15 seconds before incubating at room temperature for 10 minutes, prior to centrifugation for 10 minutes in the cold room. This separation formed a pellet at the bottom of the Eppendorf tube and a supernatant liquid, which was discarded, leaving a pellet, which was washed with 1 mL of 75% ethanol. This addition was followed by vortexing and centrifuging for 5 minutes in the cold room. Lastly, the supernatant was removed, and the pellet was allowed to air dry for 5 minutes prior to suspension in 25 µL of RNase-free water.

RNA samples were treated with deoxyribonuclease (DNase) to remove possible DNA contamination. 1 µL of DNase 1 (Invitrogen) was added per 10 µL of RNA suspension and incubated at room temperature for 15 minutes. The reaction was stopped with EGTA and heated at 65^{o}C for 10 minutes. The purity and abundance of RNA were quantified via absorbance using a NanoDrop spectrophotometer. Nucleic acids and proteins absorb ultraviolet light at 260 nm and 280 nm, respectively. Absorbance at the 230 nm wavelength is the result of salt contamination. To guarantee the purity of the RNA sample, the A260/A280 ratio was targeted between 1.8 and 2.0 and the A260/A230 ratio between 2.0 and 2.2. Pure RNA was stored at -80^{o}C for future use.

2.5 Complementary DNA (cDNA) synthesis

Reverse transcriptase is an enzyme that synthesises complementary DNA (cDNA) from RNA. The RNA isolate from CCSM crura was synthesised into cDNA using the SuperScript^{TM} II RNase-H reverse transcriptase kit (Invitrogen), and all incubations were facilitated using a Techne TC-512 thermal cycler. The reaction was initiated with the addition of 50 ng/uL of random hexamers used to reverse-transcribe 1 ug of RNA with the addition of a deoxyribonucleotide triphosphate (dNTP) mix (10 mM). The mixture was added to a nuclease-free microcentrifuge tube and heated at 65^{o}C for 5 minutes, followed by a 2-minute chill on ice. The contents were collected by centrifugation, followed by the addition of 4 µL of 5x First-Strand Buffer and 2 µL of 0.1

M dithiothreitol (DTT). The contents of the tube were mixed gently by trituration and incubated at 25°C for 2 minutes. Following, 1 µL of SuperScript II RNase-H Reverse Transcriptase (Invitrogen) was added and mixed by gentle trituration. The mixture was incubated at 25°C for 10 minutes, followed by 42°C for 50 minutes, and finished with heating to 70°C for 15 minutes. All cDNA samples were stored at -20°C for future use.

2.6 Reverse transcriptase-polymerase chain reaction (RT-PCR)

Synthesised cDNA from CCSM crura was used to commence PCR of the gene of interest. If the target gene of interest is within the cDNA sample, the PCR protocol is able to amplify the sequence to form millions of copies over many cycles. The sequence begins with denaturation (to separate the double-stranded cDNA) at high temperatures, followed by annealing of forward and reverse primers to cDNA strands, and finally, an extension phase of the new DNA strand. The process of PCR requires *Taq* polymerase, a thermostable DNA polymerase able to synthesise cDNA strands from an existing template. A commercially popular mastermix was employed for the PCR in this study: Amplitaq Gold PCR Mastermix (Applied Biosystems), containing all reagents, including buffer containing Mg^{2+} (the co-factor for DNA polymerase) and dNTPs. The PCR reaction mixture utilised was as follows:

12.5 µL Amplitaq Gold PCR Mastermix

8.5 µL DNase-free water

1 µL forward primers

1 µL reverse primers

2 µL cDNA or 2 µL of DNase-free water (for non-template controls, NTCs)

The sequence of forward and reverse primers for genes of interest are listed in Table 1:

Primer	Genbank ID/ Ref	Sequence (5’ to 3’)	Amplicon size (bp)
Rapgef3 F	NM_001177810.1	CCTGCCCCATAAAGTACGGA	211
Rapgef3 R	(*Rapgef3*)	CATCATCCGCATCTTCTCAAAG	
Rapgef4 F	NM_001204165.1	TGGATAAAAGGCCGTTGGAG	287
Rapgef4 R	(*Rapgef4*)	TCCAAAGGCTGTCCCAATTC	
*Kcnq*1 F	NM_008434.2	AGCACACCCCATTTCTTGAG	274
*Kcnq*1 R	(*Kcnq*1)	ACTGATCCAGCCTTCTCTGT	
*Kcnq*2 F	NM_010611.3	CGGCAGAATTCAGAAGAAGCA	211
*Kcnq*2 R	(*Kcnq*2)	CCGAGTACTGTTCGATGACG	
*Kcnq*3 F	NM_152923.2	CCAGCAGTCTCCAAGGAATG	204
*Kcnq*3 R	(*Kcnq*3)	GCCCCCTTAGTTGGGTAGTA	
*Kcnq*4 F	NM_001081142.2	CGATCACACTGACGACCATT	216
*Kcnq*4 R	(*Kcnq*4)	ACGCAGCCTGGATGAGATTA	
*Kcnq*5 F	NM_001160139.1	TCTTGGCTCAGGTTTTGCAT	193
*Kcnq*5 R	(*Kcnq*5)	CTTCTGATTGGTAGGGCTGC	
β-Actin F	NM_007393.3	CTAGGCACCAGGGTGTG	205
β-Actin R	(*Actb*)	GTGAGCAGCACAGGGT	

Table 1. Primer sequences (5’ to 3’) and amplicon sizes used for RT-PCR and qPCR.

RT-PCR was carried out in a Techne TC-512 thermal cycler pre-programmed to the setting listed in Table 2:

Step	Temperature (°C)	Time (min)
Denaturation	95	5
40 cycles of:		
1) Denaturation	95	0.5
2) Annealing*	56	1
3) Extensions	72	1
Final Extension	72	7

Table 2. Thermal cycling protocol for a standard PCR reaction. * Annealing temperature varied based on the melting temperature (T_M) of forward and reverse primers.

2.7 Agarose gel electrophoresis and imaging

To analyse the results of RT-PCR, gel electrophoresis was utilised based on its functionality of being able to distinguish components of a nucleic acid sample based on amplicon size (bp). In this case, agarose gel was used, as it forms a porous matrix when solid at room temperature. In this matrix, PCR-amplified genetic samples are able to move across the matrix from cathode to anode in an electric field. The migration speed is indicative of the amplicon size of DNA fragments inside the PCR sample. The smaller fragments migrate farther than the larger fragments within the same time, and therefore, we can identify DNA fragments in PCR samples.

Agarose gel (2%) was prepared via a combination of Ultra-Pure agarose powder (Invitrogen; 2.0 g) and Tris-Acetic Acid-EDTA (TAE; Sigma; 1X; 100 mL) buffer. The mixture was heated until bubbling, between which were multiple sessions of swirling. It was then allowed to cool at room temperature until approximately 55°C. After cooling, a SYBR-Safe DNA gel stain (Invitrogen; 1X; 5 µL) was added, allowing visualisation of a PCR-amplified genetic sample under excitation by UV light. The mixture was moulded in an electrophoresis-casting tray with a comb inserted at one end to allow the application of samples. The mixture was left to solidify for 30 minutes, at which point the comb was removed and the gel was submerged in an electrophoresis chamber filled with TAE (1X) buffer connected to a power supply. The gel was oriented so the sample loading wells were closer to the cathode.

Each PCR product (10 µL) was mixed with DNA loading buffer (2 µL) before being pipetted into the respective loading wells. The DNA ladder (Thermo Scientific; 100 bp; 3 µL) was loaded in a single well with 2 µL DNA loading dye, and the residual volume was made up to 12 µL with 7 µL TAE (1X) buffer to serve as an amplicon size reference. After all samples were loaded, gel electrophoresis was initiated at 80 V for approximately 90 minutes. After which, the gel was removed and placed inside an INGENIUS gel documentation system (Syngene Bio Imaging), in which UV light (312 nm) allowed visualisation of bands, indicative of the migration of DNA fragments from PCR-amplified cDNA samples across the gel. Gel images were captured and annotated for use as figures.

2.8 Real time quantitative PCR (qPCR)

Real-time quantitative PCR (qPCR) is a molecular technique used to quantify the amplification of a DNA sequence using a fluorescent reporter dye, in which the fluorescent signal is directly proportional to the quantity of accumulating PCR amplicons produced during repeated PCR reactions in real time. In this case, SYBR Green was used as the nucleic acid stain for qPCR. SYBR Green Master Mix (Applied Biosystems) contains a fluorescent dye that binds to double-stranded DNA, enabling the amplification of the target DNA sequence. The dye absorbs light at 488 nm and emits light at 522 nm when a dye-DNA complex is formed.

The PCR protocol was carried out using a Techne-Quantica real-time thermal cycler, running the PCR protocol listed in Table 2. During each amplification, the intensity of the emitted light was recorded by Quansoft software, allowing measurements of amplification in real time. All samples were performed in triplicate, including NTCs. Each gene under investigation and their subsequent standard curve were compared to β-actin, a conserved cytosolic structural protein, as a housekeeping gene.

In this study, primer sets with a percentage efficiency value between 90% and 110% were used for qPCR analysis. The determination of primer efficiency involved the preparation of serial dilutions of mouse brain cDNA at 1:3, 1:10, 1:30, and 1:100 concentration ratios. These respective cDNA dilutions were then used as templates to run a qPCR analysis to obtain the respective cycle threshold (Ct) values. These values were used to construct a standard curve, which was then used to calculate the percentage efficiency of a primer set. The equation used was listed below:

$$\text{Efficiency}\,(\%) \;=\; (10^{\frac{-1}{\text{slope}}} - 1) \;\times\; 100$$

Melting curve analysis was also performed after the qPCR reaction, in which the temperature was ramped from 70°C to 90°C to denature double-stranded DNA. A single peak indicated that only one PCR product had been amplified during the qPCR process.

2.9 Single cell intracellular Ca^{+} imaging

Isolated CCSM cells were dispersed as previously described (section 2.3) and loaded with the Ca^{2+} indicator dye, Fluo-4-AM (Molecular Probes). The WillCo-dish® containing cell dispersal solution, 2 mL, was mounted on the stage of a Nikon Eclipse T*i* microscope, and cells were allowed to stick to the bottom of the dish for 30 minutes. Fluo-4-AM at a concentration of 0.4 μM was added to the cell dispersal solution and incubated for 5 minutes in a dark environment. The Fluo-4-AM was washed out with a persistent perfusion of Hanks' (Solution 3) maintained at 37°C with a glass heat exchanger. The perfusion system was custom-built using an array of 20 mL syringes acting as drug reservoirs, each fitted with a three-way tap to control drug delivery. The drug reservoirs were placed ascendant to the glass bottom dish, allowing drug perfusion to operate via gravity through a 1 mL syringe via polyurethane tubing of equal length and sealed with silicon-based sealant (Fig2.3). A glass micropipette tip (tip diameter = 200 μm) was connected to the 1 mL syringe and manoeuvred approximately 300 μm from the cell of interest. A perfusion tip further away may induce time delays in drug effects, and a tip too close may result in pressure artifacts. To prevent perfusion artefacts, the cell was perfused with Hanks' solution, and the three-way tap of the drug reservoir was turned on at the same time as Hanks' reservoir was turned off.

Ca^{2+} events in CCSM cells were captured using a confocal microscope. Confocal microscopy excludes light not present in the focal plane. This exclusion is achieved through the maximal focus of light rays onto the tissue specimen by an objective lens through a series of pinhole apertures, invoked by a Nipkow spinning disc. The returning light rays pass through a detector pinhole disc and are collected by a photomultiplier or charge-coupled device, transducing the light rays into an electrical signal. Detector pinholes are situated confocal to the source pinhole, at which point returning light rays come into focus, improving the resolution of the specimen. An illustration of this principle is shown in Figure 2.4.

A krypton-argon laser (Melles Griot, UK) was used to excite the Fluo-4-AM dye at 488 nm, and the resulting fluorescent emissions were detected at wavelengths >510 nm. The fluorescent light rays emitted from the specimen returned through the objective lens and Nipkow spinning disc were reflected using a dichroic mirror to the imaging point. An electron multiplying charge coupled device (EMCCD) camera, the Andor iXon 887 (Andor Technology Belfast, UK, 512 x 512 pixels, pixel size 16 x 16 μm), was coupled to a dual Nipkow spinning disc (CSU22, Yokogawa, Electric Corporation, Tokyo, Japan) to image CCSM cells (Fig2.5). Experiments on intracellular Ca^{2+} events of CCSM cells were operated using a x60 objective lens (Nikon Plan Apo VC, 1.4/NA) and utilised a 15 frames per second (FPS) rate to capture images (pixel size 0.266 x 0.266 μm). An illustration of the confocal imaging setup used for single-cell intracellular Ca^{2+} imaging is shown in Figure 2.5.

The acquisition of image recordings from the EMCCD camera was captured using Andor IQ software (Andor, Belfast). Files were saved as a stack of tagged image file format (TIFF) images. ImageJ software (version 1.53t, National Institute of Health, MD, USA) was utilised for analysis of TIFF stacks. Firstly, the subtraction of background fluorescence was achieved by subtraction of the mean fluorescence of a null frame throughout the stack to obtain ‘F’. A pseudo-linescan was drawn with a freeform line corresponding to the length of the CCSM cell and using the 'reslice' function in ImageJ. The linescan is oriented to rotate 90° and align the linescan so that the x axis corresponds to time (s) and the y axis corresponds to length of cell (μm). The intensity of the spatiotemporal map was altered so that high-intensity Ca^{2+} signals were represented with warm colours (red, orange, and yellow) and low-intensity with cold colours (black, purple, and blue). To obtain normalised data on the intensity of fluorescent events, the mean value of a null area is taken (F_0), and using the ‘divide’ option, the entire spatiotemporal map is divided by F_0. Each Ca^{2+} signal is subsequently represented as F/F_0. An intensity plot was generated form the entire spatiotemporal map showing F/F_0 values against time. From this intensity plot, frequency was acquired by the enumeration of Ca^{2+} oscillations within a specified period, and amplitude was calculated by the change in fluorescent signal from basal to peak, known as $\Delta F/F_0$. The threshold for detecting Ca^{2+} oscillations was set at ≥10% of the maximal $\Delta F/F_0$ within each trace when a large transient was present; in the absence of a large transient, an absolute threshold of $\Delta F/F_0 \geq 0.1$ was applied.

2.10 Cell culture

Human embryonic kidney (HEK) cells are widely used as host systems for heterologous expression of recombinant proteins due to their mammalian origin and capacity for post-translational modifications, enabling proper protein folding and biological function (Baldi *et al*., 2007). HEK-293 cells were maintained in a mixed medium of Dulbecco's Modified Eagle Medium (DMEM, Gibco) and Minimum Essential Medium (MEM, Gibco) supplemented with 10% foetal bovine serum (FBS, Gibco) and 1% penicillin-streptomycin (Gibco). Cultures were incubated at 37°C in a humidified atmosphere containing 5% CO_2. Subculturing was performed by rinsing confluent cultures with sterile 1xPBS followed by enzymatic detachment using 0.05% Trypsin-EDTA (Gibco) for 2-3 minutes.

For long-term storage, HEK-293 cells were cryopreserved by combining an equal volume of cell suspension with freezing medium containing 10% dimethyl sulfoxide (DMSO), followed by controlled cooling at -80°C for 30 minutes before transfer to liquid nitrogen. For recovery, vials were rapidly thawed in a 37°C water bath and the contents transferred to 5 mL of pre-warmed growth medium in a 15 mL falcon tube. Cells were centrifuged at 2000 rpm for 3 minutes to remove DMSO, resuspended in 5 mL of growth medium, and cultured in T25 flasks under standard conditions to promote growth.

HEK-293 cells were cultured in 100 mm dishes to near confluence (8-10 $x10^6$ cells). Following trypsinisation, cells were resuspended in 9 mL of fresh growth medium and seeded into 35 mm dishes containing 2 mL medium per dish at a density of 1 $x10^5$ cells per dish. After 18-24 h, cultures reached approximately 40-50% confluence (4 $x10^5$ cells), at which point plasmid transfections were performed.

2.11 Transfection

HEK-293 cells were transfected with the plasmid cDNA for human $K_V7.5$, with and without $\alpha_{1A}R$ plasmid cDNA. The $K_V7.5$ plasmid was kindly supplied as gifts from Prof Søren Peter Olesen, University of Copenhagen, Denmark, while the $\alpha_{1A}R$ plasmid (pRP[Exp]-eGFP-CAG>mAdra1a[NM_001422092.1]) was designed and synthesised by VectorBuilder and contained an eGFP reporter to facilitate identification of transfected cells.

$K_V7.5$ and/or $\alpha_{1A}R$ plasmid DNA was diluted in 100 µL serum-free medium. In parallel, Lipofectamine reagent (0.3 µL per 100 ng DNA) was diluted in 100 µL serum-

free medium (Fig2.6). The solutions were combined and incubated for 20 minutes at room temperature to allow complex formation. Culture medium was replaced with serum- and antibiotic-free medium prior to transfection, and 200 µL of the plasmid DNA-Lipofectamine mixture was added dropwise to each dish. After 3 hours, transfection was terminated by replacing the medium with fresh complete growth medium.

2.12 Electrophysiology

HEK-293 cells transfected with $K_v7.5$ and/or $\alpha_{1A}R$ were used for electrophysiological recordings using the whole-cell patch-clamp technique at room temperature, as described by Zavaritskaya *et al*. (2020). Voltage-clamp mode was employed to control membrane potential and measure ionic currents elicited by defined voltage steps.

Voltage-clamp recordings were carried out using a glass patch pipette containing a chlorided silver wire electrode and filled with whole-cell K^+ solution (solution 4). Patch pipettes were pulled from borosilicate glass capillaries (Havard Apparatus, UK) with an outer diameter of 1.5 mm and an inner diameter of 1.17 mm, using a Flaming/Brown micropipette puller (model-P97, Sutter Instruments, CA, USA). Pipette tips were around 1-2 µm in diameter. New glass pipettes were used for each experiment. A similar silver electrode was present in the bath which acted as an earth electrode.

The bath was continuously perfused with Hanks' solution (solution 3). In addition, the recorded cell was locally superfused using a custom-built gravity-fed system enabling rapid drug application or solution exchange. Multiple 20 mL syringe reservoirs were connected via polyurethane tubing to a 1 mL syringe sealed with silicone to prevent backflow. The outlet consisted of a glass pipette (200-300 µm tip diameter) positioned approximately 100 µm from the cell using a micromanipulator. Flow from individual reservoirs was controlled via three-way taps. Solution changes were performed by activating the new reservoir before deactivating the previous one to minimise mechanical artefacts.

Using a micromanipulator, the patch pipette was positioned adjacent to the target HEK-293 cell and gentle suction (~0.1 mL) was applied via a 1 mL syringe to form a gigaseal (≥10 GΩ), electrically isolating the membrane patch from the extracellular solution. Subsequent stronger suction (~0.5 mL) ruptured the membrane,

establishing the whole-cell configuration and enabling electrical access to the cell interior.

2.12.1 Patch-clamp recordings

Voltage-clamp commands were delivered using an Axopatch 1D patch-clamp amplifier (Molecular Devices, Sunnyvale, CA, USA), with the patch pipette connected to the inverting (–) input and the command potential (V_{com}) applied to the non-inverting (+) input. A high-gain feedback resistor enabled continuous comparison of the pipette potential (V_p) with V_{com}; any deviation generated a compensatory feedback current injected through the pipette to clamp V_p to V_{com}. This feedback current, equal and opposite to the net transmembrane ionic current, which formed the measured whole-cell current. Data acquisition and protocol control were performed via a Digidata 1440A AD/DA converter (Molecular Devices) interfaced to a Dell PC running Clampex 10.2 software (Molecular Devices). Signals were sampled at 100 kHz and low-pass filtered at 1 kHz by the amplifier. A HumBug noise-elimination device (Quest Scientific) was placed between the amplifier and the converter to remove 50/60 Hz mains interference and harmonics by real-time reconstruction and subtraction of the noise waveform, without altering the frequency characteristics of the physiological signal. Leak currents were subtracted offline using Clampfit 11.4.1 software (Molecular Devices). Experiments routinely did not use series resistance compensation, as voltage errors were estimated to be less than 15 mV (see section 2.12.3).

2.12.2 Pipette resistance

The electrical activity of cells arises from the movement of ions across the plasma membrane through selective ion channels, as the lipid bilayer itself is effectively impermeable to ions. Ionic flux constitutes an electrical current (I), which is driven by the electrochemical gradient. Voltage (V, mV) represents the electrical potential difference for ion movement, while resistance (R, Ω) quantifies the opposition to current flow. These variables are related by Ohm's law:

$$V = IR$$

Therefore:

$$R = \frac{V}{I}$$

When current is applied through a conductive fluid-filled patch pipette, the electrical resistance of the patch pipette is defined as the ratio of voltage drop across the pipette tip to the applied current. Together with access (R_a) resistance, pipette resistance (R_p) influences current flow during patch-clamp recordings and can be described by Ohm's law:

$$R_p = \frac{V_{test}}{I_p}$$

Prior to gigaseal formation, R_p was measured in the bath solution using a square voltage test (V_{test}) pulse (5 mV step for 400 ms). The typical resulting current was approximately 2 nA, therefore the R_p can be calculated:

$$R_p = \frac{5\ x10^{-3}}{2\ x10^{-9}} = 2.5\ M\Omega$$

This value lies within the optimal range (1-5 MΩ) for whole-cell patch-clamp recordings. Upon contact with the cell membrane, resistance increased as evidenced by a reduction in current amplitude. After the formation of the gigaseal, the same square voltage test pulse produced current less than 5 pA, corresponding to a seal resistance (R_s) of 1 GΩ.

2.12.3 Series resistance

During whole-cell patch-clamp recordings, current passing through the pipette flows via resistances in series with the cell membrane, including the pipette resistance (R_p) and access resistance (R_a). The combined resistance between the amplifier and the cell membrane is defined as the series resistance (R_{series}):

$$R_{series} = R_p + R_a$$

High R_{series} can introduce significant voltage errors, by opposing pipette current (I_p) given by:

$$\Delta V_{error} = I_p \times R_{series}$$

This voltage error results in the actual membrane potential (V_m) deviating from the amplifier command voltage (V_{cmd}), such that the membrane is not clamped at the intended potential:

$$V_m = V_{cmd} - (I_p \times R_{series})$$

Therefore:

$$V_m = V_{cmd} - \Delta V_{error}$$

This error becomes increasingly significant during recordings of large ionic currents, leading to distortion of voltage dependence and current-voltage relationships (Odgen, 1994). In addition, R_{series} contributes to dynamic voltage-clamp errors by introducing a temporal lag in membrane potential changes, limiting accurate measurement of rapid currents. The time constant (τ) describing this delay is given by:

$$\tau = R_{series} \times C_m$$

Series resistance was determined by analysing passive capacitive transients evoked by a voltage-step protocol consisting of 10 mV depolarising increments from a holding potential of -80 mV. The decay phase of the capacitive current was fitted with a single-exponential function to obtain τ, from which R_{series} was calculated. Membrane capacitance (Cm) was determined as:

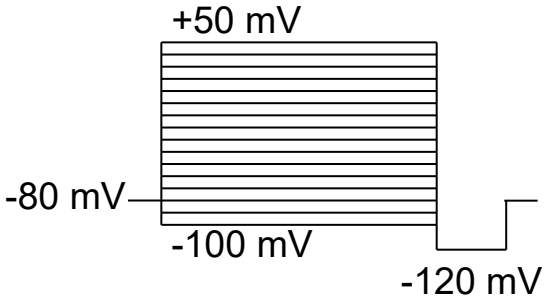
$$C_m = \frac{Q_c}{\Delta V_m}$$

Where Q_c is the total charge transferred during the transient and ΔV_m is the applied voltage step.

In HEK-293 cells, the mean R_{series} was approximately 4 MΩ, comprising an R_a of 1.5 MΩ and R_p of 2.5 MΩ. This predicted an uncompensated voltage-clamp error of approximately 10 mV during large current recordings. Electronic series resistance compensation was not applied; therefore, to minimise voltage-clamp errors, cells exhibiting control current amplitudes exceeding 2 nA at +50 mV were excluded from analysis.

2.12.4 Voltage-clamp protocols

All experiments were performed in the whole-cell configuration utilising the same voltage-step protocol. Cells were held at -80 mV and subjected to 1 s depolarising voltage steps from -100 mV to +50 mV in 10 mV increments, with an inter-sweep interval of 10 s. Steady-state activation curves were constructed from tail currents evoked by repolarisation to -120 mV following each depolarising step. This voltage-clamp protocol can be denoted schematically as:



Conductance-voltage (G-V) relationships were fitted using the Boltzmann equation:

$$\frac{G}{G_{max}} = \frac{1}{1 + \exp\left[\frac{V_{0.5} - V_m}{Slope}\right]}$$

Where G is the conductance at test potential, G_{max} is the maximal conductance and $V_{0.5}$ is the voltage at which conductance is half-maximal.

2.13 Immunocytochemistry

Dispersed cells were left at 4°C for 40 minutes to adhere to the dish, then incubated in 2% paraformaldehyde (PFA, Sigma Aldrich) for 20 minutes at room temperature and washed x3 with 1x Dulbecco's Phosphate Buffered Saline (DPBS, Gibco). Cells were then permeabilised with 0.1% Triton X-100 (Sigma Aldrich) for 10 minutes, then washed x3 with DPBS. Cells were blocked with 50% SEA BLOCK blocking buffer (Thermo Scientific) for 2 hours prior to incubation with the primary antibody: anti-K_v7.5 antibody (rabbit polyclonal anti-mouse, 1:200 dilution, Invitrogen Cat# PA5-101768, RRID:AB_2851200), anti-smooth muscle myosin heavy chain 11 antibody (rabbit polyclonal anti-mouse, 1:200 dilution, Abcam Cat# ab53219, RRID:AB_2147146), anti-EPAC1 antibody (rabbit polyclonal anti-mouse, 1:200 dilution, Invitrogen Cat# PA5-76094, RRID:AB_2719821) overnight at 4°C. Then they were washed x3 with 1x DPBS, followed by incubation of cells in secondary antibody conjugated to Alexa Fluor™ 488 (donkey polyclonal anti-rabbit antibody, 1:1000 dilution, Molecular Probes Cat# A-21206, RRID:AB_2535792) for 2 hours at room temperature and then washed x4 with 1x DPBS. Secondary antibody-only controls were prepared simultaneously.

Additional validation experiments were performed to confirm antibody specificity. For the anti-K_V7.5 antibody, untransfected and *Kcnq5*-transfected HEK-293 cells were used. For the anti-EPAC1 antibody, untransfected HEK-293 cells and mouse kidney cortex (positive control tissue) were included. All control samples were processed in parallel with experimental samples and imaged using identical acquisition parameters.

Immunofluorescence of CCSM, kidney cortex and HEK-293 cells was imaged using an Axioskop 2 LSM 510 Meta confocal microscope (Zeiss, Germany). Laser excitation (488 nm) was used to visualize immunoreactivity in the cells. The emission filter used was 505-530nm. Confocal micrographs were generated from Z-series scans taken at 0.5μm depth intervals.

2.14 Statistical analysis

Summary data for each experiment were presented as the mean ± standard error of the mean (S.E.M.). Statistical analyses were performed using analytical software, GraphPad Prism 10.0, to calculate the statistical significance of each experiment, taking $P<0.05$ as statistically significant. Unless otherwise stated and the control data passed the Kolmogorov-Smirnov normality test, pairs of columns were compared using a Student's paired t test, while multiple comparisons were made using one- or two-way ANOVA, as appropriate, corrected for multiple comparisons using the Holm-Šidák or Šidák test, respectively. When control data failed the normality test, the data were compared using Friedman's test, correcting for multiple comparisons using the Dunn test. N refers to the number of animals used, and n represents the number of cells or crura used. The minimum N number used in these experiments was 6, with a minimum n of 6. For RT-PCR/qPCR/ICC experiments, tissue from two animals was pooled to generate a single biological replicate. Therefore, each RT-PCR/qPCR/ICC replicate represents one pooled sample (N=3 pools, comprising a total of 6 animals).

Concentration-effect data were fitted with a Hill-Langmuir equation: $Y/Y_{control} = 1/\{1 + 10\text{^}(\log[Drug] - \log IC_{50})\}$, where Y is the value recorded in the drug, $Y_{control}$ is the value in the absence of drug, IC_{50} is the half-maximal effective concentration, and [Drug] is the concentration variable. In each case, IC_{50} is stated, followed by the upper and lower 95% confidence limits (CI). IC_{50}s were compared using the extra sum-of-squares F test, $V_{0.5}$ values were also assessed for statistical significance using the same method.

2.15 Solutions

Concentrations are stated in millimolar (mM).

Solution 1: Krebs‘

NaCl (120), KCl (5.9), $NaHCO_3$ (25), Glucose (5.5), NaH_2PO_4 (1.2), $MgCl_2$ (1.2), $CaCl_2$ (2.5)

pH adjusted to 7.4 using 95% O_2 and 5% CO_2 for 20 minutes.

Solution 2: Ca^{2+} free Hanks’ for cell isolation

NaCl (125), KCl (5.36), Glucose (10), Sucrose (2.9), $NaHCO_3$ (15.5), KH_2PO_4 (0.44), Na_2HPO_4 (0.33), HEPES (10)

pH adjusted to 7.4 with NaOH.

Solution 3: Hanks’

NaCl (125), KCl (5.36), Glucose (10), Sucrose (2.9), $NaHCO_3$ (4.17), KH_2PO_4 (0.44), Na_2HPO_4 (0.33), $MgCl_2.6H_2O$ (0.5), $CaCl_2.2H_2O$ (1.8), $MgSO_4.7H_2O$ (0.4), HEPES (10)

pH adjusted to 7.4 with NaOH

Solution 4: Whole-cell K^+ patch pipette solution

KCl (133), $MgCl_2.6H_2O$ (1), EGTA (0.5), HEPES (10), Na_2ATP (1), NaGTP (0.1), Na_2-phosphocreatine (2.5)

pH adjusted to 7.2 with KOH

2.16 Drugs

Drugs were made up to stock solution concentrations using either dimethyl sulfoxide (DMSO), ethanol or distilled water (dH_2O) dependent on the solubility properties of the drug. Stock solutions of each drug were carefully aliquoted and stored as per manufacturer's instructions.

Drugs	Supplier	Solvent
Phenylephrine hydrochloride (PE)	Sigma-Aldrich	dH_2O
Forskolin (FK)	Tocris	DMSO
8-pCPT-2-O-Me'-cAMP-AM (007-AM)	Biolog	DMSO
N^6-Monobutyryladenosine- 3', 5'- cyclic monophosphate (6-MB)	Biolog	dH_2O
Nifedipine (NIF)	Tocris	DMSO
2-Aminoethoxydiphenyl borate (2-APB)	Sigma-Aldrich	DMSO
GSK-7975A (GSK)	Medchem	DMSO
Retigabine (RTG)	Tocris	DMSO
XE-991	Tocris	dH_2O
Guanethidine (GE)	Tocris	dH_2O
Phentolamine hydrochloride	Sigma-Aldrich	dH_2O
PI(4,5)P2-diC8	Echelon Biosciences	dH_2O



Figure 2.1. Picture of the mouse penis used for experiments. The ischiocavernosus skeletal muscle is excised from the tunica albuginea (white) of the corpus cavernosum smooth muscle (CCSM) crus, excised from the penile body at the dashed line.

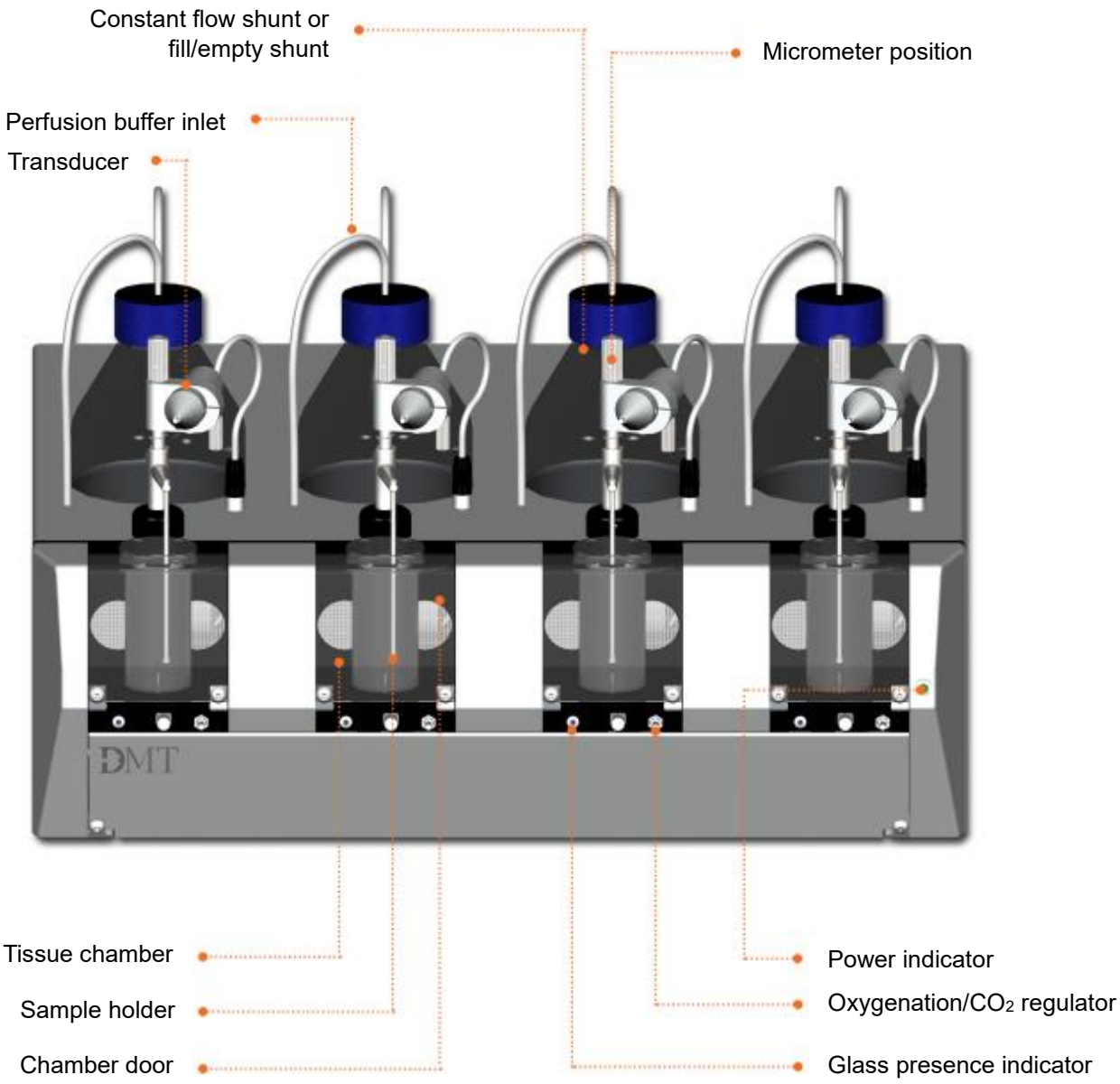


Figure 2.2. Danish Myo Technology (DMT) Tissue Organ Bath Systems (TOBS) 750. (Adapted from DMT TOBS750 User Guide)

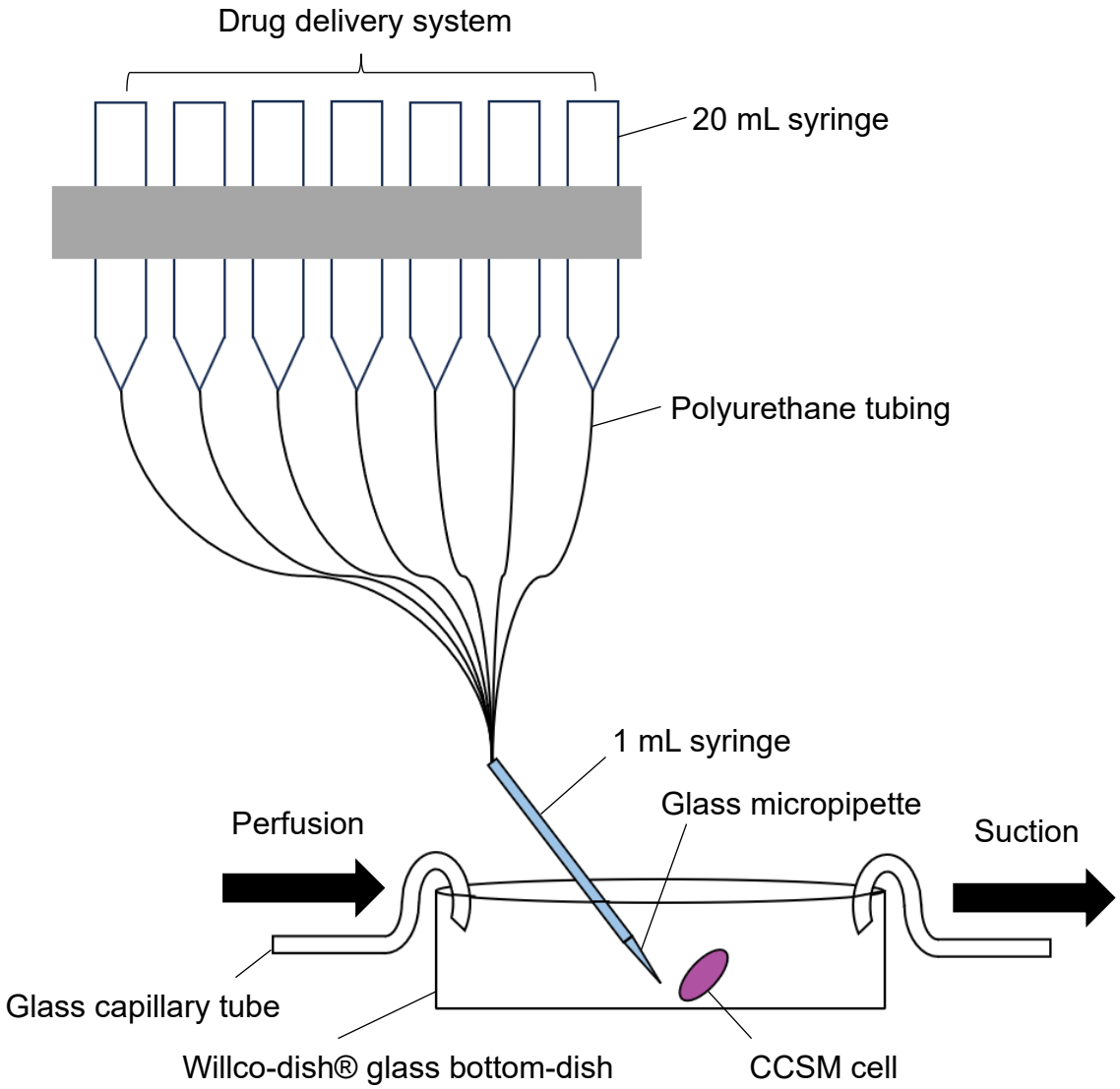


Figure 2.3. Illustration of the drug perfusion system used for confocal imaging experiments. Drug reservoirs (20 mL syringes) were gravity fed to a 1 mL syringe via silicon tubing. CCSM cells were continuously perfused with Hanks' solution maintained at 37^{o}C through a glass exchanger. Overflow of Hanks' solution from Wilco-dish® glass bottom-dish was prevented via suction using a glass capillary tube.

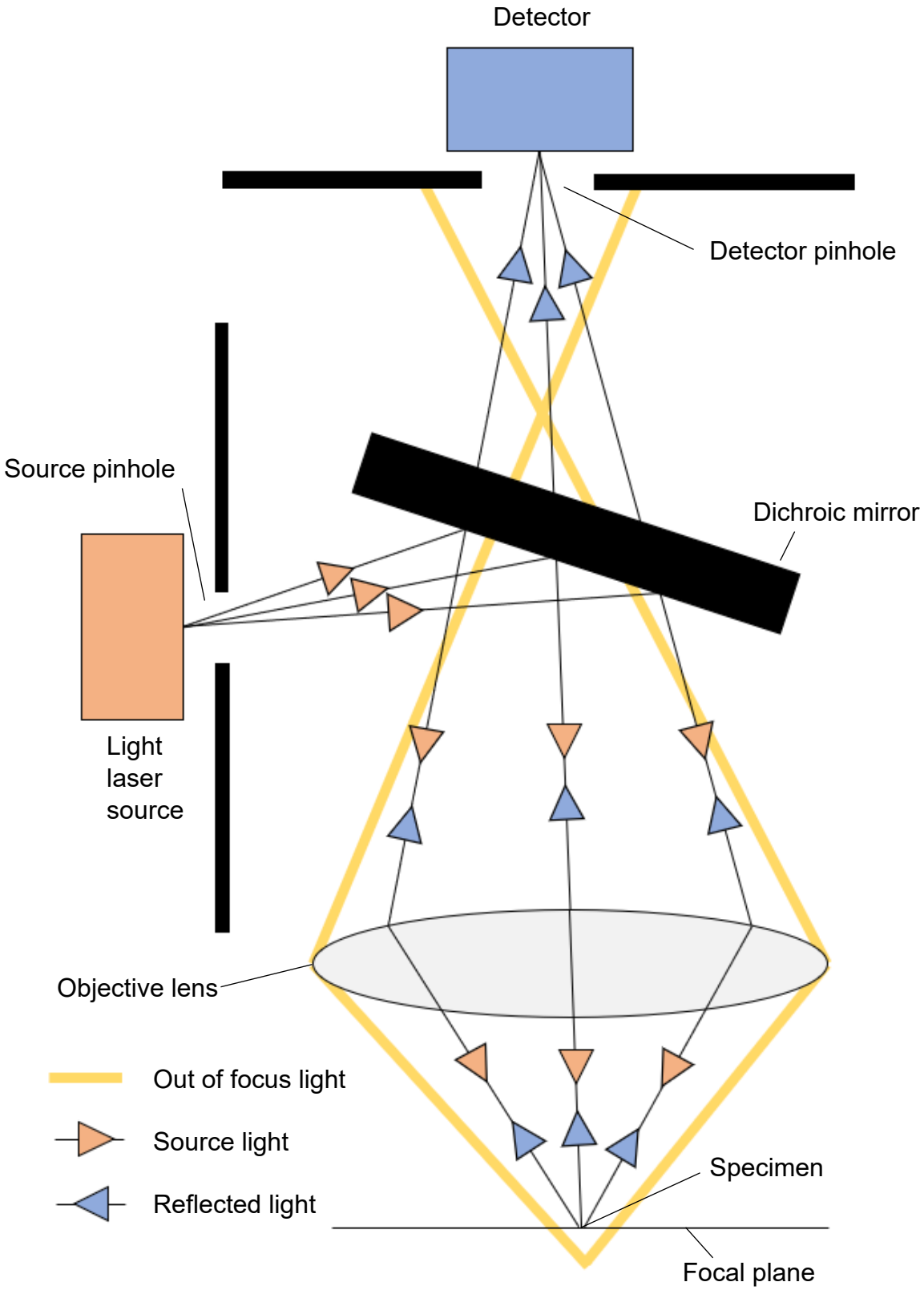


Figure 2.4. Simplified light paths of a confocal microscope

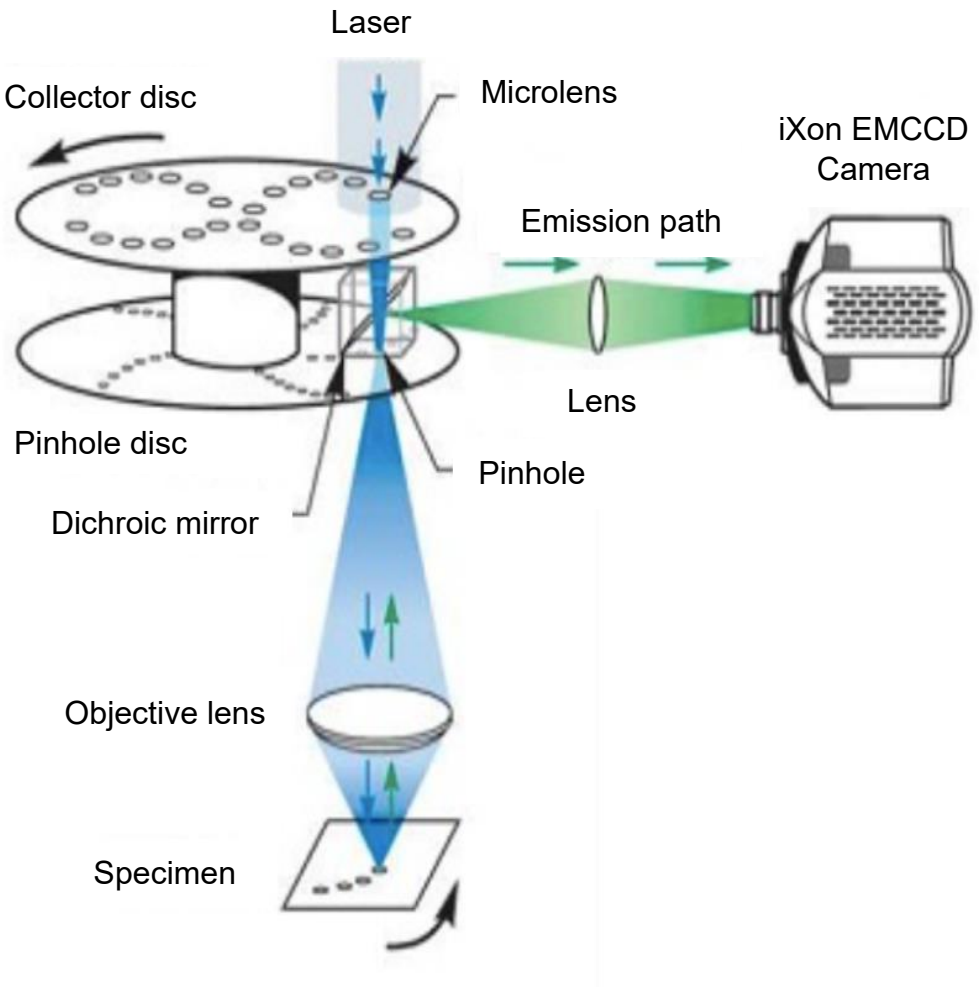


Figure 2.5. Representative image of the Nipkow spinning disc and microlens array (image adapted from Andor Technology Ltd, Belfast, Northern Ireland).

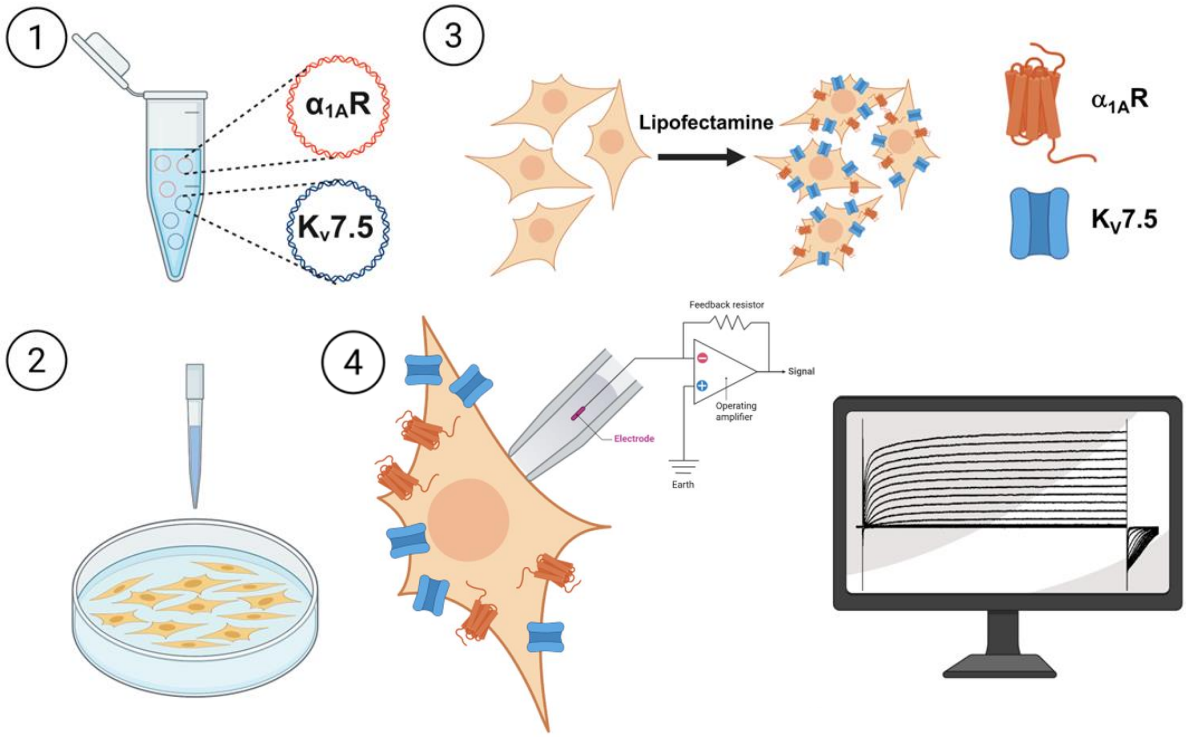


Figure 2.6. Workflow for HEK-293 cell transfection and electrophysiological recordings. **1.** $K_v7.5$ and $\alpha_{1A}R$ plasmid DNA was diluted in 100 µL serum-free medium and complexed with Lipofectamine. **2.** The 200 µL plasmid DNA-Lipofectamine mixture was added dropwise to cultured HEK-293 cells. **3.** After 3 h of transfection, the medium was replaced with fresh growth medium to allow expression of $K_v7.5$ and $\alpha_{1A}R$. **4.** Transfected cells were subsequently used for whole-cell patch-clamp electrophysiology.

3. Results Chapter 1:

Distinct Ca^{2+} signalling pathways underlie phasic and tonic contractions in corpus cavernosum smooth muscle

3.1 Introduction

Adrenergic signalling is a principal determinant of CCSM tone, maintaining penile flaccidity through α_1-adrenoceptor activation. Activation of α_1-adrenoceptors elicits tonic responses in human (Christ *et al*., 1990; 1992), rat (Wingard *et al*., 2003), rabbit (Saenz de Tejada *et al*., 1989a) and guinea pig (Hashitani *et al*., 2002) CCSM. Yet, human CCSM elicits phasic spontaneous contractions (Christ, 1990). Phasic contractions have been suggested to reflect periodic intracellular Ca^{2+} transients, whereas tonic contractions arise from prolonged elevations in Ca^{2+} and sustained activation of the contractile filaments (Nelson *et al*., 1990; Berridge *et al*., 1993).

However, evidence from traditionally tonic smooth muscles, including urethra and internal anal sphincter, suggests that sustained tone may arise through the temporal and spatial summation of asynchronous phasic Ca^{2+} oscillations across multiple smooth muscle bundles rather than from a maintained global elevation in cytosolic Ca^{2+} (Thornbury et al., 2011; Drumm et al., 2018; Cobine et al., 2020). Consistent with this concept, whole-tissue Ca^{2+} imaging in rabbit CCSM has shown that detumescent tone is associated with asynchronous propagation of phasic Ca^{2+} oscillations (Sergeant et al., 2009). However, comparable whole-tissue Ca^{2+} imaging studies have not been performed in mouse CCSM, and therefore the Ca^{2+}-signalling mechanisms underlying phasic and tonic contractions in this species remain unclear.

CCSM cells exhibit a relatively depolarised resting membrane potential (-41 to -50 mV; Hashitani *et al*., 2005), therefore, it could be suggested that even a modest depolarisation may be sufficient to recruit LTCCs and drive Ca^{2+} influx and excitability (Nelson *et al*., 1990). One likely source of depolarisation is provided by Ca^{2+}-activated Cl^- channels encoded by ANO1, which are expressed in mouse and rabbit CCSM, coupling SR Ca^{2+} release to membrane depolarisation (Hannigan et al. 2017; Lim et al., 2022b). Concurrently, intracellular Ca^{2+} release via IP_3Rs and RyRs contributes to the generation/propagation of Ca^{2+} oscillations (Keizer & De Young, 1995; Bolton, 2006). SOCE mediated by Ca^{2+}-release–activated Ca^{2+} (CRAC) channels, replenishes SR store Ca^{2+} content and sustains Ca^{2+} release under continuous receptor activation (Prakriya and Lewis, 2015). Notably, Sevilleja-Ortiz et al. (2020) demonstrated increased CRAC channel contributions to adrenergic hypercontractility in CCSM from men with ED, suggesting that enhanced SR Ca^{2+} store refilling via SOCE may represent a pathological mechanism by which sustained SR-dependent adrenergic tone is amplified in the CCSM and strongly opposes detumescence.

In support of this, STICs recorded in mouse CCSM cells were abolished by inhibition of IP_3Rs, RyRs, CRAC channels and SERCA, which indicated that spontaneous depolarising activity was initiated by SR-dependent Ca^{2+} release and sustained by store-refilling mechanisms (Lim et al., 2022b). Since ANO1 inhibition abolishes phasic contractions in mouse CCSM but suppresses tonic contractures in rabbit CCSM (Hannigan et al., 2017; Lim et al., 2022b), these channels may serve important functions in linking SR Ca^{2+} release activity to membrane depolarisation, and therefore initiate phasic activity in mouse CCSM.

Therefore, the present study aimed to determine the underlying signalling mechanisms governing phasic and tonic contractile responses in mouse CCSM, but more specifically, this chapter sought to:

1. Characterise the concentration dependence of PE-evoked contractions in mouse CCSM and determine how phasic and tonic components vary across the agonist range.
2. Define the contribution of membrane excitability pathways, including LTCCs and ANO1 channels, to each component of contractility.
3. Determine the role of intracellular SR Ca^{2+} release pathways, including IP_3Rs and SOCE via CRAC channels, in adrenergic contractions.
4. Assess how low- versus high-PE concentrations differentially regulate intracellular Ca^{2+} oscillations in isolated CCSM cells and their sensitivity to pharmacological modulation of LTCC, IP_3R, RyR and CRAC channels.

3.2 Results

3.2.1 PE evokes concentration-dependent phasic and tonic contractions

Cumulative application of PE (1 $x10^{-7}$ M - 3 $x10^{-5}$ M) produced two distinct contractile responses in CCSM (Fig3.1A). At low concentrations (≤1 $x10^{-6}$ M), rhythmic phasic contractions predominated, characterised by oscillatory increases in tension (9.3 min^{-1}; amplitude 0.85 mN; n=8, N=8). At higher concentrations (≥3 $x10^{-6}$ M), these oscillations were superimposed upon large tonic contractions (increase in tone 0.3-1.0 mN; n=8, N=8).

These contractile responses exhibited distinct concentration dependence. Phasic contractions were present across the entire concentration range and showed limited concentration dependence of amplitude or frequency, whereas tonic contractures required higher PE concentrations to produce substantial increases in tension. Notably, the amplitude of phasic contractions, even at low concentrations of PE (e.g., 1 $x10^{-7}$ M), was comparable to the maximal tonic response observed at the highest concentration.

Subsequent to a 40-min washout period consisting of six washes, followed by a 20-min equilibration period, a repeat addition of the cumulative PE concentrations demonstrated attenuation, but not complete abolition, of the PE response (Fig. 3.1B). On the second application, phasic contraction frequency (1 $x10^{-7}$ M to 1 $x10^{-5}$ M PE: $P<0.01$) and amplitude (3 $x10^{-7}$ M and 1 $x10^{-6}$ M PE: $P<0.01$) were significantly reduced compared with the first (Fig3.1C-D), and tonic tension also appeared to increase modestly, yet, this difference was not statistically significant (at 3 $x10^{-5}$ M, $P=0.8346$; Fig3.1E; n=8, N=8).

Taken together, these results indicate run-down of PE-induced phasic responses upon repeated exposure. Although both phasic and tonic components remained detectable, the marked reduction in phasic frequency and amplitude demonstrates that the response is not conserved across repeated applications. Accordingly, the second application reflects an attenuated, but not abolished, contractile response, providing only a limited reference for temporal changes in subsequent experiments and should therefore be interpreted with appropriate caution.

3.2.2 PE-evoked phasic contractions were selectively abolished by NIF and Ani-9

Phasic contractions were selectively abolished by modulators of membrane excitability. The LTCC blocker NIF (1 x10^{-6} M) abolished phasic contractions (Fig3.2B-D; frequency and amplitude: P<0.0001) with tonic responses unaffected, except at 1 x10^{-6} M PE (Fig3.2E; P<0.01; n=6, N=6). Blockade of ANO1 with Ani-9 (3 x10^{-6} M) also abolished phasic contractions (Fig3.3C, frequency: P<0.0001; Fig3.3D, amplitude: P<0.0001) without affecting tonic responses, except for slight, yet significant, increases at 3 x10^{-6} M and 1 x10^{-5} M PE (Fig3.3E; P<0.05; n=6, N=6).

3.2.3 PE-evoked tonic contractions were abolished by 2-APB and GSK-7975A

Inhibition of IP_3Rs with 2-APB (1 x10^{-4} M) abolished both phasic and tonic activity evoked by PE (Fig3.4A-B). Analysis of summary data showed significant reductions in phasic contraction frequency (Fig3.4C, P<0.05) and amplitude (Fig3.4D, P<0.05), as well as a pronounced decrease in tone (Fig3.4E, P<0.0001 at 3 x10^{-5} M; n=6, N=6).

The CRAC channel inhibitor GSK-7975A (1 x10^{-5} M) preferentially attenuated tonic responses (Fig3.5E, P<0.01 at 3 x10^{-5} M). Phasic frequency was significantly decreased (Fig3.5C, P<0.0001), yet the amplitude and duration of phasic events were significantly increased at higher concentrations of PE (3 x10^{-6} M - 3 x10^{-5} M; Fig3.5D, amplitude: P<0.001 at 3 x10^{-5} M; Fig3.5F, duration: P<0.05 at 3 x10^{-5} M; n=6, N=6).

3.2.4 PE evoked Ca^{2+} oscillations

Ca^{2+} imaging confirmed two distinct PE responses. Low PE (1 x10^{-7} M) evoked robust Ca^{2+} oscillations (Fig3.6A), whereas high PE (1 x10^{-5} M) produced a transient Ca^{2+} elevation, followed subsequently by (smaller) sustained oscillations (Fig3.7A). Over 2 min of application, low PE oscillation frequency was stable (Fig3.6B, P=0.2162), while amplitude declined modestly (Fig3.6C, P=0.0426). At high PE, both parameters remained unchanged over time (Fig3.7B, frequency: P=0.7029; Fig3.7C, amplitude: P=0.7512). While Ca^{2+} oscillation frequency and amplitude did not differ between low and high PE (32.5 vs 29.0 min^{-1}, P=0.8408; 1.74 vs 1.68 F/F_0, P=0.9181; n=6, N=6), high PE significantly prolonged Ca^{2+} oscillation duration compared to low PE (0.91 vs 0.71 s; P=0.0276; data not shown).

3.2.5 Low-concentration PE-evoked Ca^{2+} oscillations were selectively abolished by NIF

Imaging of isolated CCSM cells confirmed that the addition of NIF abolished only low-PE Ca^{2+} oscillations (Fig3.8A-C; frequency: P=0.0217; amplitude: P=0.0047; n=6, N=6), with no recovery on washout. The oscillation frequency was 23.00 ± 5.83 min^{-1} under low-PE conditions, which was reduced to 0.00 ± 0.00 min^{-1} in the presence of NIF, with a partial recovery to 1.50 ± 1.03 min^{-1} on washout. Similarly, oscillation amplitude was 1.72 ± 0.30 F/F_0 under low-PE conditions, falling to 0.00 ± 0.00 F/F_0 with NIF, with a partial recovery to 0.45 ± 0.30 F/F_0 on washout. In contrast, NIF had no significant effect on high-PE oscillations (Fig3.9A-C; frequency: P=0.1240; amplitude: P=0.9276; n=6, N=6), where frequency remained comparable across control (42.00 ± 7.18 min^{-1}), NIF (31.00 ± 3.35 min^{-1}), and washout (31.50 ± 3.70 min^{-1}) conditions. Likewise, amplitude was preserved across control (1.22 ± 0.22 F/F_0), NIF (1.20 ± 0.24 F/F_0), and washout (1.00 ± 0.20 F/F_0) conditions.

3.2.6 High-concentration PE-evoked Ca^{2+} oscillations were inhibited by 2-APB, GSK-7975A and TC

The results of this chapter are consistent with low-PE–induced Ca^{2+} oscillations driving phasic contractions, as evidenced by their shared sensitivity to NIF. In contrast, high-PE Ca^{2+} oscillations underpin tonic contractures, demonstrated by their insensitivity to NIF. Consistent with this interpretation, 2-APB abolished both phasic and tonic PE-induced activity in previous experiments (Fig3.4). Similarly, high-PE Ca^{2+} oscillations were abolished by 2-APB (Fig3.10A-B; frequency: P=0.0092; Fig. 3.10C; amplitude: P=0.0113; n=6, N=6), with recovery upon washout. Oscillation frequency under control conditions was 25.50 ± 5.24 min^{-1}, which was completely abolished in the presence of 2-APB (0.00 ± 0.00 min^{-1}), with partial recovery to 17.00 ± 6.51 min^{-1} on washout. Oscillation amplitude followed the same pattern, measuring 1.38 ± 0.30 F/F_0 at control, falling to 0.00 ± 0.00 F/F_0 with 2-APB, and partially recovering to 0.61 ± 0.29 F/F_0 on washout.

CRAC channel inhibition with GSK-7975A additionally had a significant impact on tonic activity. In isolated cells, GSK-7975A significantly attenuated high-PE oscillation frequency (Fig3.11A-B, P=0.0049), from 50.00 ± 10.35 min^{-1} at control to 14.00 ± 4.36 min^{-1} with GSK-7975A, with partial recovery to 28.50 ± 8.23 min^{-1} on washout, while amplitude remained unaffected (Fig3.11C, P=0.7132; n=6, N=6),

measuring 1.52 ± 0.28 F/F_0 at control, 1.33 ± 0.31 F/F_0 with GSK-7975A, and 1.49 ± 0.28 F/F_0 on washout. Interestingly, GSK-7975A abolished low-PE oscillations (Fig3.12A-B, frequency: P=0.0163; Fig3.12C, amplitude: P=0.0363; n=6, N=6), with frequency falling from 17.50 ± 4.13 min^{-1} at baseline PE to 0.00 ± 0.00 min^{-1} with GSK-7975A, with a partial recovery to 4.00 ± 1.00 min^{-1}. Similarly, amplitude was reduced from 2.65 ± 0.77 F/F_0 at baseline PE to 0.00 ± 0.00 F/F_0 with GSK-7975A, partially recovering to 1.20 ± 0.47 F/F_0 on washout; consistent with the abolition of phasic contractions at low concentrations of PE in tension (1 $x10^{-7}$ M PE, Fig3.5B-C). Taken together, these findings indicated that IP_3Rs are indispensable for both phasic and tonic contractions, whereas CRAC channels are implicated in Ca^{2+} influx and SOCE that sustains SR Ca^{2+} load.

Application of TC (1 $x10^{-4}$ M), a RyR antagonist, initially suppressed high PE-evoked Ca^{2+} oscillations, reducing both frequency and amplitude within 10-20s (Fig3.13A). However, this effect was transient: oscillations reappeared despite continued presence of TC, a well-documented “breakthrough” phenomenon in RyR pharmacology (Overend *et al*., 1997). Grouped analysis confirmed no sustained inhibition (Fig3.13B, frequency: P=0.0605; Fig3.13C, amplitude: P=0.8631; n=6, N=6), with frequency measuring 48.50 ± 17.28 min^{-1} at control, 11.50 ± 6.41 min^{-1} in the presence of TC, and recovering to 42.50 ± 9.31 min^{-1} on washout. Amplitude similarly showed no sustained inhibition, measuring 0.75 ± 0.16 F/F_0 at control, 0.71 ± 0.27 F/F_0 in the presence of TC, and 0.51 ± 0.09 F/F_0 on washout. Nonetheless, these data suggested RyR involvement in the initiation of high-PE oscillations, given that TC initially abolished activity.

3.2.7 Caffeine-evoked store-release Ca^{2+} spikes are not inhibited by 2-APB

To verify that the effects of 2-APB on PE-evoked Ca^{2+} oscillations were not attributable to non-specific inhibition of RyRs or depletion of SR Ca^{2+} stores, its effect on caffeine-evoked Ca^{2+} spikes was examined as a control. Caffeine (1 $x10^{-2}$ M) was used as a RyR opener to evoke SR Ca^{2+} release. Application of 2-APB (1 $x10^{-4}$ M) did not significantly inhibit caffeine-evoked Ca^{2+} spikes (Fig3.14A-B; P=0.8606; n=6, N=6), yet showing a non-significant increase from 3.170 ± 0.47 F/F_0 to 3.547 ± 0.49 F/F_0 in the presence of 2-APB. These data indicate that the abolition of phasic and tonic contractions, as well as high-PE Ca^{2+} oscillations, by 2-APB is most likely not due to non-specific suppression of SERCA function or RyR-mediated Ca^{2+} release.

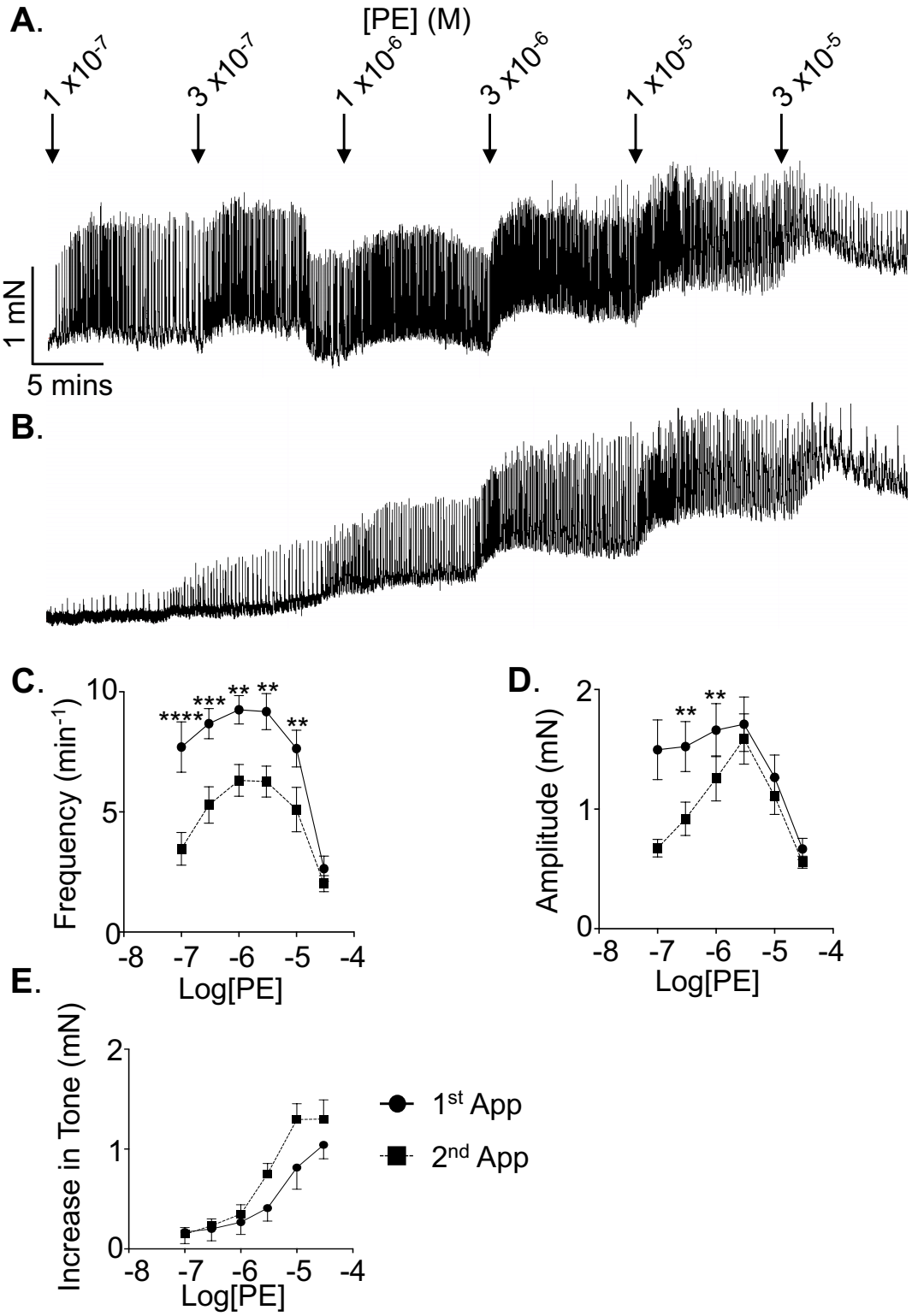


Figure 3.1: Repeated concentration-effect responses to phenylephrine (PE).

A. Representative isometric tension recording demonstrating the effect of incremental concentrations of PE (1 x10^{-7} M to 3 x10^{-5} M). **B.** Representative isometric tension recording, from the same preparation, demonstrating the second application of incremental concentrations of PE. **C+D+E.** Summary data for the effect of a second application (square) on phasic contraction frequency (C), and amplitude (D), as well as the increase in tone (E). *P<0.05, **P<0.01, ***P<0.001, ****P<0.0001 (n=8, N=8).

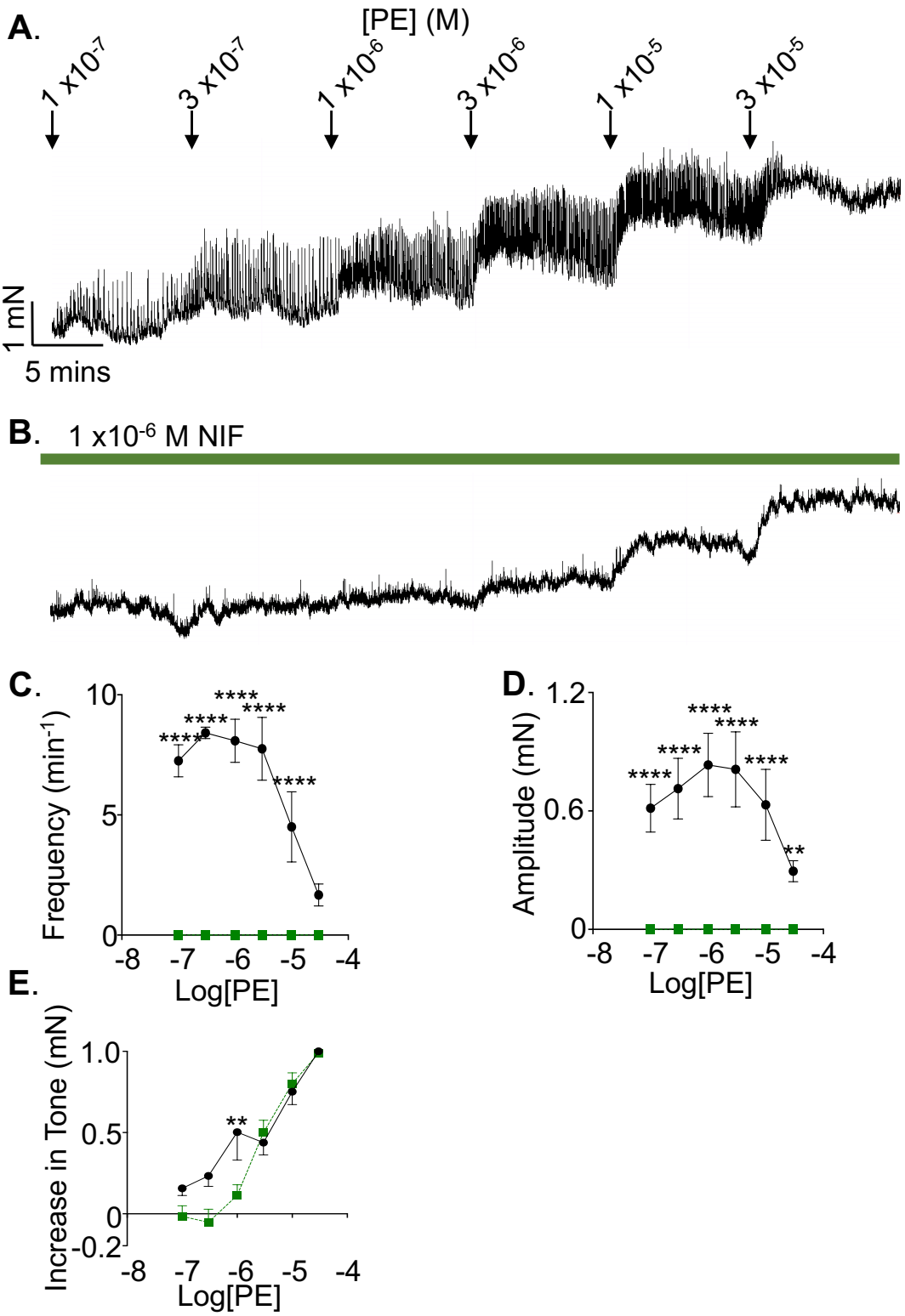


Figure 3.2: The LTCC blocker, nifedipine (NIF), abolished phasic, and not tonic, phenylephrine (PE)-induced contractions.
A. Representative isometric tension recording demonstrating the effect of incremental concentrations of PE (1 x10^{-7} M to 3 x10^{-5} M). **B.** Representative isometric tension recording, from the same preparation, demonstrating the effect of incremental concentrations of PE in the presence of 1 x10^{-6} M NIF. **C+D+E.** Summary data for the effect of NIF (green) on phasic contraction frequency (C), and amplitude (D), as well as the increase in tone (E). *P<0.05, **P<0.01, ***P<0.001, ****P<0.0001 (n=6, N=6).

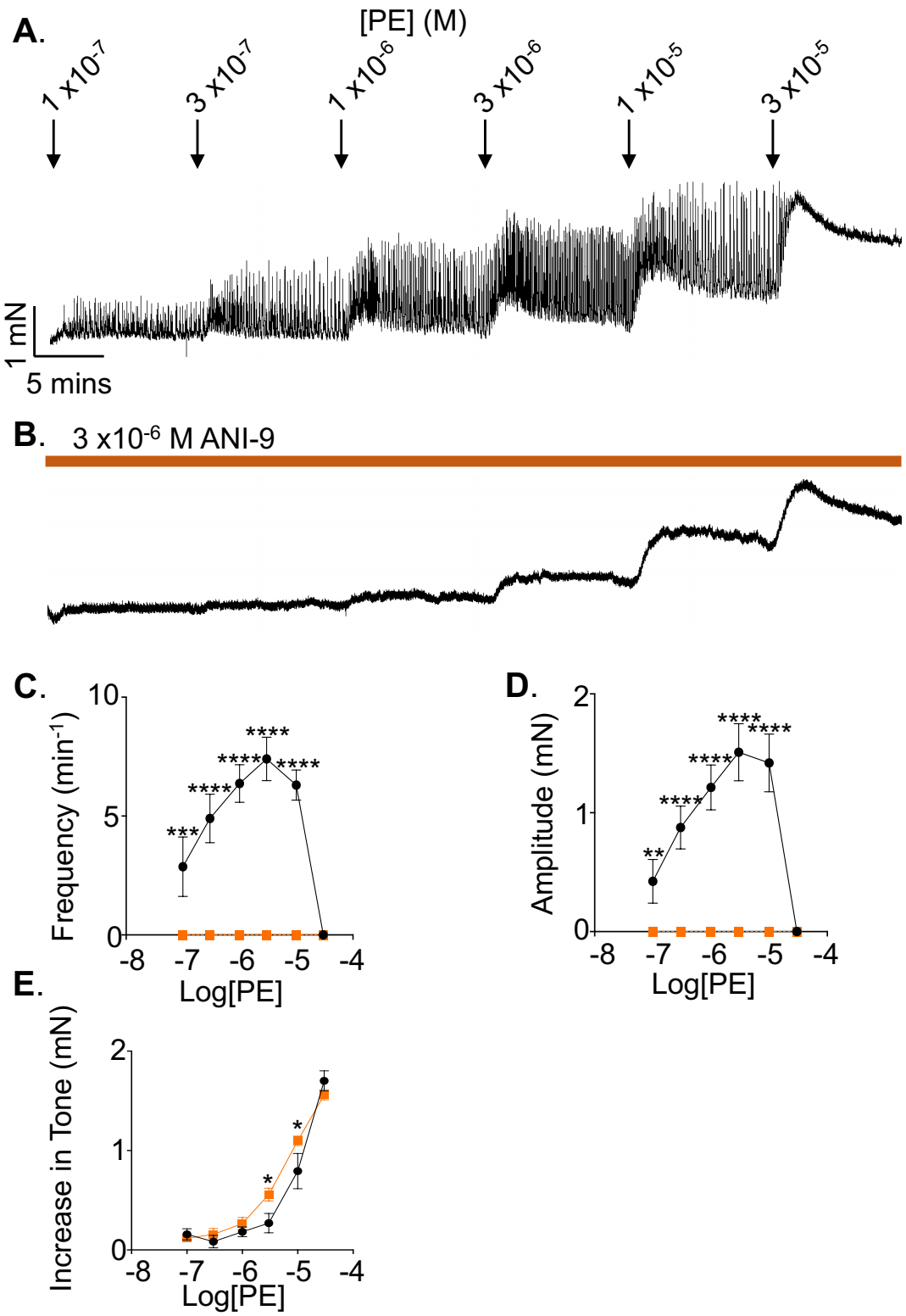


Figure 3.3: The ANO1 inhibitor, Ani-9, abolished phasic, and not tonic, phenylephrine (PE)-induced contractions.
A. Representative isometric tension recording demonstrating the effect of incremental concentrations of PE (1 x10^{-7} M to 3 x10^{-5} M). **B.** Representative isometric tension recording, from the same preparation, demonstrating the effect of incremental concentrations of PE in the presence of 3 x10^{-6} M Ani-9. **C+D+E.** Summary data for the effect of Ani-9 (orange) on phasic contraction frequency (C), and amplitude (D), as well as the increase in tone (E). *P<0.05, **P<0.01, ***P<0.001, ****P<0.0001 (n=6, N=6).

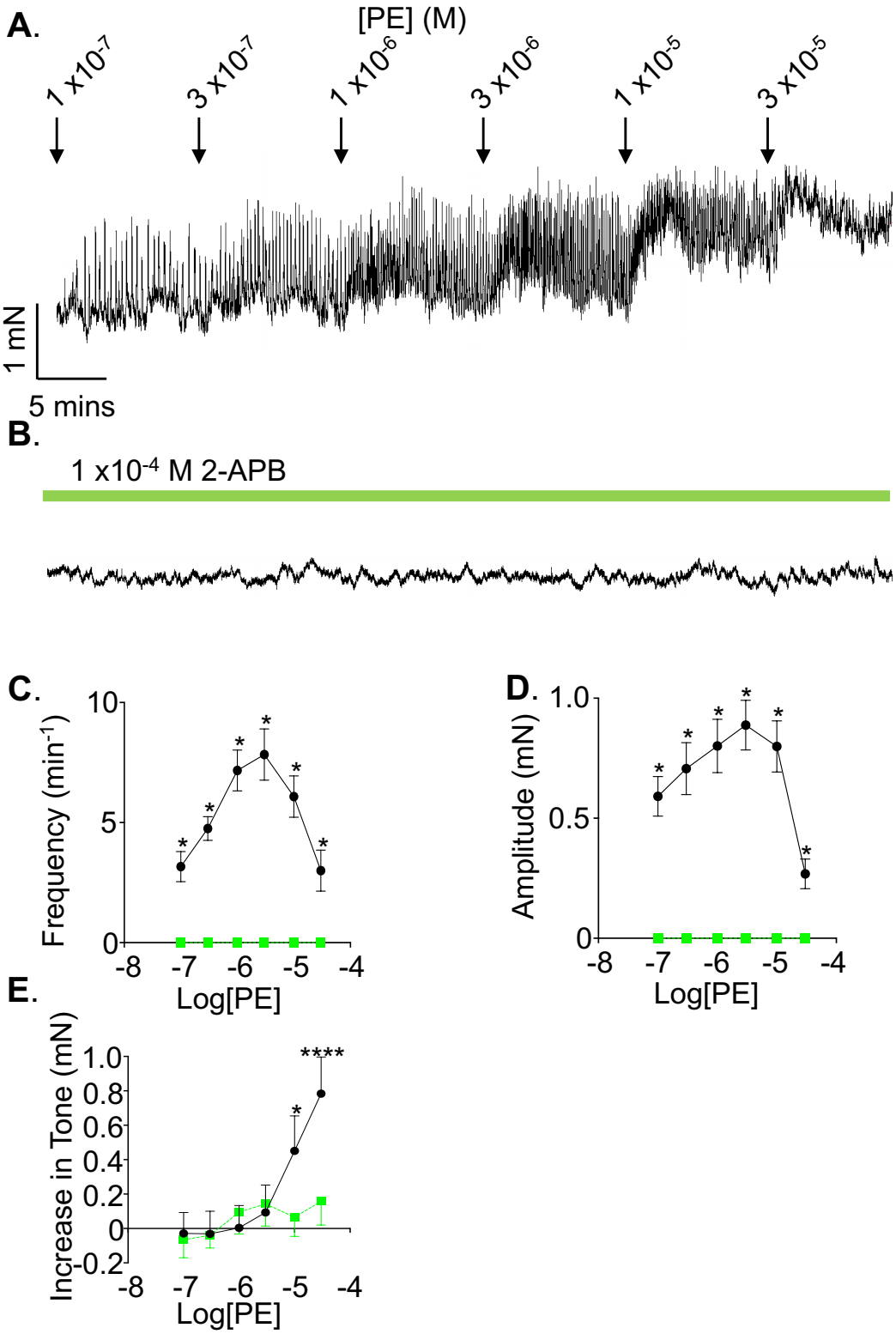


Figure 3.4: IP_3R antagonist, 2-Aminoethoxydiphenyl borate (2-APB), abolished phasic and tonic phenylephrine (PE)-induced contractions.

A. Representative isometric tension recording demonstrating the effect of incremental concentrations of PE (1 x10^{-7} M to 3 x10^{-5} M). **B.** Representative isometric tension recording, from the same preparation, demonstrating the effect of incremental concentrations of PE in the presence of 1 x10^{-4} M 2-APB. **C+D+E.** Summary data for the effect of 2-APB (lime green) on phasic contraction frequency (C), amplitude (D), as well as the increase in tone (E). *P<0.05, ****P<0.0001 (n=6, N=6).

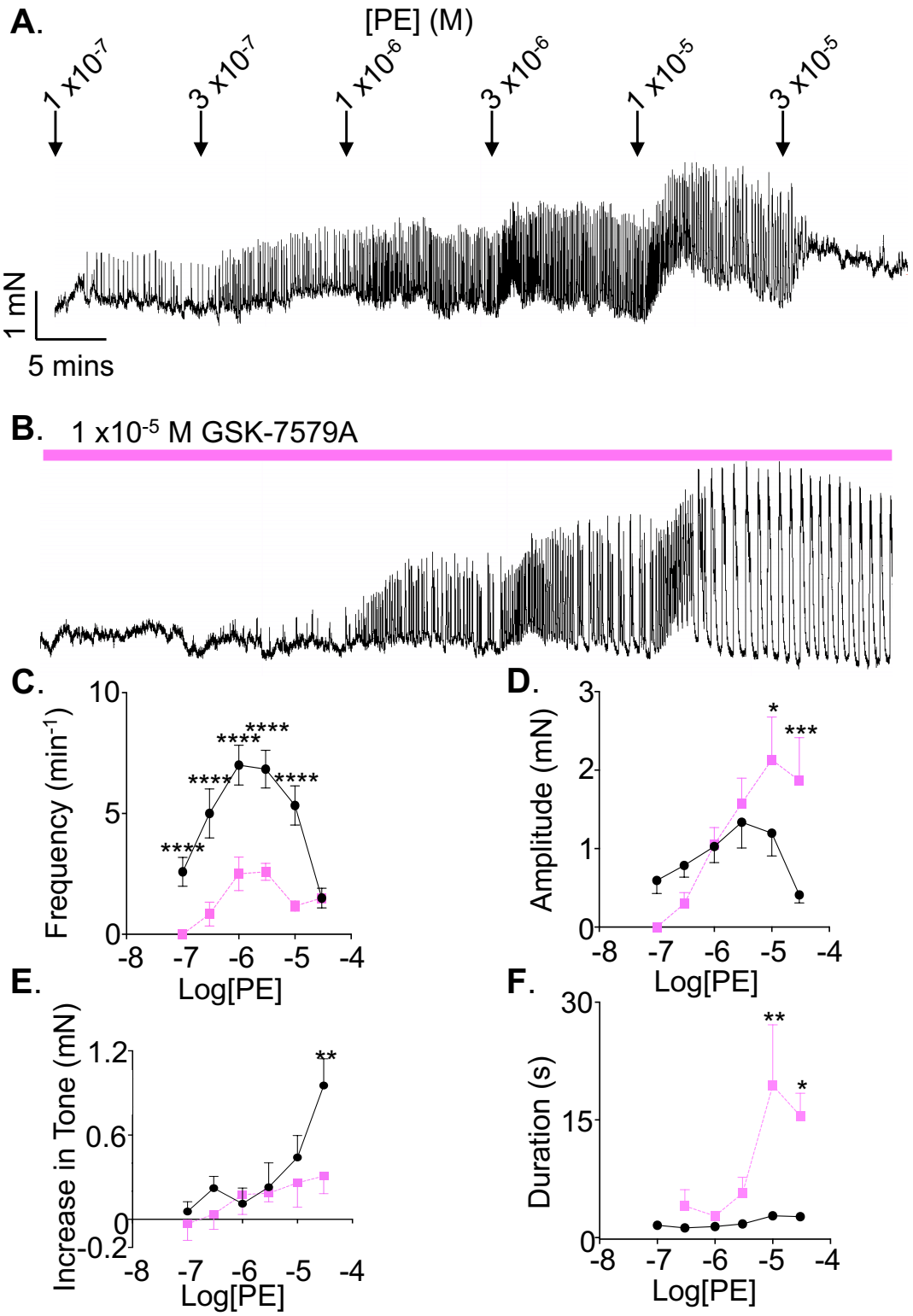


Figure 3.5: The effect of CRAC inhibitor, GSK-7975A (GSK), on phenylephrine (PE)-induced contractions.
A. Representative isometric tension recording demonstrating the effect of incremental concentrations of PE (1 x10^{-7} M to 3 x10^{-5} M). **B.** Representative isometric tension recording, from the same preparation, demonstrating the effect of incremental concentrations of PE in the presence of 1 x10^{-5} M GSK. **C+D+E+F.** Summary data for the effect of GSK (pink) on phasic contraction frequency (C), amplitude (D) and duration (F), as well as the increase in tone (E). *P<0.05, **P<0.01, ***P<0.001, ****P<0.0001 (n=6, N=6).

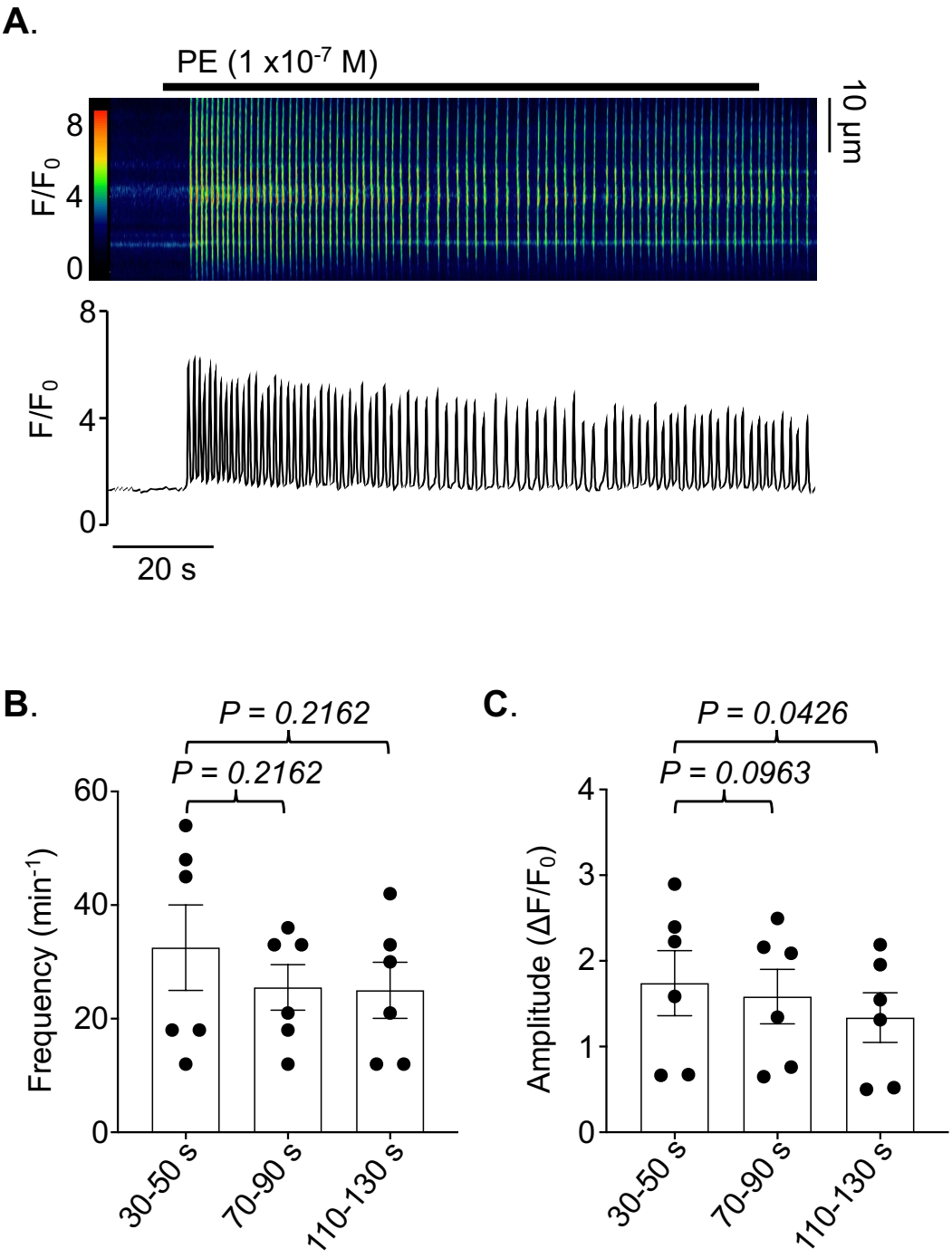


Figure 3.6: Time control of low-PE-induced Ca^{2+} oscillations in isolated cells.

A. Representative spatiotemporal map and associated intensity plot of Ca^{2+} oscillations, evoked by 2 min application of 1 x10^{-7} M PE. **B+C.** Summary data for Ca^{2+} oscillation frequency (min^{-1}) and amplitude ($\Delta F/F_0$), respectively. Ca^{2+} oscillation frequency no significant decrease over the 2 min application period, whereas amplitude showed a significant decrease between '30-50 s' and '110-130 s' periods (P=0.0426; n=6, N=6).

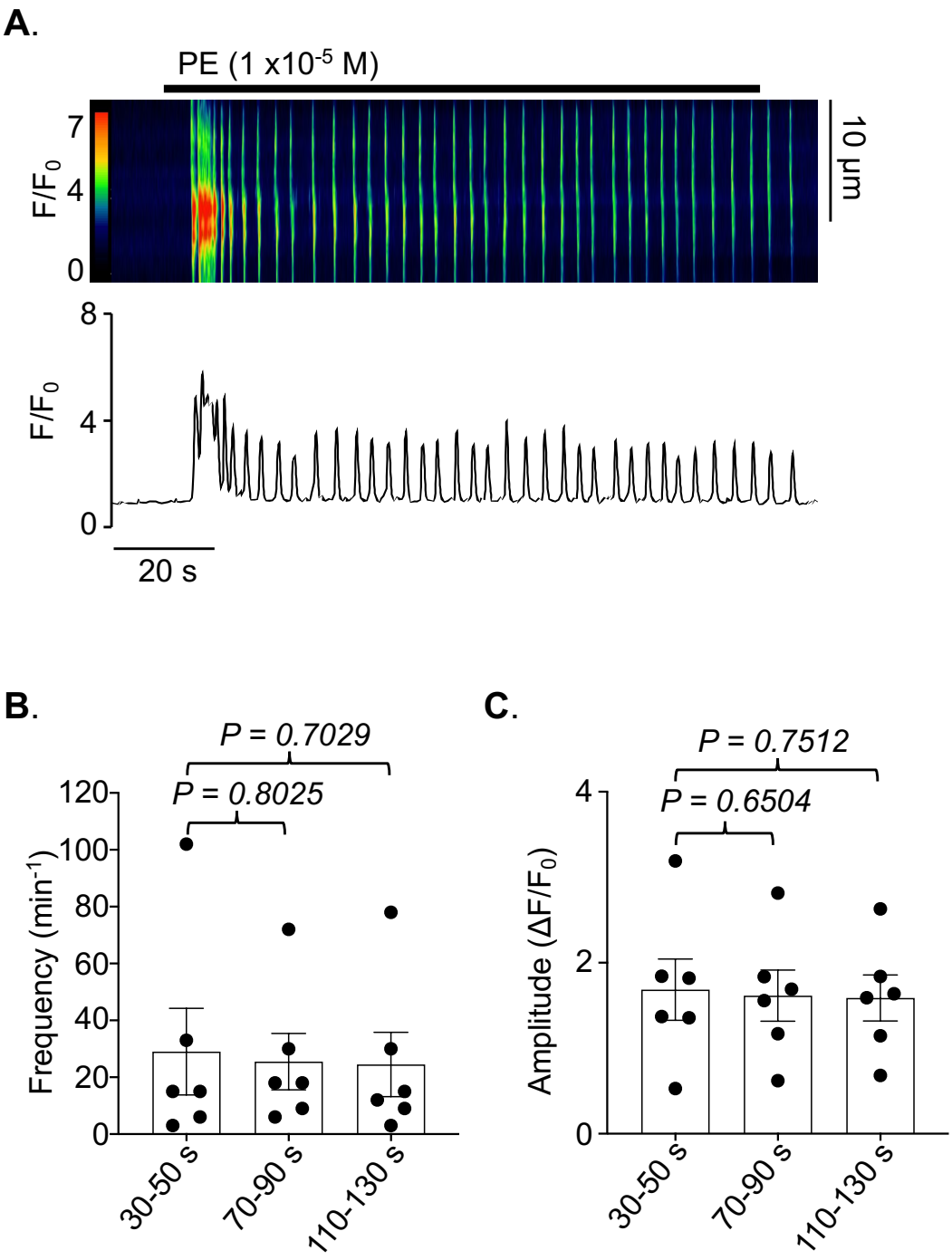


Figure 3.7: Time control of high-PE-induced Ca^{2+} oscillations in isolated cells.
A. Representative spatiotemporal map and associated intensity plot of Ca^{2+} oscillations, evoked by 2 min application of 1 x10^{-5} M PE. **B+C.** Summary data for Ca^{2+} oscillation frequency (min^{-1}) and amplitude ($\Delta F/F_0$), respectively. Ca^{2+} oscillation frequency and amplitude showed no significant decrease over the 2 min application period (n=6, N=6).

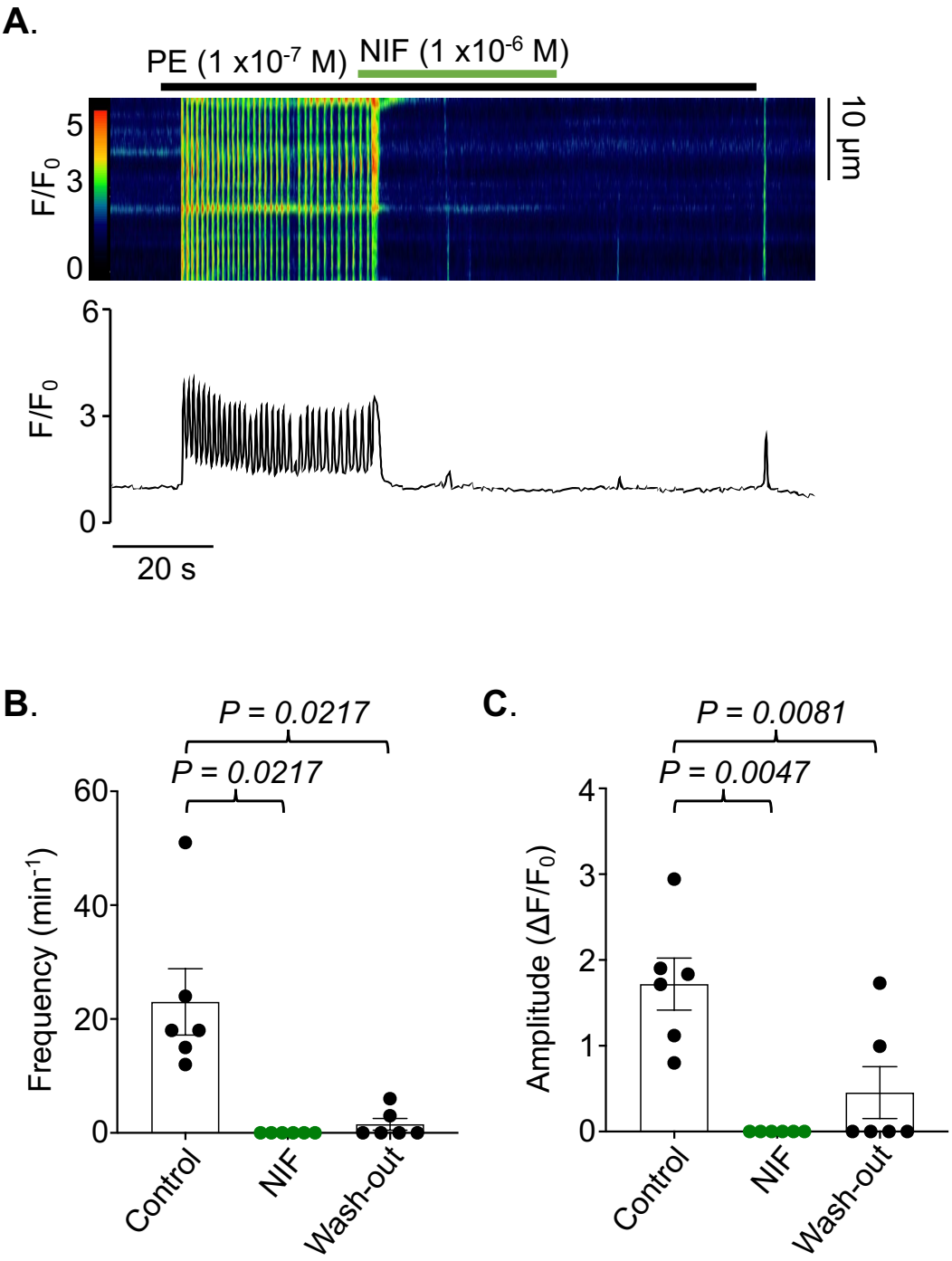


Figure 3.8: Effect of LTCC blocker, nifedipine (NIF), on low-PE-induced Ca^{2+} oscillations in isolated cells.
A. Representative spatiotemporal map and associated intensity plot of Ca^{2+} oscillations, evoked by 2 min application of 1 x10^{-7} M PE, and abolished by 1 x10^{-6} M NIF. **B+C.** Summary data for Ca^{2+} oscillation frequency (min^{-1}) and amplitude ($\Delta F/F_0$), respectively. Ca^{2+} oscillation frequency and amplitude were abolished in the presence of NIF (P=0.0217 and P=0.0047, respectively). A subsequent wash-out of NIF was unsuccessful and the frequency and amplitude of Ca^{2+} oscillations remained greatly attenuated (P=0.0217 and P=0.0081, respectively; n=6, N=6).

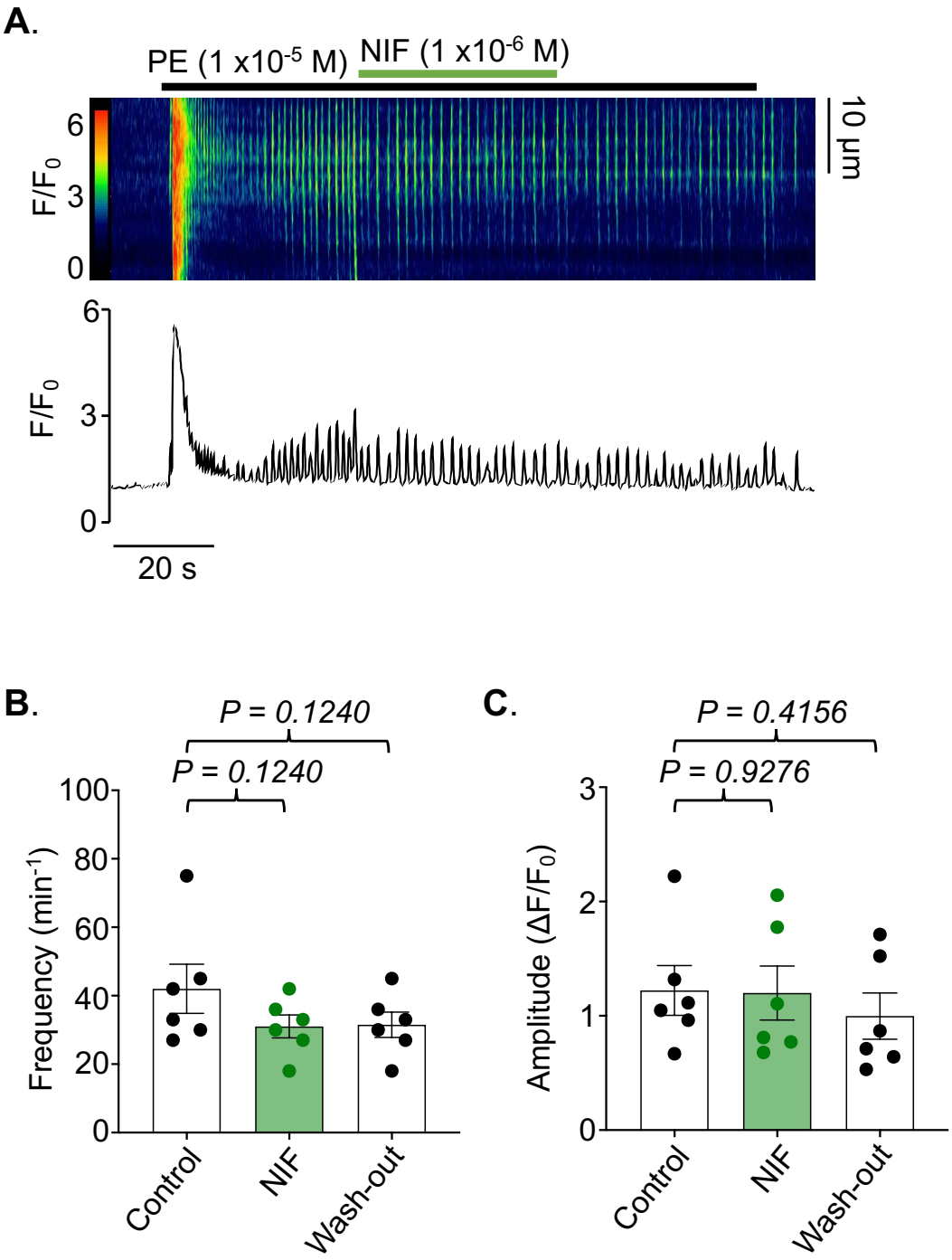


Figure 3.9: Effect of LTCC blocker, nifedipine (NIF), on high-PE-induced Ca^{2+} oscillations in isolated cells.
A. Representative spatiotemporal map and associated intensity plot of Ca^{2+} oscillations, evoked by 2 min application of 1 x10^{-5} M PE, and unaffected by 1 x10^{-6} M NIF. **B+C.** Summary data for Ca^{2+} oscillation frequency (min^{-1}) and amplitude ($\Delta F/F_0$), respectively. Ca^{2+} oscillation frequency and amplitude showed no significant effect in the presence of NIF (P=0.1240 and P=0.9276, respectively; n=6, N=6).

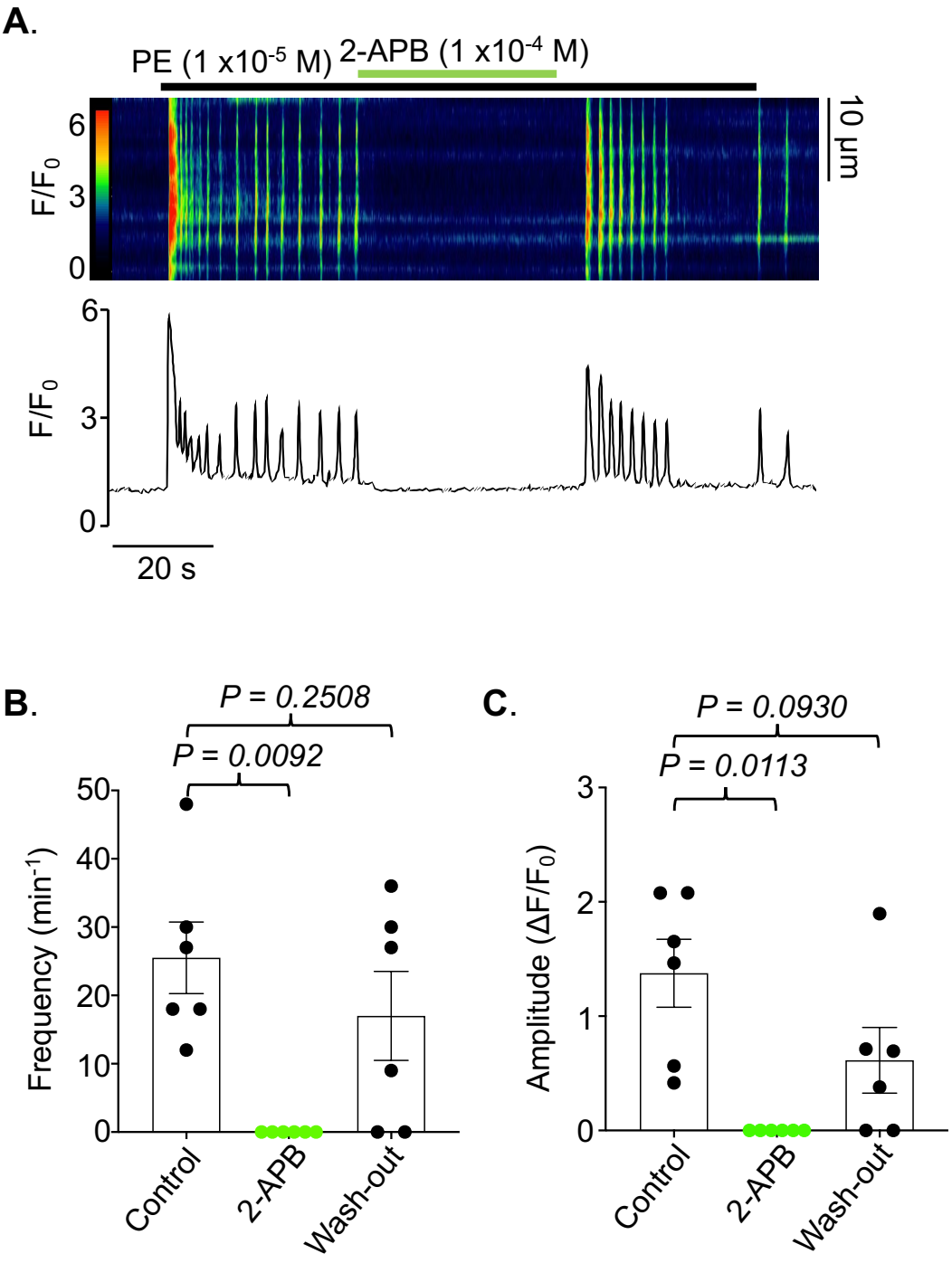


Figure 3.10: Effect of IP_3R antagonist, 2-Aminoethoxydiphenyl borate (2-APB), on high-PE-induced Ca^{2+} oscillations in isolated cells.

A. Representative spatiotemporal map and associated intensity plot of Ca^{2+} oscillations, evoked by 1 x10^{-5} M PE, and abolished by 1 x10^{-4} M 2-APB. **B+C.** Summary data for Ca^{2+} oscillation frequency (min^{-1}) and amplitude ($\Delta F/F_0$), respectively. Ca^{2+} oscillation frequency and amplitude were abolished in the presence of 2-APB (P=0.0092 and P=0.0113, respectively), and a subsequent wash-out of 2-APB returned Ca^{2+} oscillation frequency and amplitude similar to control levels (P=0.2508 and P=0.0930, respectively; n=6, N=6).

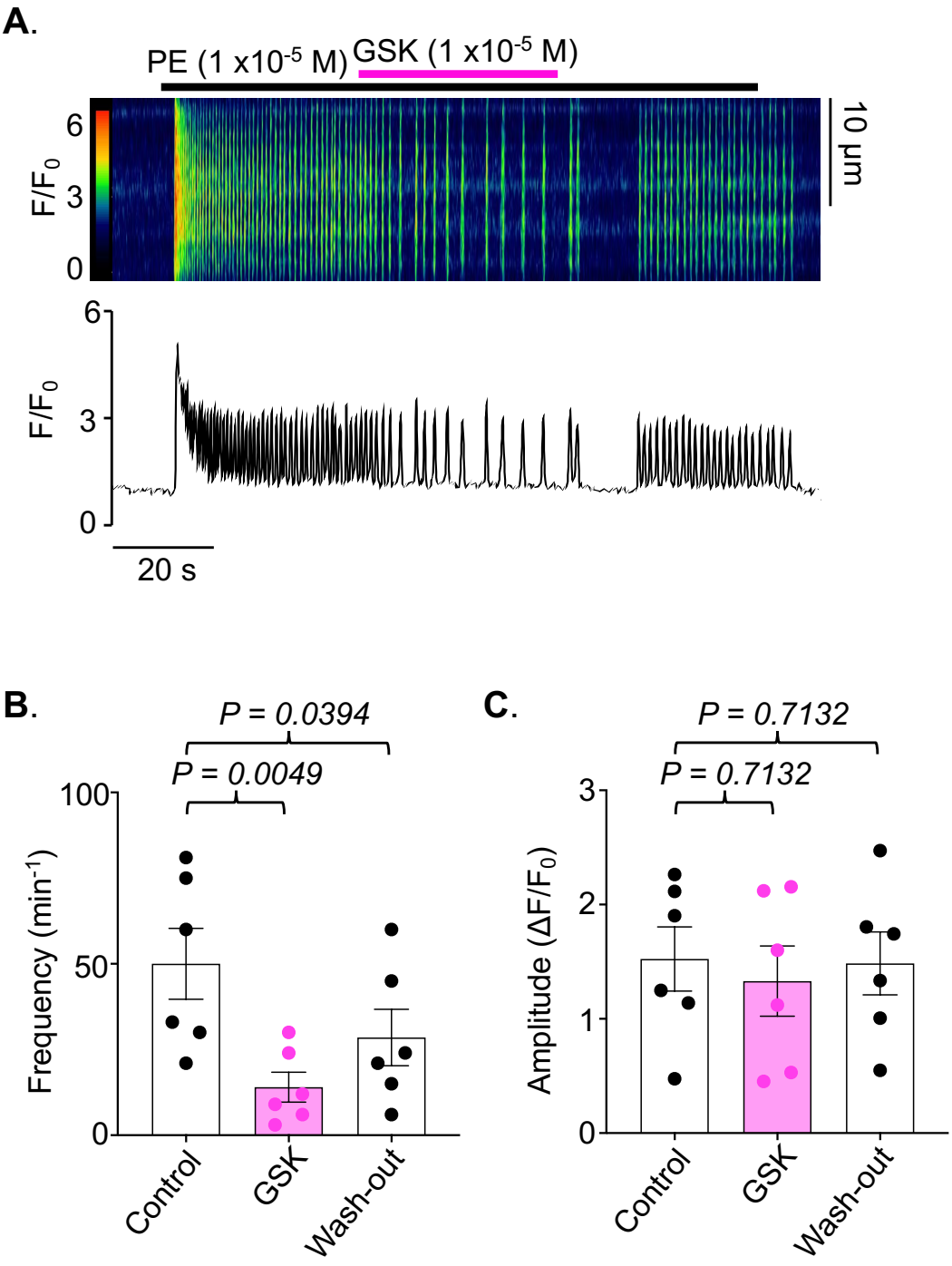


Figure 3.11: Effect of CRAC inhibitor, GSK-7975A (GSK), on high-PE-induced Ca^{2+} oscillations in isolated cells.
A. Representative spatiotemporal map and associated intensity plot of Ca^{2+} oscillations, evoked by 2 min application of 1 x10^{-5} M PE, and attenuated by 1 x10^{-5} M GSK. **B+C.** Summary data for Ca^{2+} oscillation frequency (min^{-1}) and amplitude ($\Delta F/F_0$), respectively. Ca^{2+} oscillation frequency was greatly attenuated in the presence of GSK (P=0.0049), and a subsequent wash-out of GSK was unable to return Ca^{2+} oscillation frequency and amplitude back to control levels (P=0.0394). Ca^{2+} oscillation amplitude was not-affected by GSK (P=0.7132; n=6, N=6).

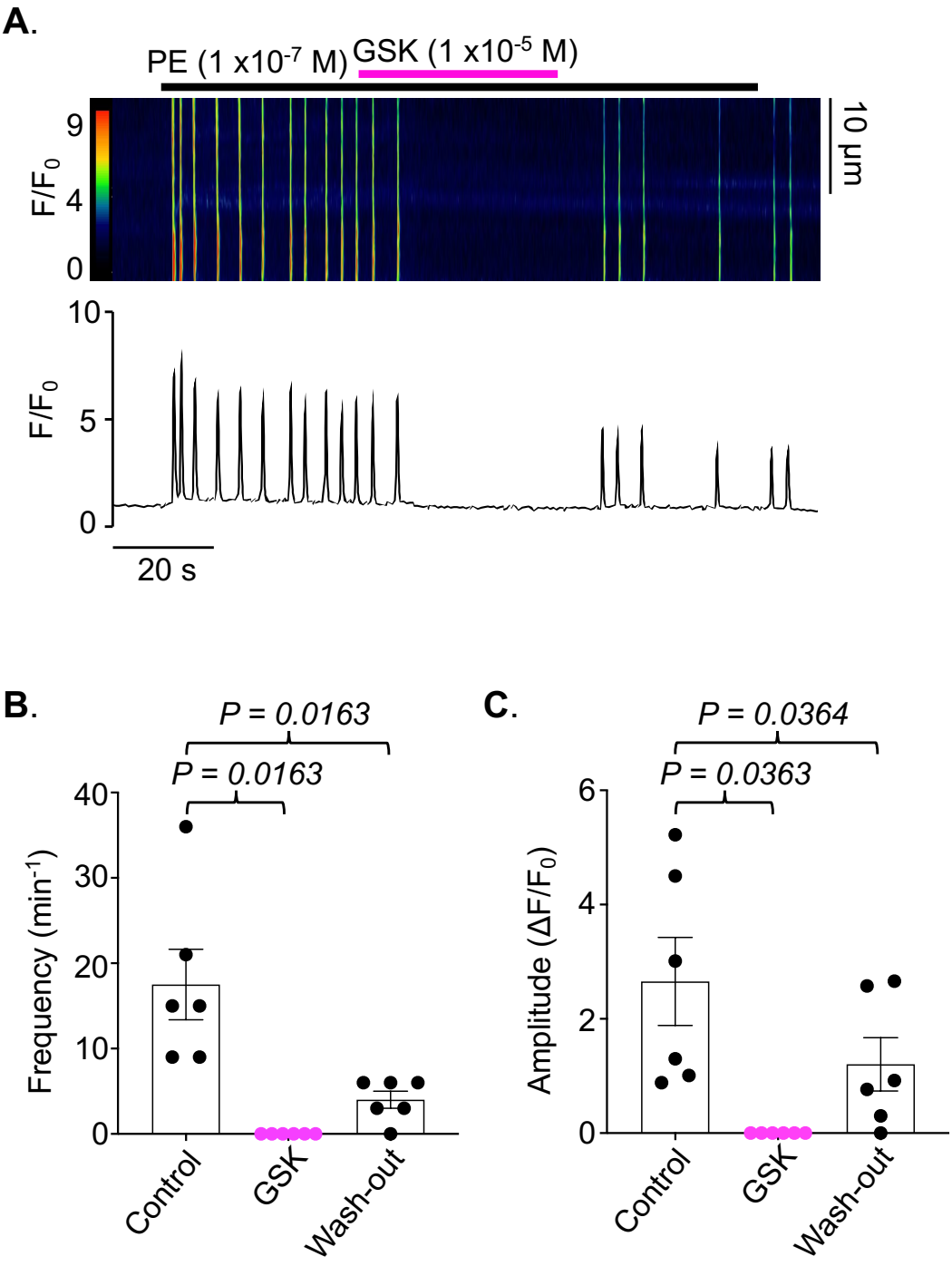


Figure 3.12: Effect of CRAC channel inhibitor, GSK-7975A (GSK), on low-PE-induced Ca^{2+} oscillations in isolated cells. **A.** Representative spatiotemporal map and associated intensity plot of Ca^{2+} oscillations, evoked by 2 min application of 1 x10^{-7} M PE, and abolished by 1 x10^{-5} M GSK. **B+C.** Summary data for Ca^{2+} oscillation frequency (min^{-1}) and amplitude ($\Delta F/F_0$), respectively. Ca^{2+} oscillation frequency and amplitude were abolished in the presence of GSK (P=0.0163 and P=0.0363, respectively), and a subsequent wash-out of GSK was unable to return Ca^{2+} oscillation frequency and amplitude back to control levels (P=0.0163 and P=0.0364, respectively; n=6, N=6).

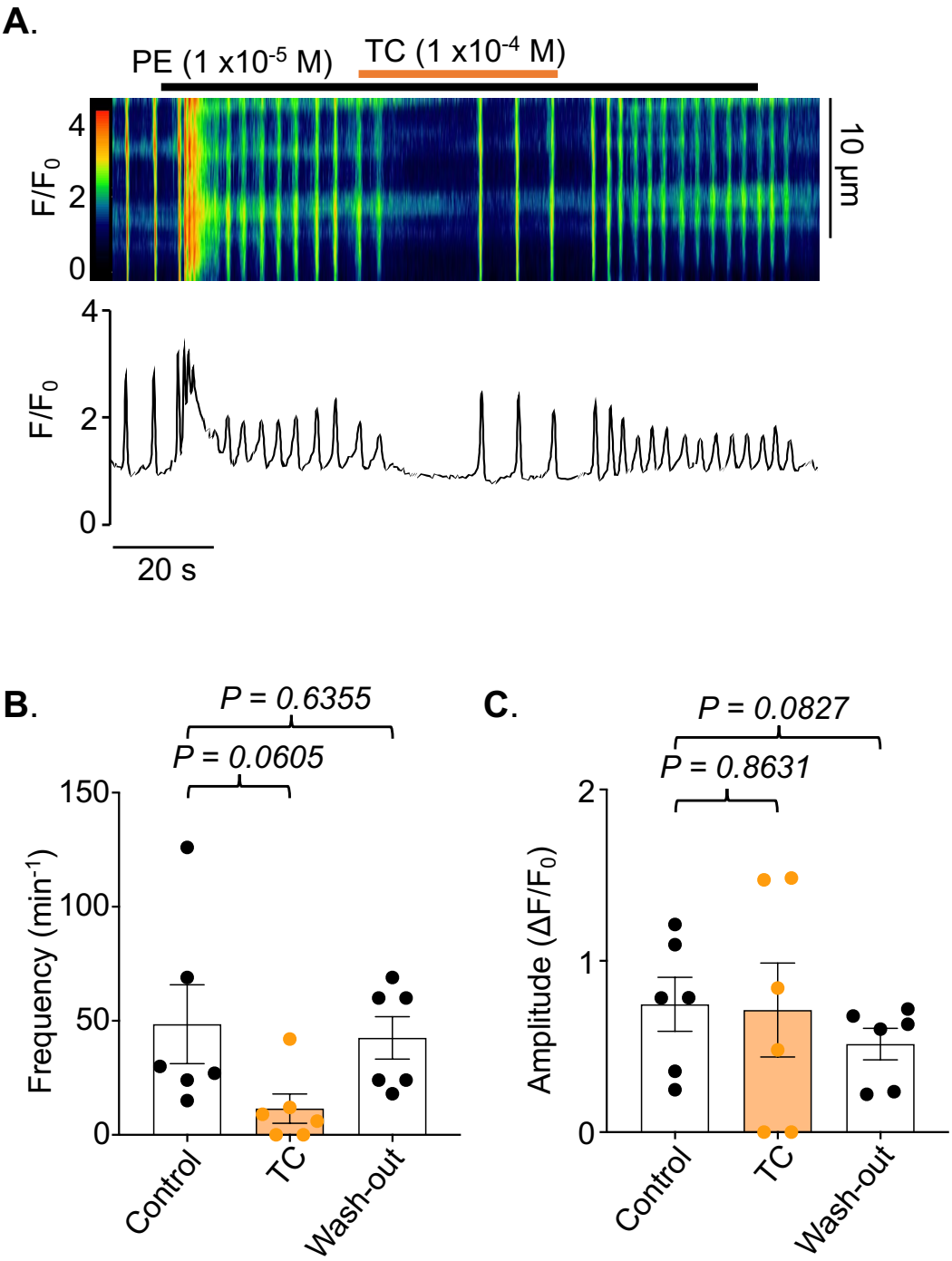


Figure 3.13: Effect of RyR antagonist, Tetracaine (TC), on high-PE-induced Ca^{2+} oscillations in isolated cells.
A. Representative spatiotemporal map and associated intensity plot of Ca^{2+} oscillations, evoked by 1 x10^{-5} M PE, and the addition of 1x10^{-4} M TC. **B+C.** Summary data for Ca^{2+} oscillation frequency (min^{-1}) and amplitude ($\Delta F/F_0$), respectively. Ca^{2+} oscillation frequency and amplitude were not significantly affected in the presence of TC (P=0.1235 and P=0.4174, respectively; n=6, N=6).

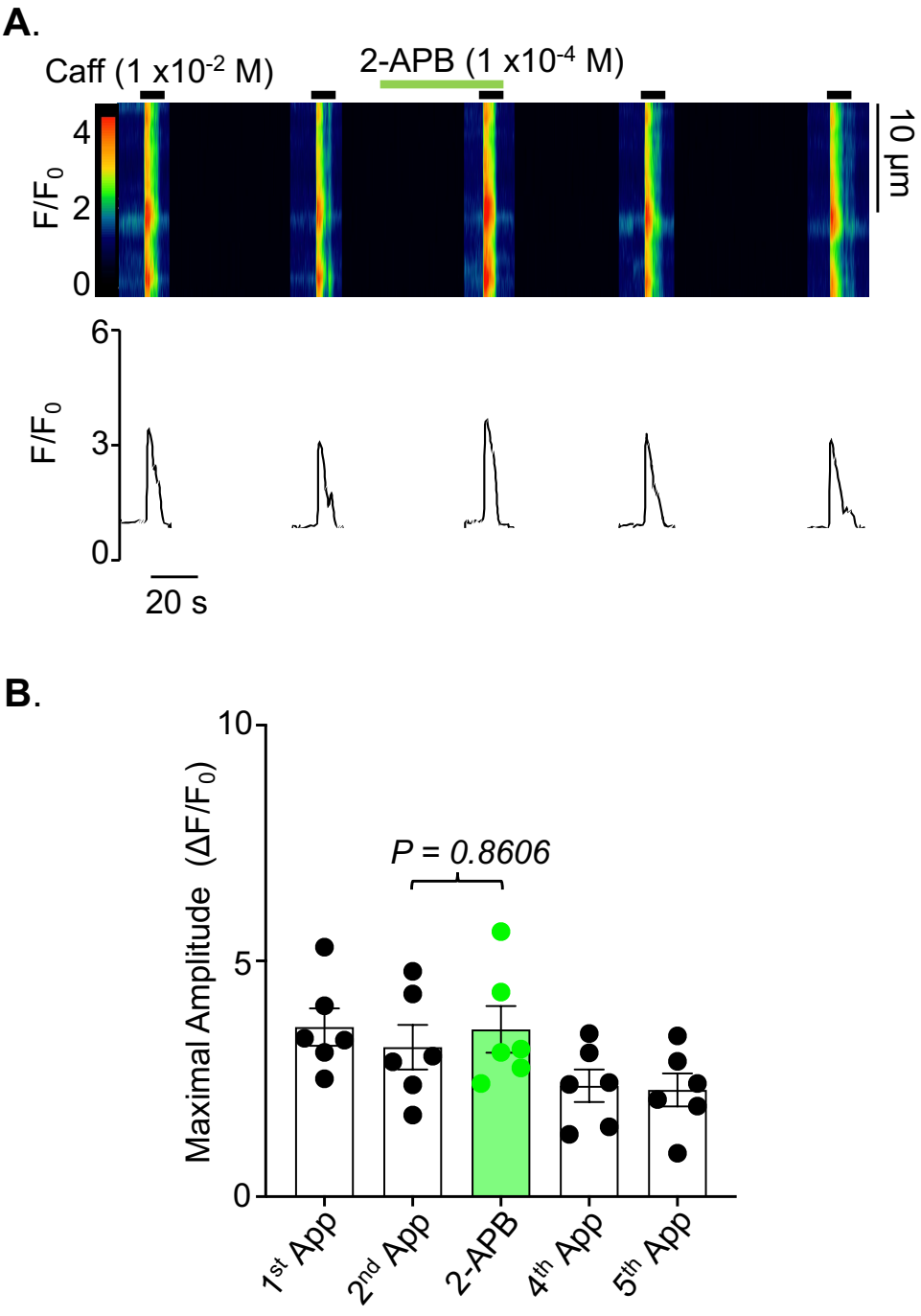


Figure 3.14: The effect of IP_3R antagonist, 2-Aminoethoxydiphenyl borate (2-APB), on caffeine (Caff)-induced store-release calcium spikes in isolated cells.
A. Representative spatiotemporal map and associated intensity plot of the effect of 1 x10^{-4} M 2-APB on Ca^{2+} spikes, evoked by 1 x10^{-2} M Caff. **B.** Summary data for maximum amplitude ($\Delta F/F_0$). Maximum amplitude showed no significant change in the presence of 2-APB (P=0.8606; n=6, N=6).

3.3 Discussion

The present study identified clear differences in the signalling mechanisms underlying the phasic and tonic components of α_1-adrenoceptor-mediated contractions in mouse CCSM. The findings indicated that phasic contractions depended critically on membrane excitability, Ca^{2+} influx through LTCCs, and depolarising ANO1 currents. In contrast, tonic contractions were primarily maintained by intracellular SR Ca^{2+} release and SOCE. Both modes ultimately rely on IP_3R activation, establishing IP_3R signalling as a central driver of adrenergic contractions and cytosolic Ca^{2+} rise in CCSM.

3.3.1 PE evoked concentration-dependent phasic and tonic contractions

Cumulative application of PE elicited two distinct forms of contraction. At low PE concentrations, rhythmic phasic contractions predominated, exhibiting minimal concentration dependency and persisting across all PE concentrations tested. In contrast, tonic contractures, characterised by large, sustained increases in tension, occurred only at higher PE concentrations and showed clear concentration dependence. These findings are consistent with prior observations in rabbit CCSM, where PE induced a transient rise in tone, followed by a sustained elevation in tension with superimposed phasic contractions (Hannigan *et al*., 2016).

Similarly, human CCSM exhibits spontaneous phasic contractions under basal conditions; however, increasing PE concentrations (1 $x10^{-7}$ M to 1 $x10^{-4}$ M) predominantly evoke tonic responses (Christ *et al*., 1990; Regadas *et al*., 2010). In the present study, using mouse CCSM, even low-PE-induced phasic contractions produced forces comparable to maximal tonic tension, suggesting that rhythmic contractile activity contributes substantially to basal tone during physiological sympathetic stimulation.

Following washout, phasic and tonic contractions to PE were modestly attenuated, likely reflecting α_1-adrenoceptor desensitisation or reduced G_q/PLC signalling (Lohse *et al*., 1990; Balla, 2013). However, the persistence of PE-evoked responses confirmed that the subsequent pharmacological effects were genuine and not due to tissue rundown.

3.3.2 Excitability dependence of phasic contractions

Low-PE-evoked phasic activity was abolished by NIF and Ani-9. NIF implicated LTCCs directly, whereas Ani-9, via inhibition of ANO1, was expected to hyperpolarise CCSM cells and suppress LTCC activation, thereby inhibiting the Ca^{2+} influx required for phasic contractions. Thus, phasic contractions appear to depend critically on voltage-dependent Ca^{2+} influx.

3.3.2.1 Role of LTCCs in contractility

Patch-clamp recordings in isolated rabbit CCSM cells identified voltage-dependent Ca^{2+} currents sensitive to NIF, confirming LTCC activity. McCloskey *et al*. (2009) further demonstrated that NIF abolished spontaneous Ca^{2+} waves in these cells, supporting LTCC-dependent Ca^{2+} influx. Although a Ni^{2+}-sensitive voltage-dependent Ca^{2+} current consistent with T-type Ca^{2+} channels was also detected, it did not contribute functionally to Ca^{2+} wave propagation. The present findings extend this work by showing that low PE concentrations evoke LTCC-sensitive Ca^{2+} oscillations, whereas high PE concentrations produce LTCC-insensitive oscillations, indicating a voltage-independent mechanism. This interpretation is supported by Doyle et al. (2012), who showed that PE enhances spontaneous Ca^{2+} waves, depolarisations and Ca^{2+}-activated Cl^- currents, while reducing NIF-sensitive LTCC current by ~30%. This inhibition was abolished by 2-APB, implicating IP_3R-mediated Ca^{2+} release from the SR. The resulting rise in cytosolic Ca^{2+} may promote Ca^{2+}-dependent inactivation of LTCCs via calmodulin binding to the channel C-terminus (Peterson et al., 1999). Accordingly, the reduced sensitivity of high-PE responses to NIF may reflect prior suppression of LTCC activity, shifting dependence toward alternative Ca^{2+} influx and/or release pathways.

Classic studies on human corpus cavernosum demonstrated a significant role for LTCCs, with channel blockers such as NIF, diltiazem, and verapamil suppressing tonic contractures induced by electrical field stimulation (Fovaeus *et al*., 1987). This tonic response was proposed to depend on sustained Ca^{2+} influx via LTCCs (Christ, 1995). This sustained influx is thought to reflect the LTCC “window current,” a voltage range where activation and inactivation overlap, allowing a steady, non-inactivating Ca^{2+} entry near the resting membrane potential (Catterall, 2000; Perez-Reyes, 2003). In arterial smooth muscle, this window current represents a key mechanism for maintaining myogenic tone, providing continuous Ca^{2+} influx to sustain basal

intracellular Ca^{2+} levels and contractility (Nelson *et al*., 1990). McCloskey *et al*. (2009) reported overlapping activation and inactivation curves of LTCCs in rabbit CCSM cells between -45 mV and -10 mV, supporting the potential for sustained influx in this tissue. However, in the present study, tonic tension in mouse CCSM was not affected by NIF, indicating that sustained contractions occur independently of LTCC activity.

In line with the role of the “window current” in resistance arteries, sustained tone is LTCC-dependent, as smooth-muscle-specific $Ca_V1.2$ deletion abolishes myogenic tone (Moosmang *et al*., 2003). In contrast to this, but in agreement with the present findings, both rat and human myometrial smooth muscle exhibit phasic contractions that depend on LTCCs; likewise, human detrusor smooth muscle develops phasic, LTCC-dependent contractions (Chien *et al*., 1996; Yart *et al*., 2022; Jezior *et al*., 2001). Tissue-specific differences in contractile responses may therefore be functionally significant: resistance arteries must maintain a steady lumen diameter and allow fine-tuning of vascular resistance, whereas the bladder, uterus, and corpus cavernosum must produce rapid, transient contractions during voiding, parturition, and detumescence, respectively.

3.3.2.2 Role of ANO1 channels in contractility

Blockade of ANO1, with Ani-9, abolished phasic activity, suggesting that Ca^{2+}-activated Cl^- currents may have an involvement in the depolarisation necessary to activate LTCC influx and phasic contractions. Given the relatively high intracellular concentration of Cl^- in smooth muscle cells which sets E_{Cl} positive to the resting membrane potential, activation of ANO1 channels is known to permit Cl^- efflux and inward currents, leading to membrane depolarisation and thereby facilitating recruitment of LTCCs. Recent work on mouse CCSM cells indicated that ANO1 is crucial for excitability, with current-clamp recordings showing that blockers of ANO1 (Ani-9 or CaCC(inh)-A01) prevented spontaneous transient depolarisations, inhibited STICs and phasic contractions (Lim *et al*., 2022b). These findings are consistent with observations in rabbit CCSM, where the Ca^{2+}-activated Cl^- channel blocker niflumic acid hyperpolarised cells by ~5 mV and abolished spontaneous action potentials (Hashitani et al., 2005). In contrast to the present findings and the work of Lim et al. (2022b), Ca^{2+}-activated Cl^- channel inhibition abolished STICs and attenuated tonic contractures in rabbit CCSM (Hannigan et al., 2017). These data underscore species-dependent differences in excitation–contraction coupling, whereby ANO1-mediated depolarisation in mouse CCSM predominantly underlies phasic contractility, whereas

in rabbit CCSM, Ca^{2+}-activated Cl^- currents contribute more substantially to sustained depolarisation and tonic contractures.

Similar electrophysiological evidence of Ca^{2+}-activated Cl^- currents influencing excitability has been reported in vascular and airway smooth muscles, where Ca^{2+}-release-induced activation of Cl^- channels produces depolarising inward Cl^- currents that trigger LTCC-dependent Ca^{2+} influx and contraction (Large & Wang, 1996; Leblanc *et al*., 2005; Wray *et al*., 2021). Consistent with this mechanism, 2-APB abolished both phasic and tonic contractions, supporting the hypothesis that IP_3R-driven Ca^{2+} release activates ANO1, leading to depolarisation and subsequent LTCC influx. This model aligns with classic work in rabbit corpus cavernosum, where Ca^{2+}-activated Cl^- currents underlie STICs modulated by NO-cGMP signalling (Craven *et al*., 2004), and subsequent evidence that Ca^{2+} waves trigger depolarising inward currents and LTCC recruitment (Sergeant *et al*., 2009; McCloskey *et al*., 2009). Evidence of a relationship between IP_3R, ANO1 and LTCCs ($Ca_v1.2$) is widespread. In mouse pulmonary arterial smooth muscle, genetic ablation or pharmacological inhibition of ANO1, $Ca_v1.2$, or IP_3Rs each similarly attenuates agonist-evoked Ca^{2+} waves and vascular tone (Akin *et al*., 2023). In lymphatic smooth muscle, IP_3R_1 activity is required for diastolic ANO1 activation and pressure-dependent chronotropy, establishing that IP_3R-derived Ca^{2+} release facilitates ANO1-mediated depolarisation that, in turn, mediates voltage-gated Ca^{2+} influx (Zawieja *et al*., 2023).

3.3.3 SR Ca^{2+} release dependence of tonic contractions

In contrast to phasic contractions, high-PE-induced tonic contractures persisted despite LTCC blockade with NIF and ANO1 inhibition with Ani-9, indicating a membrane potential-independent mechanism. Instead, IP_3R and CRAC channel inhibitors profoundly attenuated tonic contractures, indicating that these pathways sustain cytosolic Ca^{2+} through store release and refilling.

3.3.3.1 Role of IP_3Rs in contractility

IP_3Rs have well-established functional roles in smooth muscle tone. *In vivo* aortic smooth muscle showed markedly attenuated contractility to vasoconstrictors in a smooth muscle-specific IP_3R-knockout (Lin *et al*., 2016). Pharmacological inhibition of IP_3Rs with 2-APB or xestospongin C similarly reduces constriction in isolated aortic and mesenteric arteries, indicating that IP_3R activity provides the initial Ca^{2+} release necessary to maintain depolarisation and Ca^{2+} influx (Fransen *et al*., 2015; Eid *et al*.,

2018). Moreover, mouse aortic smooth muscle exhibits phasic and tonic responses to α_1-adrenergic stimulation, yet, in contrast to our findings in CCSM, the phasic component was sensitive to IP_3Rs and the sustained tonic response maintained by LTCC and non-selective cation channel influx (Fransen *et al*., 2012; 2015).

2-APB abolished both phasic and tonic components of mouse CCSM contractions; given that α_1-adrenoceptor activation stimulates phospholipase C, generating IP_3, these results position IP_3R-mediated Ca^{2+} release as the initiator for both types of contraction. Consistent with this, rabbit CCSM studies demonstrate that SR Ca^{2+} release underlies cellular excitability, with STICs and spontaneous depolarisations abolished by SERCA inhibitor cyclopiazonic acid (CPA) and 2-APB (Craven et al. 2004; Hashitani et al. 2005). The dependence of tonic contractures on SR Ca^{2+} release may reflect a phenomenon in which high intracellular Ca^{2+} stimulated by high concentrations of PE inactivates LTCCs, thereby shifting reliance toward intracellular Ca^{2+} mobilisation to sustain contraction (Doyle et al., 2012). These tonic responses may be sustained via activation of SOCE, utilising CRAC (Orai) channels.

3.3.3.2 Role of CRAC channels in contractility

STIM-Orai-mediated SOCE is present and functionally contributes to contractions in rat and human CCSM (Sevilleja-Ortiz *et al*., 2020; 2021; 2022). Human CCSM express STIM-1 and Orai-1 proteins and contribute to SOCE after store-depletion, by thapsigargin (SERCA inhibitor), which was subsequently inhibited with CRAC channel blockers (SKF96365; Sung *et al*., 2012). Human CCSM contractile studies showed that Orai channel inhibition, with YM-58483, attenuated tonic contractures (Sevilleja-Ortiz *et al*., 2020). In CCSM from men with ED, adrenergic hypercontractility was reversed by Orai channel inhibition, while tonic contractions exhibited increased sensitivity to Orai inhibition, coinciding with elevated Orai-1/3 protein expression; this suggested a pathophysiological up-regulation of this pathway that contributed to CCSM tone (Sevilleja-Ortiz *et al*., 2020). The findings of this study support these findings, as tonic contractures were abolished by GSK-7975A.

However, the mechanism underlying the increase in phasic contraction amplitude and duration in the presence of GSK-7975A, despite a decrease in frequency, remained unclear. In Ca^{2+} imaging experiments, GSK-7975A reduced the frequency, but did not abolish Ca^{2+} oscillations induced by high-PE, and it did not reduce their amplitude. Under physiological conditions, Ca^{2+} influx with Orai channels

contributes to the refilling of the SR Ca^{2+} content. Inhibition of this influx, causes partial SR Ca^{2+} depletion, requiring the recovery period to be increased between Ca^{2+} release events and decreasing frequency (Verkhratsky *et al*., 2005; Takahashi *et al*., 2013). Notably, a reduction in oscillation frequency may permit greater SR Ca^{2+} recovery between events, resulting in preservation of Ca^{2+} oscillation amplitude despite reduced Ca^{2+} influx. Interestingly, phasic contractions in the presence of GSK-7975A were increased in both duration and amplitude, suggesting that the total force generated over a given time interval may be maintained relative to control conditions. This indicated that inhibition of SOCE did not reduce Ca^{2+} signalling, but instead shifts from high-frequency, short-duration events to lower-frequency, more sustained contractions.

Furthermore, GSK-7975A abolished low-PE Ca^{2+} oscillations and phasic contractions, indicating that Orai channels contribute to the Ca^{2+} influx underlying these events. While phasic activity likely involves IP_3R-mediated SR Ca^{2+} release, ANO1 activation, membrane depolarisation and subsequent LTCC opening, the rapid onset of GSK-7975A effects argues against a mechanism solely dependent on SR Ca^{2+} depletion. Instead, Orai-mediated Ca^{2+} influx may provide a subplasmalemmal Ca^{2+} increase that sensitises IP_3R/RyR-dependent release and supports Ca^{2+} wave propagation. Inhibition of this pathway would impair Ca^{2+}-induced Ca^{2+} release and oscillatory activity independently of SR store depletion. This interpretation is supported by Chen and Sanderson (2016), who showed that GSK-7975A abolished Ca^{2+} oscillations in airway smooth muscle cells without preventing IP_3-mediated SR Ca^{2+} release following photolysis of caged IP_3.

A discrepancy was observed between Ca^{2+} imaging and tension recordings during high-PE stimulation. GSK-7975A evoked large-amplitude, long-duration, low-frequency contractions, while Ca^{2+} imaging showed only a reduction in oscillation frequency, with no change in amplitude or duration. This dissociation suggested that the enhanced phasic contractions are likely driven by altered Ca^{2+} sensitisation mechanisms rather than by changes in cytosolic Ca^{2+} levels.

Ca^{2+} sensitisation of smooth muscle contraction is mediated by inhibition of myosin light-chain phosphatase via RhoA/ROCK-dependent phosphorylation of MYPT1 and PKC-dependent phosphorylation of CPI-17, thereby increasing force at a given cytosolic Ca^{2+} concentration (Kimura *et al*., 1996; Somlyo and Somlyo, 2003). SOCE via the STIM-1/Orai-1 pathway may contribute indirectly to Ca^{2+} sensitisation by providing sustained Ca^{2+} entry capable activating Ca^{2+}-dependent PKC and RhoA-

associated pathways. Consistent with this, Ca^{2+} influx has been shown to promote activation of both PKC and RhoA signalling (Mogami et al., 2003; Singh et al., 2007). However, STIM-1 has also been reported to regulate RhoA activity independently of Orai-mediated Ca^{2+} influx (Shinde et al., 2013), suggesting that coupling between SOCE and Ca^{2+} sensitisation may involve both Ca^{2+}-dependent and Ca^{2+}-independent mechanisms.

Building on these findings, it is important to recognise that STIM/Orai-mediated Ca^{2+} influx is not limited to contractility but also plays a critical role in phenotypic remodelling (Trebak, 2012). In VSM, enhanced SOCE via STIM1 and Orai-1 has been shown to promote proliferation and migration, reflecting a shift away from a contractile phenotype towards a synthetic, non-contractile state (Potier et al., 2009). Similarly, Orai-1-dependent Ca^{2+} entry has been linked to activation of transcriptional pathways such as NFAT signalling, which are associated with cellular growth and phenotypic switching (Gwack et al., 2007). Evidence from airway smooth muscle further supports this concept, where STIM-1 and Orai-1 are required for both proliferation and remodelling responses (Johnson et al., 2022).

Importantly, phenotypic remodelling has been demonstrated in corpus cavernosal smooth muscle cells. Experimental models of ED, as well as human tissue studies, have shown a shift from a differentiated contractile phenotype towards a synthetic state, characterised by downregulation of contractile proteins, such as α-actin and myosin heavy chain, alongside increased extracellular matrix deposition and fibrosis (Ferrini et al., 2006; Zhang et al., 2011). In this context, the upregulation of Orai-1/3 protein expression observed in CCSM from patients with ED (Sevilleja-Ortiz et al., 2020; 2021) may represent a pathological adaptation that enhances Ca^{2+} influx and SR refilling to support contractile activity. However, given the established role of STIM/Orai-mediated Ca^{2+} entry in driving smooth muscle proliferation and phenotypic modulation in smooth muscle, it is also plausible that increased SOCE contributes to the transition towards a synthetic phenotype in CCSM.

3.3.3.3 Role of RyRs in high-PE Ca^{2+} oscillations

Initial suppression of high-PE Ca^{2+} oscillations by TC implies that ryanodine receptors (RyRs) are integral to the propagation of Ca^{2+} waves, although the transient nature of the inhibition (breakthrough) complicates this interpretation. The breakthrough phenomenon during continuous TC exposure, also observed in cardiac

muscle (Overend *et al*., 1997), is thought to result from SR Ca^{2+} overloading that triggers spontaneous RyR reopening (store-overload-induced Ca^{2+} release; Overend *et al*., 1997).

In smooth muscle, RyRs are not typically the primary initiators of Ca^{2+} release but instead serve to amplify IP_3R-mediated signals through Ca^{2+}-induced Ca^{2+} release (CICR). Small, localised Ca^{2+} elevations from IP_3R clusters can activate adjacent RyR channels, producing Ca^{2+} sparks or propagating Ca^{2+} waves (Iino *et al*., 1994; Boittin *et al*., 1999; Jaggar *et al*., 2000). Yet, RyRs in rat CCSM cells generate prominent Ca^{2+} sparks with unusually large spatial spread and duration, indicating robust SR Ca^{2+} release (Williams and Sims, 2007). Rabbit and mouse CCSM cells generate spontaneous Ca^{2+} waves, which are attenuated with 2-APB, yet small localised events remain, suggesting RyR-dependent Ca^{2+} release is required for initiation, and IP_3Rs are required for propagation (Sergeant *et al*., 2009; Thornbury *et al*., 2019). Consistent with this, in rabbit urethral interstitial cells, Ca^{2+} wave propagation depends on IP_3R-mediated Ca^{2+} release and sensitisation via Ca^{2+} influx mechanisms, while localised release events can persist independently of IP_3R activity, supporting a model in which RyR-mediated Ca^{2+} release events contribute to initiation (Drumm et al., 2015). In contrast, the present data demonstrate that PE-evoked Ca^{2+} oscillations are abolished by 2-APB, indicating that agonist-induced oscillations are initiated via IP_3R-mediated Ca^{2+} release. Together, these findings support a model in which RyRs predominantly amplify Ca^{2+} events, initiated via IP_3Rs, via CICR under agonist-stimulated conditions.

3.3.4 Physiological and therapeutic implications

PE-induced phasic contractions of mouse CCSM occur at frequencies of ~5-10 per minute with amplitudes comparable to maximal tonic responses, indicating they can significantly contribute to maintaining penile flaccidity by preventing venous trapping of blood. Their dependence on LTCC Ca^{2+} influx and membrane potential suggests a mechanism in which IP_3R-mediated Ca^{2+} release activates ANO1 channels, causing depolarisation and subsequent Ca^{2+} entry through LTCCs. This depolarisation-driven coupling may synchronise activity between adjacent myocytes via gap junctions, coordinating propagating Ca^{2+} waves that underpin rhythmic contractions.

In contrast, tonic contractions emerge at higher agonist concentrations and appear independent on membrane potential or LTCCs, instead reflecting direct SR Ca^{2+} release through IP_3R and possibly RyR pathways. It could be speculated that given the unphysiological conditions required to generate tonic responses, these contractions likely correspond to pathophysiological adrenergic activation, as might occur during stress or impaired NO signalling, leading to prolonged constriction and ED.

Together, these findings support a model in which phasic activity maintains the flaccid state under physiological conditions, while tonic contractures contribute to pathological hypercontractility. The dependence of phasic contractions on LTCC-mediated Ca^{2+} influx and ANO1-driven depolarisation, and of tonic contractures on IP_3R- and CRAC-mediated Ca^{2+} signalling, identifies multiple pharmacologically distinct targets that could facilitate CCSM relaxation through mechanisms independent of current PDE5-based therapies

3.3.5 Limitations and future directions

Several limitations warrant consideration. Although 2-APB is widely used as an IP_3R inhibitor, structural studies indicate it can also bind to RyR domains (Ansari et al., 2014); moreover, having effects on SR store Ca^{2+} refilling (Diver et al., 2001) and SOCE (Bootman et al., 2002). 2-APB was found not to inhibit caffeine-evoked Ca^{2+} spikes, suggesting no inhibitory effects on store-refilling or RyRs (Fig3.14). Yet, TC has been shown to inhibit IP_3Rs (MacMillan et al., 2005), and GSK-7975A has been suggested to modestly inhibit LTCCs and TRPV6 channels in HEK-293 cells (Derler et al., 2013). Contrary to this, experiments performed by Dwivedi et al. (2023) GSK-7975A had no inhibitory effects on LTCC current in bronchial myocytes.

Taken together, despite the well-established potency of the pharmacological tools used, off-target effects cannot be entirely excluded. Future studies employing photolysis of caged IP_3 to isolate IP_3R function, selective isolation of SOCE to define STIM-Orai involvement, and complementary genetic approaches using isoform-specific silencing would further support the findings of this chapter.

Second, Ca^{2+} imaging was performed only on isolated cells, limiting a possible extrapolation to tissue-level CCSM activity. Future experiments employing whole-tissue Ca^{2+} imaging in WT or transgenic (Acta2-GCaMP8.1-mVermilion-expressing mice) sections of CCSM are necessary to differentiate phasic and tonic Ca^{2+}

responses. This approach would provide mechanistic insight into the propagation of Ca^{2+} waves underlying phasic and tonic contractions, thereby clarifying their functional significance.

4. Results Chapter 2:

KCNQ-encoded voltage-dependent potassium (K_V7) alpha-subunits are expressed and form functional channels in corpus cavernosum smooth muscle

4.1 Introduction

The findings of Chapter 3 established that phasic contractions in mouse CCSM are critically dependent on membrane excitability, requiring Ca^{2+} influx through LTCCs and depolarising currents through ANO1 channels. These findings implicate membrane potential as a central determinant of phasic contractile activity, and by extension, of the underlying coordinated Ca^{2+} signalling. Consistent with this, synchronised activity within the CCSM has long been postulated to arise from electrical coupling through connexin-43-containing gap junctions, which allow electrical signals and second messengers to propagate between adjacent cells, effectively enabling the CCSM to function as a syncytium (Campos de Carvalho et al., 1993; Moreno et al., 1993). Consistent with this concept, rabbit CCSM tissue displayed rapid intercellular Ca^{2+} waves, hypothesised to be dependent on membrane depolarisation (Sergeant et al., 2009). Thus, regulation of the resting membrane potential is likely a critical determinant of CCSM contractility, and its pharmacological manipulation may provide therapeutic avenues for ED.

Potassium (K^+) channels are major regulators of membrane potential in smooth muscle. Their opening promotes K^+ efflux, leading to membrane hyperpolarisation, deactivation of voltage-dependent Ca^{2+} channels (VDCCs), reduced Ca^{2+} influx, and ultimately relaxation through inhibition of Ca^{2+}-calmodulin-dependent myosin light chain kinase (MLCK) activation (Hayase *et al*., 2009). Among these, BK_{Ca} channels have been extensively studied. They are expressed at both transcript and protein levels in human CCSM (Andersson, 2011), and their pharmacological activation (e.g., with GoSlo-SR5-130) reduces spontaneous contractile activity, an effect reversed by the BK_{Ca} blocker iberiotoxin (Hannigan *et al*., 2017). In mouse models, genetic deletion of BK_{Ca} ($KCNMA1^{-/-}$) leads to heightened responsiveness to adrenergic agonists and impaired neurogenic relaxations, underscoring their functional significance (Werner *et al*., 2005).

Despite the established role of BK_{Ca} channels, CCSM cells retain outward K^+ currents in the presence of iberiotoxin or following genetic deletion of BK_{Ca}, suggesting contributions from additional K^+ channels (Malysz *et al*., 2001; Werner *et al*., 2005). Other K^+ channel families, such as ATP-sensitive (K_{ATP}) and intermediate/small-conductance Ca^{2+}-activated K^+ channels (IK_{Ca}/SK_{Ca}), have been implicated in CCSM relaxation (Seino and Miki, 2003; Jackson, 2022; Comerma-Steffensen *et al*., 2017,

2022). However, increasing attention has focused on voltage-dependent K^+ (K_v) channels, particularly those encoded by the *Kcnq* gene family (K_v7 channels).

K_v7 channels are slowly activating, non-inactivating K^+ channels that play key roles in setting the resting membrane potential in smooth muscle. In the CCSM, *KCNQ4*/*Kcnq4* and *KCNQ5*/*Kcnq5* have been identified as the predominant isoforms in humans and rats, respectively. Corresponding $K_v7.4$ and $K_v7.5$ α-subunits have been identified by immunocytochemistry (Jepps *et al*., 2016; Lee *et al*., 2020a). Functional evidence supports their contribution to CCSM excitability, with application of K_v7 activators (ML213 and BMS204352) eliciting endothelium-independent relaxations of pre-contracted CCSM strips, albeit, requiring high concentrations of activator to achieve modest effects; while blockade of K_v7 channels with XE-991 enhanced contractile tone (Jepps *et al*., 2016; Lee *et al*., 2020a).

Importantly, pathological models of ED showed reduced *Kcnq4* and *Kcnq5* expression. In diabetic and spontaneously hypertensive rats, diminished $K_v7.4/5$ expression correlated with impaired CCSM relaxation, suggesting that K_v7 dysfunction contributes to ED pathophysiology and that these channels may represent promising therapeutic targets (Jepps *et al*., 2016; Lee *et al*., 2020a). Similar alterations in K_v7 channel expression and function have also been reported in mesenteric (Ng *et al*., 2011), coronary (Morales-Cano *et al*., 2015), renal (Chadha *et al*., 2012) arteries during cardiovascular disease reinforcing their importance in smooth muscle physiology (Baresse *et al*., 2018).

However, despite this emerging evidence, the functional role of K_v7 channels in CCSM remains unclear, particularly in mouse tissue, which is widely used for mechanistic and transgenic studies of ED. Moreover, it is unclear how K_v7 channel activity influences both spontaneous and agonist-induced contractility, or how these effects relate to intracellular Ca^{2+} signalling, a key determinant of coordinated CCSM activity. Therefore, the present study aimed to characterise *Kcnq* expression in mouse CCSM and to determine the effects of K_v7 modulators on contractile behaviour and Ca^{2+} signalling.

4.2 Results

4.2.1 Expression of K_v7 channel subunits in mouse CCSM

To determine which K_v7 isoforms are expressed in mouse corpus cavernosum, end-point PCR was performed using cDNA extracted from crural tissue. Amplicons corresponding to *Kcnq1, Kcnq3, Kcnq4*, and *Kcnq5* were detected, whereas *Kcnq2* was not observed (Fig4.1A). The specificity of each primer pair was confirmed using mouse brain cDNA as a positive control (Fig4.1B), and no amplification was observed in non-template controls (Fig4.1C). Quantitative PCR (qPCR) revealed a clear expression hierarchy, with *Kcnq5* transcripts most abundantly expressed relative to *β-actin*, while *Kcnq1, Kcnq3*, and *Kcnq4* were present at lower levels (Fig4.1D; n=6, N=3).

To corroborate these findings at the protein level, immunocytochemical staining was performed on freshly isolated CCSM cells. Cells displayed strong peripheral immunoreactivity for $K_v7.5$ α-subunits (Fig4.2A; n=6; each dispersal was from tissue pooled from two animals). Smooth muscle identity was confirmed by smooth muscle myosin heavy chain staining in parallel preparations (Fig4.2B; n=6). Positive controls using HEK-293 cells transfected with *Kcnq5* showed comparable $K_v7.5$ staining (Fig4.2C; n=6), whereas untransfected cells (Fig4.2D; n=6) and secondary-only controls were negative. Collectively, these data demonstrate that $K_v7.5$ is robustly expressed in CCSM at both the transcriptional and protein level, suggesting that this subunit is the principal functional isoform in this tissue.

4.2.2 K_v7 modulators modulate adrenergic contractions

Activation of α_1-adrenoceptors with PE (3×10^{-7} M) induced rhythmic phasic contractions, often superimposed on a modest increase in baseline tone (Fig4.3A). Time-control experiments demonstrated that neither the frequency (Fig4.3B; P=0.6827) nor the amplitude (Fig4.3C; P=0.3200; n=6, N=6) of these phasic contractions significantly changed over a 40 min observation period. However, these phasic contractions were affected by K_v7 pharmacological agents.

Application of the $K_v7.2$-5 activator retigabine (RTG, 1×10^{-5} M) rapidly reduced the frequency and amplitude of PE-induced contractions before abolishing them entirely (Fig4.4A-C; frequency: P=0.0038; amplitude: P=0.0235; n=6, N=6); with frequency falling from 6.20 ± 1.22 min^{-1} under 300 nM PE to 0.00 ± 0.00 min^{-1} in the

presence of RTG, and amplitude falling from 0.89 ± 0.28 mN to 0.00 ± 0.00 mN. Notably, RTG had no effect on the tone generated by 3 x10^{-7} M PE. To investigate this further, the effect of RTG was examined in mouse CCSM contracted across a range of PE concentrations.

Using a protocol consistent with Chapter 3 (Fig3.1-3.5), cumulative concentrations of PE (1 x10^{-7} M to 3 x10^{-5} M) were applied to generate distinct phasic and tonic contractile responses (Fig4.5A). Following a washout period, RTG was applied and the protocol repeated. RTG abolished phasic contractions (Fig4.5B), significantly reducing both frequency (Fig4.5C; P<0.0001) and amplitude (Fig4.5D; P<0.0001), while leaving tonic contractions intact (Fig4.5E; n=8, N=8). In contrast, XE-991 significantly potentiated PE-induced contractions at 3 x10^{-7} M, increasing both frequency and amplitude (Fig4.6A-C; frequency: P<0.0001; amplitude: P=0.0205; n=6, N=6), with frequency rising from 3.97 ± 0.63 min^{-1} under PE alone to 10.08 ± 0.97 min^{-1} in the presence of XE-991, representing a 154% increase, and amplitude increasing from 0.92 ± 0.25 mN to 1.25 ± 0.33 mN, a 36% increase.

Transcriptional analysis of *Kcnq* isoforms in CCSM indicated a small proportion of *Kcnq1* transcripts (Fig4.1D). To investigate whether K_v7.1 contributes to this activity, selective modulators were employed. The K_v7.1 blocker chromanol-293B (3 x10^{-5} M) produced no significant change in contraction frequency (Fig4.7A-B; P=0.1580) or amplitude (Fig4.7C; P=0.1267; n=6, N=6), with frequency measuring 6.70 ± 0.32 min^{-1} under PE alone and 6.23 ± 0.43 min^{-1} in the presence of chromanol-293B, and amplitude measuring 0.74 ± 0.19 mN and 0.70 ± 0.20 mN respectively. Similarly, the K_v7.1 activator ML277 (1 x10^{-5} M) failed to inhibit PE-induced phasic activity (Fig4.8A-C; frequency: P>0.9999; amplitude: P=0.2461; n=6, N=6), with frequency remaining unchanged at 5.63 ± 1.27 min^{-1} under PE alone and 5.63 ± 1.35 min^{-1} in the presence of ML277, and amplitude measuring 0.62 ± 0.10 mN and 0.60 ± 0.09 mN respectively. These findings indicated that K_v7.1 channels do not contribute significantly to contractile regulation in mouse CCSM.

A report by Rubi *et al*. (2017) indicated that RTG, at concentrations exceeding 1 x10^{-5} M, may exert off-target inhibitory effects on LTCCs. In these experiments, RTG abolished PE-induced phasic contractions, and subsequent application of XE-991 restored phasic activity, which is dependent on LTCC influx (Fig4.9A). Summary data confirmed that RTG significantly reduced contraction frequency from 6.38 ± 0.83 min^{-1}

^{1} under PE alone to 0.00 ± 0.00 min^{-1} (P=0.0001), and amplitude from 0.62 ± 0.11 mN to 0.00 ± 0.00 mN (P=0.0026), while XE-991 reinstated both parameters, restoring frequency to 13.50 ± 1.15 min^{-1} (P<0.0001) and amplitude to 0.70 ± 0.15 mN (P=0.0049; Fig4.9B-C; n=8, N=8). These findings suggested that RTG at 1 x10^{-5} M does not significantly block LTCCs, as the restoration of phasic contractions by XE-991 requires functional LTCC activity.

4.2.3 Effects of K_v7 blockade in the presence of endothelial and neurogenic inhibitors

To test whether K_v7 channels act independently of endothelial NO signalling or neurogenic transmitter release, tissues were treated with either the NOS inhibitor L-NNA (Fig4.10A; 1 x10^{-4} M) or the sympathetic neurotransmission inhibitor guanethidine (Fig4.11A; GE, 1 x10^{-5} M). Both inhibitors induced phasic contractions prior to PE application, with L-NNA evoking a frequency of 1.75 ± 0.46 min^{-1} and amplitude of 0.56 ± 0.26 mN, and GE evoking a frequency of 3.67 ± 0.40 min^{-1} and amplitude of 1.07 ± 0.20 mN (Fig4.10A/Fig4.11A).

In both conditions, application of XE-991 (1 x10^{-5} M) significantly enhanced the frequency of PE-induced phasic contractions (Fig4.10B, L-NNA: P=0.0106; Fig4.10B, GE: P=0.0065; n=6, N=6), with frequency increasing from 5.08 ± 1.36 min^{-1} under PE alone to 14.83 ± 1.26 min^{-1} with XE-991 in the L-NNA condition, representing a 192% increase, and from 7.08 ± 0.57 min^{-1} to 13.33 ± 1.01 min^{-1} in the GE condition, representing an 88% increase. However, contraction amplitude was unaffected (Fig4.11C, L-NNA: P=0.1992; Fig4.11C, GE: P=0.2041), measuring 0.73 ± 0.28 mN and 0.65 ± 0.26 mN under PE and XE-991 respectively in the L-NNA condition (a non-significant 11% decrease), and 1.68 ± 0.40 mN and 1.14 ± 0.21 mN respectively in the GE condition (a non-significant 32% decrease). These data suggested that K_v7 modulators exert their effects directly on smooth muscle excitability, independent of endothelial or neurogenic influences.

4.2.4 Effects of K_v7 modulators on PE-evoked Ca^{2+} oscillations

As established in Chapter 3, Ca^{2+} oscillations elicited in isolated CCSM cells by low- and high-PE concentrations were dependent and independent on membrane potential, respectively. To build upon this finding and elucidate the mechanism by

which K_v7 channels regulate phasic contractions, the effects of K_v7 modulators were examined on these Ca^{2+} oscillations.

Imaging of isolated CCSM cells confirmed that RTG suppressed low-PE Ca^{2+} oscillations (Fig4.12A-C; frequency: P=0.0147; amplitude: P=0.0021), with oscillation frequency falling from 23.00 ± 5.29 min^{-1} under PE alone to 0.00 ± 0.00 min^{-1} in the presence of RTG, with partial recovery to 11.00 ± 2.86 min^{-1} on washout (P=0.0536). Similarly, amplitude was reduced from 2.42 ± 0.36 F/F_0 to 0.00 ± 0.00 F/F_0 with partial recovery to 1.38 ± 0.33 F/F_0 on washout (P=0.0295). This contrasts with the effect of RTG on high-PE Ca^{2+} oscillations, which persisted in the presence of the drug (Fig4.13A-C; frequency: P=0.8585; amplitude: P=0.0669; n=6, N=6), with frequency remaining comparable across control (26.50 ± 5.45 min^{-1}), RTG (25.00 ± 3.44 min^{-1}), and washout (26.50 ± 3.04 min^{-1}) conditions, and amplitude measuring 1.54 ± 0.34 F/F_0, 1.23 ± 0.24 F/F_0, and 1.04 ± 0.21 F/F_0, respectively. Consistent with these findings, blockade of K_v7 channels with XE-991 potentiated low-PE Ca^{2+} oscillation frequency (Fig4.14A-B; P=0.0049) but had no significant effect on amplitude (Fig4.14C; P=0.3774; n=6, N=6), with frequency increasing from 9.50 ± 3.04 min^{-1} under PE alone to 26.00 ± 3.52 min^{-1} in the presence of XE-991, representing a 174% increase, with partial return to 14.00 ± 2.86 min^{-1} on washout, while amplitude remained comparable across PE (1.89 ± 0.31 F/F_0), XE-991 (1.57 ± 0.19 F/F_0), and washout (1.14 ± 0.27 F/F_0) conditions.

4.2.5 K_v7 channel modulators regulate spontaneous contractions

Approximately 50% of corpus cavernosum preparations developed spontaneous phasic contractions during equilibration, with no instances of notable spontaneous tone. Once established, spontaneous phasic activity persisted for at least 30 min (Fig4.15A), with a mean frequency of 3.2 min^{-1} (Fig4.15B) and amplitude of 1 mN (Fig4.15C). Time-control experiments demonstrated that neither the frequency (Fig4.15B; P=0.0826) nor the amplitude (Fig4.15C; P=0.6693) of these contractions changed significantly over successive 10 min intervals during a 30 min observation period (n=6, N=6).

Application of RTG (1 $x10^{-5}$ M) produced a progressive suppression of this spontaneous activity. In representative recordings, RTG first reduced contraction frequency before abolishing contractions completely within several minutes

(Fig4.16A). Grouped data confirmed that RTG significantly decreased both contraction frequency (Fig4.16B) and amplitude (Fig4.16C) compared with control (frequency: P<0.0001; amplitude: P=0.0009; n=6, N=6), with frequency falling from 3.13 ± 0.25 min^{-1} under spontaneous activity to 0.00 ± 0.00 min^{-1} in the presence of RTG, and amplitude falling from 0.96 ± 0.14 mN to 0.00 ± 0.00 mN. In all tissues tested, spontaneous contractions were completely suppressed by RTG, with no recovery during the period of observation.

Conversely, the K_v7 blocker, XE-991 (1 $x10^{-5}$ M), markedly increased the phasic activity of spontaneously contracting tissues (4.17A). Summary analysis demonstrated significant increases in frequency from 2.20 ± 0.46 min^{-1} to 6.80 ± 0.53 min^{-1} (Fig4.17B; P=0.0012), representing a 209% increase, and amplitude from 0.61 ± 0.15 mN to 1.21 ± 0.24 mN (Fig4.17C; P=0.0277; n=6, N=6), representing a 96% increase. Subsequent application of the LTCC antagonist, NIF (1 $x10^{-6}$ M), abolished XE-991-enhanced contractions (Fig3.17A; frequency: P=0.0001; amplitude: P=0.0121), confirming that K_v7-blockade-induced enhancement of phasic activity depended on Ca^{2+} influx through LTCCs.

4.2.6 K_v7 modulators influence spontaneous intracellular Ca^{2+} oscillations

Isolated CCSM cells exhibited whole-cell spontaneous Ca^{2+} oscillations at a mean frequency of 12.57 ± 3.19 min^{-1}, less frequent than those elicited by low- or high-PE stimulation (Fig3.6-3.7), with a mean amplitude of 1.99 ± 0.47 F/F_0, a spatial spread of 14.15 ± 1.49 μm (87.1 ± 6.6% of individual cell length), and a mean duration of 0.65 ± 0.15 s (Data not shown; n=12, N=12). Consistent with observations during low-PE stimulation (Fig3.8), spontaneous oscillations were abolished by LTCC inhibition. Application of NIF (1 $x10^{-6}$ M) abolished spontaneous oscillatory activity in all cells, with no recovery following washout (Fig4.18A-C; frequency: P=0.0013; amplitude: P=0.0226; n=6, N=6), with frequency falling from 10.67 ± 1.41 min^{-1} under spontaneous activity to 0.00 ± 0.00 min^{-1} in the presence of NIF, with no recovery on washout; and amplitude similarly reduced from 1.14 ± 0.29 F/F_0 to 0.00 ± 0.00 F/F_0, with no recovery on washout. Consistent with its effects on contractile activity, RTG also abolished spontaneous Ca^{2+} oscillations, with spontaneous activity frequency dropping from 13.50 ± 3.26 min^{-1} to 0.00 ± 0.00 min^{-1} in the presence of RTG, with partial recovery to 7.00 ± 0.63 min^{-1} on washout. Amplitude was similarly abolished

from 1.64 ± 0.58 F/F_0 to 0.00 ± 0.00 F/F_0, with partial recovery to 1.24 ± 0.38 F/F_0 on washout.

In contrast, XE-991 (1 $x10^{-5}$ M) either enhanced existing oscillations or induced activity in previously quiescent cells (Fig4.20A/Fig4.21A). Increases in frequency were consistent across experiments (Fig4.20B/Fig4.21B; P=0.0018 and P=0.0040, respectively), with frequency rising from 1.00 ± 0.63 min^{-1} under spontaneous activity to 17.00 ± 3.35 min^{-1} in the presence of XE-991, representing a 16 fold increase, and from 1.50 ± 0.67 min^{-1} to 15.00 ± 2.19 min^{-1} in the XE-991 and NIF experiment, representing a 9 fold increase. Changes in amplitude were variable and not statistically significant (Fig4.20C/Fig4.21C; P=0.2247 and P=0.2498, respectively; n=6, N=6), with amplitude measuring 0.28 ± 0.21 F/F_0 and 1.43 ± 0.30 F/F_0 before and during XE-991 respectively, and 0.50 ± 0.28 F/F_0 and 1.03 ± 0.15 F/F_0 in the XE-991 and NIF experiment. Upon washout, oscillation frequency decreased towards baseline (Fig4.20B; P=0.2978), recovering to 6.50 ± 2.11 min^{-1}, with amplitude returning to 1.05 ± 0.29 F/F_0. Subsequent addition of NIF abolished XE-991-induced oscillations (Fig4.21A), reducing frequency from 15.00 ± 2.19 min^{-1} to 0.00 ± 0.00 min^{-1} and amplitude from 1.03 ± 0.15 F/F_0 to 0.00 ± 0.00 F/F_0 (Fig4.21B-C; P=0.0040 and P=0.0030, respectively; n=6, N=6).

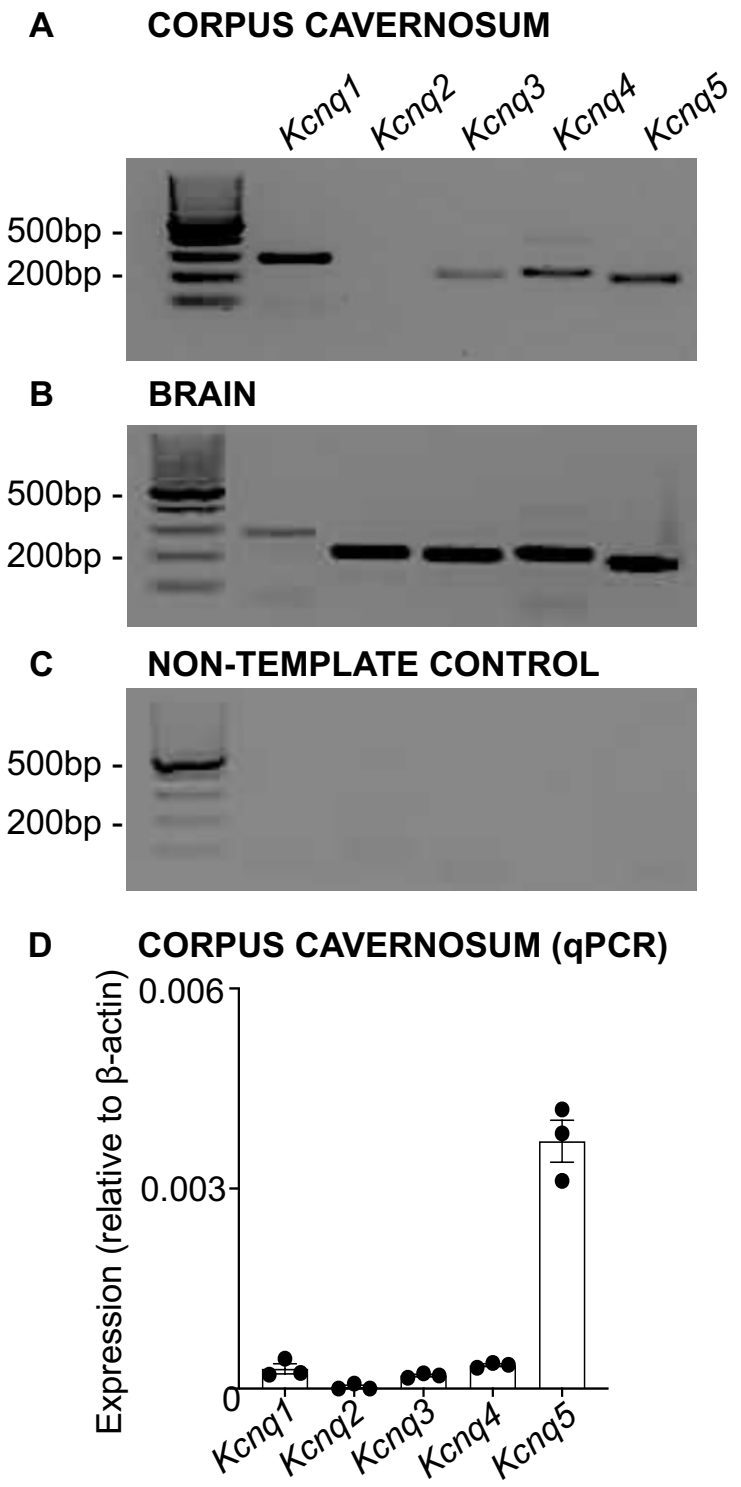


Figure 4.1: Transcriptional analysis of *Kcnq* isoforms. Expression of *Kcnq* isoform transcripts in RT-PCR using cDNA extracted from mouse corpus cavernosum (**A**), and brain (**B**), serving as a positive control. Amplicons were resolved via agarose gel (2%) electrophoresis, and visualised using SYBR safe (n=6, N=3). Non-template control was used for detection of contamination or non-specific amplification (**C**). **D**. Quantitative PCR of *Kcnq1-5* transcript expression relative to β-actin using corresponding primers used in RT-PCR (n=6, N=3).

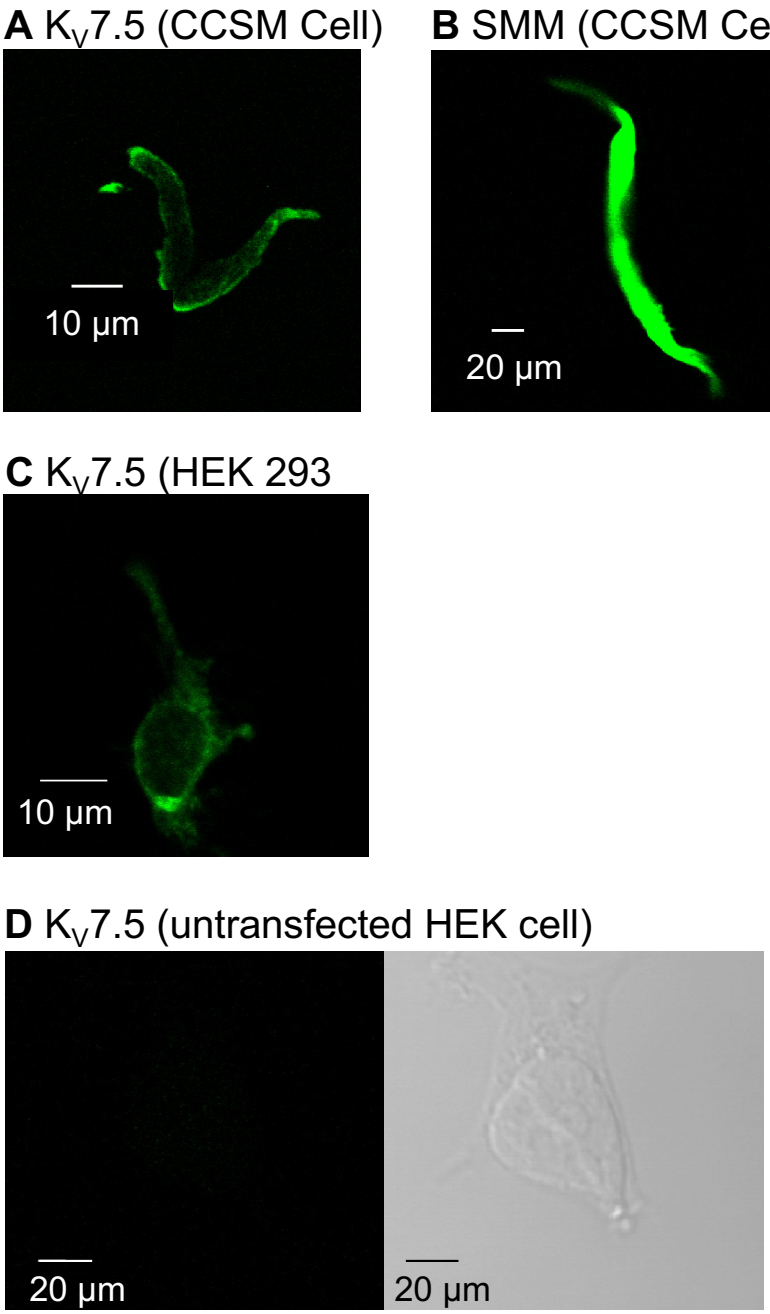


Figure 4.2: Immunocytochemical staining of K_V7.5 α-subunits. **A.** Representative photomicrograph showing that freshly isolated mouse CCSM cells were immunoreactive (green) to selective K_V7.5 antibody (n=6, N=6). **B**. Smooth muscle cells were identified by smooth muscle myosin-positive immunoreactivity (green; n=6, N=6). **C**. Positive control showing immunoreactivity in a *KCNQ5*-transfected HEK293 cell exposed to the same primary and secondary antibodies as in A. (n=6). **D**. Negative control showing lack of immunoreactivity in an untransfected HEK293 cell exposed to the same primary and secondary antibodies as in *A.* (n=6). Secondary-only antibody controls in native CCSM cells also failed to show reactivity (n=6 as for *D*, data not shown).

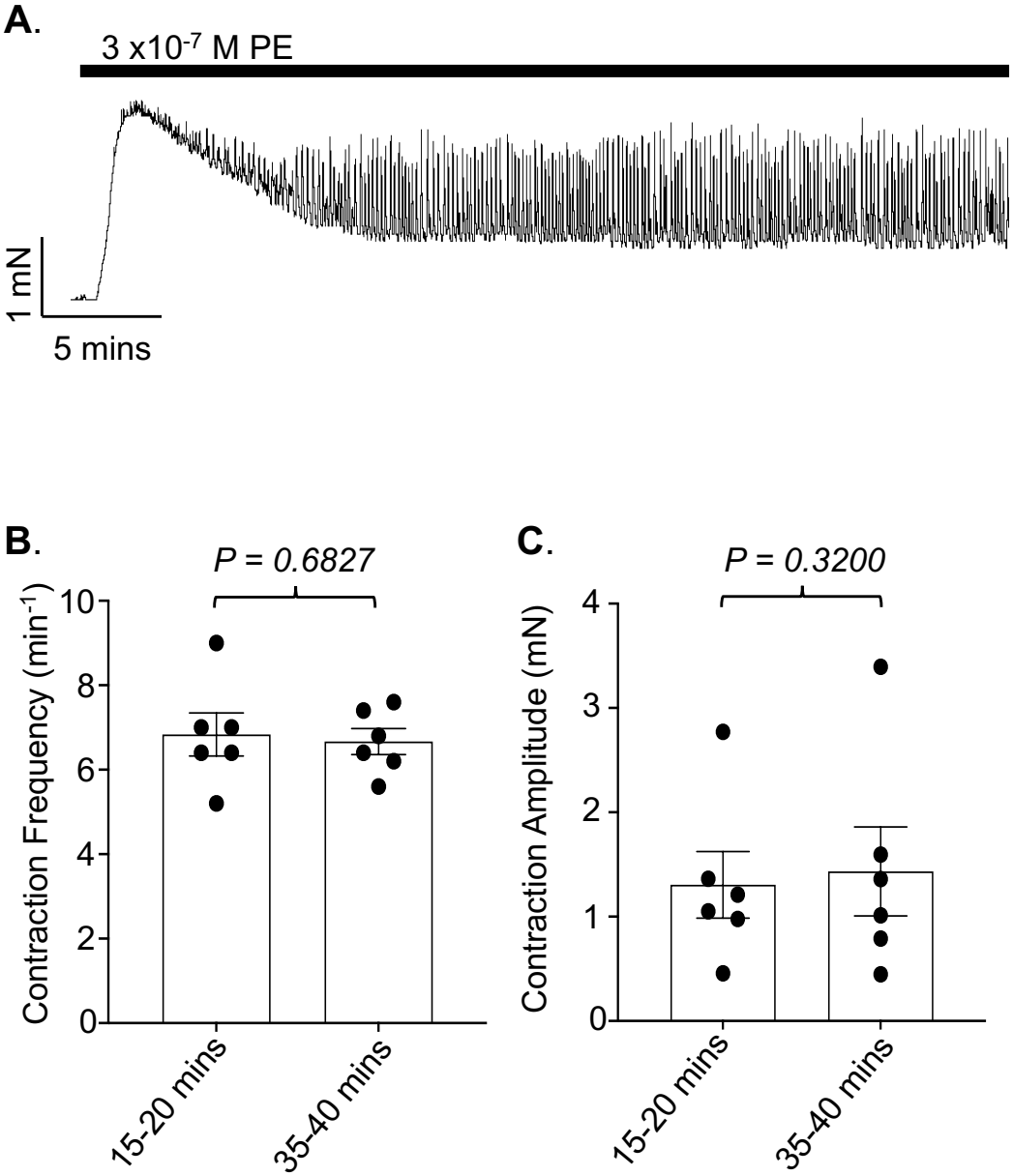


Figure 4.3: Time-control of Phenylephrine (PE)-induced phasic contractions.
A. Representative isometric tension recording demonstrating the development of phasic contractions induced by 3 x10^{-7} M PE. **B+C.** Summary data for phasic contraction frequency and amplitude, showing no significant decrease over the 40 min period (n=6, N=6).

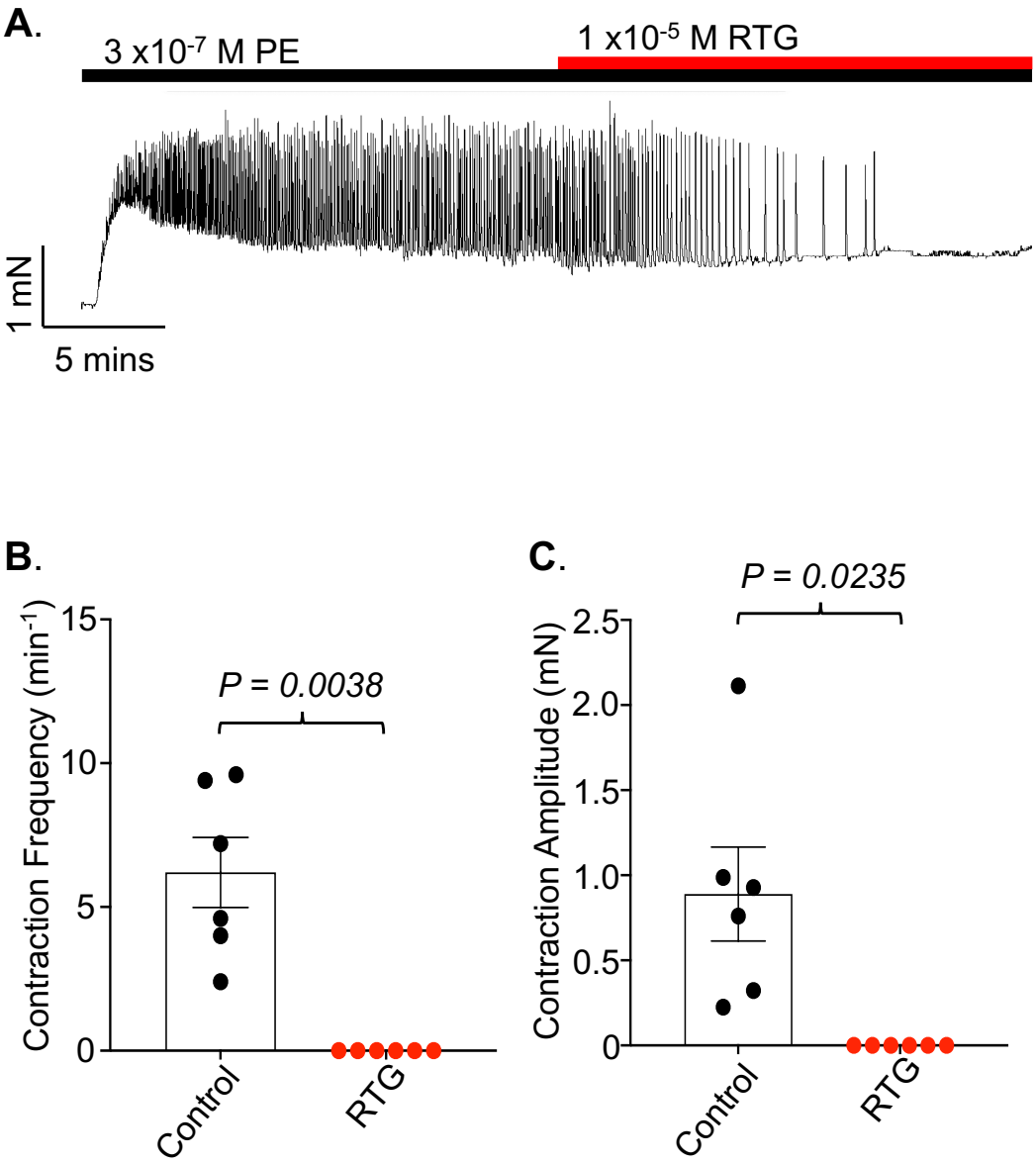


Figure 4.4: Phenylephrine (PE)-induced contractions were abolished by a K_V7.2-5 activator, retigabine (RTG).
A. Representative isometric tension recording demonstrating the effect of 1 x10^{-5} M RTG on 3 x10^{-7} M PE-induced phasic contractions. **B+C.** Summary data for the inhibitory effect of RTG on phasic contraction frequency and amplitude (P=0.0038 and P=0.0235, respectively; n=6, N=6).

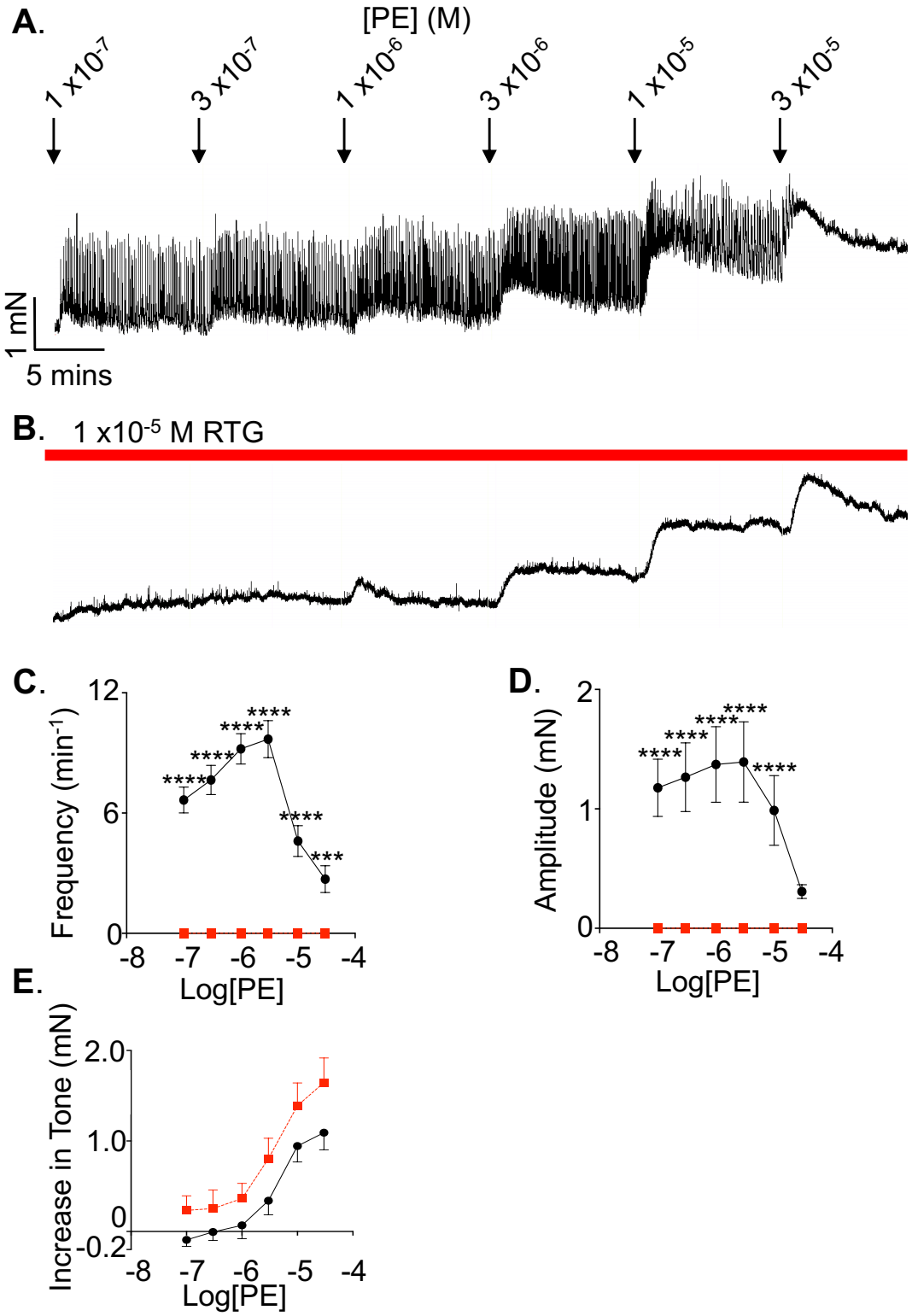


Figure 4.5: The K_v7.2-5 activator, retigabine (RTG), abolished phasic, and not tonic, phenylephrine (PE)-induced contractions.
A. Representative isometric tension recording demonstrating the effect of incremental concentrations of PE (1 x10^{-7} M to 3 x10^{-5} M). **B.** Representative isometric tension recording, from the same preparation, demonstrating the effect of incremental concentrations of PE in the presence of 1 x10^{-5} M RTG. **C+D+E.** Summary data for the effect of RTG (red) on phasic contraction frequency (C), and amplitude (D), as well as the increase in tone (E). *P<0.05, **P<0.01, ***P<0.001, ****P<0.0001 (n=8, N=8).

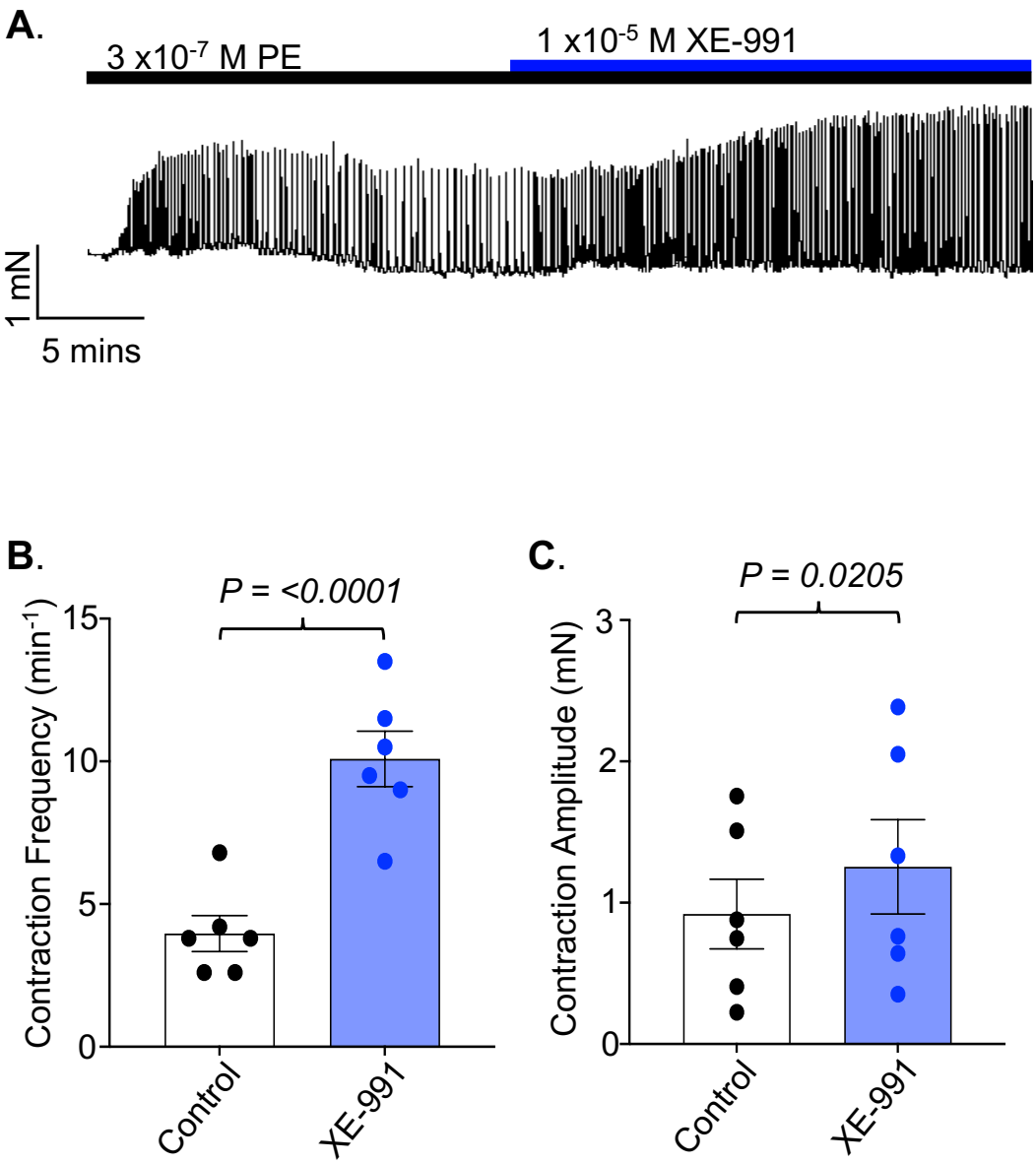


Figure 4.6: Phenylephrine (PE)-induced contractions were enhanced by a K_V7 blocker, XE-991.
A. Representative isometric tension recording demonstrating the effect of 1 x10^{-5} M XE-991 on 3 x10^{-7} M PE-induced phasic contractions. **B+C.** Summary data for the enhancement effect of XE-991 on phasic contraction frequency and amplitude (P=<0.0001 and P=0.0205, respectively; n=6, N=6).

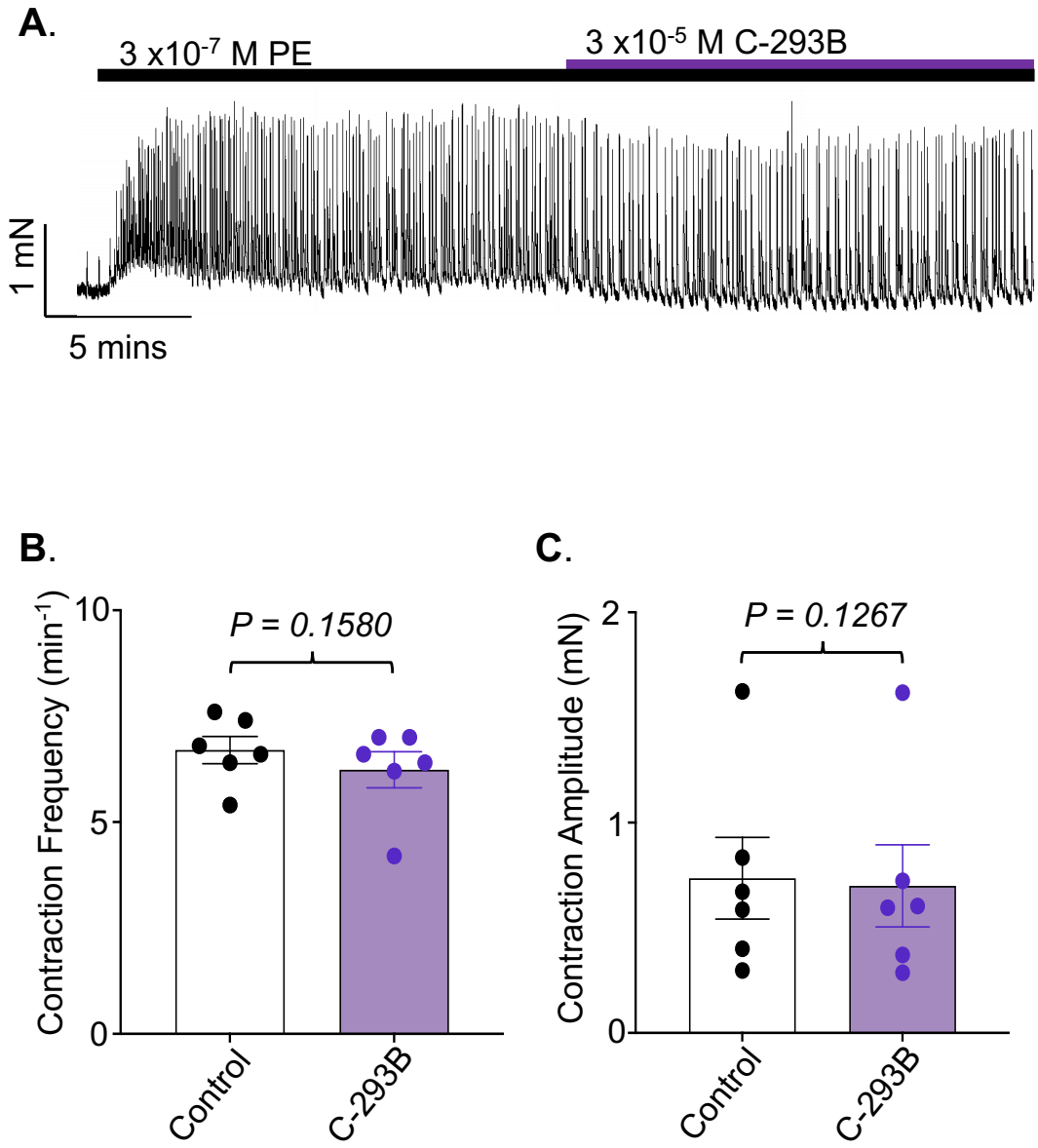


Figure 4.7: Phenylephrine (PE)-induced contractions were not enhanced by a $K_V7.1$ blocker, chromanol-293B (C-293B). **A.** Representative isometric tension recording demonstrating the effect of 3 x10^{-5} M C-293B on 3 x10^{-7} M PE-induced phasic contractions. **B+C.** Summary data shows no significant effect of C-293B on phasic contraction frequency and amplitude (P=0.1580 and P=0.1267, respectively; n=6, N=6).

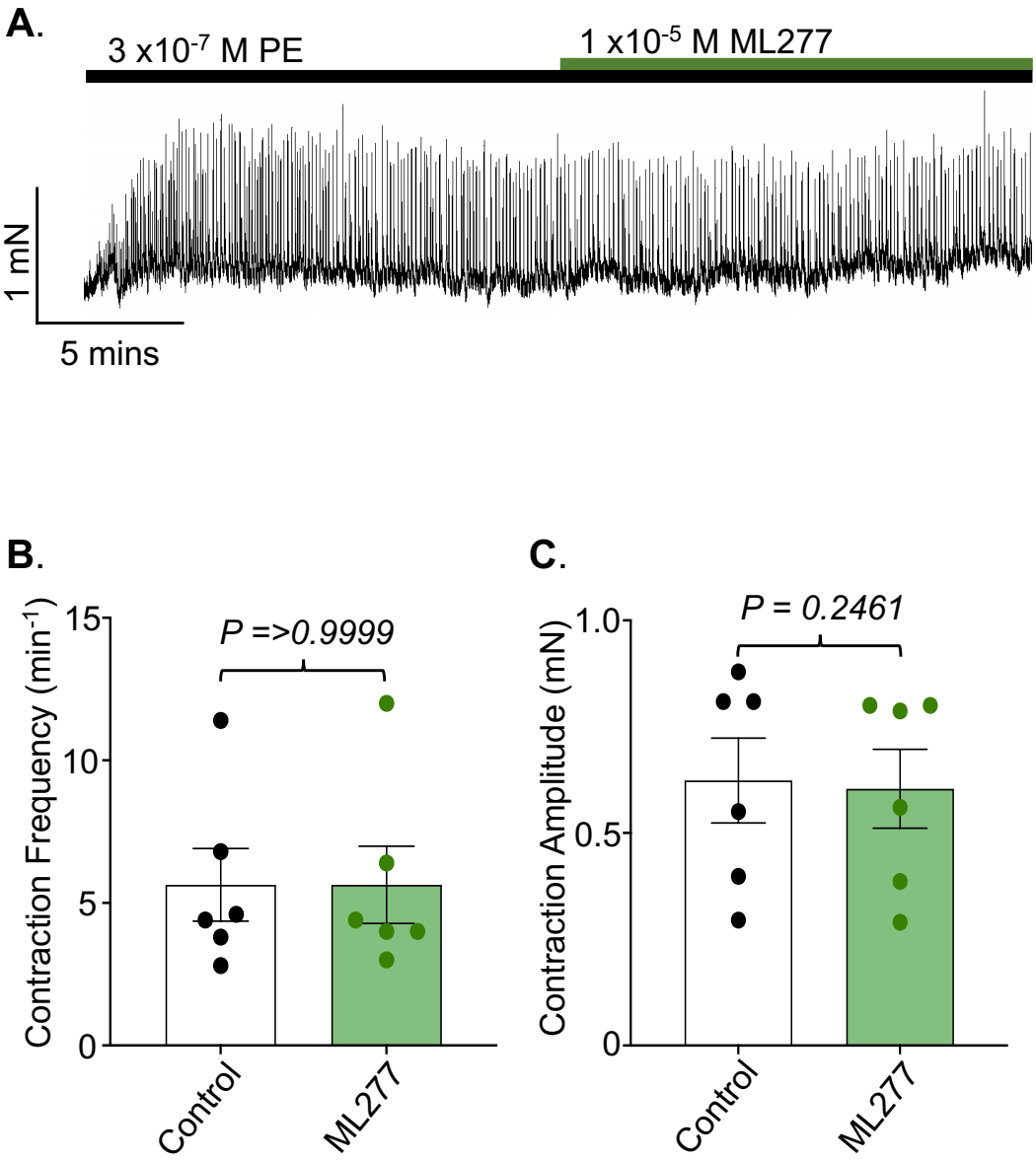


Figure 4.8: Phenylephrine (PE)-induced contractions were not inhibited by a K_V7.1 activator, ML277.
A. Representative isometric tension recording demonstrating the effect of 1 x10^{-5} M ML277 on 3 x10^{-7} M PE-induced phasic contractions. **B+C.** Summary data shows no significant effect of ML277 on phasic contraction frequency and amplitude (P=>0.9999 and P=0.2461, respectively; n=6, N=6).

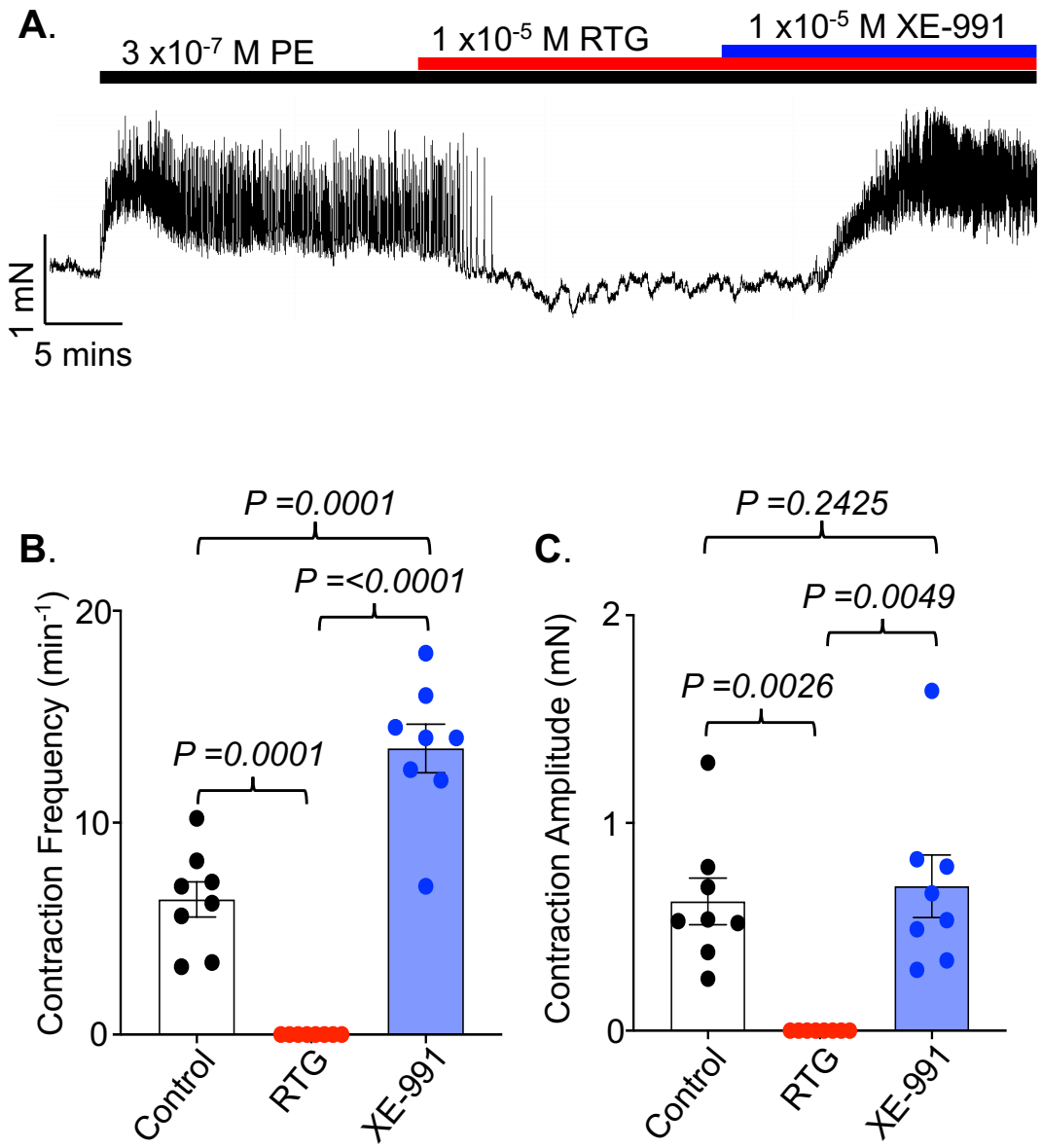


Figure 4.9: Phenylephrine (PE)-induced contractions abolished by K_V7.2-5 activator, retigabine (RTG), were restored by K_V7 blocker, XE-991.

A. Representative isometric tension recording demonstrating the inhibitory effect of 1 x10^{-5} M RTG on 3 x10^{-7} M PE-induced phasic contractions, with a subsequent restoration of phasic contractions by 1 x10^{-5} M XE-991. **B+C.** Summary data shows RTG abolished contraction frequency and amplitude (P=0.0001 and P=0.0026, respectively). Phasic contraction frequency and amplitude was restored in the presence of XE-991 (P=<0.0001 and P=0.0049, respectively).

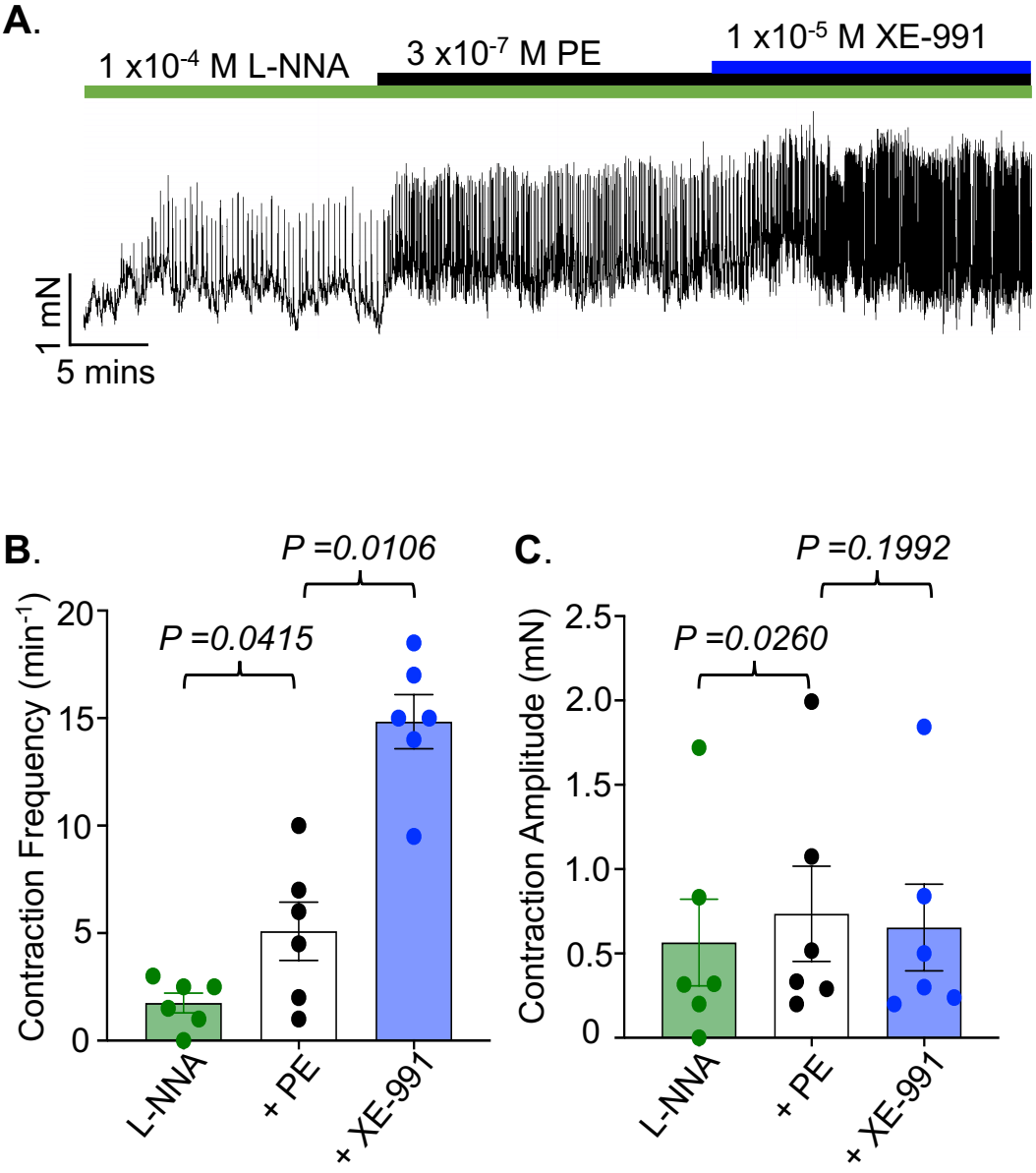


Figure 4.10: Phenylephrine (PE)-induced contraction frequency was enhanced by K_V7 blocker, XE-991, in the presence of NOS inhibitor, N_ω-Nitro-L-arginine (L-NNA). A. Representative isometric tension recording demonstrating the enhancement effect of 1 x10^{-5} M XE-991 on 3 x10^{-7} M PE-induced phasic contractions, in the continued presence of 1 x10^{-4} M L-NNA. **B+C.** Summary data shows XE-991 only enhanced contraction frequency (not amplitude) in the presence of L-NNA (P=0.0106 and P=0.1992, respectively; n=6, N=6).

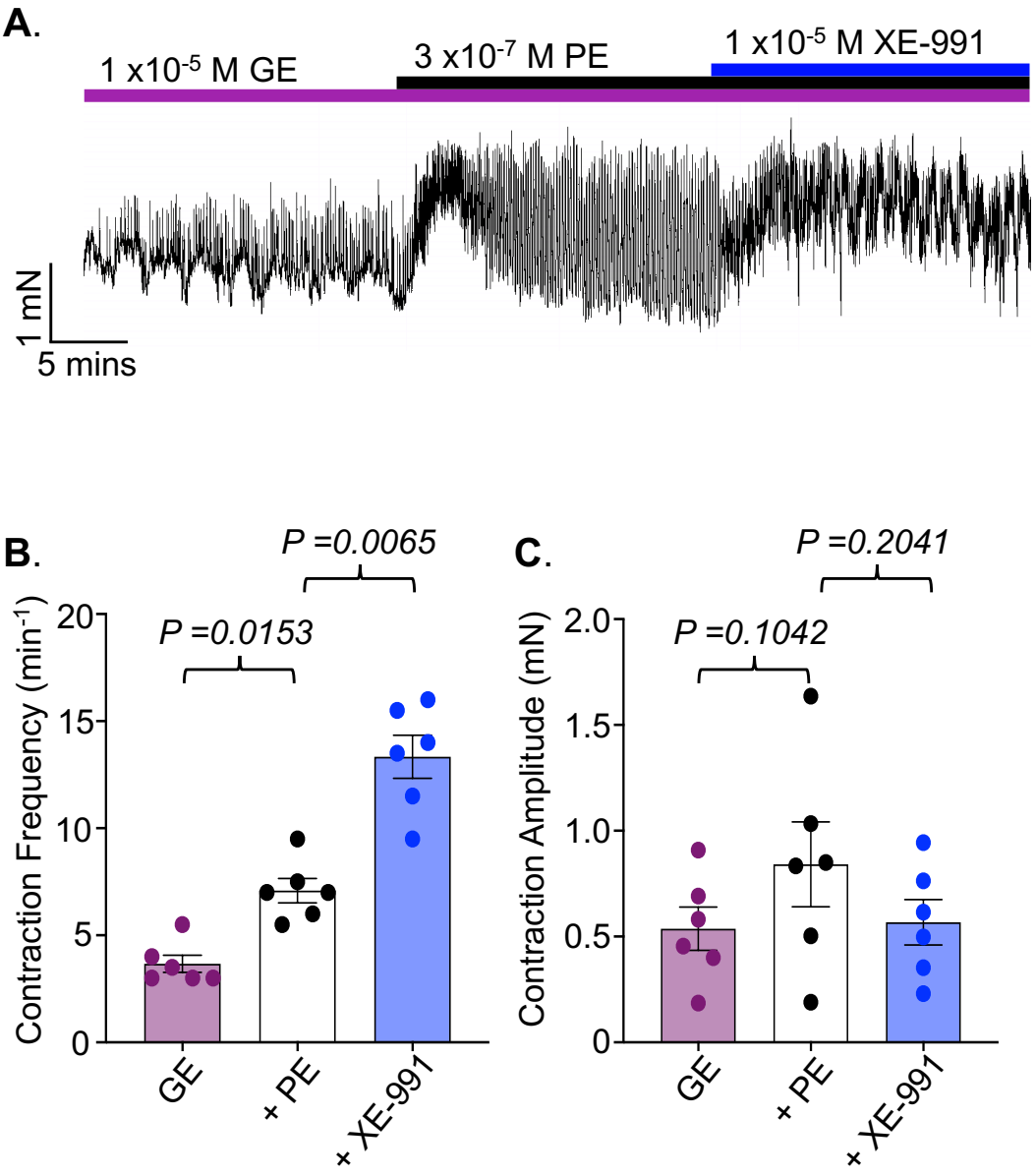


Figure 4.11: Phenylephrine (PE)-induced contraction frequency was enhanced by K_V7 blocker, XE-991, in the presence of a pre-junctional noradrenaline release inhibitor, guanethidine (GE).
A. Representative isometric tension recording demonstrating the enhancement effect of 1 x10^{-5} M XE-991 on 3 x10^{-7} M PE-induced phasic contractions, in the continued presence of 1 x10^{-5} M GE. **B+C.** Summary data shows XE-991 only enhanced contraction frequency (not amplitude) in the presence of GE (P=0.0065 and P=0.2041, respectively; n=6, N=6).

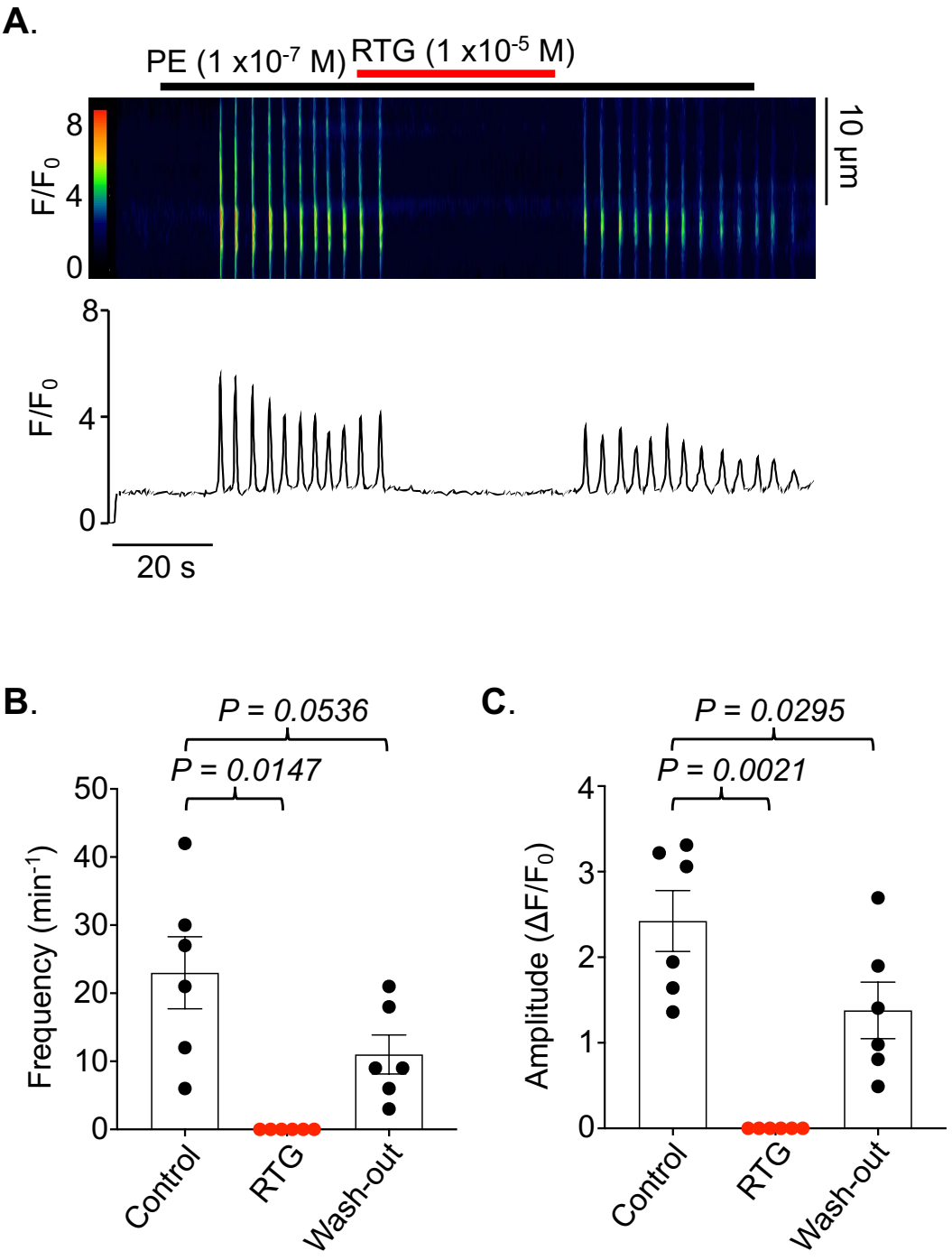


Figure 4.12: The effect of $K_v7.2$-5 activator, retigabine (RTG), on low-PE-induced Ca^{2+} oscillations in isolated cells.
A. Representative spatiotemporal map and associated intensity plot of Ca^{2+} oscillations, evoked by 2 min application of 1 x10^{-7} M PE, and abolished by 1 x10^{-5} M RTG. **B+C.** Summary data for Ca^{2+} oscillation frequency (min^{-1}) and amplitude ($\Delta F/F_0$), respectively. Ca^{2+} oscillation frequency and amplitude were abolished in the presence of RTG (P=0.0147 and P=0.0021, respectively), and a subsequent wash-out of RTG was able to return Ca^{2+} oscillation frequency closer to control levels (P=0.0536). Amplitude of Ca^{2+} oscillations during the wash-out remained significantly decreased (P=0.0295; n=6, N=6).

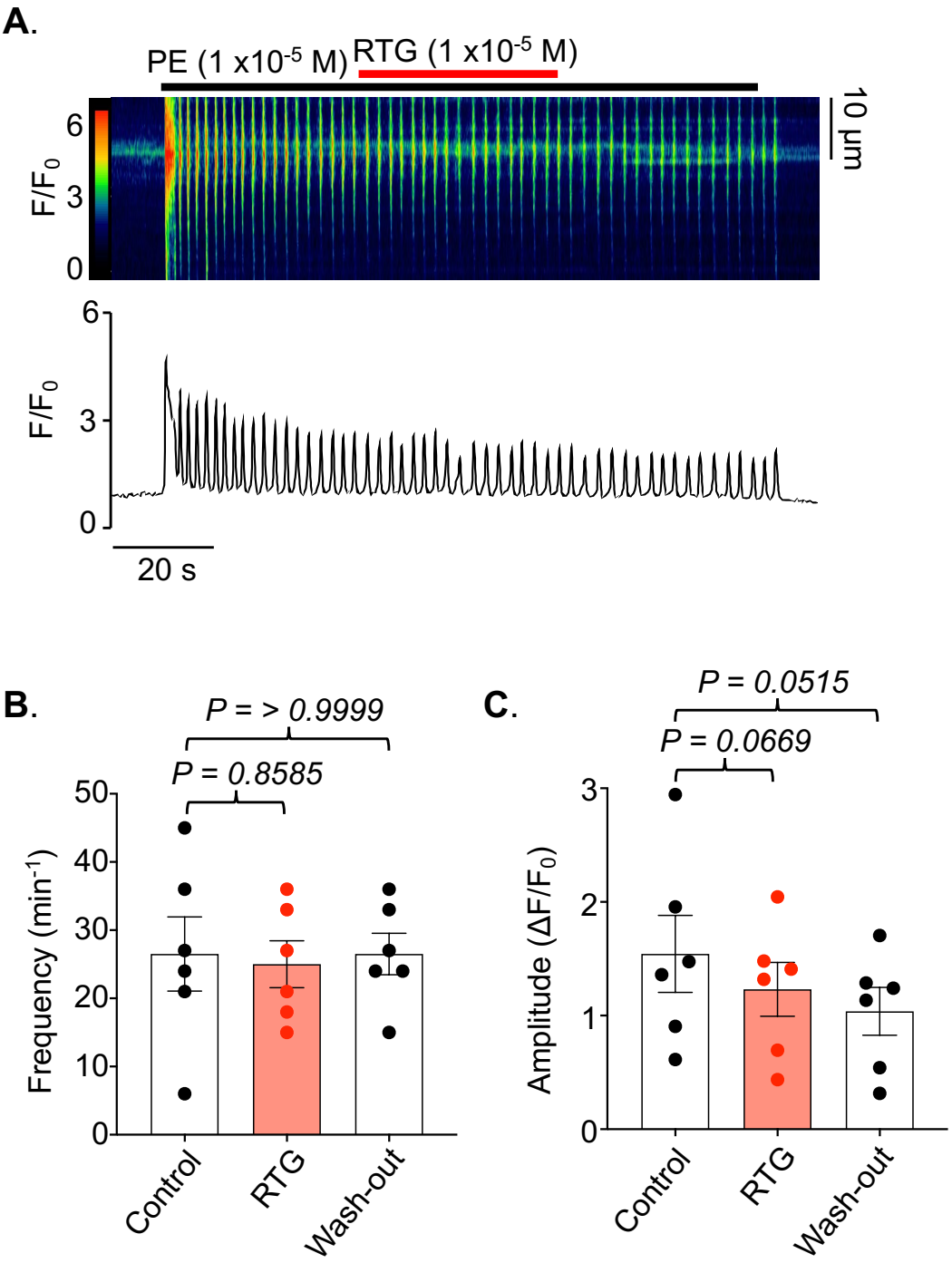


Figure 4.13: The effect of $K_v7.2$-5 activator, retigabine (RTG), on high-PE-induced Ca^{2+} oscillations in isolated cells. A. Representative spatiotemporal map and associated intensity plot of Ca^{2+} oscillations, evoked by 2 min application of 1 x10^{-5} M PE, and unaffected by 1 x10^{-5} M RTG. **B+C.** Summary data for Ca^{2+} oscillation frequency (min^{-1}) and amplitude ($\Delta F/F_0$), respectively. Ca^{2+} oscillation frequency and amplitude showed no significant effect in the presence of RTG (P=0.8585 and P=0.0669, respectively; n=6, N=6).

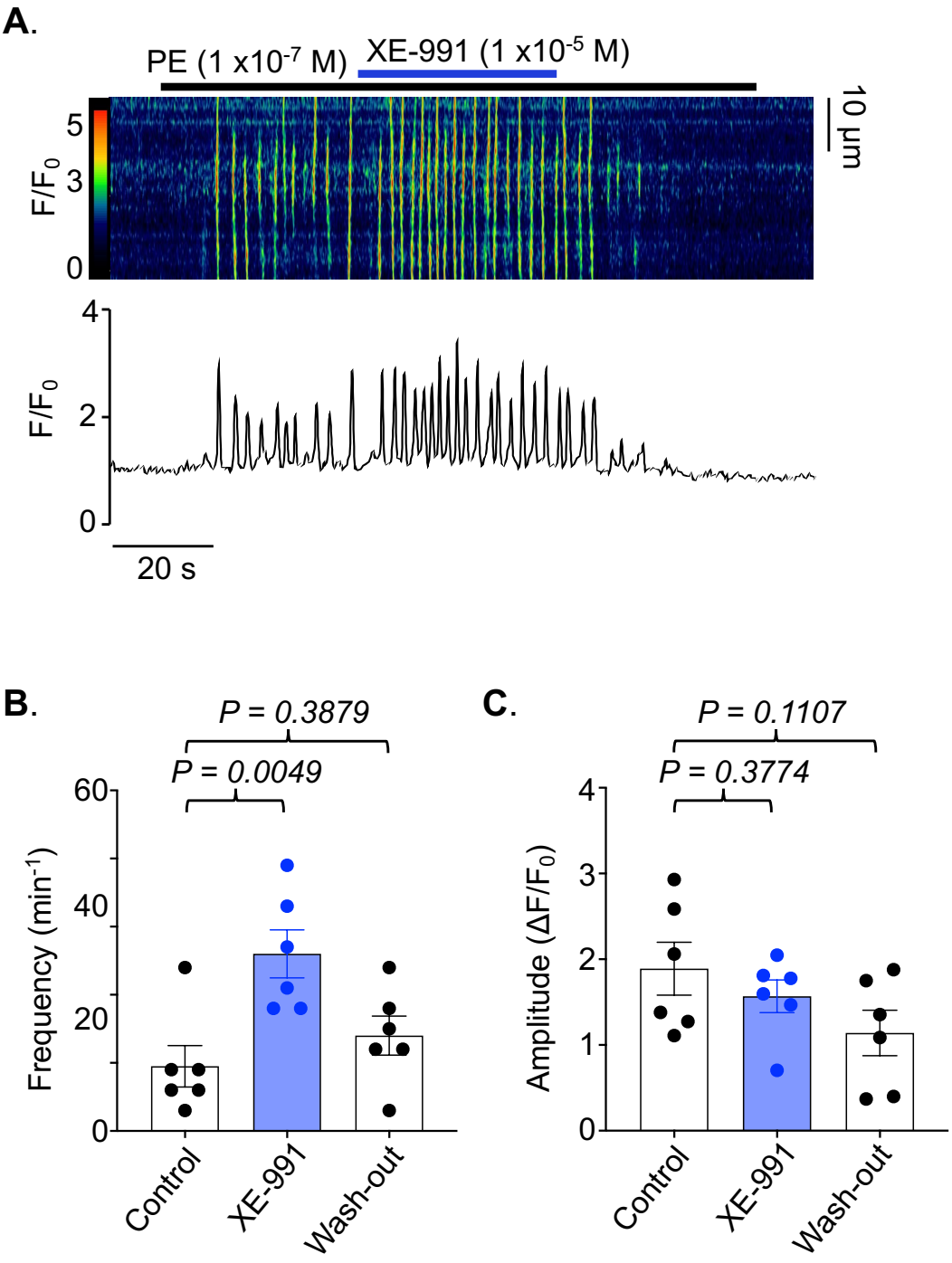


Figure 4.14: Effect of K_v7 blocker, XE-991, on low-PE-induced Ca^{2+} oscillations in isolated cells.
A. Representative spatiotemporal map and associated intensity plot of Ca^{2+} oscillations, evoked by 2 min application of 1 x10^{-7} M PE, and enhanced by 1 x10^{-5} M XE-991. **B+C.** Summary data for Ca^{2+} oscillation frequency (min^{-1}) and amplitude ($\Delta F/F_0$), respectively. Ca^{2+} oscillation frequency was enhanced in the presence of XE-991, and a subsequent wash-out returned frequency closer to control levels (P=0.0049 and P=3879, respectively). XE-991 showed no significant effect on Ca^{2+} oscillation amplitude (P=0.3774; n=6, N=6).

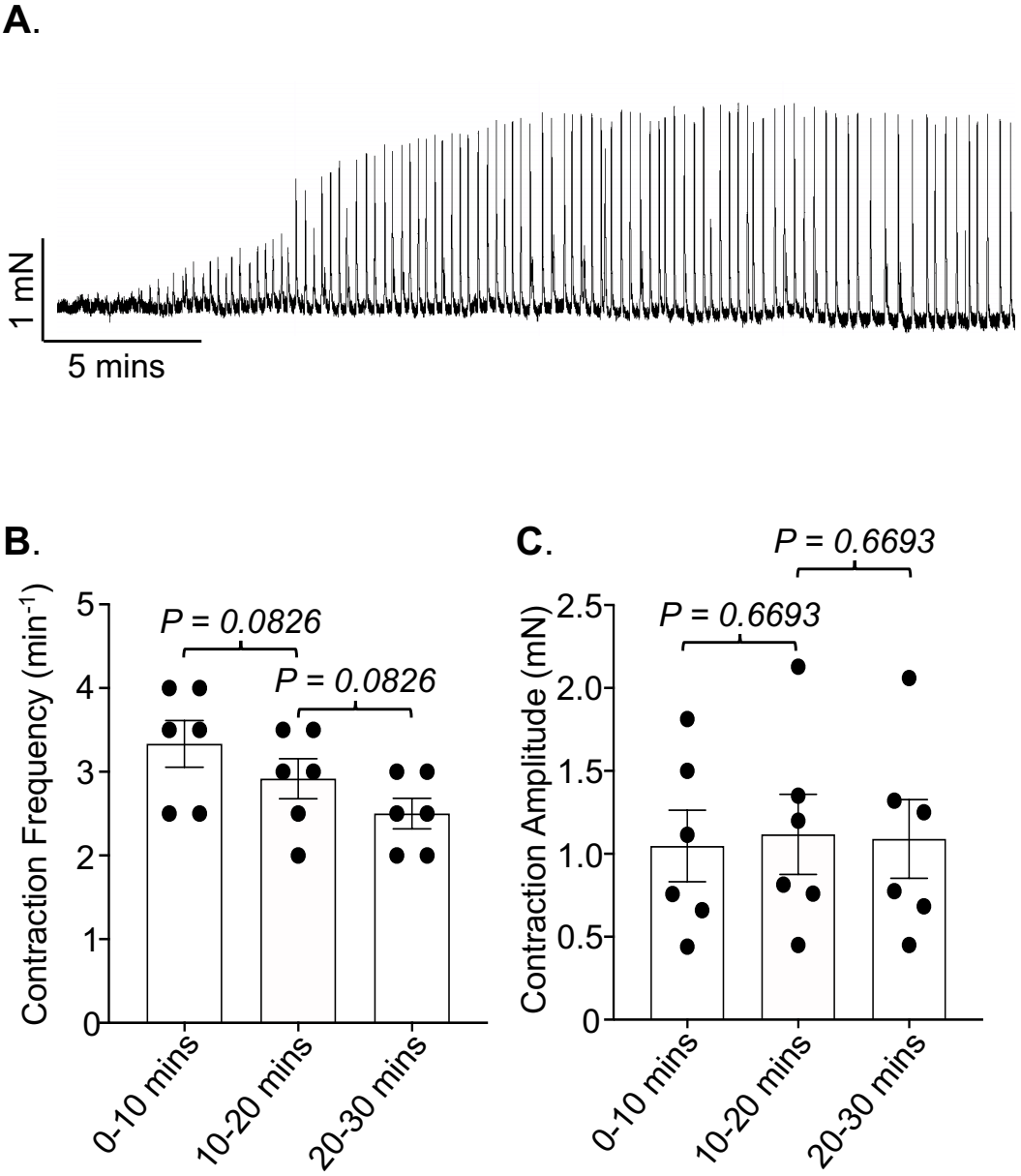


Figure 4.15: Mouse CCSM develops spontaneous phasic contractions.
A. Representative isometric tension recording demonstrating the development of spontaneous phasic contractions. **B+C.** Summary data for spontaneous phasic contraction frequency and amplitude, showing no significant decrease over the 30 min period (n=6, N=6).

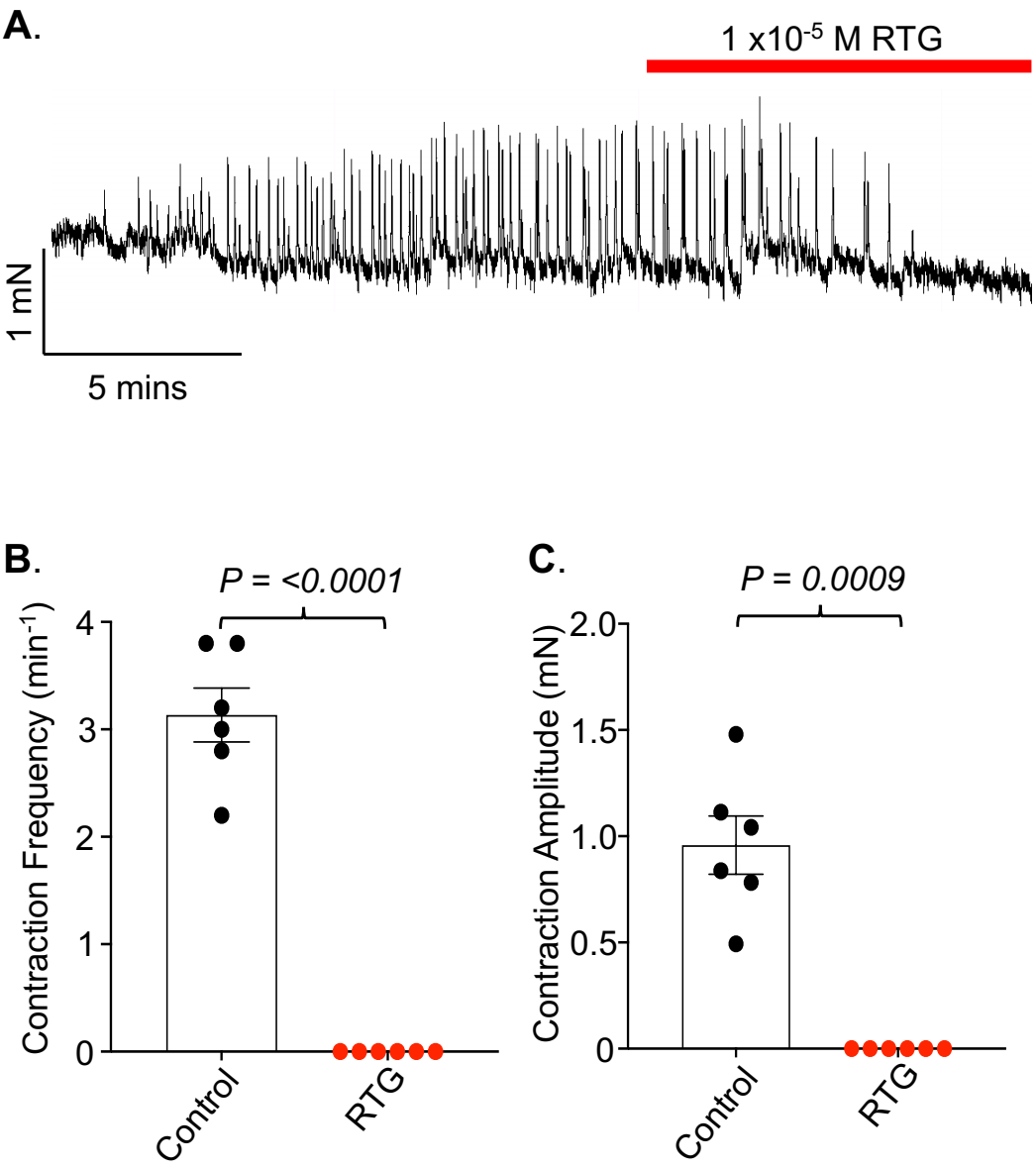


Figure 4.16: Spontaneous contractions were abolished by a K_V7.2-5 activator, retigabine (RTG).
A. Representative isometric tension recording demonstrating the effect of 1 x10^{-5} M RTG on spontaneous phasic contractions. **B+C.** Summary data for the inhibitory effect of RTG on phasic contraction frequency and amplitude (P=<0.0001 and P=0.0009, respectively; n=6, N=6).

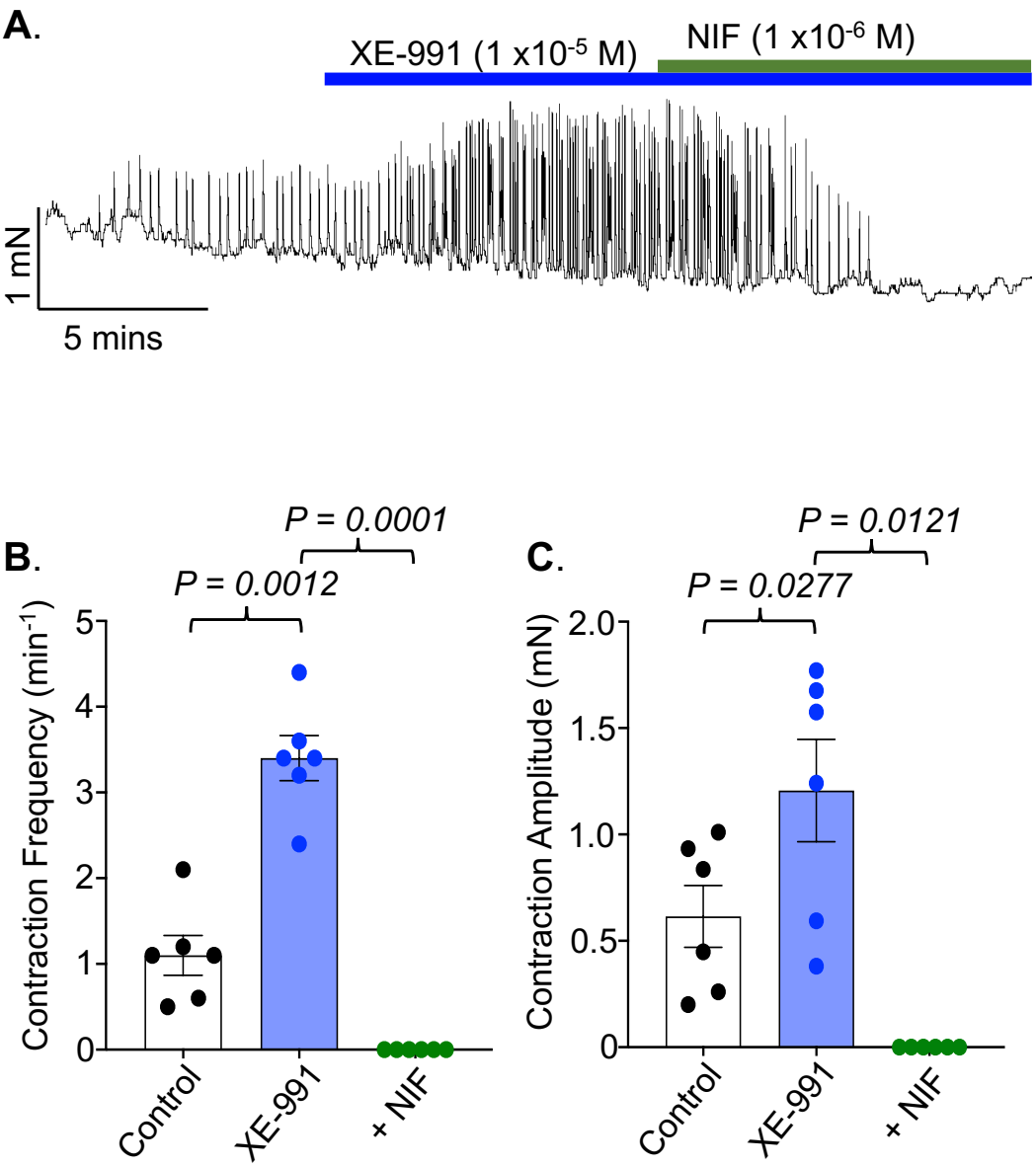


Figure 4.17: Spontaneous contractions were enhanced by a K_V7 blocker, XE-991, and abolished by LTCC blocker, nifedipine (NIF).

A. Representative isometric tension recording demonstrating the effect of 1 x10^{-5} M XE-991 on spontaneous phasic contractions, and the subsequent abolition of the enhanced activity by 1 x10^{-6} M nifedipine (NIF). **B+C.** Summary data for the enhancement effect of XE-991 on phasic contraction frequency and amplitude (P=0.0012 and P=0.0277, respectively). Addition of NIF abolished XE-991-enhanced phasic contraction frequency and amplitude (P=0.0001 and P=0.0121, respectively; n=6, N=6).

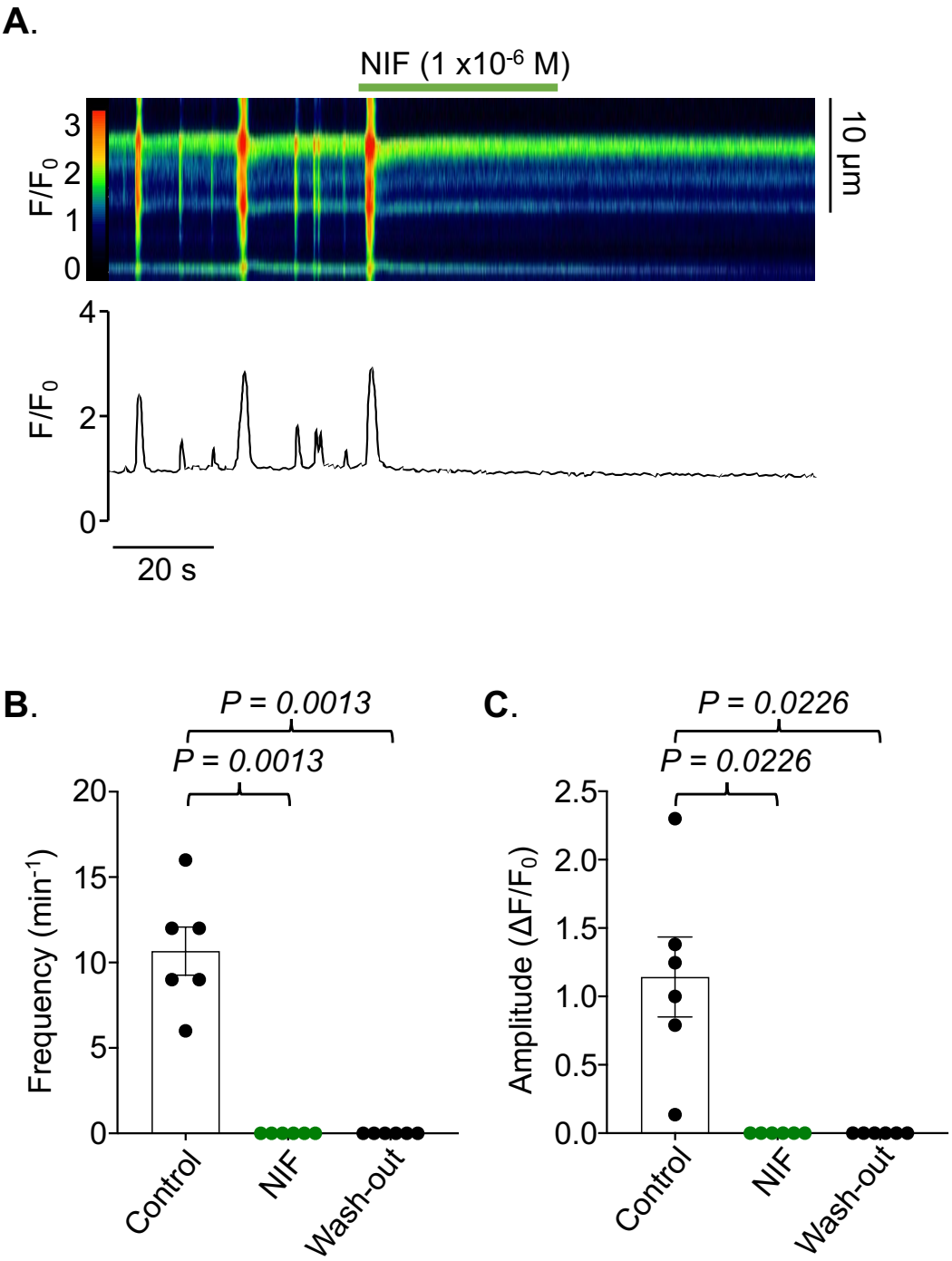


Figure 4.18: Effect of LTCC blocker, nifedipine (NIF), on spontaneous Ca^{2+} oscillations in isolated cells.
A. Representative spatiotemporal map and associated intensity plot of spontaneous Ca^{2+} oscillations and the addition of 1 x10^{-6} M NIF. **B+C.** Summary data for Ca^{2+} oscillation frequency (min^{-1}) and amplitude ($\Delta F/F_0$), respectively. Ca^{2+} oscillation frequency and amplitude were abolished in the presence of NIF (P=0.0013 and P=0.0226, respectively). A subsequent wash-out of NIF was unsuccessful and the frequency and amplitude of Ca^{2+} oscillations remained abolished (P=0.0013 and P=0.0226, respectively; n=6, N=6).

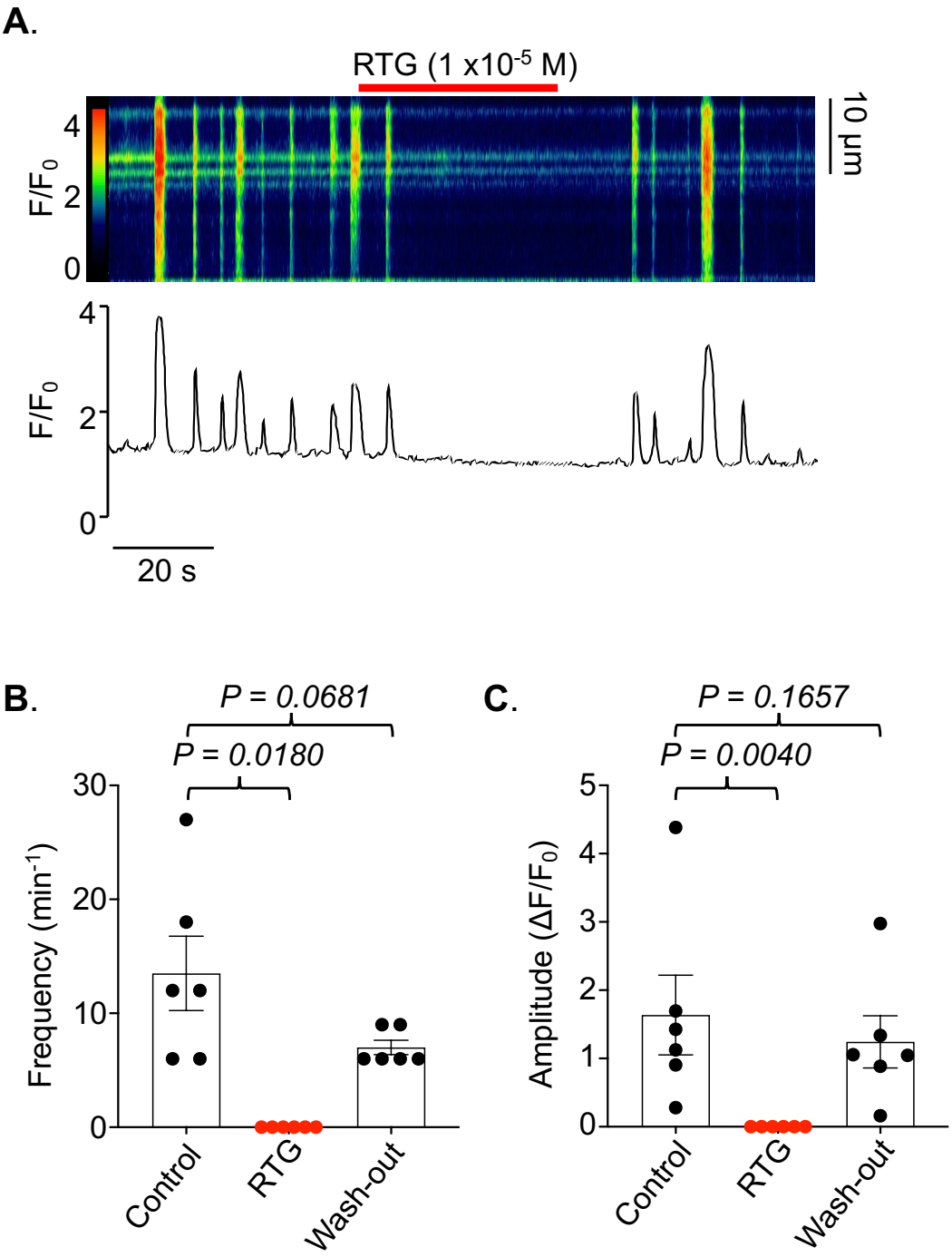


Figure 4.19: Effect of K_V7.2-5 activator, retigabine (RTG), on spontaneous Ca^{2+} oscillations in isolated cells.
A. Representative spatiotemporal map and associated intensity plot of spontaneous Ca^{2+} oscillations and the addition of 1 x10^{-5} M RTG. **B.** Summary data for Ca^{2+} oscillation frequency (min^{-1}) showed abolition in the presence of RTG (P=0.0180) and a subsequent wash-out increased frequency closer to control levels (P=0.0681). **C.** Summary data for Ca^{2+} oscillation amplitude ($\Delta F/F_0$) showed complete abolition (despite non-significant P value: P=0.0745) and subsequent wash-out returned amplitude closer to control levels (P=0.1657; n=6, N=6).

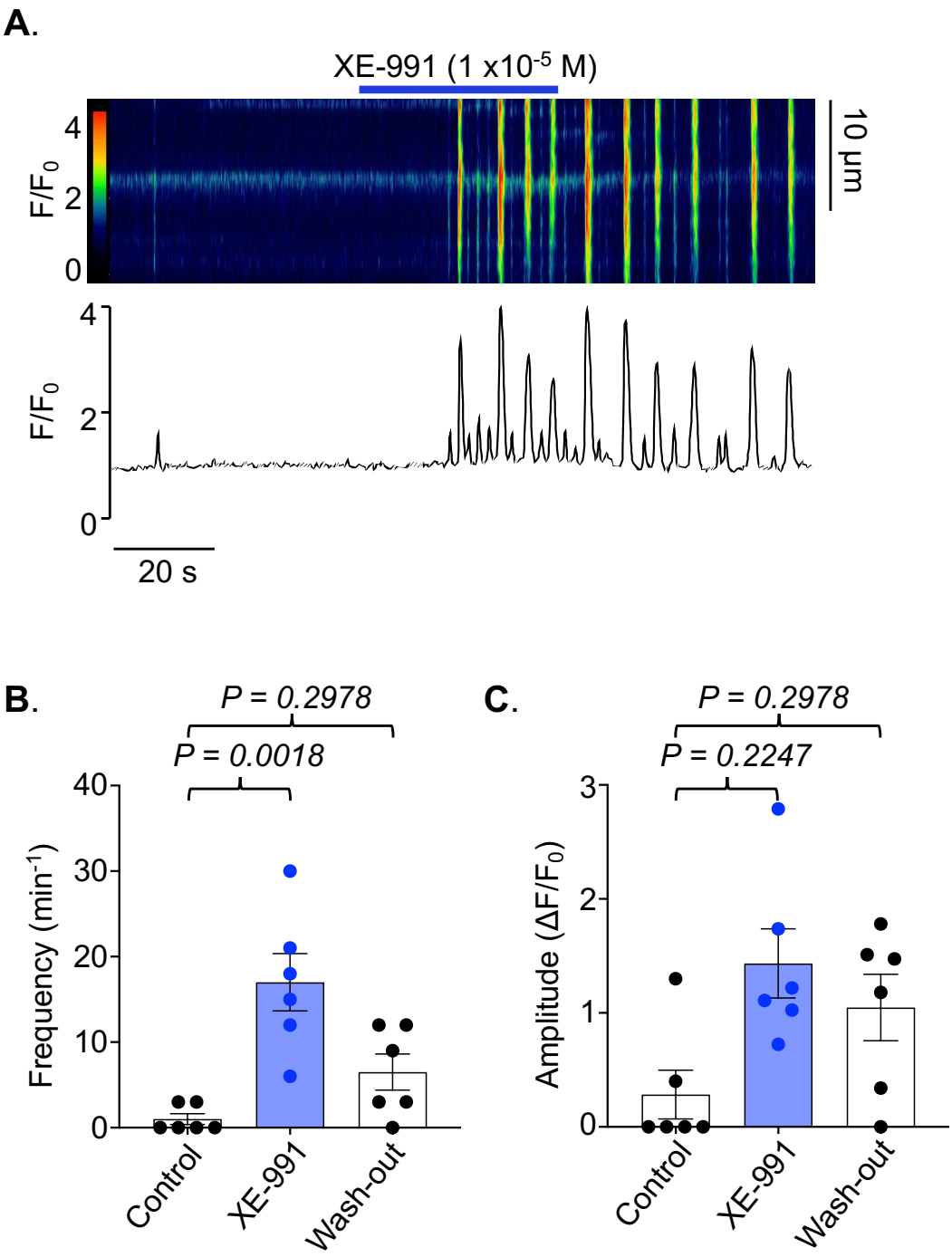


Figure 4.20: Effect of K_V7 blocker, XE-991, on spontaneous Ca^{2+} oscillations in isolated cells.
A. Representative spatiotemporal map and associated intensity plot of spontaneous Ca^{2+} oscillations and the addition of 1 x10^{-5} M XE-991. **B.** Summary data for Ca^{2+} oscillation frequency (min^{-1}) showed enhancement\induction in the presence of XE-991 (P=0.0018) and a subsequent wash-out appeared to decrease frequency, though this did not reach statistical significance (P=0.2978). **C.** Summary data for Ca^{2+} oscillation amplitude ($\Delta F/F_0$) showed no significant enhancement in the presence of XE-991 (P=0.2247; n=6, N=6).

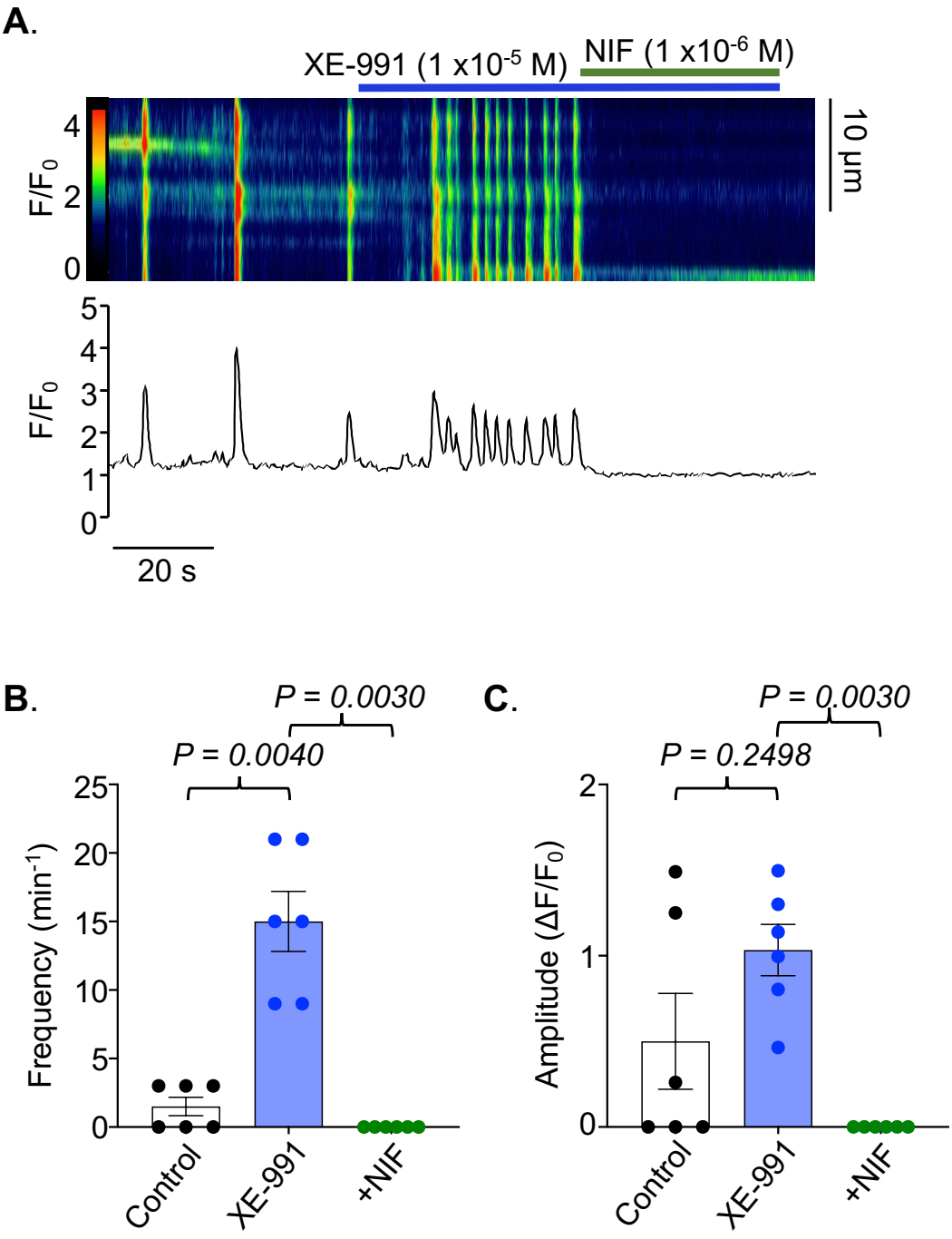


Figure 4.21: Effect of LTCC blocker, nifedipine (NIF) on XE-991-enhanced/induced Ca^{2+} oscillations in isolated cells.
A. Representative spatiotemporal map and associated intensity plot of spontaneous Ca^{2+} oscillations and the addition of 1 x10^{-5} M XE-991, followed by the addition of 1 x10^{-5} M NIF . **B.** Summary data for Ca^{2+} oscillation frequency (min^{-1}) showed enhancement\induction in the presence of XE-991 (P=0.0040) and abolition by subsequent addition of NIF (P=0.0030). **C.** Summary data for Ca^{2+} oscillation amplitude ($\Delta F/F_0$) showed no significant enhancement in the presence of XE-991 (P=0.2498), nonetheless, addition of NIF abolished the amplitude of Ca^{2+} oscillations (P=0.0030; n=6, N=6).

4.3 Discussion

The present study demonstrates that K_v7 channels, particularly $K_v7.5$, are functionally expressed in mouse CCSM and play a central role in regulating spontaneous and adrenergic-induced contractile activity via modulation of Ca^{2+} influx through LTCCs. The predominant expression of *Kcnq5*, confirmed at the transcript and protein level, alongside the marked pharmacological sensitivity of phasic contractions and Ca^{2+} oscillations to K_v7 modulators, strongly suggested that $K_v7.5$-containing channels were the dominant functional isoform in mouse CCSM.

4.3.1 K_v7 isoform expression in CCSM

Gene expression analysis revealed transcripts for *Kcnq1*, *Kcnq3*, *Kcnq4*, and *Kcnq5*, but not *Kcnq2*, with *Kcnq5* expressed most abundantly. Immunocytochemistry confirmed $K_v7.5$ protein expression at the cell periphery, consistent with plasma membrane localisation. This expression pattern mirrors findings in rat CCSM (Jepps *et al*., 2016), where *Kcnq5* was also the predominant isoform, but differs from human CCSM, where *KCNQ4* predominance has been reported (Lee *et al*., 2020). These differences highlight possible species-specific or disease-related variability. $K_v7.4$ and $K_v7.5$ can co-assemble to form heteromeric channels (Brueggemann *et al*., 2014a), yet the predominance of *Kcnq5* suggests that homomeric $K_v7.5$ channels may significantly contribute in mouse. The relatively hyperpolarised half-activation potential of $K_v7.5$ (-44 mV; Brueggemann *et al*., 2011) compared with $K_v7.4$ (-31 mV), places $K_v7.5$ activity close to the reported resting membrane potential of CCSM cells (-50 to -41 mV; Hashitani *et al*., 2005), implying a physiologically relevant contribution to resting membrane potential.

4.3.2 Adrenergic contractions and K_v7 modulation

Activation of α_1-adrenoceptors with PE induced rhythmic phasic contractions that were abolished by the $K_v7.2$-5 activator RTG and enhanced by the K_v7 blocker XE-991, consistent with K_v7 channels restraining membrane excitability under adrenergic stimulation. This aligns with electrophysiological studies across multiple smooth muscle tissues demonstrating that K_v7 activation induces membrane hyperpolarisation and reduces excitability by limiting LTCC activation. In mouse portal vein, RTG caused pronounced hyperpolarisation under current-clamp conditions, reversed by XE-991 (Yeung et al., 2008). Similarly, in detrusor smooth muscle, RTG elicited XE-991-sensitive hyperpolarisation and suppressed spontaneous action

potentials (Afeli et al., 2013), and in mesenteric arterial myocytes, K_v7 activators attenuated depolarisation-induced Ca^{2+} influx (Jepps et al., 2014). Collectively, these findings support a mechanism by which K_v7 channels stabilise resting membrane potential, limit LTCC activation, and reduce Ca^{2+} influx and contractile activity.

Importantly, K_v7 modulation selectively affected phasic but not tonic contractions, further validating the Chapter 3 finding that phasic contractility depended on voltage-dependent Ca^{2+} influx through LTCCs, whilst tonic contractility is membrane potential-independent, relying instead on SR Ca^{2+} release. This selective influence on phasic activity is consistent with findings in other phasic smooth muscles; in bladder and uterine smooth muscle, K_v7 activation inhibits phasic contractions whilst XE-991 enhances their frequency and amplitude (McCallum et al., 2009; Afeli et al., 2013). In vascular tissues, by contrast, K_v7 activity primarily modulates basal tone, with blockade eliciting tonic contractures through increased LTCC activity (Zhong et al., 2010; Jepps et al., 2014).

In rat CCSM, ML213 produced ~40% tonic relaxation, whilst penile arteries exhibited ~90% inhibition of tone, both reversed by linopirdine (Jepps et al., 2016). In rabbit CCSM, ML213 induced concentration-dependent relaxation, whereas other K_v7 activators required substantially higher concentrations for comparable effects (Lee et al., 2020a). That K_v7 modulation in rat and rabbit CCSM predominantly affects tonic rather than phasic responses suggested that LTCCs contributed more substantially to sustained tone in these species than in mouse, possibly reflecting species differences in resting membrane potential or LTCC expression. The presence of two functionally distinct contractile components in mouse CCSM therefore allows the contributions of K_v7 modulators to be more precisely delineated: K_v7 activation abolishes LTCC-dependent phasic contractions whilst tonic contractures, driven by voltage-independent pathways, remain preserved. This distinction contrasts with mouse aortic smooth muscle, where phasic contractions are IP_3R-dependent and tonic contractions are LTCC-dependent (Fransen et al., 2015), underscoring tissue-specific differences in excitation-contraction coupling.

To investigate isoform selectivity, $K_v7.1$ modulators were employed. Neither chromanol-293B nor ML277 affected PE contractions, consistent with low *Kcnq1* expression and an absence of functional $K_v7.1$ contribution in CCSM, supporting a predominant role for $K_v7.4$ and $K_v7.5$ (Brueggemann et al., 2014a; Jepps et al., 2015).

A potential caveat is that RTG has been reported to block LTCCs in cardiomyocytes at micromolar concentrations (Rubi et al., 2017). However, the restoration of phasic contractions by XE-991 following RTG treatment argues against significant LTCC blockade at the concentration employed, since functional Ca^{2+} influx through LTCCs is required for the phasic activity that XE-991 restores.

4.3.3 Independence from NOS and neurotransmitter release

The actions of K_v7 modulators were preserved in the presence of NOS inhibition (L-NNA) and sympathetic neurotransmission blockade (GE). This demonstrates that K_v7 activity is independent of endothelial NOS or neurogenic influences, reflecting direct effects on smooth muscle excitability. In rat CCSM, K_v7 channels contribute to NO- and cGMP-mediated relaxations (Jepps *et al*., 2016), supporting the idea that K_v7 channels act downstream of cyclic nucleotide signalling rather than through upstream modulation of transmitter release.

Interestingly, both L-NNA and GE induced phasic contractions in CCSM preparations. The response to NOS inhibition suggests that basal NO tonically suppresses spontaneous contractile activity within the corpus cavernosum. This is broadly consistent with Masuda et al. (2004), who showed that NOS inhibition increased tone in rabbit corpus cavernosum, with the effect being endothelium-dependent, supporting basal endothelial NO release. Further support comes from eNOS-deficient mouse corpus cavernosum, where loss of endothelial NO signalling is associated with increased RhoA/Rho-kinase pathway activity and enhanced contractile signalling (Bivalacqua et al., 2007; Priviero et al., 2010). In contrast, GE-induced phasic activity should not be interpreted simply as evidence for tonic basal NA release from adrenergic nerves. Rather, GE can transiently increase resting NA efflux by displacing NA from sympathetic nerve terminals, while ultimately inhibiting impulse-evoked adrenergic transmission. This indirect sympathomimetic phase has been demonstrated in classical radiolabelled NA studies and later by Fabiani and Story (1996), who reported increased resting NA efflux during GE exposure despite inhibition of stimulation-evoked transmitter release (Hertting et al., 1962).

4.3.4 K_v7 channels regulate spontaneous activity

Approximately half of CCSM preparations developed spontaneous phasic contractions, contrary to earlier reports that mouse CCSM is quiescent (Mizusawa *et al*., 2001). These contractions were abolished by RTG and enhanced by XE-991, with

effects reversed by NIF, demonstrating that K_v7 activity opposes LTCC-dependent excitability. Comparable, yet distinct, spontaneous activity has been described in rabbit CCSM, where phasic contractions occur alongside tonic contractures (Hannigan *et al*., 2016).

The variability in spontaneous activity likely reflects differences in electrical coupling and intracellular signalling. Gap junctions composed of connexin-43 are the primary mediators of intercellular electrical coupling in CCSM, allowing propagation of membrane depolarisation and second messengers such as IP_3 between adjacent smooth muscle cells, enabling the tissue to function as a syncytium (Campos de Carvalho et al., 1993; Moreno et al., 1993). Whole-tissue Ca^{2+} imaging in tonic smooth muscles has revealed that contractile signalling consists of temporal and spatial summation of asynchronous Ca^{2+} transients (Thornbury et al., 2011; Drumm et al., 2018; Cobine et al., 2020), suggesting that the phasic nature of mouse CCSM spontaneous activity implies a greater degree of synchronous Ca^{2+} signalling than that underlying the tonic contractures observed in rabbit CCSM. The basis for such species differences in coupling is unclear. Connexin-43 expression has not been compared across CCSM from different species, and even where expression is equivalent, gap junction permeability can be dynamically regulated through PKC- or Src kinase-mediated phosphorylation (Lampe and Lau, 2004). Whether differences in connexin expression, phosphorylation state, or downstream Ca^{2+} signalling account for the distinct contractile phenotypes observed between mouse and rabbit CCSM remains to be determined.

The mechanism is consistent with K_v7 regulation of resting membrane potential. XE-991 depolarises CCSM cells into the LTCC activation range, yet this does not necessarily produce sustained Ca^{2+} influx. LTCCs undergo strong Ca^{2+}-dependent inactivation mediated by calmodulin binding to the cytosolic C-terminus (Peterson et al., 1999), providing an intrinsic negative feedback mechanism that limits Ca^{2+} entry and favours rhythmic Ca^{2+} influx and contraction. Human CCSM studies likewise reported XE-991-induced depolarisation (~10 mV) and K_v7 activator-induced hyperpolarisation (Lee et al., 2020).

4.3.5 K_v7 modulation of Ca^{2+} oscillations

Ca^{2+} imaging in isolated CCSM cells confirmed that spontaneous oscillations were abolished by RTG and NIF and enhanced by XE-991, consistent with tension

experiments. XE-991 could also induce oscillations in previously quiescent cells, further supporting a role for K_v7 channels in stabilising resting membrane potential. XE-991-induced oscillations were suppressed by NIF, confirming dependence on LTCC activity.

Critically, RTG selectively abolished low-PE Ca^{2+} oscillations whilst leaving high-PE Ca^{2+} oscillations intact, and XE-991 enhanced low-PE Ca^{2+} oscillations. This dissociation mirrors precisely the pattern established in Chapter 3, where pharmacological agents modulating membrane potential, namely NIF and Ani-9, selectively abolished phasic contractions and low-PE Ca^{2+} oscillations, whilst tonic contractures and high-PE Ca^{2+} oscillations were preserved. The present findings therefore extend and reinforce that framework: K_v7 channels operate within the same membrane potential-dependent pathway as LTCCs and ANO1, selectively governing the excitability that underlies phasic contractility.

While these single-cell recordings are consistent with a K_v7-LTCC axis governing excitability, it is important to acknowledge that Ca^{2+} oscillations in isolated cells may not fully represent the Ca^{2+} signalling that generates phasic or tonic contractions at the whole-tissue level. In intact tissue, the contractile output reflects the integrated behaviour of a coupled syncytium rather than the activity of individual cells. Sergeant et al. (2009) demonstrated that isolated rabbit CCSM myocytes exhibit spontaneous Ca^{2+} oscillations modulated by the NO-cGMP pathway, and proposed that detumescent tone may be maintained not by a sustained elevation of cytosolic Ca^{2+}, but rather by the summation of Ca^{2+} oscillations. If the same principle applies in mouse CCSM, then K_v7 activation would be predicted to selectively abolish the synchronised, propagating Ca^{2+} transients that underlie phasic contractions, while leaving asynchronous IP_3R-mediated SR Ca^{2+} release underlying tonic contractility, as identified in Chapter 3, relatively intact. This is consistent with the preservation of tonic PE responses following RTG application and LTCC blockade observed in the isometric tension data.

Species differences in Ca^{2+} signalling responses were also evident: in human CCSM, XE-991 induces large transient Ca^{2+} elevations (Lee et al., 2020), whereas rhythmic oscillations predominated in mouse CCSM, mirroring the distinct spontaneous contractile phenotypes described above. These differences likely reflect species-specific coupling between K_v7 channels, LTCCs, and Ca^{2+} release pathways, and underscore the need for future whole-tissue imaging to determine how

membrane potential regulation translates into coordinated contractile behaviour in mouse CCSM.

4.3.6 Physiological implications and therapeutic potential

These findings highlighted that $K_v7.5$-containing channels are key regulators of excitability in mouse CCSM. By stabilising the resting membrane potential, K_v7 channels suppressed LTCC-driven phasic activity while leaving tonic responses intact. This suggested that K_v7 channels selectively modulated rhythmic excitability. Given that phasic contractions may contribute to maintaining penile flaccidity, K_v7 activation could facilitate erection by reducing basal excitability, while K_v7 blockade may exacerbate contractility and contribute to ED. K_v7 channels therefore represent a potential therapeutic target, complementing PDE5 inhibitors, particularly in conditions of impaired NO signalling.

4.3.7 Limitations and future directions

A major finding of this chapter is that Kv7 modulation preferentially affects phasic rather than tonic contractile activity. Isolated exceptions were observed, which may reflect temporal summation of phasic events inducing tone, though further validation is required to substantiate this. Moreover, several pharmacological limitations warrant consideration. XE-991, while widely used as a K_v7 inhibitor, shows limited off-target activity at higher concentrations; at 1 $x10^{-5}$ M, it can partially block $K_v1.2/1.5$ and $K_v2.1/9.3$ heteromeric channels, though this inhibition is substantially weaker than its effect on $K_v7.4$, and there is currently no evidence that these non-K_v7 channels are expressed in CCSM (Zhong et al., 2010). RTG is commonly employed as a $K_v7.2$-5 activator; however, partial LTCC inhibition has been reported as an off-target effect. In detrusor smooth muscle, approximately 19% block was observed at 1 $x10^{-5}$ M (Tykocki et al., 2019), whereas studies in guinea pig heart and heterologously expressed human LTCCs report minimal inhibition (<6%) at the same concentration (Rubi et al., 2017). However, the restoration of phasic contractions by XE-991 following RTG treatment argues against significant LTCC blockade at the concentration employed, since functional Ca^{2+} influx through LTCCs is required for the phasic activity that XE-991 restores

Beyond these pharmacological considerations, several questions regarding isoform selectivity and signalling remain unresolved. While $K_v7.5$ appears dominant in mouse CCSM, the contribution of $K_v7.4$ cannot be excluded, and isoform-specific

knockdown or selective pharmacology will be required to dissect their relative roles. Although K_v7 channels contribute to NO/cGMP-mediated relaxation of rat CCSM (Jepps et al., 2016), the coupling between K_v7 isoforms and cAMP/PKA or cGMP/PKG signalling in mouse CCSM remains unresolved, in contrast to the well-developed characterisation in VSM (Stott et al., 2016; Brueggemann et al., 2018). Finally, translation to human physiology requires caution, as expression patterns differ between species, predominant *Kcnq5* in mouse versus *KCNQ4* in human, and comparative studies in human CCSM will be essential for determining the therapeutic relevance of K_v7 channels in erectile function.

5. Results Chapter 3:

Activation of α_{1A}-adrenoceptors (α_{1A}Rs) inhibit *KCNQ*-encoded voltage-gated potassium isoform 5 (K_V7.5) channels

5.1 Introduction

Voltage-dependent K^+ (K_V) channels serve as key regulators of smooth muscle excitability, maintaining the resting membrane potential and thereby controlling Ca^{2+} influx through LTCCs (Nelson & Quayle, 1995; Cox, 2005; Jackson, 2017). In mouse CCSM, K_V7 channels are abundantly expressed (with *Kcnq5* being the predominant transcriptional isoform) and play a functional role in membrane excitability (Mercer *et al*., 2025). Activation of K_V7 channels promotes K^+ efflux and membrane hyperpolarisation, leading to LTCC deactivation and reduced Ca^{2+} influx, whereas pharmacological blockade depolarises the membrane, facilitates LTCC activation, and enhances contractile activity (Jepps *et al*., 2016; Lee *et al*., 2020a; Mercer *et al*., 2025).

K_V7 channels are critically dependent on membrane phosphatidylinositol 4,5-bisphosphate (PIP_2), which binds to conserved C-terminal domains to stabilise the open state of the pore (Zhang *et al*., 2003; Falkenburger *et al*., 2010). Beyond PIP_2, K_V7 activity is modulated by protein kinases and calmodulin (CaM). Activation of protein kinase C (PKC) inhibits K_V7 activity, reducing $K_V7.2/3$ (M-current) and vascular $K_V7.4/5$ channels via phosphorylation of cytosolic residues (Schroeder *et al*., 1998; Brueggemann *et al*., 2014b). In contrast, PKA enhances K_V7 currents, as shown in cardiomyocyte $K_V7.1$-minK (IK_S) currents and $K_V7.5$ currents in human airway and VSM (Marx *et al*., 2002; Mani *et al*., 2016; Brueggemann *et al*., 2018). CaM acts as both a structural subunit and Ca^{2+} sensor; apo-CaM is constitutively bound to C-terminal helices, and the subsequent binding of Ca^{2+} to CaM (Ca^{2+}-CaM) decreases channel open probability (Yus-Nájera *et al*., 2002; Gamper & Shapiro, 2003; Delmas & Brown, 2005).

Evidence from cardiac myocytes demonstrates that α_1-adrenoceptor (α_1R) activation suppresses K^+ currents through intracellular signalling pathways consistent with $G_{q/11}$-PLC coupling. In rat ventricular cells, α_1-agonists prolong the action potential by inhibiting voltage-dependent K^+ currents (Apkon & Nerbonne, 1988). Similarly, in atrial and other cardiac myocytes, α_1-stimulation reduces the transient outward K^+ current (I_{out}) and the inward-rectifier K^+ current (I_{K1}), with these effects attributed to PKC-mediated phosphorylation (Fedida & Shimoni, 1990; Fedida *et al*., 1991; Braun *et al*., 1992; Ivanova *et al*., 2021). Moreover, α_1R activation can modulate G-protein-gated inward-rectifier K^+ channels (GIRK) through PIP_2 depletion, as demonstrated in atrial myocytes where α_1-agonists or endothelin reduce

GIRK activity via PLC-mediated hydrolysis of PIP_2 (Cho *et al*., 2001;2002;2005; Bender *et al*., 2002). In neurons, α_1R activation also inhibits M-current, though the relative roles of PKC and PIP_2 are unresolved (Filippov and Brown, 2012; Wang *et al*., 2022). Collectively, these findings indicated that α_1R signalling inhibits K^+ currents through PKC-dependent phosphorylation and/or PIP_2 depletion.

Findings from the preceding chapters established that K_v7 channels are functionally important regulators of CCSM excitability, given pharmacological activation abolished phasic adrenergic contractions, and blockade enhanced them. These observations indicated that K_v7 channels provided a significant hyperpolarising influence that constrained contractile responses. Accordingly, adrenergic stimulation may enhance contraction, at least in part, by reducing this K_v7-mediated influence.

Given the predominant expression of *Kcnq5* in mouse CCSM, K_v7 currents are likely to be largely mediated by channels containing $K_v7.5$ α-subunits, although contributions from other isoforms, including $K_v7.4$, cannot be excluded. On this basis, it was hypothesised that activation of α_1Rs suppresses $K_v7.5$ channel activity via $G_{q/11}$-dependent signalling. Such inhibition would be expected to reduce K^+ efflux, depolarise the membrane, increase the open probability of LTCCs, and thereby facilitate phasic contractile activity.

To establish this mechanism, HEK-293 cells were used to determine if α_{1A}R-activation will inhibit $K_v7.5$ channels, and if this effect is mediated by PIP_2 depletion and/or PKC activation. Therefore, this chapter sought to:

1. Determine whether α_{1A}R-activation suppresses $K_v7.5$ current in HEK-293 cells.
2. Establish α_{1A}R-dependence using pharmacological antagonism of αRs (phentolamine) and $K_v7.5$-only controls.
3. Assess whether PKC activation can mimic this inhibitory effect using phorbol 12,13-dibutyrate (PDBu), or PKC inhibitors, GF109203X and chelerythrine chloride, can prevent the effect.
4. Determine whether intracellular supplementation with exogenous PIP_2 prevents α_{1A}R-mediated $K_v7.5$ inhibition.

5.2 Results

5.2.1 $K_v7.5$ currents are inhibited by $\alpha_{1A}R$ activation

To determine whether $\alpha_{1A}R$ activation modulates $K_v7.5$ channel activity, HEK-293 cells were co-transfected with plasmids encoding $K_v7.5$ and $\alpha_{1A}R$, and whole-cell currents were recorded using the voltage-clamp protocol shown in Fig5.1A. Under control conditions, depolarising voltage steps elicited characteristic slowly activating, non-inactivating outward currents typical of $K_v7.5$ channels. Application of the α_1R agonist, PE (1 $x10^{-5}$ M), significantly reduced current amplitude across all test potentials (Fig5.1B), with maximal relative conductance (G/G_{max}) significantly reduced to 0.25 ± 0.01 ($P<0.0001$). Boltzmann fits to tail currents showed a hyperpolarising shift in the voltage-activation curve (Fig5.1C), with the half-activation voltage ($V_{0.5}$) shifting from -52.53 ± 1 mV (control) to -59.32 ± 7 mV following PE application ($P=0.2478$; $n=6$). These data indicate that $\alpha_{1A}R$ activation by PE inhibits $K_v7.5$ currents.

To assess whether $\alpha_{1A}R$-mediated inhibition of $K_v7.5$ was near maximal at 1 $x10^{-5}$ M PE, a higher concentration of PE (1 $x10^{-4}$ M) was tested under identical conditions. Similar to the lower concentration, PE (1 $x10^{-4}$ M) markedly suppressed $K_v7.5$ currents in HEK-293 cells co-expressing $\alpha_{1A}Rs$ (Fig5.2A-B). Activation curves demonstrated a pronounced hyperpolarising shift of $V_{0.5}$ from -54.39 ± 1 mV (control) to -69.69 ± 7 mV after PE ($P=0.0162$; Fig. 5.2C), accompanied by a significant reduction in maximal conductance to 0.22 ± 0.02 G/G_{max} ($P<0.0001$; $n=6$).

5.2.2 PE does not affect $K_v7.5$ currents in the absence of $\alpha_{1A}R$

To verify that the inhibitory effect of PE requires $\alpha_{1A}R$ activation, HEK-293 cells expressing $K_v7.5$ alone were exposed to a maximal concentration of PE (1 $x10^{-4}$ M). Under these conditions, PE had no significant effect on current amplitude ($P=0.0546$; Fig5.3A-B). The voltage-activation relationship shifted (Fig5.3C), with $V_{0.5}$ values of -42.70 ± 1 mV (control) and -55.81 ± 3 mV following PE ($P<0.0001$; $n=6$), and maximal conductance of 1.04 ± 0.03 G/G_{max}. These results confirm that the inhibitory effects of PE are mediated specifically via $\alpha_{1A}R$ activation and not through direct interaction with $K_v7.5$ channels.

5.2.3 Phentolamine prevented PE-induced inhibition of $K_v7.5$ currents

To further confirm $\alpha_{1A}R$ dependence, experiments were performed in the presence of the non-selective α-adrenergic antagonist phentolamine (1 $x10^{-6}$ M). Co-

application of maximal concentration PE (1 x10^{-4} M) and phentolamine prevented current inhibition in cells co-expressing K_v7.5 and α_{1A}R (P=0.4694; Fig5.4A-B). The voltage-activation curves before and after drug application showed no significant shifts (P=0.5097; Fig5.4C), with $V_{0.5}$ values of -45.67 ± 2 mV (control) and -48.84 ± 3 mV (PE + phentolamine), and maximal conductance of 0.95 ± 0.02 G/G_{max} (n=6). This further confirms that PE-induced suppression of K_v7.5 currents is mediated through α_{1A}R activation.

5.2.4 Protein kinase C activation reduces K_v7.5 currents

To evaluate whether PKC contributes to K_v7.5 channel inhibition, the potent PKC activator phorbol 12,13-dibutyrate (PDBu, 1 x10^{-6} M) was applied to cells expressing only K_v7.5. Application of PDBu resulted in a notable significant decrease in current amplitude, with a reduction in maximal conductance to 0.38 ± 0.03 G/G_{max} (P<0.0001; Fig 5.5A-B). The mean voltage-activation curve showed no significant change in $V_{0.5}$ from -47.46 ± 1 mV (control) to -43.38 ± 6 mV following PDBu application (P=0.4076; Fig. 5.5C; n=6). Although less pronounced than the effects of α_{1A}R activation, these data suggested that PKC activation alone could suppress K_v7.5 current amplitude, consistent with a possible parallel inhibitory mechanism downstream of receptor stimulation.

5.2.5 PKC inhibitors attenuate K_v7.5 currents

Pilot experiments were performed to assess the effect of PKC inhibition on K_v7.5 currents using a single-step voltage protocol (holding potential -80 mV, depolarising step to 0 mV for 1 s, followed by a hyperpolarising step to -120 mV). Application of the PKC inhibitors GF109203X or chelerythrine chloride (tested in separate experiments at 1 x10^{-6} M) reduced K_v7.5 current amplitude (Fig5.6A-B; n=2). Given the exploratory nature of these experiments and the unexpected direction of the effect, full current-voltage relationships were not generated

5.2.6 Exogenous PIP_2 prevents α_{1A}R-mediated inhibition of K_v7.5 currents

To assess whether PIP_2 depletion mediates α_{1A}R–induced inhibition, experiments were repeated using pipette solutions containing the soluble PIP_2 analogue $PI(4,5)P_2$ -diC_8 (2 x10^{-4} M). In the presence of exogenous PIP_2, application of PE (1 x10^{-4} M) failed to inhibit K_v7.5 currents, with no reduction in maximal conductance (1.02 ± 0.04 G/G_{max}; P=0.2179; Fig5.7A-B). The $V_{0.5}$ values showed a significant depolarising shift from -47.36 ± 2 mV in control + PIP_2 compared to -39.19

± 3 mV in PE + PIP_2 (P=0.0167; Fig5.7C; n=6). These findings indicated that preservation of membrane PIP_2 levels prevents α_{1A}R-mediated suppression of K_v7.5 activity, suggestive of PIP_2 depletion being the primary mechanism of α_{1A}R inhibition of K_v7.5 currents.

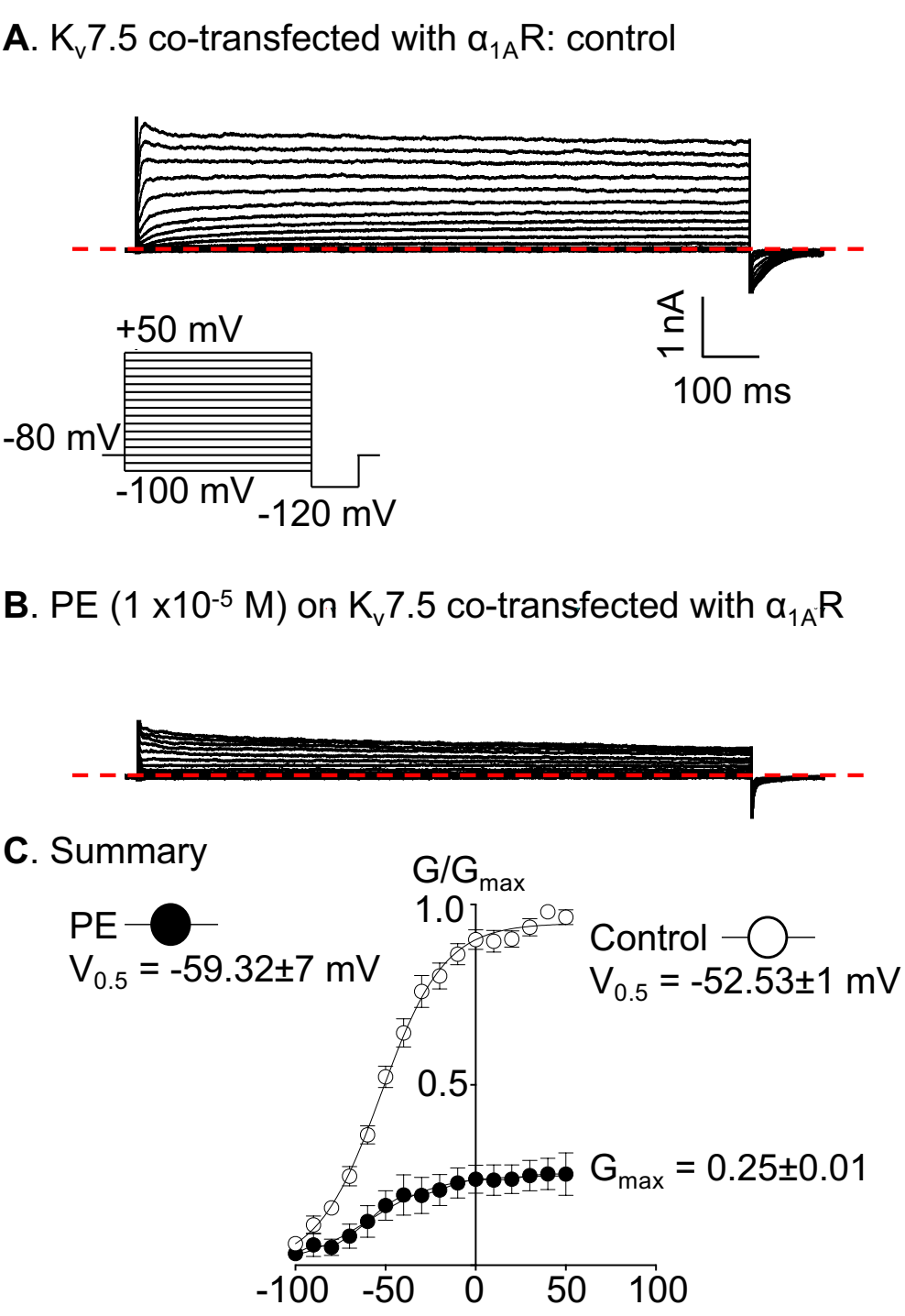
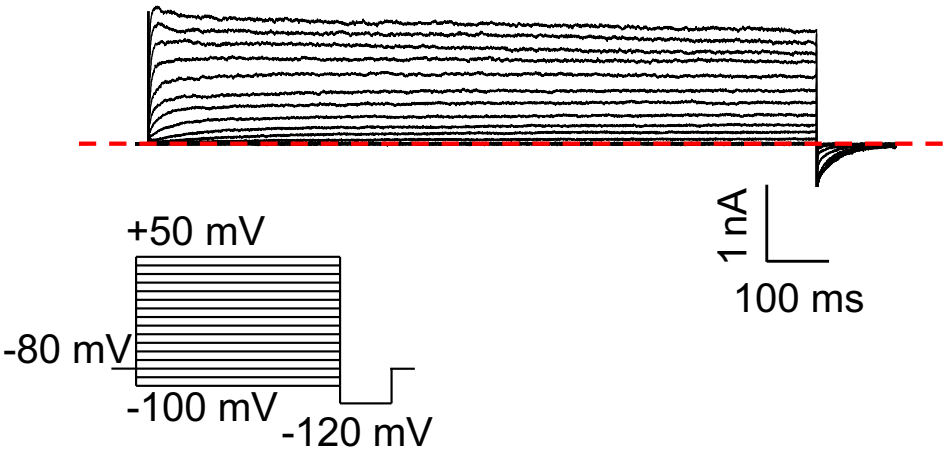


Figure 5.1: Effect of 1 x10^{-5} M PE on K_v7.5 channels co-expressed with α_{1A}Rs.
A. A typical family of currents obtained from HEK-293 cells expressing K_v7.5 channels and α_{1A}Rs. Voltage clamp protocol is described in the inset. Dotted lines represent the zero current level. **B.** The effect of 1 x10^{-5} M PE on currents from the same cell. **C.** Summary activation curves obtained from measuring tail currents in six cells before (white circles) and after (black circles) application of PE (n=6). The curves were fit with the Boltzmann equation. G/G_{max} ($P<0.0001$) and $V_{0.5}$ ($P=0.2478$).

A. $K_v7.5$ co-transfected with α_{1A}Rs: control



B. PE (1 x10^{-4} M) on $K_v7.5$ co-transfected with α_{1A}R



C. Summary

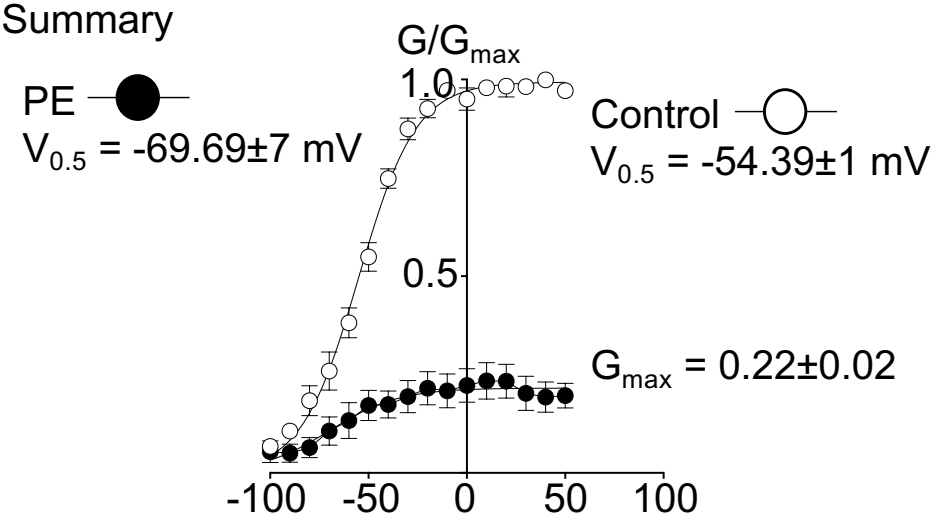


Figure 5.2: Effect of 1 x10^{-4} M PE on $K_v7.5$ channels co-expressed with α_{1A}Rs.
A. A typical family of currents obtained from HEK-293 cells expressing $K_v7.5$ channels and a_{1A}Rs. Voltage clamp protocol is described in the inset. Dotted lines represent the zero current level. **B.** The effect of 1 x10^{-4} M PE on currents from the same cell. **C.** Summary activation curves obtained from measuring tail currents in six cells before (white circles) and after (black circles) application of PE (n=6). The curves were fit with the Boltzmann equation. G/G_{max} ($P<0.0001$) and $V_{0.5}$ ($P=0.0162$).

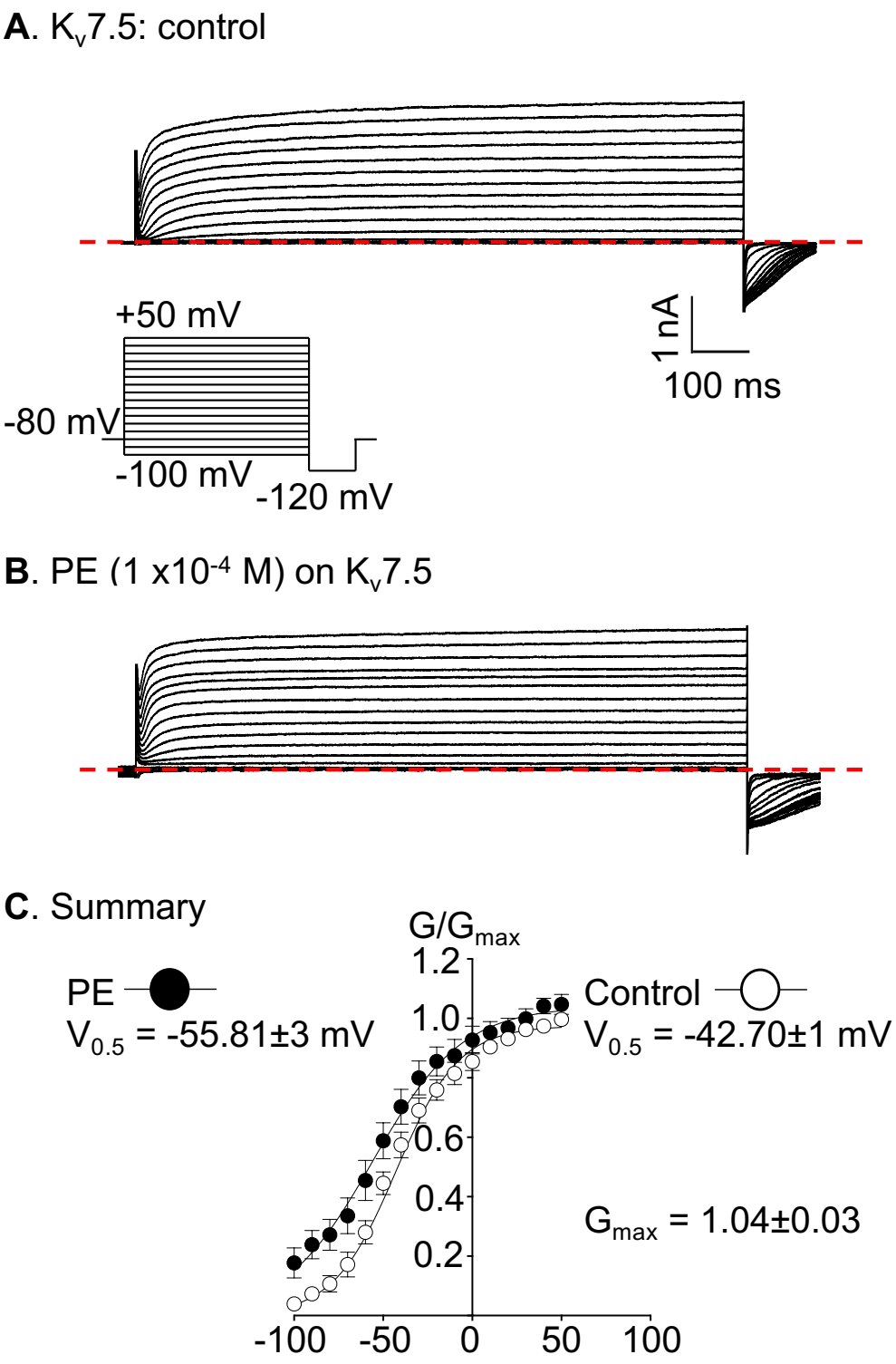
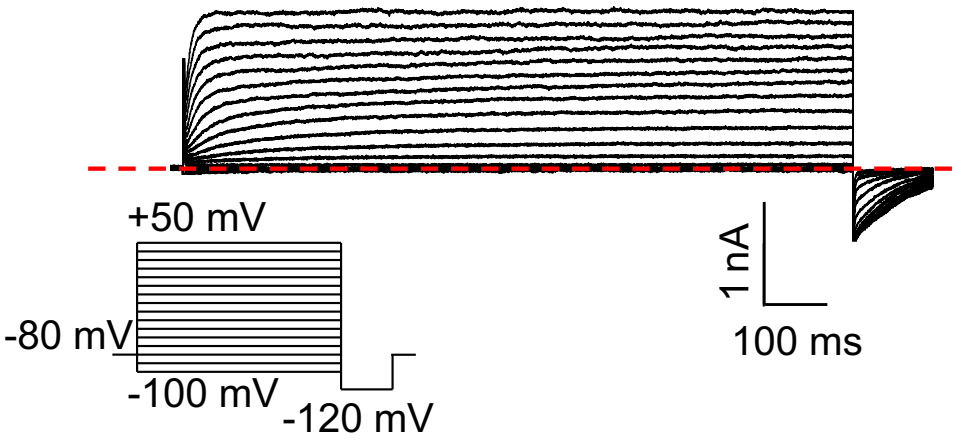
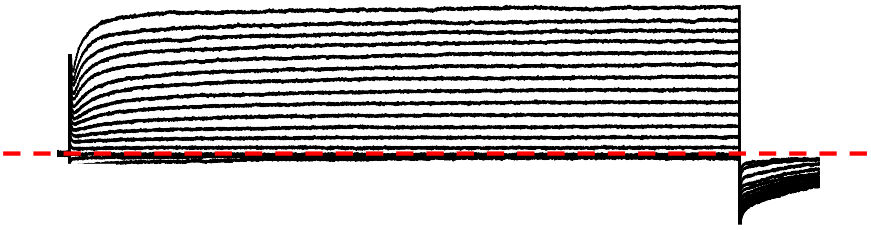


Figure 5.3: Effect of 1 x10^{-4} M PE on K_v7.5 channels.
A. A typical family of currents obtained from HEK-293 cells expressing K_v7.5 channels. Voltage clamp protocol is described in the inset. Dotted lines represent the zero current level. **B.** The effect of 1 x10^{-4} M PE on currents from the same cell. **C.** Summary activation curves obtained from measuring tail currents in six cells before (white circles) and after (black circles) application of PE (n=6). The curves were fit with the Boltzmann equation. G/G_{max} (P=0.0546) and $V_{0.5}$ (P<0.0001).

A. $K_v7.5$ co-transfected with $\alpha_{1A}R$: control



B. PE (1 x10^{-4} M) and Phentolamine (1 x10^{-6} M) on $K_v7.5$ co-transfected with $\alpha_{1A}R$



C. Summary

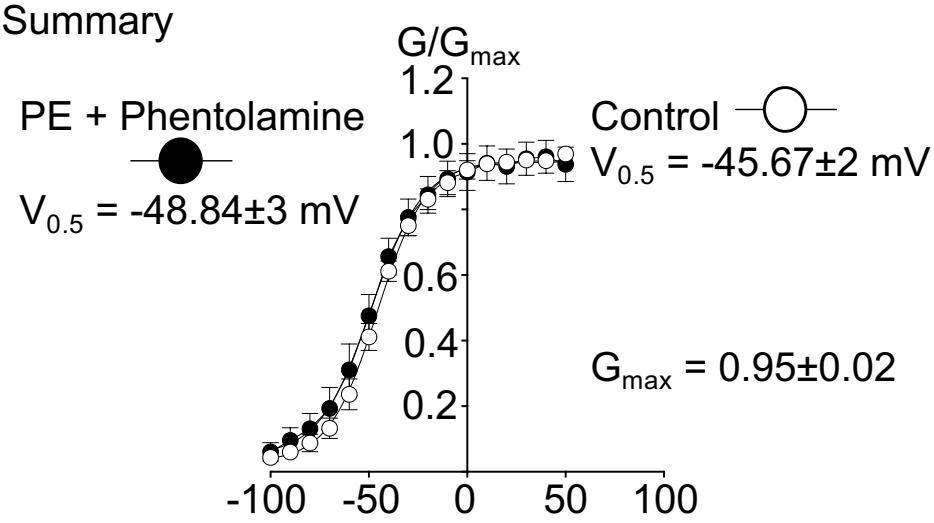


Figure 5.4: Effect of 1 x10^{-4} M PE on $K_v7.5$ channels co-expressed with α_{1A}Rs in the presence of an alpha-adrenergic blocker, 1 x10^{-6} M Phentolamine.

A. A typical family of currents obtained from HEK-293 cells expressing $K_v7.5$ channels and α_{1A}Rs. Voltage clamp protocol is described in the inset. Dotted lines represent the zero current level. **B.** The effect of 1 x10^{-4} M PE and 1 x10^{-6} M Phentolamine on currents from the same cell. **C.** Summary activation curves obtained from measuring tail currents in six cells before (white circles) and after (black circles) application of PE (n=6). The curves were fit with the Boltzmann equation. G/G_{max} (P=0.4694) and $V_{0.5}$ (P=0.5097).

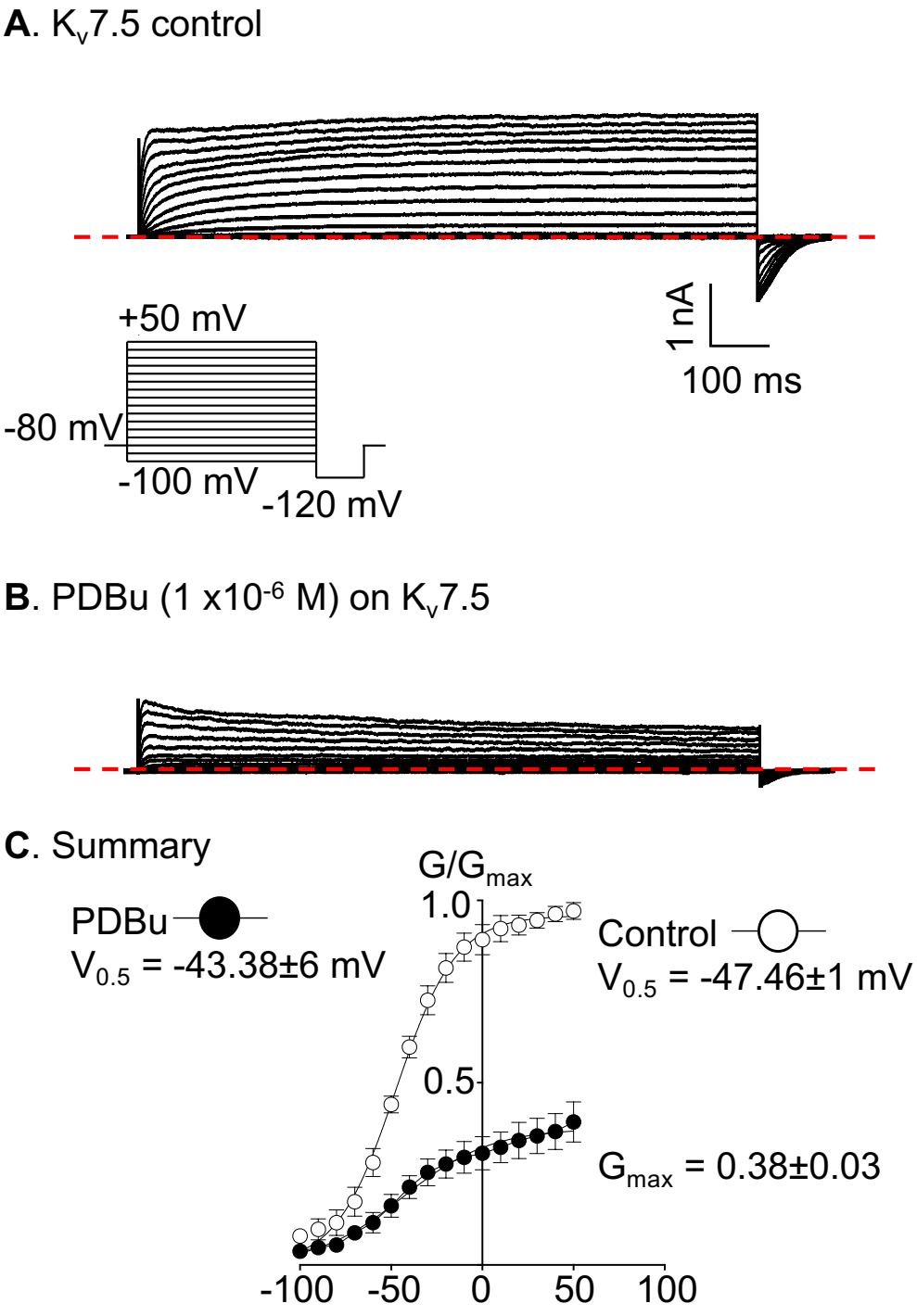
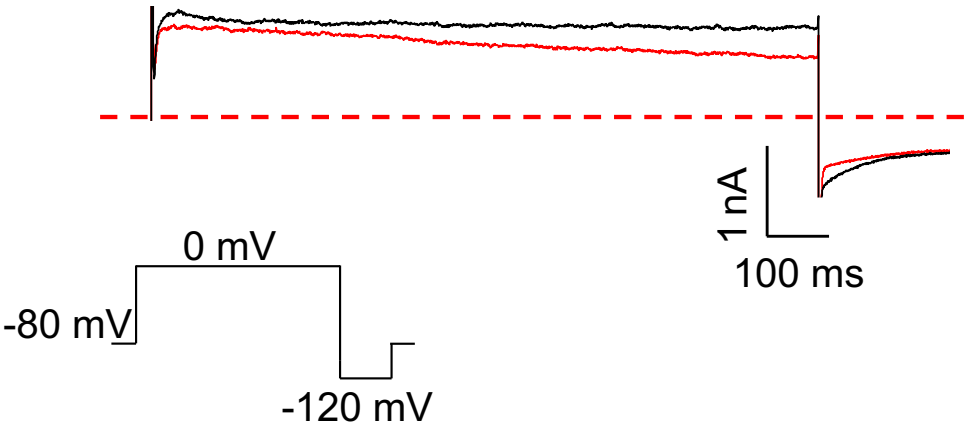


Figure 5.5: Effect of 1 x10^{-6} M phorbol 12,13-dibutyrate (PDBu) on K_v7.5 channels.
A. A typical family of currents obtained from HEK-293 cells expressing K_V7.5 channels. Voltage clamp protocol is described in the inset. Dotted lines represent the zero current level. **B.** The effect of 1 x10^{-6} M PDBu on currents from the same cell. **C.** Summary activation curves obtained from measuring tail currents in six cells before (white circles) and after (black circles) application of PDBu (n=6). The curves were fit with the Boltzmann equation. G/G_{max} ($P<0.0001$) and $V_{0.5}$ ($P=0.4076$).

A. GF109203X (1 x10^{-6} M) on K_v7.5 co-transfected with α_{1A}R



B. Chelerythrine chloride (1 x10^{-6} M) on K_v7.5 co-transfected with α_{1A}R

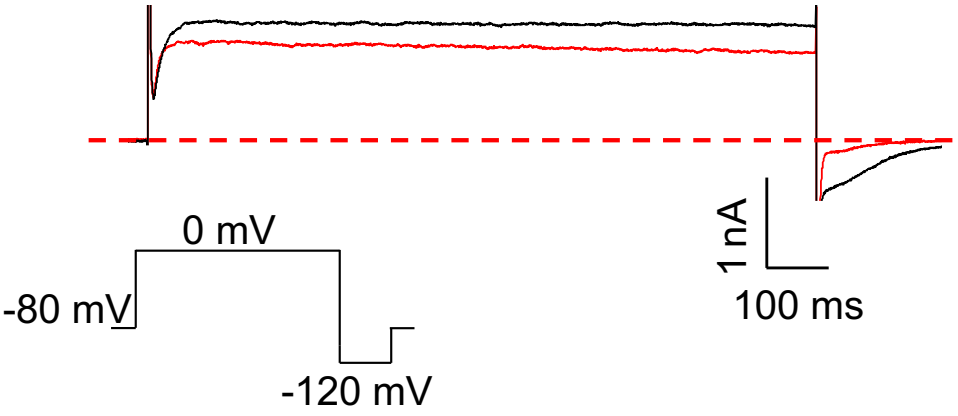
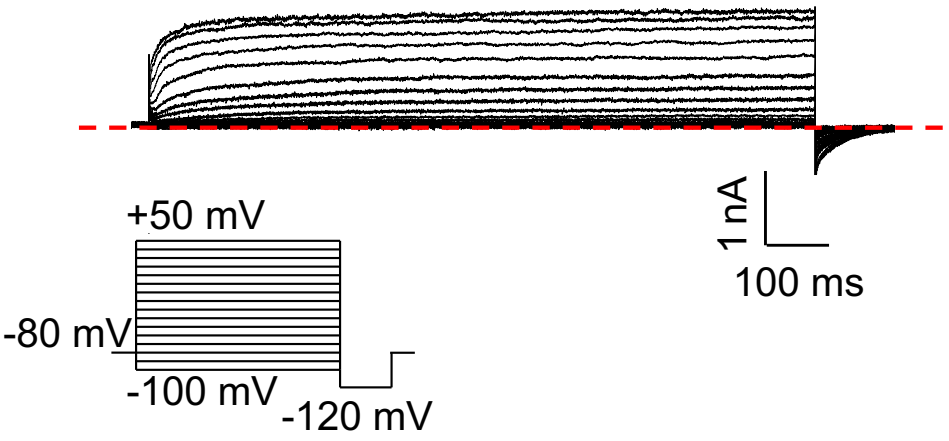
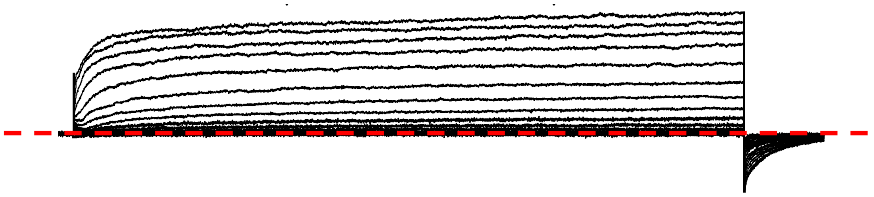


Figure 5.6: Effect of PKC inhibitors (GF109203X and chelerythrine chloride) on K_v7.5 channels co-expressed with α_{1A}Rs.
HEK-293 cells, expressing K_v7.5 channels and α_{1A}Rs, were held at a holding potential of -80 mV and subjected to a depolarizing step to 0 mV (1s), followed by a hyperpolarizing step to -120 mV.
A. The black trace is a control trace, and the red trace indicates the reduction current in the presence of 1 x10^{-6} M GF 109203X (n=2).
B. The black trace is a control trace, and the red trace indicates the reduction current in the presence of 1 x10^{-6} M chelerythrine chloride (n=2).

A. $K_v7.5$ co-transfected with $\alpha_{1A}R$: control with $PI(4,5)P_2$-diC8 (2×10^{-4} M) in the pipette solution



B. PE (1×10^{-4} M) with $PI(4,5)P_2$-diC8 (2×10^{-4} M) in the pipette solution on $K_v7.5$ co-transfected with $\alpha_{1A}R$



C. Summary

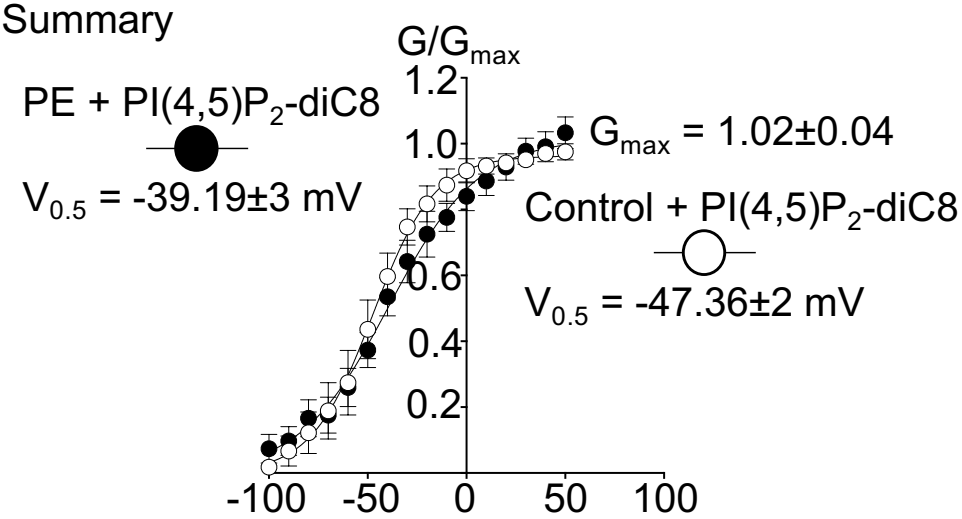


Figure 5.7: Effect of 1×10^{-4} M PE on $K_v7.5$ channels co-expressed with α_{1A}Rs in the presence of exogenous PIP_2 analogue - 2×10^{-4} M $PI(4,5)P_2$-diC8.

A. A typical family of currents obtained from HEK-293 cells expressing $K_v7.5$ channels and α_{1A}Rs, in the presence of 2×10^{-4} M $PI(4,5)P_2$-diC8 in the pipette solution. Voltage clamp protocol is described in the inset. Dotted lines represent the zero current level. **B.** The effect of 1×10^{-4} M PE and 2×10^{-4} M $PI(4,5)P_2$-diC8 on currents from the same cell. **C.** Summary activation curves obtained from measuring tail currents in six cells before (white circles) and after (black circles) application of PE (n=6). The curves were fit with the Boltzmann equation. G/G_{max} (P=0.2179) and $V_{0.5}$ (P=0.0167).

5.3 Discussion

This chapter was undertaken to test whether α_{1A}R activation can directly suppress K_v7.5 channel activity, thereby providing a plausible molecular mechanism linking adrenergic stimulation to enhanced CCSM excitability. Previous chapters demonstrated that pharmacological activation and inhibition of K_v7 channels abolished and enhanced phasic contractions in mouse CCSM, respectively. These contractions were shown to be dependent on LTCC-mediated Ca^{2+} influx, consistent with K_v7 channels providing a hyperpolarising influence that limits LTCC recruitment.

The present study provided insight into the molecular mechanisms underlying α_1R-dependent phasic contractility. PE inhibited K_v7.5 current in an α_{1A}R-dependent manner, and this effect was prevented by intracellular supplementation with an exogenous PIP_2 analogue. PKC activation partially mimicked this inhibitory effect; however, its contribution could not be clearly defined, as pharmacological inhibition using GF109203X and chelerythrine chloride was unsuccessful.

Taken together, these findings are consistent with a mechanism in which α_{1A}R-mediated inhibition of K_v7.5 channels occurs via PLCβ-dependent depletion of membrane PIP_2, with a possible additional contribution from PKC. These data therefore provided a mechanistic basis by which adrenergic stimulation may enhance phasic contractility in mouse CCSM. Inhibition of K_v7.5-mediated K^+ efflux would be expected to depolarise the membrane, increase LTCC open probability, and thereby facilitate Ca^{2+} influx.

5.3.1 Mechanism of α_{1A}R-mediated inhibition of K_v7.5 channels

The canonical $G_{q/11}$-PLCβ pathway is initiated with the stimulation of the α_1R, dissociation of the α-subunit of the $G_{q/11}$ complex, activation of PLCβ, which in turn hydrolyses membrane PIP_2 into diacylglycerol (DAG) and inositol-1,4,5-trisphosphate (IP_3; Berridge, 2016).

5.3.1.1 Role of PIP_2 depletion

Ichishima *et al*. (2010) confirmed that activation of α_1R in ventricular myocytes causes a reduction in membrane PIP_2 via fluorescence-based imaging. PIP_2 is essential for stabilising the open state of K_v7 channels by coupling voltage-sensor domain (VSD) movement to pore opening (Zhang *et al*., 2003; Falkenburger *et al*., 2010). In K_v7.1 channels, the depolarisation-induced conformational change of the

VSD facilitates PIP_2 binding, which in turn, facilitates the open-state of the pore (Zaydman *et al*., 2013; Mandala and MacKinnon, 2023). The results of this study supported PIP_2 depletion as the dominant mechanism of α_{1A}R-induced inhibition of $K_v7.5$ currents, given the prevention of this effect in the presence of exogenous PIP_2. Similar evidence has been reported in atrial myocytes, in which α_1R-activation suppressed G-protein-gated inward-rectifier K^+ (GIRK) currents, and was prevented with exogenous PIP_2 (Cho *et al*., 2001;2002;2005; Bender *et al*., 2002). These findings on GIRK modulation by α_1Rs parallel those for K_v7 channels, as both rely on membrane PIP_2 to sustain VSD-pore coupling and gating (Suh and Hille, 2002).

5.3.1.2 Role of PKC-mediated phosphorylation

The relative importance of PKC remains unresolved. α_{1A}R-mediated production of DAG, via the $G_{q/11}$-PLCβ pathway, activates PKC, a well characterised modulator of K_v7 channels. PKC has been shown to be anchored in close proximity to the C-terminal helices of K_v7 α-subunits, allowing the phosphorylation of serine/threonine residues (Brueggemann *et al*., 2014b). This phosphorylation induces conformational changes in the C-terminal regulatory region, including the PIP_2-binding domain, thereby reducing channel affinity for PIP_2. The consequent destabilization of the open state results in decreased current amplitude (Delmas and Brown, 2005; Fosmo and Skraastad, 2017; Brueggemann *et al*., 2020). $K_v7.5$ currents are reported to be relatively resistant to PKC-mediated inhibition, via arginine vasopressin and phorbol 12-myristate 13-acetate, than $K_v7.4$ in VSM (Brueggemann *et al*., 2014b). As of yet, the exact residues phosphorylated by PKC in $K_v7.5$ are not clear. Haick *et al*. (2017) showed histamine suppressed $K_v7.5$ currents in human trachealis smooth muscle in a PKC-dependent manner, and mutation of serine 441 (S441), in the proximal C-terminus of $K_v7.5$, abolished this effect, suggesting that S441 is a functionally important PKC phosphorylation site.

Evidence from excitable tissues support an established role for PKC in α_1R-induced inhibition of K^+ channels. In cardiac myocytes, α_1R stimulation suppressed voltage-dependent K^+ (K_v) currents and prolonged action potentials. This mechanism appears to be PKC-dependent, with α_1-agonist-induced inhibition of outward K^+ currents was mimicked by phorbol esters (PKC activators) and prevented by PKC inhibitors (Apkon and Nerbonne, 1988). Furthermore, rabbit atrial and ventricular myocytes showed α_1-agonist induced inhibition of outward (I_{out}) and inward-rectifier

(I_{K1}) currents, again, mimicked by PKC activators and prevented with PKC inhibitors (Fedida and Shimoni, 1990; Fedida *et al*., 1991; Braun *et al*., 1992).

Given evidence that PKC-mediated phosphorylation typically inhibits K_v7 channels, PKC inhibition would be expected to enhance or at least not attenuate $K_v7.5$ currents. To investigate the involvement of PKC in α_{1A}R-mediated inhibition of $K_v7.5$, pilot studies were conducted using two widely used PKC inhibitors, GF109203X (otherwise known as bisindolylmaleimide I) and chelerythrine chloride at 1 $x10^{-6}$ M. Both inhibitors have shown functional effects in electrophysiological experiments at 1 $x10^{-6}$ M, consistent with their use here (Zhu *et al*., 2005; Salzer *et al*., 2014). Unexpectedly, both inhibitors attenuated $K_v7.5$ currents, which may be explained by the non-selective nature of these compounds. Both inhibitors elicited blockade of the human Ether-a-go-go Related Gene (hERG) K^+ channel heterologously expressed in HEK-293 cells (Harmati *et al*., 2011). A comprehensive screening of GF109203X kinase inhibition selectivity revealed a concentration of 5 $x10^{-7}$ M inhibited (in a similar extent to the inhibitory effects of PKC) ten additional protein kinases (Anastassiadis *et al*., 2011). Moreover, chelerythrine chloride was found to not inhibit PKC, or any additional protein kinases tested (Davies *et al*., 2000). This signals a misleading marketing of chelerythrine chloride as a PKC inhibitor, however, it has been found to cytotoxic and an inducer of apoptosis, via one mechanism involving PKC-independent inhibition of pro-survival Bcl-2 family proteins (Yamamoto *et al*., 2001; Chan *et al*., 2003).

5.3.1.3 Role of Ca^{2+}-CaM

Constitutively bound CaM to the proximal C-terminus (helices A and B) of K_v7 channels functions as a structural subunit essential for channel assembly, trafficking, and gating (Yus-Nájera *et al*., 2002; Gamper & Shapiro, 2003; Delmas & Brown, 2005). The interaction between CaM and the K_v7 C-terminus was first resolved by X-ray crystallography, revealing the characteristic “CaM-hug” configuration in which CaM wraps around helices A and B of $K_v7.1$ (Wiener *et al*., 2008; Sachyani *et al*., 2014; Tobelaim *et al*., 2017). Subsequent cryo-EM studies by Sun and MacKinnon (2020) confirmed this arrangement in the full-length $K_v7.1$-CaM-PIP_2 complex and demonstrated that CaM stabilises the closed state of the pore. PIP_2 binding in the presence of Ca^{2+}-free (apo-) CaM induces conformational rearrangements within the C-terminal helices that relieve this inhibition and promote channel opening. Conversely, Ca^{2+} binding to CaM alters the shape of the PIP_2 binding site, reducing

channel affinity open for PIP_2 and decreasing probability (Sun and MacKinnon, 2020). X-ray crystallography has confirmed that this mode of CaM binding and Ca^{2+}-dependent conformational switching is conserved across K_v7 isoforms, although cryo-EM evidence remains unavailable for $K_v7.5$ (Xu *et al*., 2013; Chang *et al*., 2018).

Given function of structurally bound CaM to the $K_v7.5$ C-terminus as a Ca^{2+} sensor, the mobilisation of Ca^{2+}, via the canonical $G_{q/11}$-PLCβ pathway, via IP_3Rs in the ER membrane during $\alpha_{1A}R$-activation may serve a significant function. In rat sympathetic neurons, activation of bradykinin receptor 2, with a downstream G_q-PLC pathway, suppressed M-current; an effect requiring ER store Ca^{2+} release, and prevented via store depletion (Cruzblanca *et al*., 1998). Interestingly, in the same cell type, muscarinic receptor 1 ($G_{q/11}$-PLC pathway) activation inhibited M-current, yet in a PIP_2-dependent mechanism, independent of Ca^{2+} release (Suh and Hille, 2002). The results of the present study indicate a predominantly PIP_2-dependent mechanism, consistent with the protection conferred by exogenous PIP_2 analogues. However, the potential contribution of Ca^{2+} release via IP_3Rs was not examined here and should be investigated in future experiments.

5.3.1.4 Role of Gβγ subunits

So far, we have discussed the canonical $\alpha_{1A}R$ signalling pathway utilising $G_{q/11}$ and PLCβ, yet the activation of $\alpha_{1A}Rs$, will release Gβγ subunits, which have been shown to modulate K_v7 channel function. Stott *et al*. (2015) demonstrated that Gβγ subunit application to $K_v7.4$ channels, in HEK-293 cells, dramatically increased current amplitude and shifted the $V_{0.5}$ to more hyperpolarised potentials, an effect prevented in the presence of Gβγ subunit inhibitors (gallein, GRK2i and a β-subunit antibody). Furthermore, K_v7 currents in native renal arterial myocytes were enhanced by the presence of Gβγ subunits, likewise, the Gβγ subunit inhibitor, gallein, inhibited these currents (Stott *et al*., 2015b). The initial findings were only relevant to $K_v7.4$ overexpression in HEK-293 cells, yet the suggested dominant expression of K_v7 channels in VSM is heteromeric $K_v7.4/5$, suggestive that the mechanism of Gβγ-enhancement may be shared in $K_v7.5$ and relevant to our study (Chadha *et al*., 2014; Brueggemann *et al*., 2014).

The mechanism by which Gβγ subunits enhance $K_v7.4$ currents is not fully understood, yet a recent study has provided valuable insight. Gβγ subunits may interact with the C-terminus of $K_v7.4$ channels, and increase affinity for PIP_2, stabilising

the open state (Povstyan *et al*., 2017). Povstyan *et al*. (2017) demonstrated this relationship using inside-out patches of HEK-293 cell overexpressing $K_v7.4$ channels, PIP_2-mediated activation was inhibited in the presence of Gβγ subunit inhibitors.

The role of Gβγ subunits in regulating K_v7 channel activity is complex. With five Gβ ($Gβ_{1-5}$) and twelve Gγ ($Gγ_{1-12}$) isoforms identified in mammalian cells, multiple Gβγ combinations can form, each potentially conferring distinct regulatory effects (Smrcka, 2008). Greenwood and Stott (2020) have partly elucidated these distinct effects, with $Gβ_3$ knockdown in rat renal artery myocytes markedly attenuating native K_v7 current amplitude, resting membrane potential and enhancement to $K_v7.2$-5 activator, RTG. Moreover, $Gβ_1$ knockdown decreased protein expression of $K_v7.4$, and $Gβ_5$ knockdown had no observable effect (Greenwood and Stott, 2020). Taken together, these findings suggested that, given the strong PIP_2 dependence of $K_v7.5$ and the diverse modulatory potential of Gβγ subunit combinations, Gβγ subunits may enhance $K_v7.5$ currents in spite of the predominant $α_{1A}$R-induced inhibition.

The enhancement effects of Gβγ subunits may serve as one possible explanation for the contradictory findings of this study, in which notable hyperpolarising shifts in $V_{0.5}$ were recorded despite a dramatic inhibition of $K_v7.5$ currents following $α_{1A}$R activation. The results indicate a predominant PIP_2-depletion effect; however, a residual current remained after PE application (approximately 22% of G_{max}). One likely explanation is that these remaining, not fully PIP_2-depleted, $K_v7.5$ channels are enhanced by the abundance of Gβγ subunits released upon activation of overexpressed $α_{1A}$Rs, thereby shifting the $V_{0.5}$ in a hyperpolarising direction.

Given the work of Povstyan *et al*. (2017), we would expect these Gβγ subunits to increase PIP_2 affinity in the remaining, not fully PIP_2-depleted, $K_v7.5$ channels, thus stabilising the open state at more hyperpolarised potentials. Yet, a hyperpolarising shift in $V_{0.5}$ was also observed when PE was applied to HEK-293 cells expressing $K_v7.5$ alone. One plausible explanation for this is the existence of endogenously expressed $α_1$Rs in HEK-293 cells. Pillay *et al*. (2020) confirmed endogenous expression of $α_1$Rs in HEK-293 cells via western blotting and identified transcripts for $α_{1A}$Rs (ADRA1A) and $α_{1D}$Rs (ADRA1D). Therefore, it is likely that these endogenous $α_1$Rs are stimulated by PE, releasing Gβγ subunits that enhance $K_v7.5$ currents. The associated effects on PKC activation, PIP_2 depletion, and Ca^{2+} release are likely inconsequential due to the overexpression of $K_v7.5$ and the comparatively low levels of endogenous $α_1$Rs. This explanation is further supported by the finding that, in HEK-293 cells co-expressing

$K_V7.5$ and α_{1A}Rs, PE application in the presence of phentolamine produced no shift in $V_{0.5}$.

5.3.2 Beyond $G_{q/11}$-PLCβ: additional pathways of $K_V7.5$ regulation

Canonically, α_1Rs are coupled to $G_{q/11}$ proteins, yet non-canonical coupling has been described in multiple studies. Horie *et al*. (1995) demonstrated that in CHO cells expressing α_{1B}Rs, agonist stimulation increased both cytosolic Ca^{2+} and cAMP. The rise in Ca^{2+} was abolished by the PLC inhibitor U-73122, whereas cAMP production remained unaffected. Notably, the increase in cAMP was inhibited with G_s α-subunit antiserum, indicating α_1Rs couple to non-canonical G proteins (Horie *et al*., 1995). Interestingly, this does not appear to apply uniformly for all α_1Rs, with α_{1A}Rs and α_{1B}Rs able to couple to G_s proteins, but not α_{1D}Rs. Mutational chimera studies identified key amino acid residues (Thr136 and Val138) in the second intracellular loop of α_{1A}Rs are required for coupling to G_s proteins (Shinoura *et al*., 2002).

Aside from G_s proteins, α_1Rs have also been implicated to couple to $G_{i/o}$ proteins. Tohkin *et al*. (1990) showed that pertussis toxin (PTX, a $G_{i/o}$ inhibitor) decreased α_1R-stimulation induced PLC activation. Moreover, these effects have been detected in rabbit aortic myocytes, in which α_1R-stimulation elicited a PTX-sensitive Ca^{2+} influx, calmodulin interaction, phospholipase A_2 activation, resulting in prostacyclin production (Nebigil and Malik, 1993). Taken together, these data support a model in which α_1Rs predominantly couple to $G_{q/11}$ proteins, yet non-canonical coupling to G_s/$G_{i/o}$ proteins can result from receptor subtype and expression level (Cotecchia, 2010; Akinaga *et al*., 2019; Kim *et al*., 2020; Pérez, 2021). Given that HEK-293 cells express endogenous α_1Rs, it is plausible that similar non-canonical coupling may occur in this model system, and this warrants further investigation.

5.3.2.1 Role of PKA

Activation of G_s stimulates AC, elevating cAMP and thereby activating PKA, on the other hand, $G_{i/o}$ inhibits AC, decreasing cAMP and attenuating PKA activity (Neves *et al*., 2002; Sadana and Dessauer, 2009). PKA phosphorylates specific serine and threonine residues on target proteins, thereby altering their biophysical properties and regulatory interactions. Consequently, PKA serves as a key modulator of ion-channel function, including the K_V7 channels relevant to the present study (Taylor *et al*., 2013; Conti *et al*., 2014).

The PKA-mediated phosphorylation of $K_v7.1$, resulting in increased amplitude, occurs at serine-27 of the N-terminus (Kurokawa *et al*., 2004). In cardiomyocytes, Kv7.1 co-assembles with minK (encoded by *Kcne1*) to form the I_{Ks} current, important in the repolarisation phase of the cardiac action potential, and displays enhancement by PKA phosphorylation, with increased current amplitude and channel expression (Thompson *et al*., 2020). Marx *et al*. (2002) found that PKA-phosphorylation of $K_v7.1$ is dependent on tethering via A-kinase-anchoring protein 9 (AKAP9/Yotiao), bound to the C-terminus of $K_v7.1$ via a leucine zipper. Loss-of-function mutations in $K_v7.1$ or its auxiliary subunit minK (encoded by *Kcne1*) reduce I_{Ks} and are associated with congenital long-QT syndrome (LQTS). Notably, the LQTS-associated $K_v7.1$ mutation G589D disrupts Yotiao binding, thereby preventing PKA-mediated phosphorylation resulting in impaired channel function (Marx *et al*., 2002).

Relevant to the focus of this study, PKA has demonstrated modulatory effects on $K_v7.5$ channels. In human airway smooth muscle cells, activation of β-receptors (βRs), coupled to G_s proteins, stimulate AC, increase cellular cAMP and activate PKA, which in turn, increases $K_v7.5$ current amplitude, via phosphorylation of a N-terminal residue, serine-53 (S53). Confirming the importance of this phosphorylation site, a mutation (S53A) abolished the enhancement effect of PKA (via βR stimulation, FK and IBMX). The authors suggested phosphorylation of this site increased PIP_2 affinity, given that sensitivity to PIP_2 depletion was reduced after PKA activation (Brueggemann *et al*., 2018). Mani *et al*. (2016) showed endogenous K_v7 currents of A7r5 rat aortic myocytes, predominantly $K_v7.5$, were markedly enhanced by PKA activation. Furthermore, the heteromeric $K_v7.4/5$ channels, endogenously expressed in rat mesenteric artery smooth muscle cells or exogenously expressed in A7r5 cells, showed decreased enhancement to PKA activation, and lastly, homomeric $K_v7.4$ channels showed no enhancement (Mani *et al*., 2016). The isoform-specific effects were further supported by evidence that a chimera of $K_v7.4$ with the $K_v7.5$ N-terminus, conferred the cAMP sensitivity (Brueggemann *et al*., 2020).

In summary, PKA is a strong positive regulator of $K_v7.5$. While α_{1A}Rs have been reported to couple to non-canonical G proteins (G_s or $G_{i/o}$), raising the possibility in HEK-293 cells that α_{1A}R stimulation could activate PKA and augment $K_v7.5$ currents, the opposite outcome is also plausible, that α_{1A}R activation could lower cAMP, inhibit PKA, and thus potentiate $K_v7.5$ suppression. The recruitment of G_s proteins via α_{1A}R-stimulation serves as another potential explanation for the hyperpolarising shift in the

$V_{0.5}$ during PE stimulation of HEK-293 cells expressing α_{1A}Rs and K_v7.5; whereby, the non-PIP_2 depleted K_v7.5 channels become phosphorylated by PKA, stabilising the open state at more hyperpolarised potentials.

5.3.3 Physiological implications

Penile flaccidity is maintained by sympathetic outflow of noradrenaline (NA) acting on α_1Rs (predominant expression of α_{1A}Rs and α_{1D}Rs) in CCSM cells (Traish *et al*., 1995; Daussé *et al*., 1998; Dean & Lue, 2005; Docherty, 2009; Jung *et al*., 2014). In healthy men, intracavernosal NA decreases during tumescence and rises during detumescence, whereas men with ED exhibit increased NA release during sexual stimulation, consistent with sustained sympathetic tone and maintenance of flaccidity (Becker *et al*., 2000; 2002). Accordingly, ED is correlated to states of increased sympathetic tone such as hypertension, ageing, and diabetes. Spontaneously hypertensive rats display impaired erectile responses and enhanced CCSM contractions to PE (Behr-Roussel *et al*., 2003; Ushiyama *et al*., 2006). Moreover, aged human and rat corpus cavernosum show elevated CCSM contractility, with rat models additionally showing elevated tyrosine hydroxylase expression in line with elevated sympathetic tone (Christ *et al*., 1991; Silva *et al*., 2014). Lastly, diabetic models exhibited dysregulated neurogenic and endothelial signalling, in line with reduced NO release and bioavailability due to endothelial dysfunction and peripheral neuropathy; indicating a dominant adrenergic over an impaired nitrergic signalling pathway (De Tejada, 2004). Contrary to this, decreased adrenoceptor responsiveness has been reported in penile tissue from men with T2DM (Iñigo Sáenz de Tejada, personal communication). It remains unclear if ED conditions produce a concomitant increase in α_1R expression, with one study finding preserved transcriptional expression, with a slight decrease in α_1R, β_1R and soluble guanylate cyclase (sGC) in middle-aged vs young rats (Silva *et al*., 2014). Despite this uncertainty, it remains clear that sympathetic overactivity and enhanced adrenergic contractile responses contribute to ED pathophysiology.

With this pathophysiological context in mind, the findings of the present study suggested that heightened sympathetic tone would increase α_1R activation and thereby amplify downstream $G_{q/11}$ signalling, resulting in enhanced PIP_2 hydrolysis, PKC activation, and SR Ca^{2+} release. Collectively, these signalling events are predicted to maintain endogenously expressed K_v7.5 (and other K_v7 isoforms) in a PIP_2-depleted state. Given the fundamental role of K_v7 channels in CCSM in stabilising

the membrane potential and limiting LTCC activity, persistent suppression of K_v7 currents would be expected to depolarise CCSM, increase LTCC-mediated Ca^{2+} influx, and thereby enhance contractility to maintain flaccidity (Mercer *et al*., 2025). Furthermore, K_v7 channels act as downstream effectors of cyclic-nucleotide signalling pathways in CCSM (cAMP and cGMP), meaning their inhibition could also blunt relaxation mechanisms that depend on cAMP or cGMP-mediated signalling (Jepps *et al*., 2016; Lee *et al*., 2020a; van der Horst *et al*., 2020).

5.3.4 Limitations and future directions

This study demonstrated a α_{1A}R-dependent mechanism of $K_v7.5$ inhibition, likely involving PIP_2 depletion. Several limitations should be considered. Firstly, only $K_v7.5$ was examined within an interplay with α_{1A}R. Relatively low amounts of *Kcnq4* and *Kcnq1* transcripts have been detected in mouse CCSM (Fig3.1D). $K_v7.5$ was chosen for relevancy, based on its relatively high transcriptomic presence (Fig3.1D) and the presence of $K_v7.5$ α-subunits in mouse CCSM cells (Fig3.2A). Yet, studies on rat and human CCSM detected higher quantities of *Kcnq4*, making it physiologically relevant, and VSM cells have been suggested to form heteromeric $K_v7.4/5$ channels, with distinct electrophysiological characteristics (Chadha *et al*., 2014; Brueggemann *et al*., 2014; Jepps *et al*., 2016; Lee *et al*., 2020a). Furthermore, K_v7 isoforms have distinct PIP_2 affinities and sensitivity to PKC, indicating each α_{1A}R-dependent mechanism may show a variety of sensitivities (Hernandez *et al*., 2009; Brueggemann *et al*., 2014). Therefore, future work should examine the effects of α_{1A}R-activation of homomeric $K_v7.4$ and heteromeric $K_v7.4/5$ channels.

Next, PDBu was used to activate PKC, inhibiting $K_v7.5$ currents, yet a PKC inhibitor, given the pharmacological promiscuity, was not employed to determine the extent of protection from the α_{1A}R-dependent inhibition. Furthermore, the contribution of Ca^{2+}-CaM formation from the activation of the $G_{q/11}$-PLCβ pathway was not assessed. Therefore, future experiments utilising selective pharmacological inhibition of PKC and IP_3Rs, or a Ca^{2+} chelator, would distinguish the relative contributions of these components of the activated $G_{q/11}$-PLCβ pathway.

HEK-293 cells overexpressing $K_v7.5$ and α_{1A}Rs were utilised in this study, thus the overexpression may exaggerate the signalling pathway and not represent physiological mechanisms. Future experiments will need to isolate endogenous K_v7

currents in isolated mouse CCSM cells, and determine the inhibitory effect of α_1R-stimulation.

Lastly, the mechanism of α_{1A}R-induced inhibition was determined to be PIP_2 depletion, yet this was extrapolated based on the protection conferred by the addition of exogenous PIP_2-analogue ($PI(4,5)P_2$-diC_8) in the pipette solution. Live-cell PIP_2 biosensors, such as PH-PLCδ1-GFP, which allows real-time analysis of membrane PIP_2 levels and provides direct confirmation of the α_{1A}R-induced inhibition of K_V7.5 via PIP_2 depletion.

6. Results Chapter 4:

Modulation of contractions and cytosolic Ca^{2+} by cAMP and its downstream effector proteins, EPAC and PKA

6.1 Introduction

The penile erection is formed in part by the relaxation of the CCSM, which is mediated by the action of intracellular cyclic nucleotides and their downstream effector protein kinase signal transduction pathways (Andersson, 2011). Current ED treatments rely heavily on enhancing the NO-cGMP-PKG pathway, where PDE5Is such as sildenafil increase cGMP by inhibiting its breakdown (Francis *et al*., 2008). NO-stimulated cGMP can act via PKG isoforms, which, when stimulated by the binding of two cGMP molecules, relieves autoinhibition of the kinase domain of the PKG protein, allowing phosphorylation of target serine/threonine residues (Casteel *et al*., 2010). Yet the exact cellular events concurrent with cGMP stimulation are not fully defined; nonetheless, evidence reveals PKG I phosphorylates phospholamban, disinhibiting the SERCA pump and decreasing cytosolic Ca^{2+} concentration by increased SERCA-mediated Ca^{2+} uptake (Movsesian *et al.*, 1984; Raeymaekers and Casteels, 1988). Furthermore, PKG has the capacity to modulate ion channels, acting on LTCCs and BK_{Ca} channels (Joshi *et al*., 2012). The mechanical removal of Ca^{2+} from the cytosol and inhibition of LTCCs may cause decreased cytosolic Ca^{2+} levels and inhibit contractile activity (Andersson, 2011).

The importance of the NO-cGMP-PKG pathway cannot be overstated given the popular success of PDE5Is as a first-line oral treatment for ED. However, approximately 30-40% of men suffering from ED do not respond to PDE5I treatment (de Tejada, 2004). Non-responsiveness is most common in conditions such as diabetes mellitus, advanced vasculopathy, and neurogenic injury, all of which compromise endothelial or neuronal NO production (Fonseca *et al*., 2004; Cheng *et al*., 2007; Dubsky *et al*., 2023). Reduced NO availability limits cGMP synthesis, and because PDE5Is depend on endogenous cGMP generation to exert their effect, their efficacy falls sharply when NO signalling is impaired. These constraints highlight the need to define NO-independent mechanisms of CCSM relaxation and identify alternative therapeutic pathways for patients who do not benefit from PDE5I treatment.

Prior to the mass adoption of PDE5Is as the first line treatment of ED, pharmacological agents acting via the parallel cAMP pathway were administered by cavernosal injections of alprostadil (synthetic PGE_1; Porst *et al*., 1996). The effects of stimulating the cAMP pathway were postulated to be mediated by the protein effector PKA, a serine/threonine kinase that can be tethered to cellular targets via AKAP proteins to optimise phosphorylation activity. Such targets may include phosphorylation

of phospholamban to disinhibit SERCA (Tada *et al*., 1974; Lindemann *et al.*, 1983). Crucially, PKA directly enhances $K_V7.5$ channel activity; In vascular and airway smooth muscle, β-adrenergic/cAMP signalling enhanced K_V7 currents via PKA-dependent phosphorylation of an N-terminal residue, serine 53, of $K_V7.5$ channels (Mani *et al*., 2016; Brueggemann *et al*., 2018).

However, cAMP signalling also acts on an additional effector, EPAC, yet less is known about this cAMP-dependent pathway (de Rooij *et al*., 1998). EPAC gene transcripts (*Rapgef3* and *Rapgef4*) have not been detected at the mRNA level in CCSM, but recent studies in rat corpus cavernosum have detected the EPAC-1 protein by immunohistochemistry and western blotting (Lin *et al*., 2023). Despite this protein-level evidence in rat tissue, the functional consequences of EPAC activation have not been defined in CCSM, and its role in regulating CCSM contractility remains unknown. However, in VSM, EPAC has demonstrated the ability to promote relaxation via a reduction of cytosolic Ca^{2+}. Similar effects were also reported in the airway and detrusor smooth muscle (Roscioni *et al*., 2011; Cuíñas *et al*., 2016; Hayashi *et al*., 2016). The hypothesised mechanism involves EPAC modulation of membrane potential through activation of RyR-mediated release of Ca^{2+} to stimulate BK_{Ca} channels, promoting K^+ efflux, decreasing the probability of opening of LTCCs, and limiting Ca^{2+} influx (Roberts *et al*., 2013). Additional reports indicate EPAC-mediated inhibition of K_{ATP} channels via activation of the serine/threonine phosphatase calcineurin (Purves *et al*., 2009). Lastly, isoprenaline increased the co-localisation of EPAC downstream effectors, Rap1a and Rap2, with $K_V7.4$ α-subunits, consistent with a role for EPAC in modulating their activity (Stott *et al*., 2016).

On this basis, the present chapter sought to:

1. Identify EPAC expression, at both a transcriptional and protein level, in corpus cavernosum.
2. Determine the differential effects of cAMP, PKA, and EPAC activation via FK, N^6- Monobutyryladenosine- 3', 5'- cyclic monophosphate (6-MB), and 8-pCPT-2-O-Me-cAMP-AM (007-AM), respectively, on CCSM contractile activity.
3. Examine the effect of FK, 6-MB, and 007-AM on intracellular Ca^{2+} oscillations in isolated CCSM cells.

4. Examine whether K_v7 channels contribute to cAMP-dependent signalling pathways, using pharmacological blockade of K_v7 (XE-991) on contractile and Ca^{2+} oscillations.

6.2 Results

6.2.1 AC activation inhibits adrenergic phasic contractions through a K_v7-dependent mechanism

Activation of AC with FK produced a robust and concentration-dependent inhibition of phasic contractions evoked by 3 $x10^{-7}$ M PE (Fig6.1A/C-D). Incremental FK application (1 $x10^{-9}$ M-3 $x10^{-8}$ M) led to progressive reductions in phasic frequency and amplitude, culminating in abolition of phasic activity at higher FK concentrations. Summary data for concentration-effect-curves for reduction in contraction frequency and amplitude revealed IC_{50} values in the low-nanomolar range (Fig6.1C: 1.79 $x10^{-8}$ M; Fig6.1D: 1.721 $x10^{-8}$ M; n=6, N=6).

To determine the contribution of K_v7 channels in the FK-induced cAMP signalling pathway activation, prior to FK application, tissues were incubated in K_v7 channel blocker, XE-991 (1 $x10^{-5}$ M) for 20 mins. The potency of FK was attenuated in the presence of K_v7 blockade, although it was still able to abolish phasic contractions, requiring increased FK concentrations (Fig6.1B). Summary data for concentration-effect-curves in control and in the presence of XE-991, indicated a significant rightward shift in IC_{50} for both frequency (Fig6.1C: 1.79 $x10^{-8}$ M vs 8.310 $x10^{-8}$ M, $P<0.0001$) and amplitude (Fig6.1D: 1.721 $x10^{-8}$ M vs 6.823 $x10^{-8}$ M, $P<0.0001$; n=6, N=6).

In contrast to the phasic contractions, 1 $x10^{-4}$ M PE-elicited tonic contractures required substantially higher concentrations of FK to achieve relaxation, with an IC_{50} of 1.660 $x10^{-7}$ M (Fig6.2A/C). Importantly, K_v7 blockade, with XE-991, did not affect FK potency under these conditions, with no significant difference in the IC_{50} to FK after incubation with XE-991 (Fig6.2B/C; IC_{50}: 1.610 $x10^{-7}$ M, $P=0.1315$; n=6, N=6).

6.2.2 Selective activation of EPAC and PKA induce modest inhibitions, whereas co-activation abolishes contractile activity

Given the relatively high sensitivity of CCSM to the AC activator, FK, the effect of selectively activating individual cAMP effector pathways was examined. The effect of EPAC activation was examined using 007-AM in CCSM tissues pre-contracted with 3 $x10^{-7}$ M PE. Application of 1 $x10^{-5}$ M 007-AM produced a modest attenuation of phasic activity (Fig6.3A). Phasic activity measured in the 15-20 min control interval and the 35-40 min interval in the presence of 007-AM revealed a 25% reduction in contraction frequency from 6.87 ± 1.47 min^{-1} to 5.17 ± 1.07 min^{-1} (Fig6.3B; $P=0.0156$) and a 14%

reduction in amplitude from 1.00 ± 0.16 mN to 0.86 ± 0.16 mN (Fig6.3C; P=0.0276; n=6, N=6).

Next, the effects of PKA activation were assessed with 6-MB, on CCSM pre-contracted with 3 $x10^{-7}$ M PE. Application of 1 $x10^{-4}$ M 6-MB, like 007-AM, produced only modest attenuation of phasic contractions (Fig6.4A), with frequency decreasing from 6.70 ± 0.59 min^{-1} under PE alone to 4.57 ± 0.47 min^{-1} in the presence of 6-MB, representing a 32% reduction (Fig6.4B; P=0.0001) and no significant change in amplitude, which measured 1.47 ± 0.29 mN under PE alone and 1.37 ± 0.26 mN in the presence of 6-MB, representing an approximately 7% reduction (Fig6.4C; P=0.1814; n=6, N=6).

Given the relatively high sensitivity of CCSM to FK, potent effects of FK, yet the relatively modest effects of EPAC and PKA activators, the effect of co-activation of EPAC and PKA was assessed in CCSM preparations pre-contracted with 3 $x10^{-7}$ M PE. Co-application of 1 $x10^{-5}$ M 007-AM and 1 $x10^{-4}$ M 6-MB rapidly and consistently abolished phasic contractions (Fig6.5A), with frequency falling from 5.83 ± 0.94 min^{-1} under PE alone to 0.00 ± 0.00 min^{-1}, and amplitude falling from 0.87 ± 0.14 mN to 0.00 ± 0.00 mN. Summary data confirmed this abolition was consistent across replicates, for both contraction frequency (Fig6.5B; P=0.0016) and amplitude (Fig6.5C; P=0.0015; n=6, N=6). We found that activating EPAC or PKA alone produces no meaningful reduction in contractility, whereas co-activation of both cAMP effectors completely inhibited contraction.

6.2.3 Molecular identification of EPAC isoforms in CCSM

Given the effect of EPAC activation, in the presence of PKA activation, abolished contractile activity, the molecular expression of EPAC isoforms in mouse CCSM was examined using RT-PCR, qPCR and immunocytochemistry. RT-PCR using cDNA extracted from CCSM crura and primers designed for EPAC gene isoforms (Table 1), showed detectable transcripts only for *Rapgef3* (EPAC-1), and not *Rapgef4* (EPAC-2; Fig6.6A-B; n=6, N=3). Mouse brain was utilised as a positive control, displaying clear bands for both *Rapgef3* and *Rapgef4* amplicons (Fig6.6A-B). Lastly, non-template controls (NTCs) were completed for each transcript using reaction mixtures without mouse cDNA. NTCs confirmed the absence of contamination of foreign genetic material or non-specific amplification (Fig6.6A-B). Quantitative analysis supported these findings, qPCR results indicated *Rapgef3* expression relative to *β-actin* was

substantially higher than transcripts for *Rapgef4*, which appeared to be minimal to undetectable in mouse CCSM crura cDNA (Fig6.6C).

Given the predominant expression of *Rapgef3* transcripts, the expression of EPAC-1 protein was confirmed via immunocytochemistry. Enzymatically dispersed CCSM cells displayed immunoreactivity for EPAC-1 (Fig6.7A; n=6; each dispersal was from tissue pooled from two animals), consistent with the transcript data. Negative controls using untransfected HEK-293 cells, as well as secondary-only controls (not-shown), exhibited no detectable staining (Fig6.7B; n=6). As a positive control, sections of mouse kidney cortex, a tissue well known to express abundant EPAC-1 (Fig6.7C; Gloerich and Bos, 2010; Sun *et al*., 2011; Sugawara, 2015), displayed strong and characteristic EPAC-1 immunoreactivity (n=3, N=6). Collectively, these data demonstrate the presence of EPAC-1 at a transcriptional and protein level.

6.2.4 Differential effects of EPAC and PKA activation on PE-evoked Ca^{2+} oscillations

Data from Chapter 4 demonstrated two distinct adrenergic-induced Ca^{2+} oscillatory activity. Low-PE generated Ca^{2+} oscillations that were highly sensitive to membrane-potential-dependent pathways, being suppressed by the LTCC blocker NIF (Fig 4.12) and the $K_V7.2$-5 channel activator RTG (Fig 4.9). In contrast, high-PE oscillations were unaffected by NIF or RTG, but were inhibited by blockade of intracellular Ca^{2+} release or store-operated entry, including the IP_3R antagonist 2-APB (Fig 4.16), the CRAC channel inhibitor GSK-7975A (Fig 4.15), and the RyR antagonist TC (Fig 4.17)

To examine the effect of cAMP-signalling on adrenergic Ca^{2+} oscillations, the AC activator, FK 1 $x10^{-6}$ M, was applied to Ca^{2+} oscillations evoked by high-PE (1 $x10^{-5}$ M). Application of FK abolished Ca^{2+} oscillations (Fig6.8A), with frequency falling from 33.50 ± 9.59 min^{-1} under PE alone to 0.00 ± 0.00 min^{-1} in the presence of FK, with no recovery on washout, and amplitude similarly reduced from 0.99 ± 0.16 F/F_0 to 0.00 ± 0.00 F/F_0, with no recovery on washout, with summary data reporting abolition of both frequency (Fig6.8B; P=0.0302) and amplitude (Fig6.8C; P=0.0032; n=6, N=6).

To determine the functions of the cAMP effectors, both EPAC and PKA activators were tested on high-PE Ca^{2+} oscillations. First, EPAC activator, 007-AM 1 $x10^{-5}$ M, greatly attenuated Ca^{2+} oscillations (Fig6.9A), with frequency falling from 20.00 ± 4.00 min^{-1} under PE alone to 0.50 ± 0.50 min^{-1} in the presence of 007-AM,

representing a 98% reduction, and amplitude falling from 1.20 ± 0.32 F/F_0 to 0.31 ± 0.31 F/F_0, representing a 74% reduction, with summary data indicating that in 5/6 replicates, 007-AM abolished Ca^{2+} oscillatory activity. Summary data showed that both frequency (Fig6.9B; P=0.0087) and amplitude (Fig6.9C; P=0.0049) were significantly inhibited. Unlike FK, the inhibitory effect of 007-AM was reversible, with frequency recovering to 18.50 ± 3.83 min^{-1} and amplitude recovering to 1.75 ± 0.50 F/F_0 on washout, both returning to similar levels as control (P=0.8040 and P=0.0626, respectively; n=6, N=6).

PKA activation showed no detectable effect on high-PE Ca^{2+} oscillations (Fig6.10A). 6-MB 1 $x10^{-4}$ M showed no significant change in oscillation frequency (Fig6.10B; P=0.2108), which measured 34.00 ± 10.58 min^{-1} under PE alone, 27.00 ± 7.27 min^{-1} in the presence of 6-MB, and 20.50 ± 6.17 min^{-1} on washout, or amplitude (Fig6.10C; P=0.2353; n=6, N=6), which measured 1.16 ± 0.31 F/F_0, 1.43 ± 0.41 F/F_0, and 1.44 ± 0.48 F/F_0 across PE, 6-MB, and washout conditions respectively. To test, the concentration dependence of 6-MB, 3 $x10^{-4}$ M was used, consistent with the 6-MB concentration employed in Morgan *et al*. (2022). The higher concentration showed no concentration-dependent effect (Fig6.11A), with frequency measuring 25.67 ± 4.24 min^{-1} under PE alone, 25.17 ± 3.49 min^{-1} in the presence of 6-MB, and 19.83 ± 2.96 min^{-1} on washout, showing no significant change in frequency (Fig6.11B; P=0.8560), and amplitude measuring 1.21 ± 0.29 F/F_0, 1.03 ± 0.24 F/F_0, and 0.75 ± 0.15 F/F_0 across PE, 6-MB, and washout conditions respectively, showing no significant change in or amplitude (Fig6.11C; P=0.0657; n=6, N=6).

It appeared clear that PKA activation has no significant effect on high-PE Ca^{2+} oscillations, therefore, the effect on low-PE Ca^{2+} oscillations was examined. Application of 6-MB 3 $x10^{-4}$ M abolished Ca^{2+} oscillations induced by 1 $x10^{-7}$ M PE (Fig6.12A), with frequency falling from 9.50 ± 0.92 min^{-1} under PE alone to 0.00 ± 0.00 min^{-1} in the presence of 6-MB, and amplitude falling from 3.04 ± 0.97 F/F_0 to 0.00 ± 0.00 F/F_0. Summary data confirmed this effect across replicates, with frequency (Fig6.12B; P=0.0003) and amplitude (Fig6.12C; P=0.0445) significantly decreased. Subsequent wash-out of 6-MB returned Ca^{2+} oscillations to a similar amplitude as control, recovering to 1.56 ± 0.74 F/F_0 (Fig6.12C; P=0.0742), yet frequency remained significantly decreased, while recovering from abolition, returning to only 3.50 ± 1.43 min^{-1} (Fig6.12B; P=0.0327; n=6, N=6).

To test whether the inhibitory effect of PKA at low-PE requires K_v7 channels, oscillations were measured following K_v7 blockade with XE-991. In the presence of XE-991 (1 x10^{-5} M), 6-MB 3 x10^{-4} M no longer suppressed Ca^{2+} oscillations (Fig 6.13A), with frequency measuring 8.00 ± 1.00 min^{-1} under PE alone, increasing to 15.50 ± 2.11 min^{-1} in the presence of XE-991, representing a 94% increase, and remaining at 14.00 ± 2.41 min^{-1} following co-application of 6-MB, and amplitude measuring 3.89 ± 1.31 F/F_0 under PE alone, 3.35 ± 1.24 F/F_0 in the presence of XE-991, representing a 14% decrease, and 2.54 ± 0.93 F/F_0 following co-application of 6-MB. Neither frequency nor amplitude were significantly altered by 6-MB in the presence of XE-991 (Fig 6.13B-C; P>0.9999 and P=0.2308), demonstrating that PKA-dependent inhibition of low-PE Ca^{2+} oscillations requires functional K_v7 channels.

6.2.5 AC and EPAC activators do not inhibit caffeine responses

Caffeine (1 x10^{-2} M) was used as a ryanodine receptor (RyR) opener to assess store-release Ca^{2+} spikes. Repeated 10s applications of 1 x10^{-2} M caffeine, with 1 min intervals, produced reproducible Ca^{2+} spikes with progressively declining amplitudes across five applications (Fig6.14A). Summary data demonstrated no significant change between the 2nd and 3rd caffeine applications, measuring 4.67 ± 1.27 F/F_0 and 4.33 ± 1.13 F/F_0 respectively (Fig6.14B; P=0.5994; n=6, N=6).

Given the potent inhibition of EPAC activation on high-PE Ca^{2+} oscillations, which were shown to be sensitive to SR Ca^{2+} release, the effect of EPAC activation was examined on caffeine responses. Application of 007-AM 1 x10^{-5} M after the 2nd application of caffeine, had no significant effect on the amplitude of the 3rd caffeine response (Fig6.15A-B; P=0.6538; n=6, N=6), with amplitude measuring 4.54 ± 0.60 F/F_0 during the 2nd caffeine application and 3.98 ± 0.57 F/F_0 during the 3rd application in the presence of 007-AM. Furthermore, similar results were obtained with FK, in which application of FK showed no significant effect on caffeine amplitude (Fig6.16A-B; P=0.3747; n=6, N=6), with amplitude measuring 5.65 ± 1.52 F/F_0 during the 2nd caffeine application and 5.11 ± 1.42 F/F_0 during the 3rd application in the presence of FK. Therefore, the effects of FK and 007-AM appeared to inhibit store-release of Ca^{2+}, independently of RyRs or store-depletion.

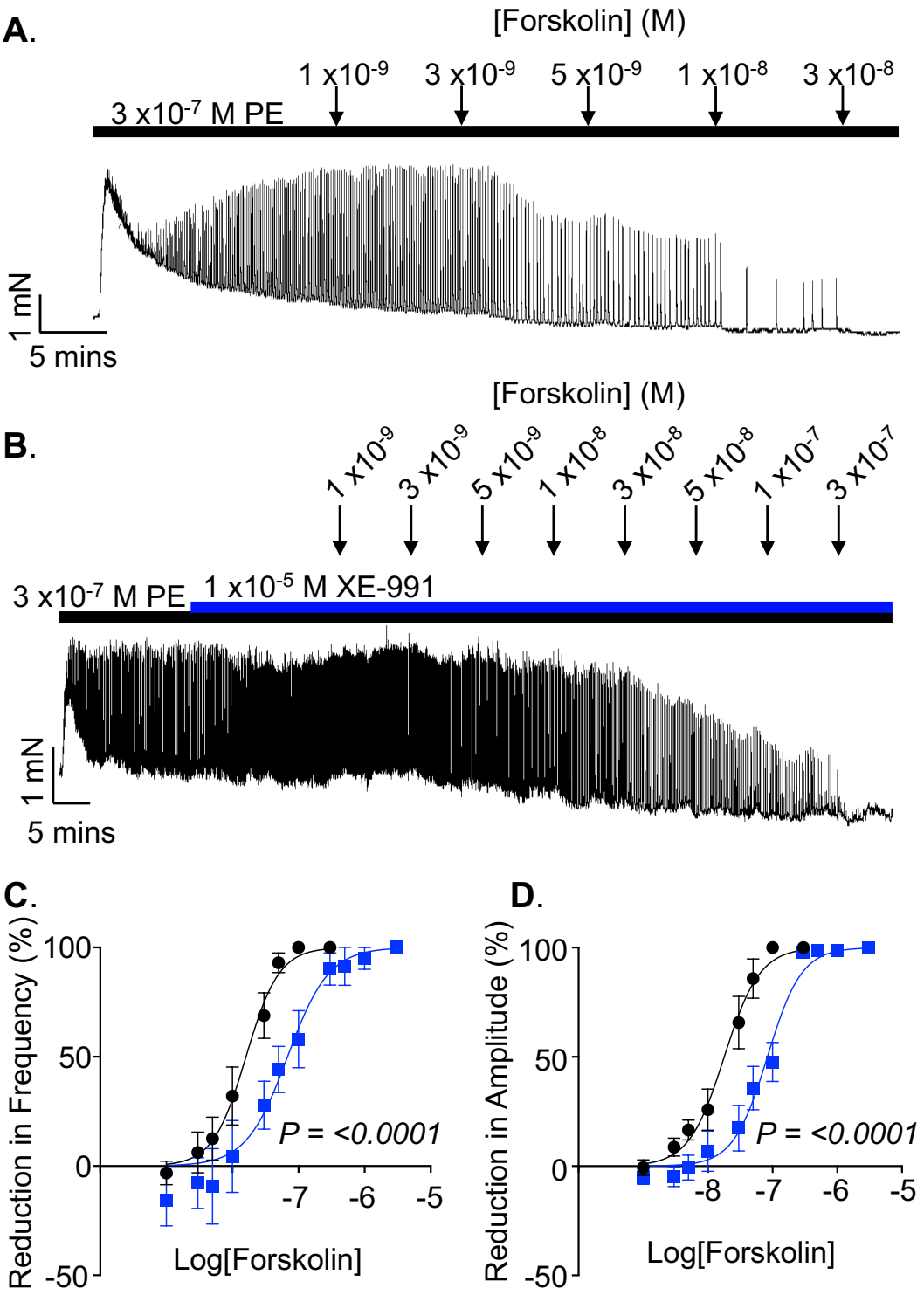


Figure 6.1: K_v7 blocker, XE-991, shifts the adenylyl cyclase activator, forskolin (FK), inhibitory concentration-effect curve.
A. Representative isometric tension recording demonstrating the effect of increasing concentrations of FK (1 x10^{-9} M to 3 x10^{-8} M) on 3 x10^{-7} M PE-induced phasic contractions **B.** Representative isometric tension recording of the effect of increasing concentrations of FK (1 x10^{-9} M to 3 x10^{-7} M) in the continued presence of 1 x10^{-5} M XE-991 . **C+D.** Summary data for the shift in FK IC_{50} in control (black) and in the presence of XE-991 (blue): for frequency (IC_{50}=1.790 x10^{-8} M vs IC_{50}=8.310 x10^{-8} M, P<0.0001) and amplitude (IC_{50}=1.721 x10^{-8} M vs IC_{50}=6.823 x10^{-8} M, P<0.0001; n=6, N=6). Statistical significance of change in IC_{50} using extra-sum-of-squares-F-test.

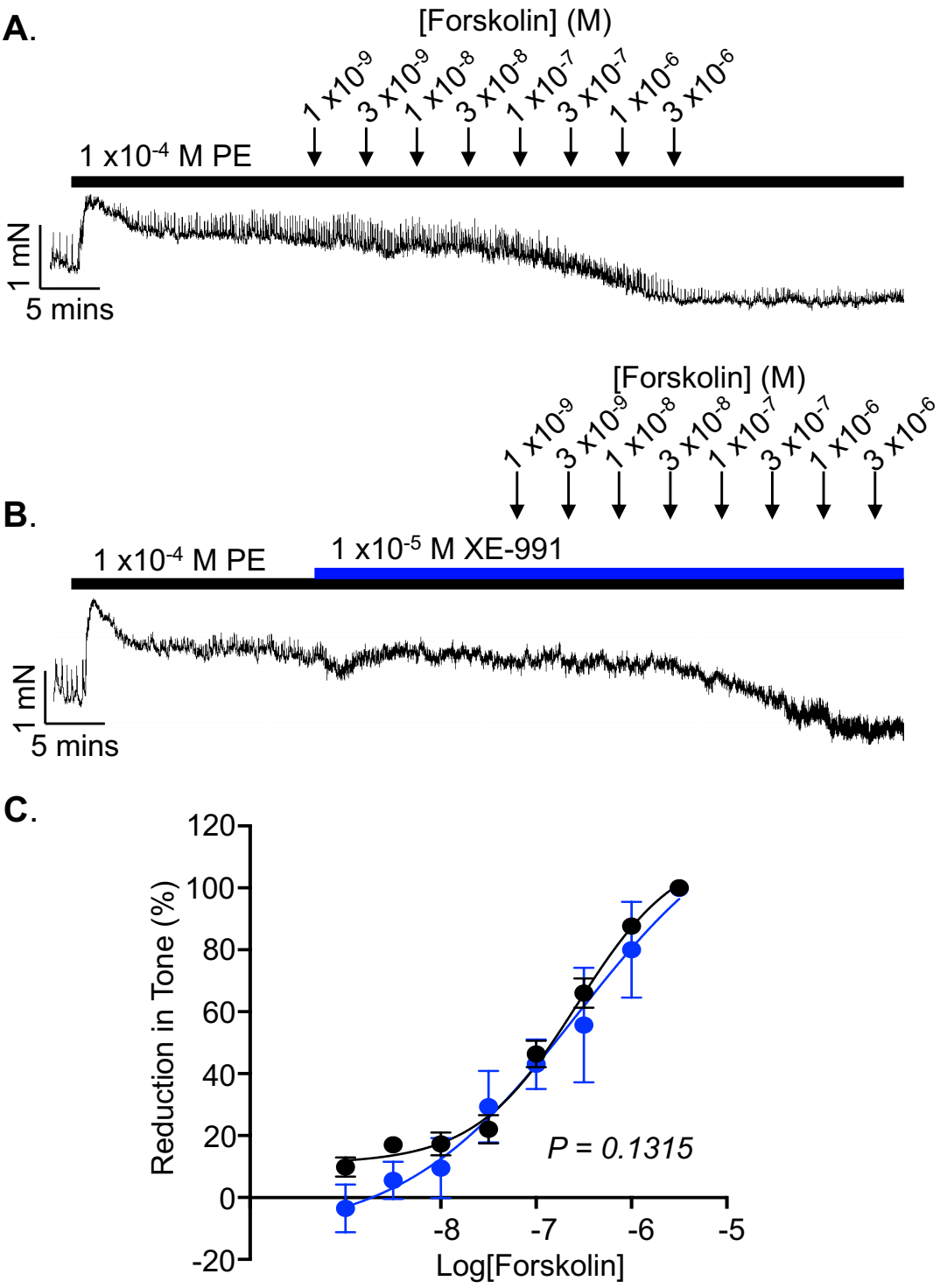


Figure 6.2: K_v7 blocker, XE-991, does not shift the adenylyl cyclase activator, forskolin (FK), inhibitory concentration-effect curve on tone. **A.** Representative isometric tension recording demonstrating the effect of increasing concentrations of FK (1 x10^{-9} M to 3 x10^{-6} M) on a 1 x10^{-4} M PE-induced tonic contraction. **B.** Representative isometric tension recording demonstrating the effect of increasing concentrations of FK (1 x10^{-9} M to 3 x10^{-6} M) on a 1 x10^{-4} M PE-induced tonic contraction, in the presence of XE-991. **C** Summary data for the shift in FK IC_{50} in control (black) and in the presence of XE-991 (blue): IC_{50}=1.660 x10^{-7} M vs IC_{50}=1.610 x10^{-7} M, P=0.1315; n=6, N=6). Statistical significance of change in IC_{50} using extra-sum-of-squares-F-test.

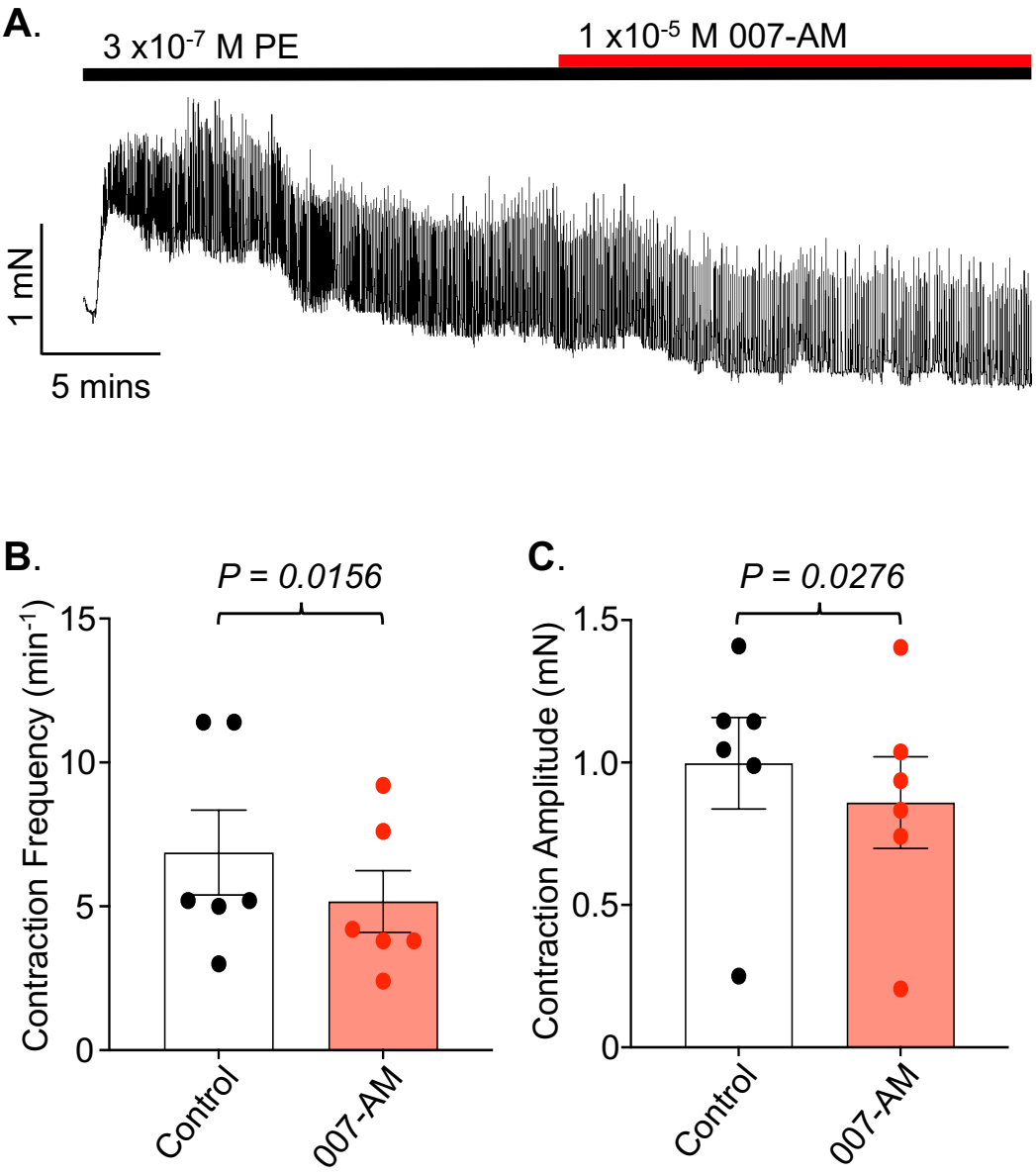


Figure 6.3: Phenylephrine (PE)-induced contractions were partially inhibited by an EPAC activator, 8-pCPT-2-O-Me-cAMP-AM (007-AM).

A. Representative isometric tension recording demonstrating the effect of 1 x10^{-5} M 007-AM on 3 x10^{-7} M PE-induced phasic contractions. **B+C.** Summary data for the partial inhibitory effect of 007-AM on phasic contraction frequency and amplitude (P=0.0156 and P=0.0276, respectively; n=6, N=6).

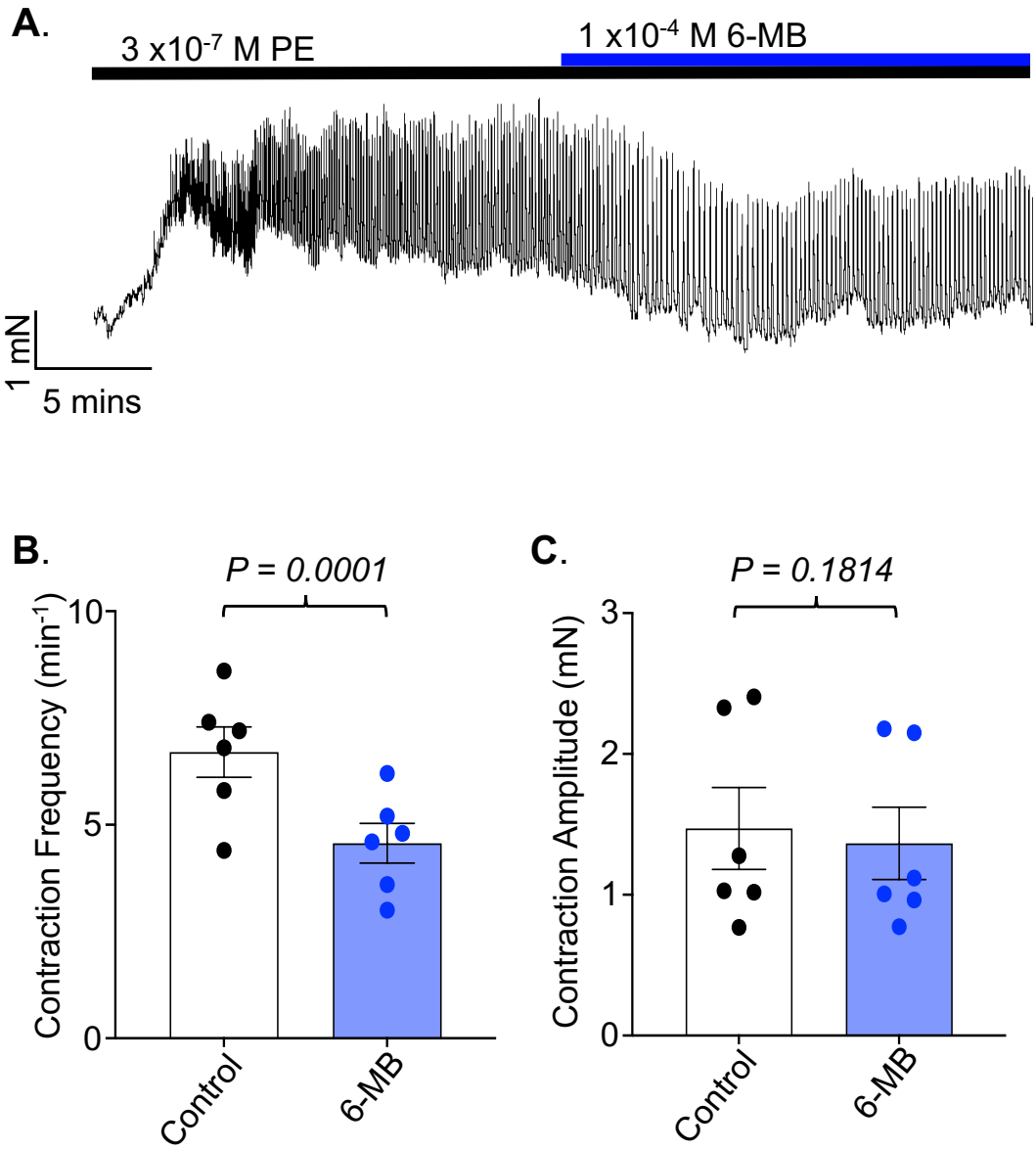


Figure 6.4: Phenylephrine (PE)-induced contractions were partially inhibited by a PKA activator, 6-MB-cAMP (6-MB). **A.** Representative isometric tension recording demonstrating the effect of 1 x10^{-4} M 6-MB on 3 x10^{-7} M PE-induced phasic contractions. **B+C.** Summary data for the partial inhibitory effect of 6-MB on phasic contraction frequency and amplitude (P=0.0001 and P=0.1814, respectively; n=6, N=6).

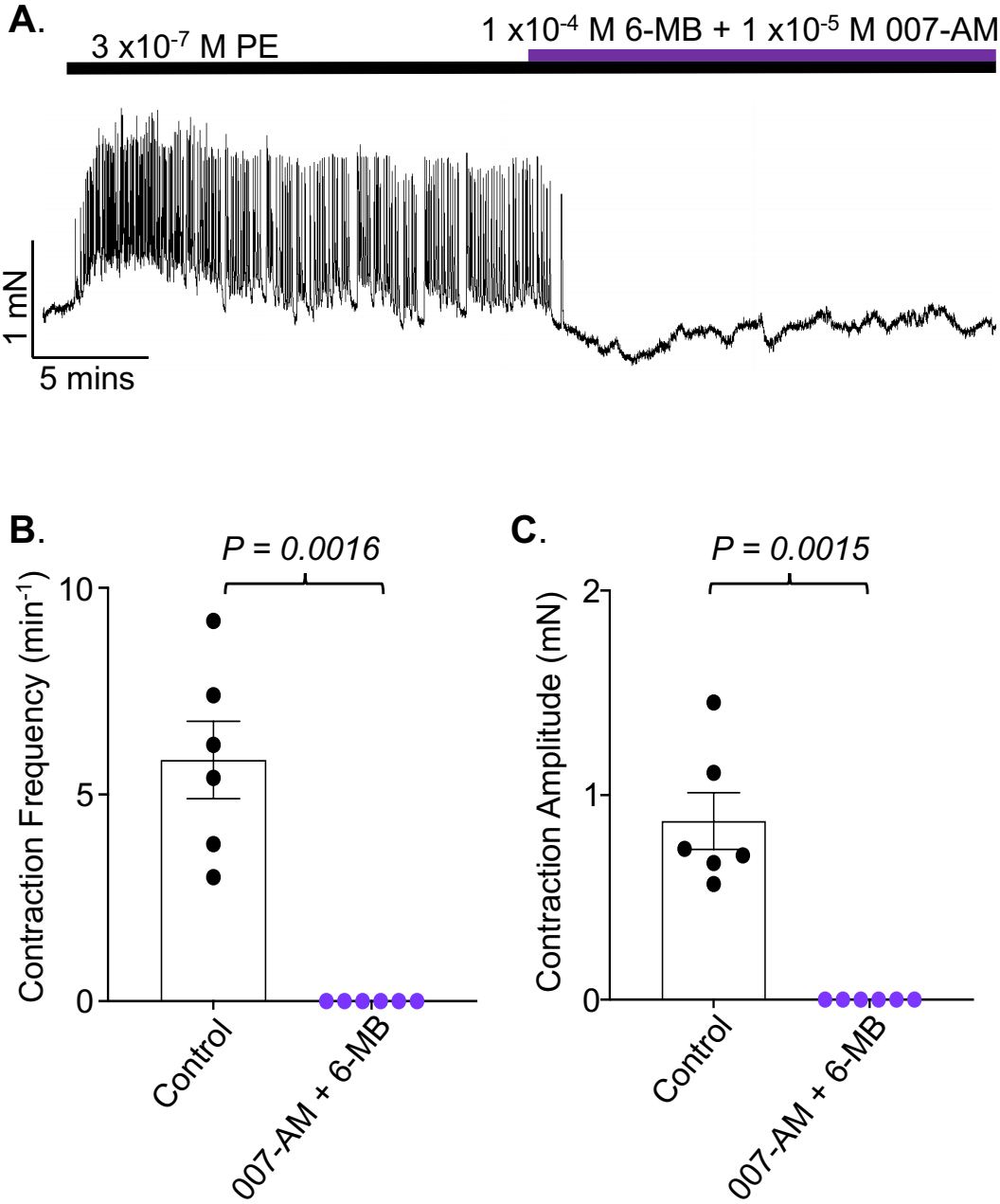


Figure 6.5: Phenylephrine (PE)-induced contractions were abolished by co-application of an EPAC and PKA activator, 8-pCPT-2-O-Me-cAMP-AM (007-AM) and 6-MB-cAMP (6-MB), respectively.

A. Representative isometric tension recording demonstrating the effect of the addition of both 1 x10^{-5} M 007-AM and 1 x10^{-4} M 6-MB on 3 x10^{-7} M PE-induced phasic contractions. **B+C.** Summary data for the partial inhibitory effect of 007-AM and 6-MB on phasic contraction frequency and amplitude (P=0.0016 and P=0.0015, respectively; n=6, N=6).

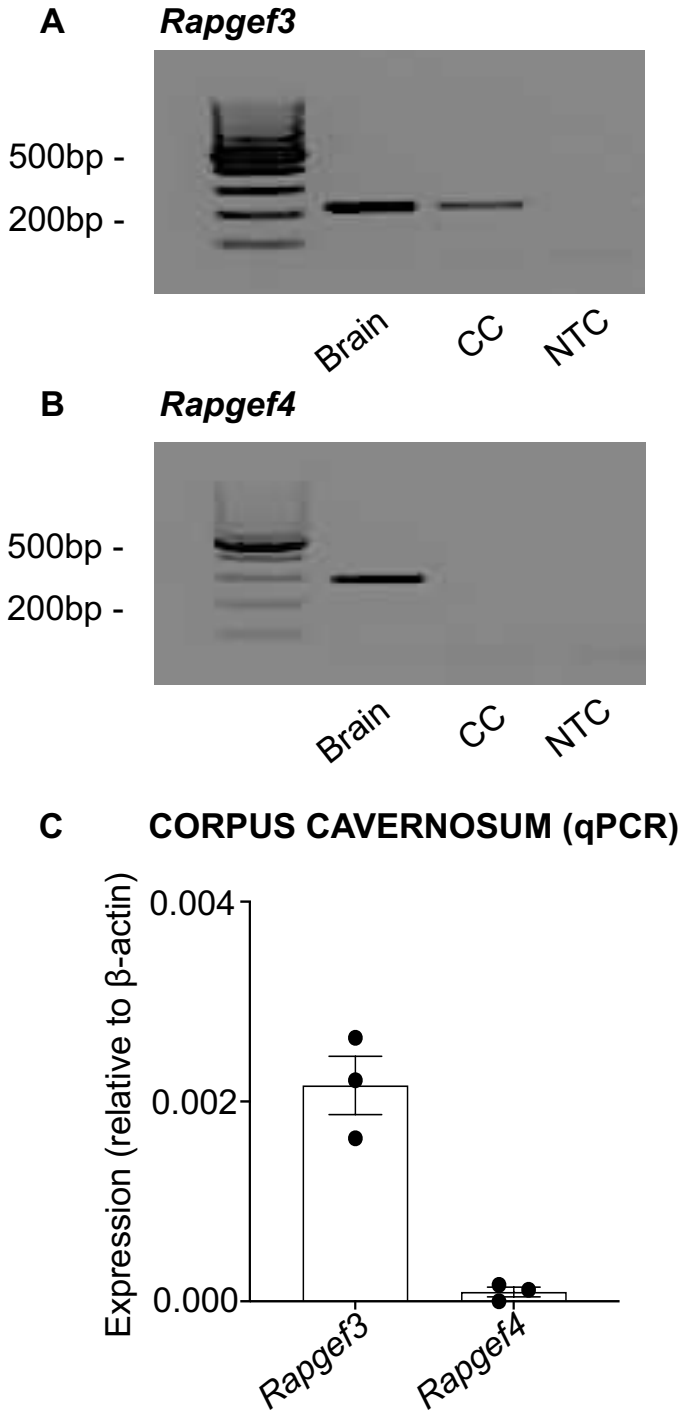


Figure 6.6: Transcriptional analysis of *EPAC* isoforms.
A. Expression of *Rapgef3* (EPAC-1) isoform transcripts in RT-PCR using cDNA extracted from mouse brain and corpus cavernosum (CC). **B**. Expression of *Rapgef4* (EPAC-2) isoform transcripts in RT-PCR using cDNA extracted from mouse brain and corpus cavernosum (CC). Both experiments employed a non-template control (NTC) for detection of contamination or non-specific amplification. Amplicons were resolved via agarose gel (2%) electrophoresis, and visualised using SYBR safe (n=6, N=3). **D**. Quantitative PCR of *Rapgef3* and *Rapgef4* transcript expression relative to β-actin using corresponding primers used in RT-PCR (n=6, N=3).

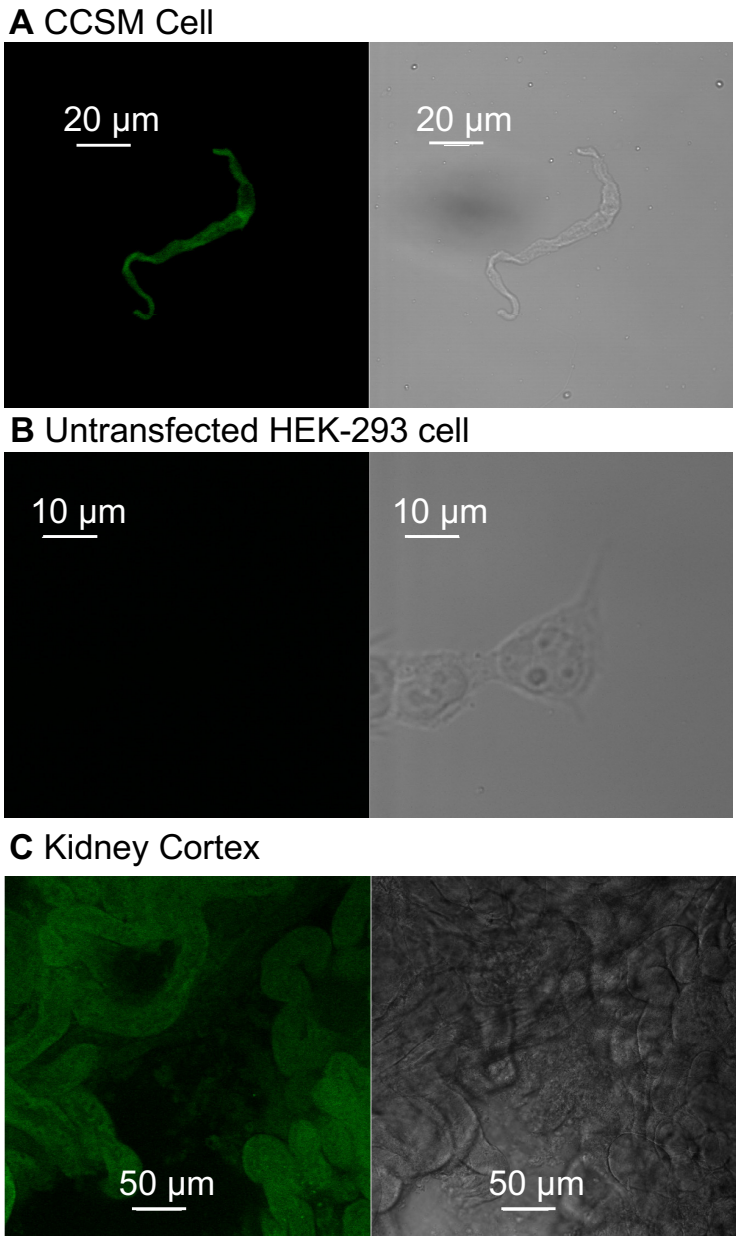


Figure 6.7: Immunocyto/histochemical staining of EPAC-1 proteins.
A. Representative photomicrograph showing that freshly isolated mouse CCSM cells were immunoreactive (green) to selective EPAC-1 antibody (n=6, N=6). Secondary-only antibody controls in native CCSM cells also failed to show reactivity (n=6 as for *A*, data not shown). **B***.* Negative control showing lack of immunoreactivity in an untransfected HEK-293 cell exposed to the same primary and secondary antibodies as in *A.* (n=6). **C.** Positive control showing high immunoreactivity (to the same antibodies used in as A) in an axial mouse kidney cortical slice (n=6). Data in this section collected by E. Barševska.

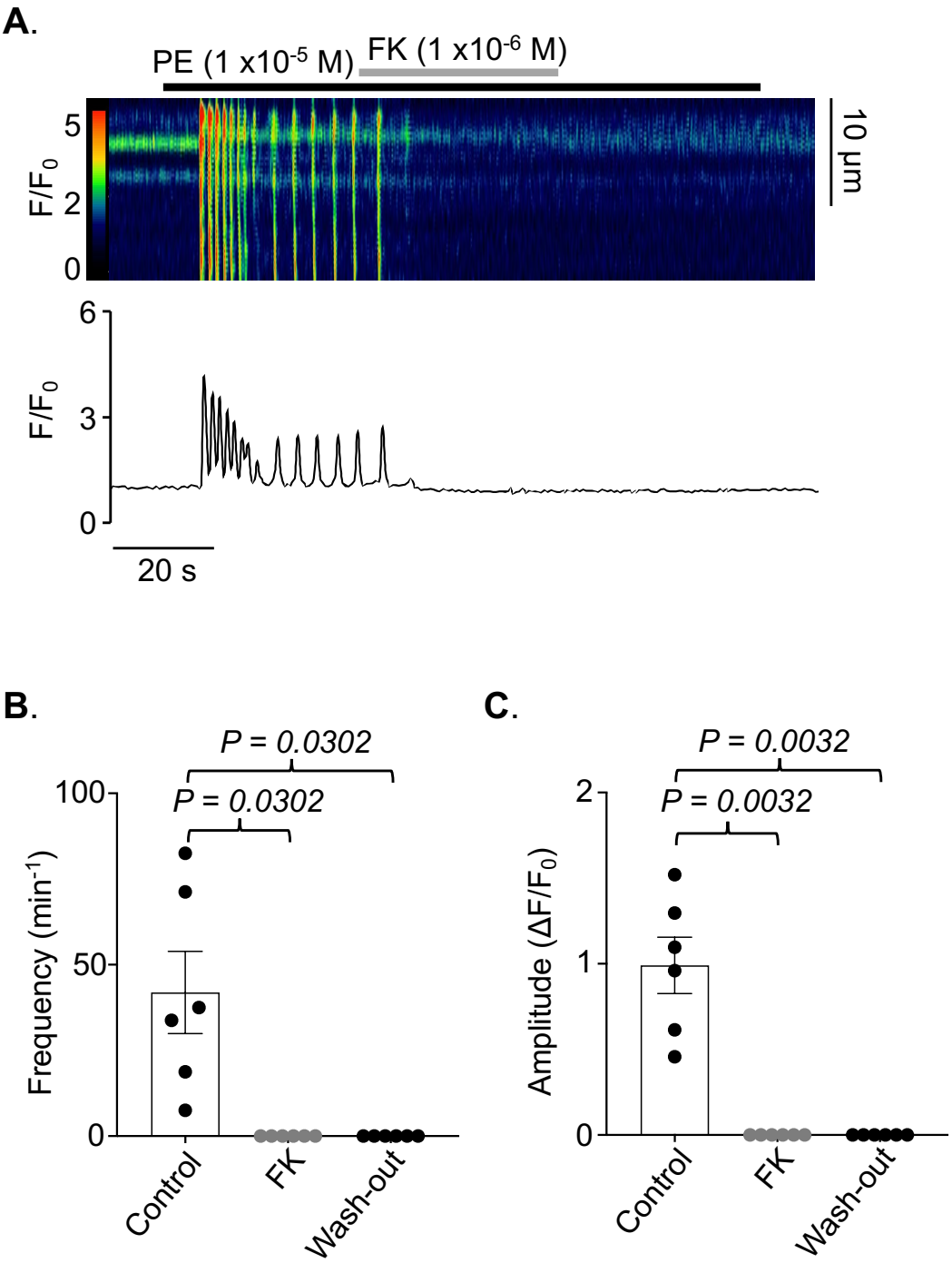


Figure 6.8: Effect of AC activator, forskolin (FK), on high-PE-induced Ca^{2+} oscillations in isolated cells.
A. Representative spatiotemporal map and associated intensity plot of Ca^{2+} oscillations, evoked by 1 x10^{-5} M PE, and the addition of 1 x10^{-6} M FK. **B+C.** Summary data for Ca^{2+} oscillation frequency (min^{-1}) and amplitude ($\Delta F/F_0$), respectively. Ca^{2+} oscillation frequency and amplitude were abolished in the presence of FK (P=0.0302 and P=0.0032, respectively). A subsequent wash-out of FK was unsuccessful and the frequency and amplitude of Ca^{2+} oscillations did not return to control level (P=0.0302 and P=0.0032, respectively; n=6, N=6).

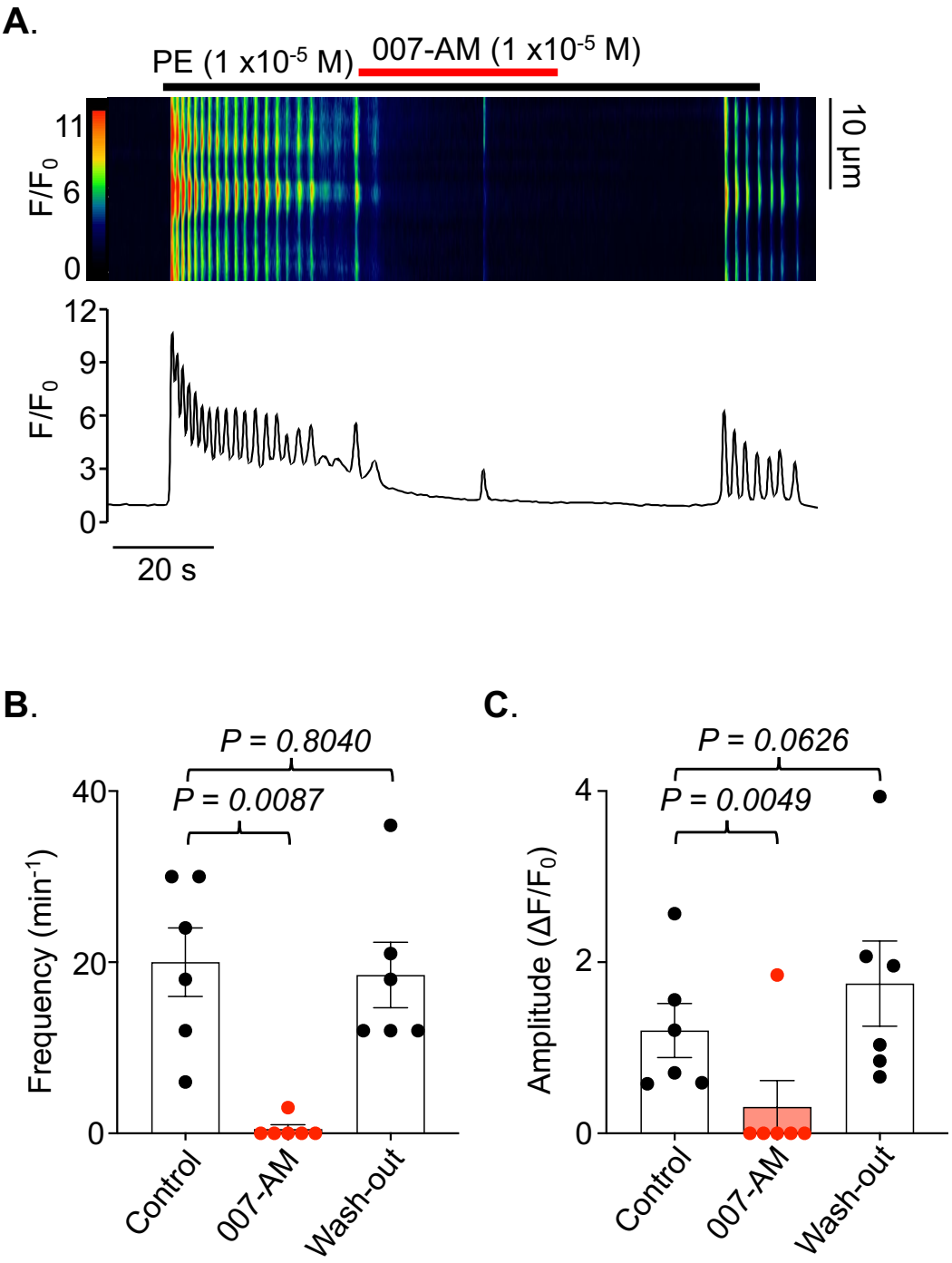


Figure 6.9: Effect of EPAC activator, 8-pCPT-2-O-Me-cAMP-AM (007-AM), on high-PE-induced Ca^{2+} oscillations in isolated cells.

A. Representative spatiotemporal map and associated intensity plot of Ca^{2+} oscillations, evoked by 1 x10^{-5} M PE, and inhibition by 1 x10^{-5} M 007-AM. **B+C.** Summary data for Ca^{2+} oscillation frequency (min^{-1}) and amplitude ($\Delta F/F_0$), respectively. Ca^{2+} oscillation frequency and amplitude were greatly attenuated in the presence of 007-AM (P=0.0087 and P=0.0049, respectively), and a subsequent wash-out of 007-AM returned Ca^{2+} oscillation frequency and amplitude similar to control levels (P=0.8040 and P=0.0626, respectively; n=6, N=6).

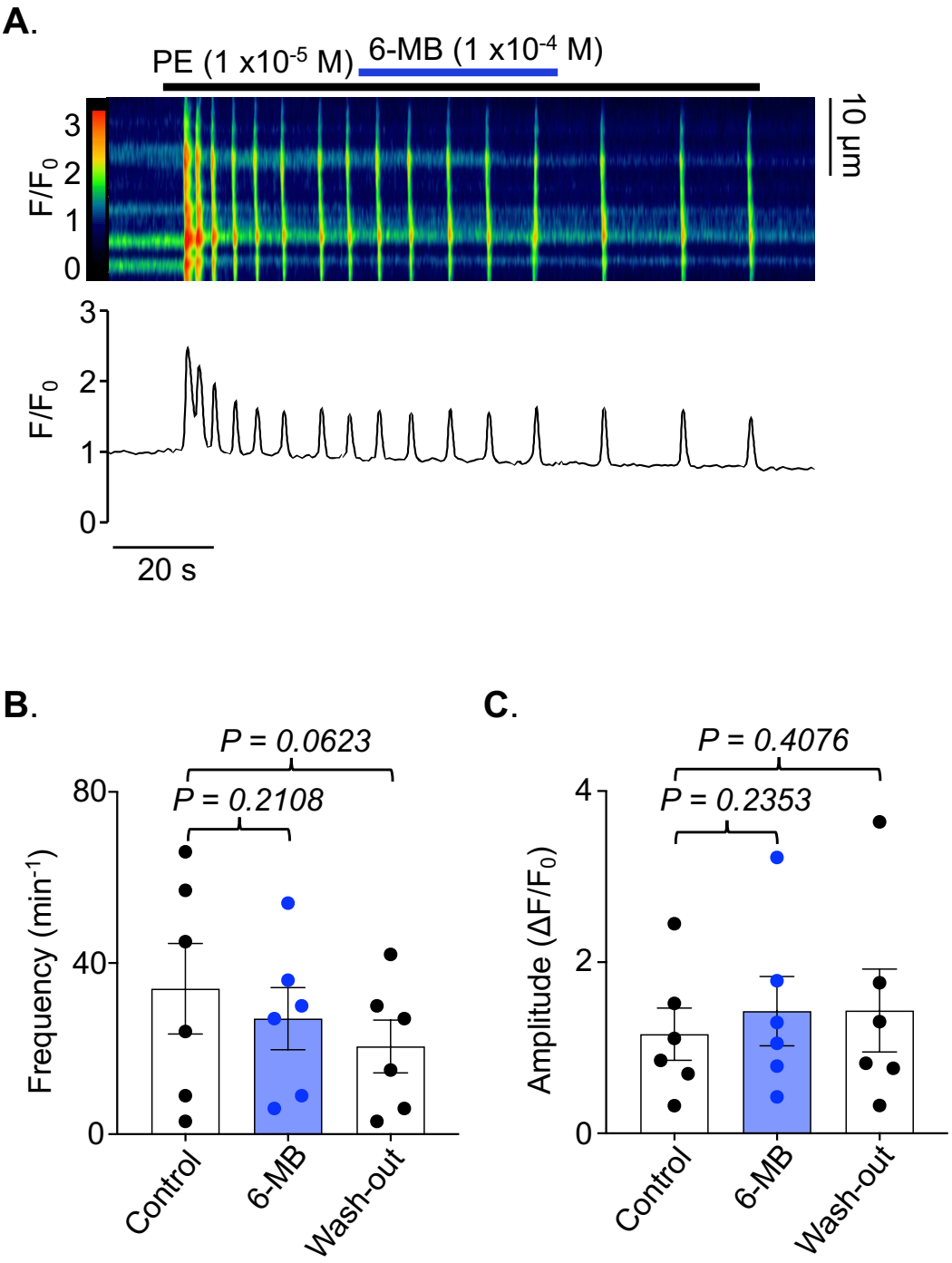


Figure 6.10: Effect of PKA activator, 6-MB-cAMP (6-MB), on high-PE-induced Ca^{2+} oscillations in isolated cells.
A. Representative spatiotemporal map and associated intensity plot of Ca^{2+} oscillations, evoked by 1 x10^{-5} M PE, and the addition of 1 x10^{-4} M 6-MB. **B+C.** Summary data for Ca^{2+} oscillation frequency (min^{-1}) and amplitude ($\Delta F/F_0$), respectively. Ca^{2+} oscillation frequency and amplitude were not significantly affected in the presence of 6-MB (P=0.2108 and P=0.2353, respectively), and a subsequent wash-out of 6-MB, showed no significant change compared to control (P=0.0623 and P=0.4076, respectively; n=6, N=6).

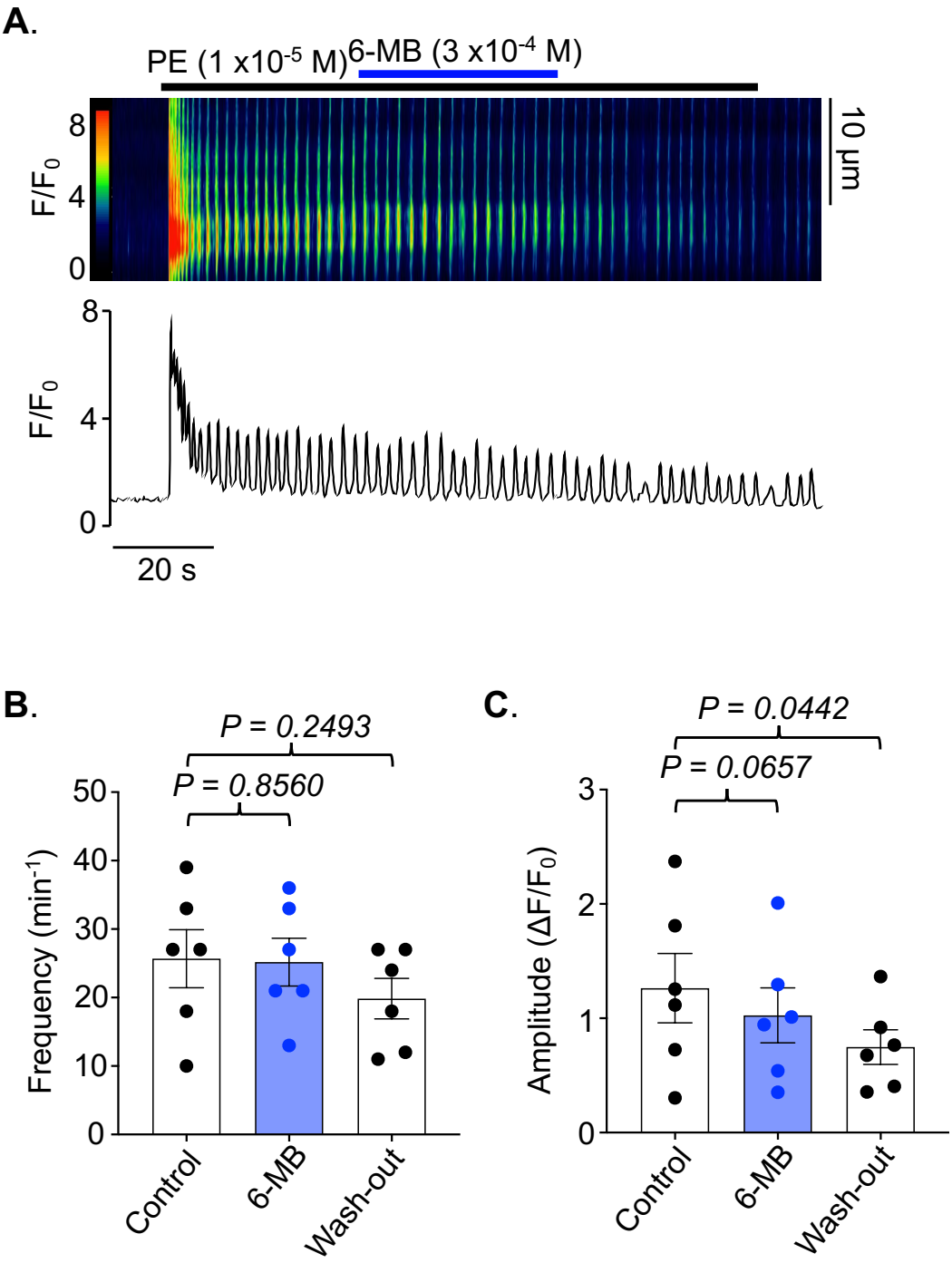


Figure 6.11: Effect of PKA activator, 6-MB-cAMP (6-MB), on high-PE-induced Ca^{2+} oscillations in isolated cells.
A. Representative spatiotemporal map and associated intensity plot of Ca^{2+} oscillations, evoked by 1 x10^{-5} M PE, and the addition of 3 x10^{-4} M 6-MB. **B+C.** Summary data for Ca^{2+} oscillation frequency (min^{-1}) and amplitude ($\Delta F/F_0$), respectively. Ca^{2+} oscillation frequency and amplitude were not significantly affected in the presence of 6-MB (P=0.8560 and P=0.0657, respectively), and a subsequent wash-out of 6-MB, showed no significant change compared to control for frequency (P=0.2493), yet amplitude showed a significant change compared to control (P=0.0442; n=6, N=6)

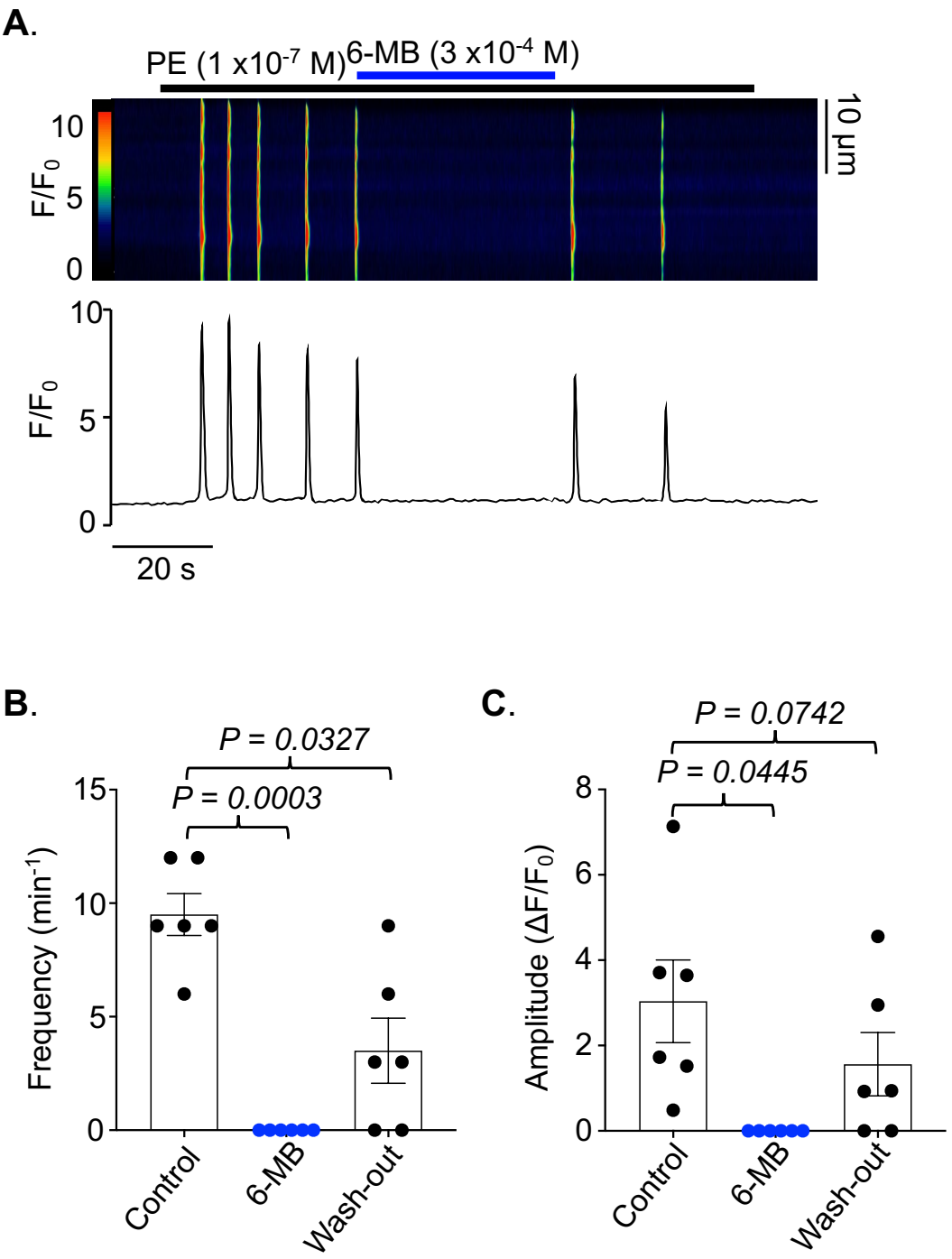


Figure 6.12: Effect of PKA activator, 6-MB-cAMP (6-MB), on low-PE-induced Ca^{2+} oscillations in isolated cells.
A. Representative spatiotemporal map and associated intensity plot of Ca^{2+} oscillations, evoked by 1 x10^{-7} M PE, and the addition of 3 x10^{-4} M 6-MB. **B+C.** Summary data for Ca^{2+} oscillation frequency (min^{-1}) and amplitude ($\Delta F/F_0$), respectively. Ca^{2+} oscillation frequency and amplitude were abolished in the presence of 6-MB (P=0.0003 and P=0.0445, respectively), and a subsequent wash-out of 6-MB, returned Ca^{2+} from abolition, yet frequency showed a significant decrease compared to control (P=0.0327; n=6, N=6)

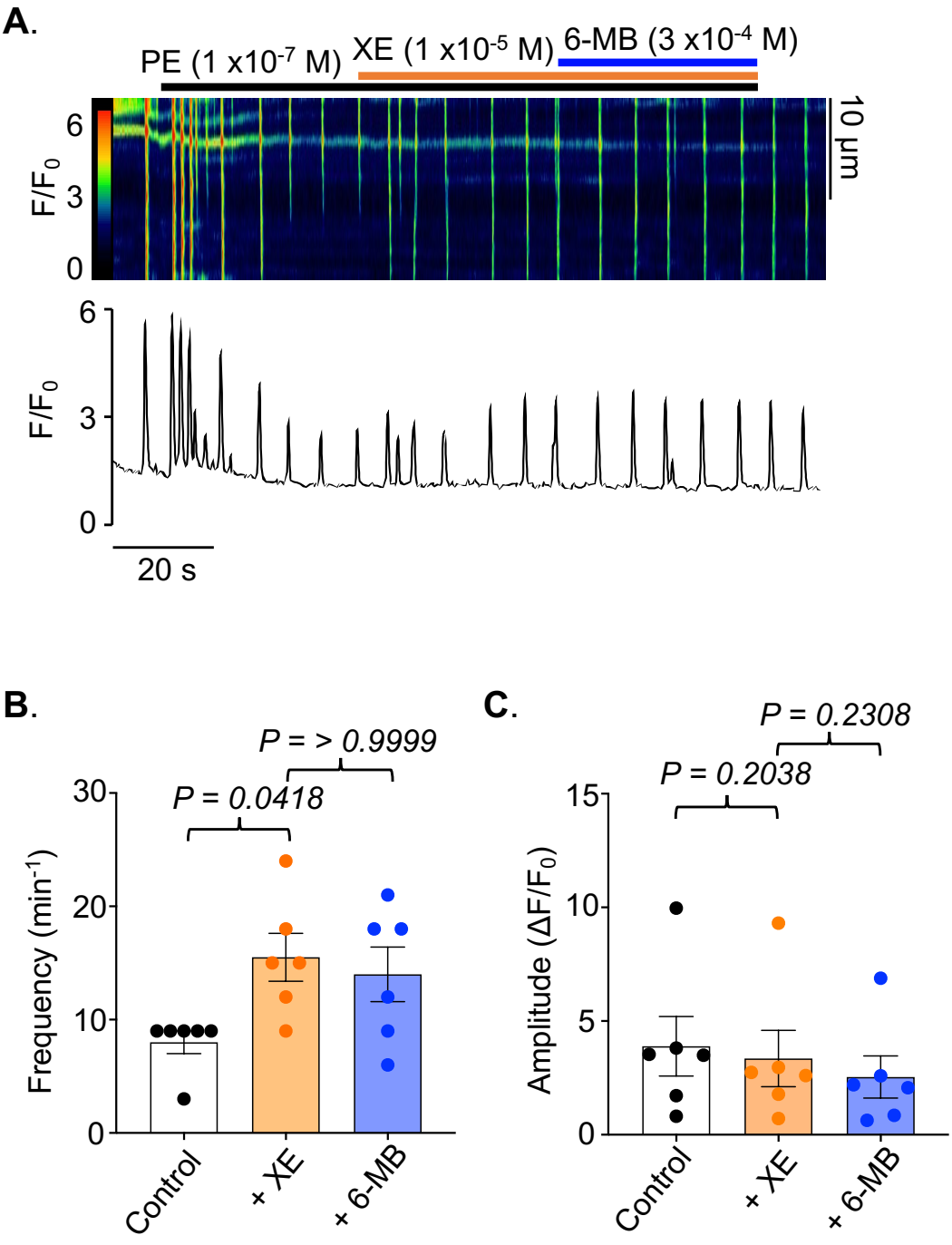


Figure 6.13: Effect of PKA activator, 6-MB-cAMP (6-MB), on low-PE-induced Ca^{2+} oscillations, in the presence of K_v7 blocker, XE-991, in isolated cells.

A. Representative spatiotemporal map and associated intensity plot of Ca^{2+} oscillations, evoked by 1 x10^{-7} M PE, later enhanced by XE-991 (XE) and the subsequent addition of 3 x10^{-4} M 6-MB. **B+C.** Summary data for Ca^{2+} oscillation frequency (min^{-1}) and amplitude ($\Delta F/F_0$), respectively. In the presence of XE, 6-MB showed no significant effect on frequency or amplitude (P=0.4896 and P=0.2308, respectively; n=6, N=6)

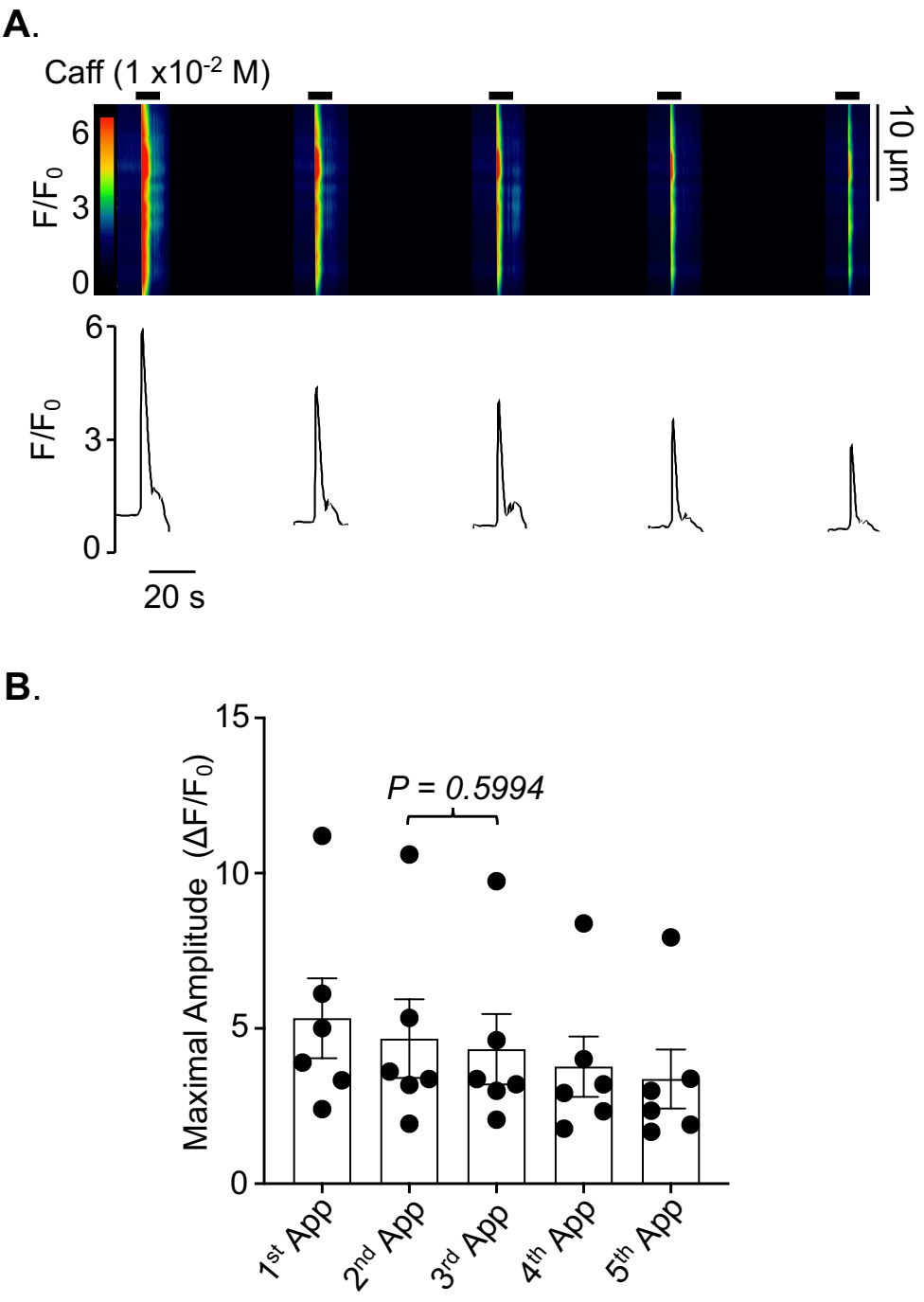


Figure 6.14: The effect of repeated caffeine (Caff)-induced store-release calcium spikes in isolated cells.
A. Representative spatiotemporal map and associated intensity plot of Ca^{2+} spikes, evoked by 1 x10^{-2} M Caff, across five applications, with 1 min intervals. **B.** Summary data for maximum amplitude ($\Delta F/F_0$). Maximum amplitude between the 2nd and 3rd applications showed no significant decrease (P=0.5994; n=6, N=6). This forms an important control for later experiments.

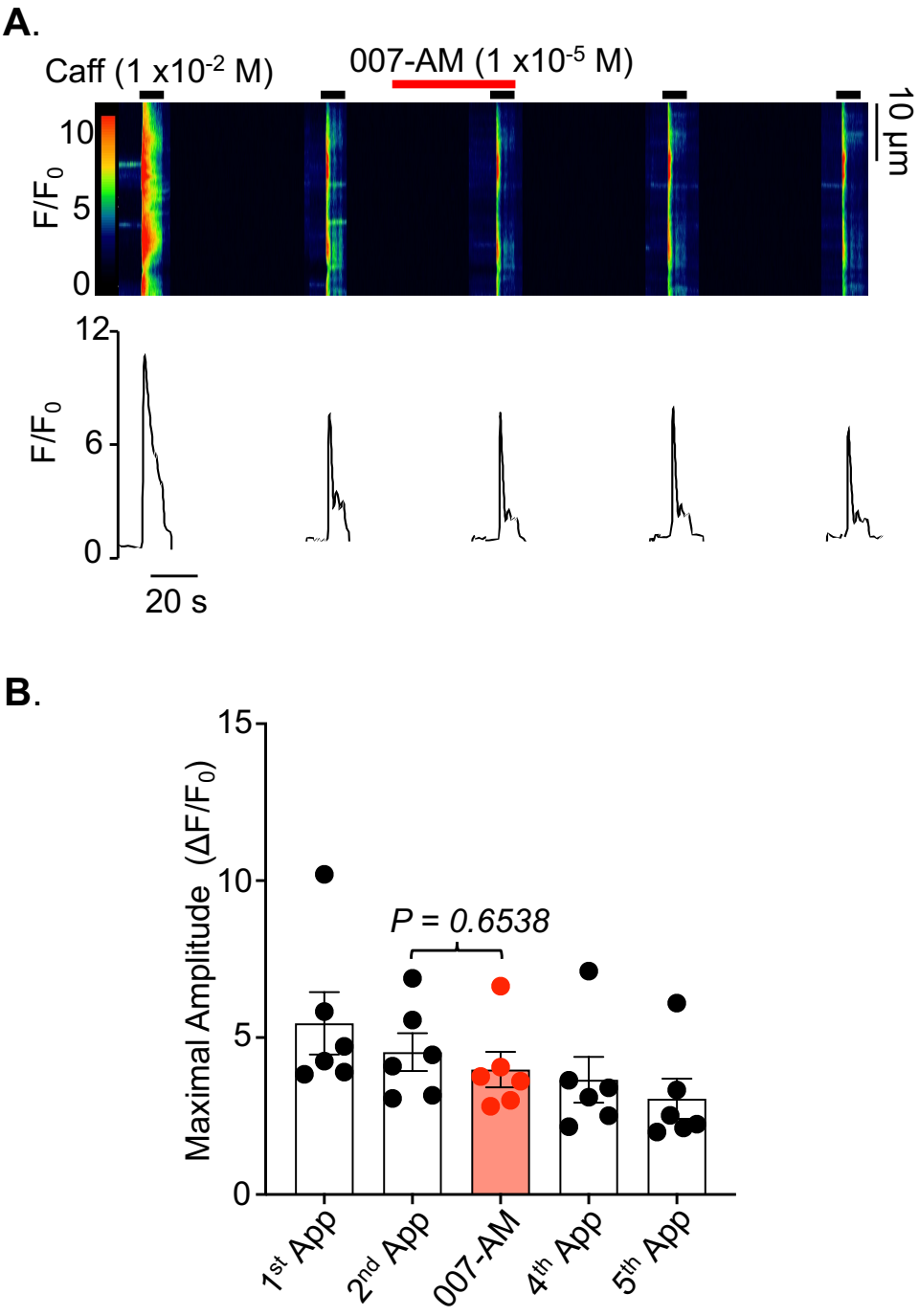


Figure 6.15: The effect of EPAC activator, 8-pCPT-2-O-Me-cAMP-AM (007-AM), on caffeine (Caff)-induced store-release calcium spikes in isolated cells.

A. Representative spatiotemporal map and associated intensity plot of the effect of 1 x10^{-5} M 007-AM on Ca^{2+} spikes, evoked by 1 x10^{-2} M Caff. **B.** Summary data for maximum amplitude ($\Delta F/F_0$). Maximum amplitude showed no significant change in the presence of 007-AM (P=0.6538; n=6, N=6).

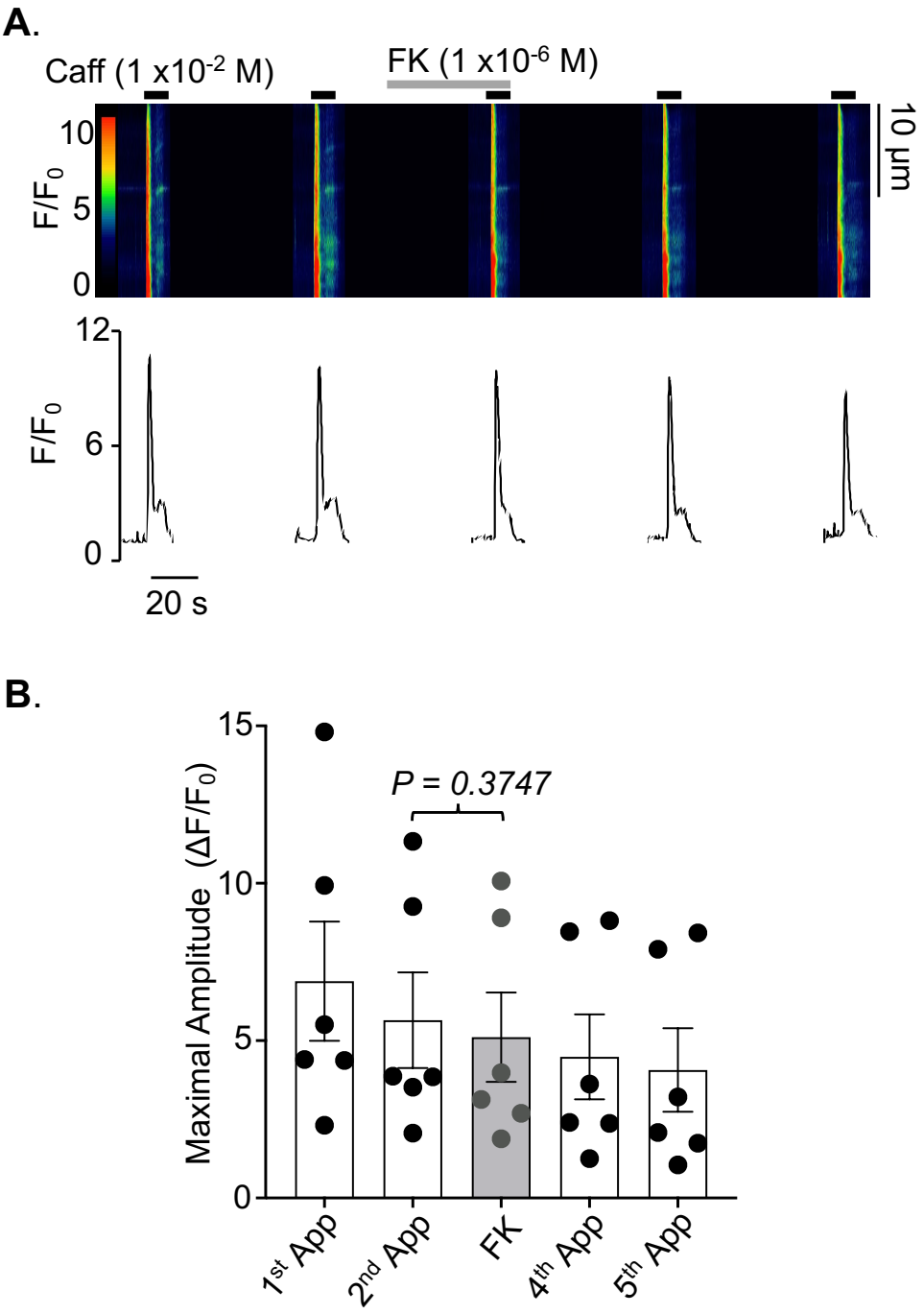


Figure 6.16: The effect of adenylyl cyclase activator, forskolin (FK), on caffeine (Caff)-induced store-release calcium spikes in isolated cells.

A. Representative spatiotemporal map and associated intensity plot of the effect of 1 x10^{-6} M FK on Ca^{2+} spikes, evoked by 1 x10^{-2} M Caff. **B.** Summary data for maximum amplitude ($\Delta F/F_0$). Maximum amplitude showed no significant change in the presence of FK (P=0.3747; n=6, N=6).

6.3 Discussion

The results presented in this chapter provide the first characterisation of both cAMP effectors, PKA and EPAC, signalling in mouse CCSM. AC activation, with low nanomolar concentrations of FK, potently inhibited adrenergic contractions, revealing an unusually high FK sensitivity. Moreover, the FK-induced relaxation was K_V7-dependent, supporting these channels as downstream targets of the cAMP-signalling pathway. Selective activation of PKA or EPAC alone produced only modest reductions in contractile activity, whereas their co-activation abolished contractions, indicating both effectors are required for CCSM relaxation. EPAC expression was confirmed with *Rapgef3* transcripts predominantly expressed and supported by immunoreactivity for EPAC-1 in isolated CCSM cells. Lastly, Ca^{2+} imaging revealed distinct actions of cAMP effectors, with PKA activation inhibiting low-PE Ca^{2+} oscillations, while EPAC activation inhibited high-PE Ca^{2+} oscillations. Moreover, the effects of PKA activation on low-PE Ca^{2+} oscillations was lost with K_V7 blockade, further implicating these channels as downstream targets of cAMP-signalling.

6.3.1 High FK sensitivity in mouse CCSM

A principal finding of this chapter is the exceptionally high potency of FK (IC_{50} in low nanomolar range) for inhibiting phasic contractions. This potency exceeds that reported in other smooth muscle types, such as rat uterus (IC_{50}: 5.5 x10^{-7} M), rat aorta (IC_{50}:1.8 x10^{-7} M), rabbit detrusor (1 x10^{-5} M used to inhibit spontaneous contractions), and mouse airway (IC_{50}:1.3 x10^{-6} M and shifted rightwards with BK_{Ca} blockade; Revuelta *et al*., 1997; Jones *et al*., 1984; Morita *et al*., 1986; Morgan, 2022). This markedly high sensitivity to FK aligns with decades of evidence supporting the efficacy of cAMP-mediated relaxation in the corpus cavernosum, such as the well-established clinical use of intracavernosal injections of alprostadil for ED (Porst, 1996; Lue and Dahiya, 1997). Alprostadil is a synthetic PGE_1 analogue, supporting CCSM relaxation via stimulation of the EP_2 and EP_4 receptors (EP_2Rs and EP_4Rs). Human tissue studies showed that EP_4Rs are the most abundantly transcribed receptor subtype, followed closely by EP_2Rs, and immunohistochemistry confirms expression of both receptors in human CCSM (Moreland *et al*., 2001; Komuro *et al*., 2006). Stimulation of EP_2Rs and EP_4Rs induces relaxation via G_s-receptor coupling to AC, and the subsequent elevation in cellular cAMP levels. Data presented in the present chapter suggesteded that activation of EPAC was also involved in cAMP-mediated inhibition.

6.3.2 K_v7 channels are downstream targets of cAMP signalling

Blockade of K_v7 channels with XE-991 significantly reduced the potency of FK in suppressing phasic contractions but spared tonic contractions. These observations highlight two points. They confirm that phasic contractility can be modulated by K_v7 channels, as shown in Chapter 4, whereas tonic contractures are K_v7-independent (Fig4.2). These data also suggested that K_v7 channels may act as downstream targets of cAMP signalling. This interpretation is strengthened by the finding that XE-991 prevents PKA-induced inhibition of low-PE Ca^{2+} oscillations.

Several studies support a link between cAMP pathways and K_v7 regulation. Lee *et al*. (2020a) reported that relaxations evoked by the $K_v7.2$-5 activator, ML213, in rabbit corpus cavernosum were attenuated by inhibition of either PKA (H-89) or EPAC (ESI-09). However, it should be noted that H-89 has been shown to inhibit other protein kinases (Davies *et al.*, 2000), and ESI-09 causes the denaturation of proteins (Rehmann, 2013). Direct enhancement of K_v7 currents by PKA has been demonstrated in airway and VSM, likely through phosphorylation of the $K_v7.5$ N-terminal domain (Mani *et al*., 2016; Brueggemann *et al*., 2018). Accordingly, $K_v7.5$ is abundantly expressed in mouse CCSM (Fig. 3.1D/3.2A; Mercer *et al*., 2025). EPAC-linked regulation is also plausible, as isoprenaline increased co-expression of EPAC downstream effectors, Rap1a/Rap2, with $K_v7.4$ in rat mesenteric arteries (Stott *et al*., 2016). In line with this interaction, 007-AM enhanced linopirdine-sensitive relaxations and currents in mesenteric and renal artery cells. However, the downstream coupling was vessel-specific; in renal artery, isoprenaline-evoked relaxations were attenuated by PKA inhibition, whereas in mesenteric artery they were selectively prevented by EPAC inhibition (Stott *et al*., 2016).

However, cAMP-K_v7 coupling is highly tissue-specific. Stott *et al*. (2016) found robust interactions between $K_v7.4$ and EPAC in mesenteric arteries, yet not in renal arteries. Van der Horst *et al*. (2020) described how tissue-specific differences arise from spatial compartmentalisation by AKAPs, localised phosphodiesterase activity and isolated cAMP microdomains by segregation of AC. Stott *et al*. (2016) showed that isoprenaline enhances co-localisation between $K_v7.4$ α-subunits and AKAP150 in mesenteric artery smooth muscle, indicating that AKAP-dependent scaffolding contributes to cAMP-mediated regulation of $K_v7.4$. Comparable signalling compartmentalisation likely underlies tissue-specific differences in K_v7 effects in other smooth muscle tissues. In pulmonary artery, cGMP- but not cAMP-dependent

relaxations are sensitive to K_v7 inhibition (Al-Chawishly *et al*., 2022), whereas β-adrenoceptor-mediated relaxations in renal artery are dependent on K_v7 channels (Chadha *et al*., 2012). By contrast, in bladder smooth muscle, although K_v7 channels modulate basal activity, blockade does not diminish β-adrenoceptor- or AC-evoked relaxations (Svalø *et al*., 2015).

6.3.3. Differential actions of cAMP effectors: EPAC and PKA

The present study revealed that both individual activation of EPAC and PKA produced only modest attenuations of phasic contractile activity, yet co-activation abolished phasic contractions. EPAC activation inhibited high-PE Ca^{2+} oscillations, and distinctly, PKA activation produced abolition of low-PE Ca^{2+} oscillations, via a mechanism dependent on K_v7 channels. These findings clearly indicated distinct signalling pathways for cAMP effectors to regulate contractility.

6.3.3.1 Role of EPAC

EPAC activation with 007-AM consistently reduced the frequency and amplitude of high-PE Ca^{2+} oscillations, abolishing activity in most recordings. Results from Chapter 4 indicated these high-PE Ca^{2+} oscillations are generated via SR store release, due to their insensitivity to LTCC- and K_v7- modulators, and sensitivity to 2-APB, GSK-7975A and TC. These results suggested that EPAC activation may have disrupted IP_3Rs, RyRs, SOCE or SR Ca^{2+} content. Given the effects of 007-AM occurred without altering caffeine-evoked RyR-mediated Ca^{2+} release, this demonstrated that EPAC does not deplete SR Ca^{2+} content or block RyRs. Comparable EPAC-dependent inhibitions in Ca^{2+} signalling have been reported in airway smooth muscle, in which activation suppressed (by approximately 60%) carbachol-evoked oscillations (Morgan *et al*., 2022).

EPAC activation has previously been shown to promote RyR-dependent Ca^{2+} release events in rat mesenteric arterial myocytes, with 007-AM increasing the frequency and amplitude of STOCs, an effect abolished by ryanodine and iberiotoxin, suggesting that EPAC may induce relaxation by facilitating Ca^{2+} sparks and BK_{Ca} activation (Roberts *et al*., 2013; Humphries *et al*., 2017). By contrast, the Ca^{2+} oscillations described in this chapter are at least partly IP_3R-dependent, based on their abolition by 2-APB. Moreover, the effects of EPAC activation and are not readily explained by localised RyR-mediated sparks, based on high-PE Ca^{2+} oscillation insensitivity to membrane potential modulators. Direct evidence for EPAC-dependent

inhibition of IP_3Rs is sparse, with EPAC often being associated with increasing IP_3R-dependent Ca^{2+} release via downstream Rap effectors and activation of PLCε (Schmidt *et al*., 2001; Dzhura *et al*., 2010; Wehbe *et al*., 2020). The only comparable effects were found in airway smooth muscle, in which EPAC inhibited carbachol-induced Ca^{2+} oscillations, which were also abolished by 2-APB (Morgan *et al*., 2022). EPAC has been functionally linked to the regulation of SOCE in several systems, although direct effects on STIM-Orai coupling remain poorly defined. In rat aortic and airway smooth muscle cells, EPAC activation decreases thapsigargin-evoked SOCE and thereby limits Ca^{2+} availability for contraction and proliferation, whereas EPAC inhibition enhances SOCE (Cuíñas *et al*., 2016; Chen *et al*., 2019). Therefore, the precise mechanism by which EPAC attenuates high-PE Ca^{2+} oscillations remains unresolved; without direct assessment of IP_3R gating (e.g. caged IP_3 photolysis) or single-cell SOCE measurements, it is not yet possible to distinguish whether EPAC acts primarily on IP_3-dependent release, store refilling, or both.

The effect of 007-AM was not tested against low-PE-evoked Ca^{2+} oscillations in the present study, and the contribution of K_V7 channels to any EPAC-mediated effect under these conditions therefore remains unresolved. Nevertheless, because EPAC activation abolished high-PE oscillations, it is plausible that EPAC suppresses SR Ca2+ release, which may contribute to the initiation of low-PE, voltage-dependent oscillatory activity, potentially via ANO1 activation (Lim et al., 2022b). Such an effect would predict inhibition of low-PE Ca^{2+} oscillations, but not necessarily through the same mechanism as PKA. Indeed, EPAC is also reported to regulate ion channels, including K_V7 family channels, raising the possibility that EPAC may additionally modulate low-PE responses through membrane potential-dependent pathways analogous to those observed with 6-MB (Stott et al., 2016; Fong et al., 2021; Matthews et al., 2023).

6.3.3.2 Role of PKA

PKA is a central mediator of cAMP-dependent relaxation in the CCSM. Classical work in human and animal CCSM shows that cAMP-elevating prostanoids such as PGE_1 and PGE_2 activate PKA to produce robust relaxation, and pharmacological inhibition of PKA attenuates these responses (Sáenz de Tejada *et al*., 1989a; Holmquist *et al*., 1991; Kim *et al*., 1998). FK and membrane-permeable cAMP analogues similarly relax CCSM through PKA-dependent mechanisms (Trigo-Rocha *et al*., 1993; Andersson and Wagner, 1995). Evidence also links PKA to ion channel

modulation in CCSM: the K_v7.2/4/5 activator ML213 produces robust relaxation, which is significantly attenuated by the PKA inhibitor H-89 (Lee *et al*., 2020a).

Despite the established importance of PKA in the corpus cavernosum, selective activation using 6-MB in the mouse yielded only modest effects on contractions. Yet, in contrast, PKA activation abolished low-PE Ca^{2+} oscillations, yet had no effect on high-PE Ca^{2+} oscillations. Chapter 4 showed that low-PE are sensitive to LTCC blockade and K_v7.2-5 activation (Fig4.9/4.12). The fact that PKA activation abolished the low-PE, but not the high-PE, Ca^{2+} oscillations, suggested that PKA may alter membrane potential, in line with the findings of Chapter 4. This is further supported by the fact that PKA-dependent abolition of low-PE Ca^{2+} oscillations was prevented by K_v7 blockade with XE-991 (Fig6.13).

One possibility is that PKA-mediated relaxation in CCSM may be partly attributable to phosphorylation and subsequent activation of K_v7 channels, limiting LTCC-dependent Ca^{2+} influx. However, this interpretation would be strengthened by demonstrating that XE-991 can reverse an established 6-MB-mediated inhibition of PE-evoked Ca^{2+} oscillations in the same isolated cell preparation. Nevertheless, the present findings remain consistent with the function of PKA, demonstrating modulatory effects on K_v7 channels, but of particular importance to the mouse CCSM, on K_v7.5 channels in particular. Brueggemann *et al*. (2018) found β-receptor activation enhanced K_v7.5 current amplitude via phosphorylation of N-terminal residue, serine-53, thereby increasing the channel's affinity for PIP_2. Of relevance to the present study, endogenous K_v7 currents in A7r5 rat aortic smooth muscle cells, predominantly K_v7.5, were enhanced by PKA activation. Moreover, heteromeric K_v7.4/5 channels showed decreased effects of PKA activation, and homomeric K_v7.4 channels showing no enhancement (Mani *et al*., 2016). The PKA selectivity of K_v7.5 was further evidenced by a chimera of K_v7.4, containing the K_v7.5 N-terminus, conferring the PKA modulation (Brueggemann *et al*., 2020). Furthermore, PKA-dependent enhancement of K_v7.1 has been shown in multiple studies, yet the relatively low expression of *Kcnq1* transcripts in mouse CCSM, suggested that they may contribute less than K_v7.5 (Marx *et al*., 2002; Kurokawa *et al*., 2004; Thompson *et al*., 2020).

The effects of PKA activation in our study are most consistent with a K_v7-dependent mechanism, in which PKA enhances K_v7.5 activity, leading to membrane hyperpolarisation and deactivation of LTCCs. A direct inhibitory action of PKA on LTCCs is unlikely. In most excitable tissues, including smooth muscle and particularly

the heart, PKA phosphorylation typically enhances Cav1.2 activity through AKAP-organised signalling complexes (Davare *et al*., 2000; Hall *et al*., 2006; Nystoriak *et al*., 2017). This well-established positive regulation contrasts with our observations, in which XE-991 completely reversed the 6-MB-induced abolition of Ca^{2+} oscillations, strongly indicating a K_V7-dependent mechanism, rather than direct inhibition of LTCCs.

6.3.3.3 Cross-talk

Co-activation of both cAMP effectors, EPAC and PKA, abolished phasic contractile activity, yet individual activation of EPAC/PKA produced small attenuations in activity. A similar pattern among the cAMP effectors has been observed in similar smooth muscles, indicating a cAMP effector cross-talk mechanism. Morgan *et al*. (2022) demonstrated that PGE_2-evoked Ca^{2+} oscillations were partly inhibited by EPAC activation, yet with co-activation of PKA almost abolished the activity (by approximately 85%). Cross-talk has been identified in VSM proliferation, where neither EPAC nor PKA inhibit cell growth, but co-activation produces a Rap1-independent anti-proliferative response (Hewer *et al*., 2011).

The cAMP effectors also exert distinct yet convergent effects on Ca^{2+} sensitisation pathways. PKA reduces Ca^{2+} sensitisation primarily through inhibition of RhoA/ROCK signalling, thereby decreasing ROCK-dependent phosphorylation of the MLCP regulatory subunit MYPT1 and relieving suppression of MLCP activity; in parallel, PKA attenuates CPI-17-mediated inhibition of MLCP, further promoting dephosphorylation of MLC_{20} (Essler et al., 2000; Bindewald et al., 2004; Goeckeler and Wysolmerski, 2005; Aslam et al., 2010). In contrast, EPAC appears to act predominantly at an upstream regulatory level via Rap1-dependent suppression of RhoA activation, rather than direct modulation of downstream contractile targets. Consistent with this, Zieba et al. (2011) demonstrated that EPAC activation reduced RhoA-GTP levels, decreased MLC_{20} phosphorylation, and relaxed rabbit portal vein smooth muscle. Collectively, these data suggested that PKA and EPAC converged on Ca^{2+} sensitisation via complementary targets; if similar signalling exists in mouse CCSM, co-activation of both pathways would be predicted to inhibit Ca^{2+} sensitisation in parallel with the observed attenuation of SR Ca^{2+} release and voltage-dependent Ca^{2+} influx, providing a plausible mechanism for the substantial inhibition of phasic contractions observed during EPAC and PKA activation.

6.3.3.4 Endothelial Involvement

The contribution of the corpus cavernosum endothelium cannot be ignored in relation to the effects of EPAC and PKA. Both cAMP effectors can stimulate eNOS, causing a concomitant increase in NO release (Roberts *et al*., 2013; Garcia-Morales *et al*., 2014; Garcia-Morales *et al*., 2017). Roberts *et al*. (2013) showed that 007-AM relaxes PE-induced tonic contractions in rat mesenteric arteries, and that this relaxation is abolished by NOS inhibition or endothelial disruption. Roberts *et al*. (2013) showed that blocking either IK_{Ca} or SK_{Ca} channels abolished the effect of 007-AM, suggesting that EPAC activation drives endothelial hyperpolarisation that either spreads to the smooth muscle through myoendothelial gap junctions (Garland and Dora, 2017) or stimulates eNOS (via influx of Ca^{2+}) with resultant release of NO. This mechanism is supported by immunohistochemical staining of rat corpus cavernosum endothelium for EPAC-1, suggesting endothelial involvement may play a role in the modest relaxations of CCSM contractility by 007-AM (Lin *et al*., 2023). However, the potent effects of 007-AM and 6-MB in isolated CCSM cells, where endothelial involvement is absent, indicated that at least part of the observed effect on contractions arose from direct actions on the CCSM itself.

6.3.4 Molecular identity of EPAC in mouse CCSM

This study indicated a *Rapgef3*-dominant transcriptional profile, with a minimal expression of *Rapgef4* and the presence of EPAC-1 protein confirmed in immunoreactive CCSM cells. This corresponds well to a study from Lin *et al*. (2023), in which rat CCSM expressed EPAC-1 in both endothelium and smooth muscle layers. Moreover, studies have indicated that although smooth muscle express both isoforms, EPAC-1 expression appears predominant. VSM cells predominantly express *Rapgef33* (EPAC-1), which has been implicated in the regulation of contractility, motility and proliferation (Wehbe *et al*., 2020; Yokoyama *et al*., 2008; Kato *et al*., 2015). Parnell *et al*. (2015) demonstrated that EPAC-1 has a broader distribution, including VSM, endothelia and cardiomyocytes, whereas EPAC-2 expression a more limited distribution, predominantly constrained to the brain, pancreas and adrenal glands.

Human airway smooth muscle expresses both isoforms, yet EPAC-1 is predominantly expressed and functionally significant in smooth muscle proliferation and remodelling (Roscioni *et al*., 2011; Oldenburger *et al*., 2012). Furthermore, exposure of human airway smooth muscle to cigarette smoke extract produced a

downregulation in *RAPGEF3*/EPAC-1, yet EPAC-2 was unaffected (Oldenburger *et al*., 2014). In human detrusor smooth muscle, EPAC-1 is clearly expressed and co-localises with β_3-adrenoceptors (Silva *et al*., 2020). Human myometrium expresses EPAC-1, which is up-regulated during early labour, whereas EPAC-2 expression appears relatively limited based on transcriptional analysis (Yulia *et al*., 2016; Li *et al*., 2021). Furthermore, and in line with the trends within the human urogenital system, both EPAC-1 and EPAC-2 are present in human prostate smooth muscle (Hennenberg *et al*., 2013). Overall, EPAC-1 expression in mouse CCSM in the present study is consistent with reports in rat corpus cavernosum and other smooth muscles, supporting EPAC-1 as the predominant functional isoform in this tissue.

6.3.5 Physiological Implications

Notably, the half-maximal cAMP concentration required to activate EPAC-1 is 30 μmol^{-1} compared to PKA with 1 μmol^{-1} (Dao *et al*., 2006); suggesting PKA is preferentially activated by small increases in cAMP, while large elevations are required to activate EPAC. In this chapter we have demonstrated that PKA preferentially inhibits Ca^{2+} influx, possibly via $K_V7.5$ activation, whilst EPAC activation inhibits SR Ca^{2+} release. Thus, when cAMP levels remain relatively low/transient, the PKA-mediated modulation of $K_V7.5$ is likely to represent an early and sensitive mechanism for limiting cytosolic Ca^{2+}. Sustained cellular cAMP would recruit EPAC-1, and limit SR Ca^{2+} release, serving as a higher-threshold, but more potent inhibitor of cytosolic Ca^{2+} elevations.

This mechanism fits well into the well-established function of G_s-coupled EP_2 and EP_4Rs in the CCSM (Moreland *et al*., 2001; Komuro *et al*., 2006). Mechanical forces associated with sinusoidal blood flow, particularly shear stress, have been shown to induce endothelial prostanoid synthesis through COX-2-dependent pathways, as demonstrated in vascular endothelial cells exposed to laminar shear stress (Topper *et al*., 1996). Shear- or stretch-induced increases in PGE_2 have been demonstrated in vascular endothelial systems (Alshihabi *et al*., 1996; Aoki *et al*., 2011). Direct evidence in the corpus cavernosum is limited, although CCSM cells are known to synthesise PGE_2 and regulate its production in response to environmental factors such as oxygen tension (Moreland *et al*., 2001). A model could be proposed in which haemodynamic changes in the corpus cavernosum sinusoids, stimulate PGE_2 production, which stimulates EP_2Rs and EP_4Rs in CCSM cells to induce relaxation. Within this context, low-level cAMP signals, stimulated by small haemodynamic

changes, may favour PKA-regulated $K_v7.5$ activation, whereas higher and sustained signals, stimulated by large or sustained haemodynamic elevations, may additionally recruit EPAC to reduce cytosolic Ca^{2+} by inhibition of SR Ca^{2+} release. This model would support the fact that co-activation abolished contractile activity in the mouse CCSM, as at high cAMP concentrations (high haemodynamic flow) both EPAC and PKA would be activated, facilitating erectile activity.

6.3.6 Limitations

There were clear differences between the effects of 007-AM in single-cell and whole-tissue preparations. While 007-AM potently inhibited Ca^{2+} oscillations in isolated CCSM cells, its effects on tissue contractions were comparatively modest. A likely explanation is hydrolysis of 007-AM. 007-AM is the acetoxymethyl (AM) ester of 8-pCPT-2′-O-Me-cAMP, designed to enhance membrane permeability; however, AM esters are highly susceptible to esterase-mediated breakdown, which limits their stability in aqueous and biological environments (Lavis *et al*., 2011). Consistent with this, high-performance liquid chromatography analysis in our laboratory demonstrated substantial spontaneous hydrolysis of 007-AM within a few hours at room temperature (Dr. Nicholas Mullins, personal communication). Degradation is therefore expected to be accelerated in the heated organ bath used for tissue experiments, reducing intracellular delivery of the active compound. This limitation is less pronounced in single-cell experiments, where the drug solution is only briefly heated and exposure is limited. In addition, diffusion barriers likely contribute, as isolated cells receive the analogue directly, whereas penetration may be restricted in intact tissue by the fibrous CCSM capsule. A similar explanation may account for the discrepancy observed with 6-MB, which strongly inhibited Ca^{2+} oscillations in isolated cells but produced only small relaxations in whole-tissue preparations.

The present study relies on pharmacological activation of AC with FK, that has long been used as a potent and direct AC activator. While FK is effective in elevating intracellular cAMP, it is also known to exert cAMP-independent effects on ion channels. Specifically, FK has been shown to modulate K^+ channels directly; Hoshi *et al*. (1988) demonstrated that high concentrations of FK (1.2×10^{-4} M) inhibited outward K^+ currents in outside-out patches from PC-12 cells independently of AC activation. However, the maximal concentration utilised in the present study was 1×10^{-6} M; at this concentration Hoshi *et al*. (1988) demonstrated a modest 10% inhibition of current. Furthermore, Boutjdir *et al*. (1990) reported FK-mediated inhibition of LTCCs in cardiac

myocytes at nanomolar concentrations, again through a non-cAMP pathway. Despite these findings, FK's ability to abolish CCSM tone and high-PE Ca^{2+} oscillations, which have been shown in Chapter 4 to be insensitive to LTCC and K_V7 channel modulation, supports the interpretation that FK-induced relaxation is mediated predominantly through AC activation and downstream cAMP signalling.

The pharmacological activation of the cAMP effectors utilised 'super-activators' of EPAC and PKA, which are chemically modified cAMP molecules, to confer specificity. 007-AM is designed to only activate EPAC, via two key modifications: the 8-pCPT moiety, which enhances lipophilicity and membrane permeability, and the 2′-O-methyl substitution, which confers high affinity for EPAC while largely preventing PKA activation (Vliem *et al*., 2008). Whereas 6-MB preferentially activates PKA, via the N^6-substitution, increasing PKA affinity by stabilising binding to the regulatory subunit and reducing interactions with EPAC. Although, these activators are designed specifically for the cyclic-nucleotide binding domain of the cAMP effectors, off-target effects have been observed. Foster *et al*. (2012) demonstrated that 8-pCPT-2′-O-Me-cAMP antagonises platelet $P2Y_{12}$ receptors independently of EPAC or PKA, and Meja *et al*. (2004) reported that the 8-pCPT moiety can inhibit equilibrative nucleoside transporters (ENT1) and activate A_2A adenosine receptors through conversion to 8-pCPT-adenosine. Moreover, Enyeart *et al*. (2010) showed that N^6-substituted cAMP analogues, including 6-MB-cAMP, directly inhibit TREK-1 ($K_2P2.1$) potassium channels via a mechanism independent of both PKA and EPAC. Lastly, the N^6-substituted analogues of 6-MB has been shown in live-cell EPAC FRET reporters to inhibit EPAC (Klarenbeek *et al*., 2015). However, the abolition of contractility observed with co-application of 007-AM and 6-MB in this study suggested that any potential EPAC antagonism by N^6-substituted analogues did not significantly impair EPAC activation under these experimental conditions.

7. General Discussion, Future Directions and Conclusions

7.1 General Discussion

The first results chapter demonstrated a predominant expression of *Kcnq5* in mouse CCSM, further supported by robust immunoreactivity in isolated cells. This profile aligns with findings in rat CCSM but contrasts with human tissue, where *KCNQ4* appears more dominant (Jepps *et al*., 2016; Lee *et al*., 2020a). Functionally, K_v7 modulation produced pronounced effects on CCSM activity, with the $K_v7.2$-5 activator RTG abolishing spontaneous and adrenergic-induced phasic contractions, whereas XE-991 enhanced them. These findings reveal an unexpectedly strong influence of K_v7 channels on phasic activity, exceeding earlier reports of moderate effects in rat and rabbit CCSM (Jepps *et al*., 2016; Lee *et al*., 2020a). The enhancement of spontaneous contractions by XE-991 was abolished by NIF, indicating that K_v7 channels normally restrain voltage-dependent Ca^{2+} influx via LTCCs. Imaging of isolated CCSM cells supported this, with RTG abolishing, and XE-991 enhancing, spontaneous Ca^{2+} oscillations. In previously quiescent cells, XE-991 induced oscillations, highlighting the integral role of K_v7 channels on resting membrane potential.

K_v7 channels in smooth muscle have been proposed to function analogously to those in neurons, where they are active at rest and help stabilise the resting membrane potential (Greenwood and Ohya, 2009). In CCSM, high transcriptional abundance of *Kcnq5* suggests that $K_v7.5$ α-subunits likely comprise the functional channels. Notably, homomeric $K_v7.5$ channels exhibit the most negative $V_{0.5}$ of activation (-44 mV) among the K_v7 family (Brueggemann *et al*., 2011). Resting membrane potential has been measured only twice in rabbit CCSM cells: Hashitani *et al*. (2005) reported values between -41 and -50 mV, whereas intracellular recordings from Professor Sean Ward indicate a more hyperpolarised potential of approximately -60 mV (Thornbury *et al*., 2019). Therefore, it is possible that a substantial proportion of channels composed primarily of $K_v7.5$ α-subunits would remain active at these potentials, generating outward stabilising currents. Inhibition of this current would depolarise the membrane, increasing the open probability of LTCCs and thereby accounting for the NIF-sensitive Ca^{2+} oscillations and phasic contractions observed with XE-991.

Chapter 4 further defined the mechanisms underlying phasic activity. Only phasic contractions were sensitive to modulators of membrane potential (RTG, NIF and the ANO1 blocker Ani-9), whereas both phasic and tonic activity were abolished by the IP_3R inhibitor 2-APB. This supports an IP_3R-dependent SR Ca^{2+} release mechanism leading to ANO1 activation, membrane depolarisation, and LTCC

activation. This aligns with Sergeant *et al*. (2009), who showed that Ca^{2+} waves in rabbit CCSM preceded Ca^{2+}-activated Cl^- currents and whole-tissue contractions. Two distinct Ca^{2+} responses to PE were identified; low-PE oscillations sensitive to RTG, XE-991 and NIF, and high-PE oscillations resistant to these modulators. These observations suggest low-PE oscillations drive phasic contractions, whereas high-PE oscillations underpin tonic responses. As SR Ca^{2+} release contributes to both phasic and tonic activity, mechanisms that maintain SR Ca^{2+} content are essential. Inhibition of CRAC channels with GSK-7975A abolished tonic contractures, consistent with tonic contractions being maintained by IP_3R-dependent SR Ca^{2+} release supported by SOCE. GSK-7975A increased phasic amplitude and duration despite abolishing low-PE oscillations, suggesting that SOCE contributes to the Ca^{2+} influx required for phasic events, and that impaired SR refilling prolongs SR Ca^{2+} release intervals. Suppression of Ca^{2+} oscillations in single cells induced by high concentration PE further indicates SOCE dependence in both phasic and tonic contractions. These findings complement studies in human tissue showing that Orai blockade suppresses CCSM tone and attenuates hypercontractility in experimental models (Sevilleja-Ortiz *et al*., 2020; 2021; 2022), supporting a conserved role for SOCE in CCSM physiology.

The findings of Chapter 6 integrate K_v7 channels into cAMP-dependent regulation of CCSM. Mouse CCSM displayed striking sensitivity to AC stimulation, with FK inhibiting phasic contractions at extremely low nanomolar concentrations. This sensitivity was markedly reduced by XE-991, positioning K_v7 channels downstream of cAMP signalling. PKA activation abolished only low-PE Ca^{2+} oscillations, an effect prevented by XE-991. These findings align with previous studies showing that K_v7 channels act as effector targets of cyclic-nucleotide pathways (Jepps *et al*., 2016; Lee *et al*., 2020a). Given the transcriptional predominance of *Kcnq5* and evidence that PKA selectively enhances $K_v7.5$ activity (Mani *et al*., 2016; Brueggemann *et al*., 2018; 2020), $K_v7.5$ likely mediates the PKA-dependent suppression of LTCC-mediated Ca^{2+} influx.

K_v7 channels are gated by PIP_2 binding at C-terminal domains (Zhang *et al*., 2003; Falkenburger *et al*., 2010). $K_v7.5$ channels are more sensitive to PIP_2 depletion than $K_v7.4$, as demonstrated by Ciona intestinalis voltage sensor-containing phosphatase (Ci-VSP)-induced PIP_2-depletion experiments (Brueggemann *et al*., 2020). PKA phosphorylation reduces this sensitivity, suggesting a PKA-dependent protective mechanism for maintaining $K_v7.5$ channel activity. Chapter 5 data support a

predominant PIP_2-depletion mechanism of α_{1A}-adrenoceptor ($\alpha_{1A}R$)-mediated $K_v7.5$ inhibition in HEK-293 cells, with exogenous $PI(4,5)P_2$ -diC_8 preventing this effect.

The combined effects of K_v7 modulators on spontaneous and adrenergic-induced phasic contractions, the predominant *Kcnq5* expression, strong $K_v7.5$ immunoreactivity, and sensitivity of $K_v7.5$ to PIP_2 depletion highlight a central role for membrane PIP_2 in CCSM contractility. Adrenergic activation, via α_1Rs, triggers $G_{q/11}$ signalling, SR Ca^{2+} release, PKC activation, and PIP_2 depletion, all of which inhibit $K_v7.5$ channels, thus, positioning $K_v7.5$ channel inhibition as an alternative mechanism to induce depolarisation and activate LTCCs, in addition to ANO1 activation. Relaxation of phasic contractions may reflect feedback mechanisms including Ca^{2+}-dependent inactivation of LTCCs, biphasic Ca^{2+} regulation of IP_3Rs, and re-synthesis of membrane PIP_2, thereby, stabilising the open-state of $K_v7.5$ channels and inducing hyperpolarisation, which together reset excitability and terminate the phasic event.

This provides a novel mechanistic framework for understanding ED pathophysiology. ED models exhibit adrenergic hypercontractility and impaired nitrergic relaxation, increasing the likelihood of sustained PIP_2 depletion and PKC activation, maintaining $K_v7.5$ channels in an inhibited state and enhancing Ca^{2+} influx via LTCCs (Behr-Roussel *et al*., 2003; De Tajada, 2004; Ushiyama *et al*., 2006; Sevilleja-Ortiz *et al*., 2020). Given that mouse phasic contractions are similar in amplitude to tonic contractures and occur at 7-10 contractions per minute, enhanced phasic activity would significantly impair sinusoidal filling. Human CCSM also exhibits spontaneous contractions of comparable amplitude to PE-induced tone (Christ *et al*., 1990), suggesting conserved functional relevance.

Diabetic ED is associated with reduced NO bioavailability and downregulation of the NO-cGMP-PKG pathway (De Tajada, 2004). K_v7 channels have been proposed to act downstream of PKG in rat CCSM, and NO signalling may increase membrane PIP_2 levels (Taoufiq *et al*., 2013; Jepps *et al*., 2016; Constantin *et al*., 2021). Jepps *et al*. (2016) reported significant reductions in *Kcnq4* and *Kcnq5* expression in spontaneously hypertensive, heart-failure prone (SHHF) ratc, suggesting $K_v7.5$ membrane expression may be limiting in disease conditions.

Given the need for therapeutic strategies for PDE5I non-responders, the relative preservation of cAMP signalling in ED is notable. Alprostadil acts as an effective salvage therapy for improving erectile function in PDE5I non-responders, although with

limitations regarding side effects and variable efficacy (Shabsigh *et al*., 2000; Jaffe *et al*., 2004; Duncan *et al*., 2019). Topical formulations avoid injection-related complications and show improved outcomes in high-risk groups (Steidle *et al*., 2002; Campbell, 2005; Rooney *et al*., 2009; Mulhall *et al*., 2013). These findings support cAMP-dependent treatments as a promising therapeutic strategy for severe ED (adjunct to PDE5Is) and PDE5I non-responders.

Within this context, the present study identifies novel signalling pathways for both PKA and EPAC in mouse CCSM. EPAC-1 appears the predominant isoform, consistent with other smooth muscle tissues (Hennenberg *et al*., 2013; Oldenburger *et al*., 2014; Parnell *et al*., 2015; Yulia *et al*., 2016; Silva *et al*., 2020; Li *et al*., 2021; Lin *et al*., 2023), and strong inhibition of high-PE Ca^{2+} oscillations by EPAC activation positions it as an important modulator of relaxation. Although the EPAC activator 007-AM is unsuitable pharmacologically, gene-based approaches utilising adenoviral delivery have been effective in ED models using eNOS or nNOS (Champion *et al*., 1999; Magee *et al*., 2002; Bivalacqua *et al*., 2005; Yoshimura *et al*., 2010). Gene therapy targeting ion channels has also been explored, with intracavernosal delivery of hSlo cDNA encoding the BK_{Ca} α-subunit improving erectile responses in ageing and diabetic animal models and progressing to a Phase I clinical trial, where plasmid hMaxi-K gene transfer produced dose-dependent improvements in erectile function without serious adverse events (Christ et al., 1998; Bivalacqua et al., 2000; Christ et al., 2001; Melman et al., 2006). However, despite this progress, cAMP-dependent pathways have not been pursued in gene therapy for ED. Given that K_v7 channels act downstream of cAMP, and with evidence of *Kcnq5* downregulation in disease (Jepps *et al*., 2016), gene therapy increasing $K_v7.5$ expression may help restore a less-depolarised resting membrane potential, and off-set ED-related hypercontractility. Additionally, approaches targeting membrane PIP_2 levels (PKG), enhancing $K_v7.5$ PIP_2 affinity (PKA), or limiting SR Ca^{2+} release (EPAC) may represent novel strategies to improve CCSM function and counteract pathophysiological changes in ED.

7.2 Future Directions

The present work highlights the importance of K_v7 channels, particularly those mediated by $K_v7.5$ α-subunits, in mouse CCSM. However, their functional contribution was inferred primarily through pharmacological modulators. Direct electrophysiological assessment of native K_v7 currents in freshly isolated mouse CCSM cells using patch-clamp would allow quantification of their biophysical properties. Such experiments would also extend the findings of α_{1A}R-mediated inhibition of $K_v7.5$ in HEK-293 cells to a more physiologically relevant model, avoiding the issue of gross overexpression. In isolated mouse CCSM cells, application of PE may suppress outward K^+ currents, which are sensitive to K_v7 channel blockers and remain sustained during prolonged depolarising voltage steps, consistent with the non-inactivating characteristic of K_v7 currents. Moreover, the involvement of PIP_2 depletion can be assessed more stringently, by using Ci-VSP in native CCSM cells.

On a similar note, K_v7 channels acting as downstream effectors of cAMP-pathway were studied using pharmacology on isometric tension recordings and single cell Ca^{2+} imaging. Isolating K_v7 currents in CCSM cells would allow direct determination of how the cAMP-pathway (FK, 007-AM, 6-MB) and cGMP-pathway (YC-1, BAY 58-2667) modulate these currents, thereby, establishing a mechanistic link between cyclic nucleotide pathways and K_v7 channel activity in CCSM cells.

To support these functional associations, evidence of the co-localisation of $K_v7.5$ with cAMP- and cGMP-effectors is required. Co-immunoprecipitation or proximity ligation assays in mouse CCSM cells could resolve interactions between $K_v7.5$ α-subunits and EPAC-1/2, their downstream GTPases Rap1/2, as well as PKA and PKG. These studies would strengthen the interpretation that K_v7 channels act as downstream effectors of cyclic nucleotide signalling.

In HEK-293 cells co-expressing α_{1A}R and $K_v7.5$, PE inhibited $K_v7.5$ current, but qPCR indicated that other *Kcnq* isoforms are present and could form homo-tetramers in their own right or hetero-tetramers with $K_v7.5$ in mouse CCSM. To better approximate the native situation in CCSM, future recombinant expression studies should examine α_{1A}R-mediated effects on $K_v7.4$ and $K_v7.1$, alone and in combination with $K_v7.5$, to resolve isoform-specific contributions.

Beyond mechanistic characterisation in healthy tissue, it would be informative to determine how these pathways are altered in disease states associated with ED.

Altered expression of BK_{Ca} and SK_{Ca} channels has been reported in db/db mice, an experimental model of T2DM (Comerma-Steffensen *et al.*, 2022), raising the possibility that K_v7 isoforms may also be remodelled in diabetic ED. Assessing K_v7 expression and function in such models may therefore clarify their pathophysiological contribution. Likewise, psychogenic ED has been associated with heightened sympathetic activity (Kim and Oh, 1992), and, given the proposed α_1R-mediated inhibition of $K_v7.5$, models with enhanced adrenergic signalling may reveal an ED phenotype involving pathological suppression of K_v7 channel activity.

This thesis relied primarily on isometric tension recordings from tissue strips and Ca^{2+} imaging in isolated CCSM cells. Because single-cell Ca^{2+} signalling does not necessarily reflect tissue-wide Ca^{2+} activity governing contractility, implementation of a whole-tissue Ca^{2+} imaging model in Acta2-GCaMP8.1-mVermilion mice would provide crucial spatial and temporal insight into Ca^{2+} signalling across intact CCSM. This approach would clarify how phasic and tonic Ca^{2+} events are initiated and propagated. Repeating pharmacological interventions (RTG, NIF, 007-AM, 6-MB) across low- and high-PE concentrations in intact tissue would further delineate the role of K_v7 channels and cAMP effectors in regulating co-ordinated Ca^{2+} signalling governing contraction.

Finally, EPAC activation in this study appeared to inhibit SR Ca^{2+} release by a mechanism independent of SR Ca^{2+} content and RyRs, suggesting potential modulation of IP_3Rs or SOCE. Direct testing of EPAC activators on SOCE in isolated CCSM cells, along with photolytic uncaging of IP_3 to directly investigate EPAC effects on IP_3R-mediated Ca^{2+} release are warranted.

7.3 Conclusions

Collectively, the data presented in this thesis identify $K_v7.5$ channels and cAMP effectors, EPAC and PKA, as key regulators of mouse CCSM contractility. Phasic contractility is markedly sensitive to pharmacological agents modulating membrane potential and likely contributes to the maintenance of detumescence. The data suggest these contractions were driven by IP_3R-driven Ca^{2+} waves activating ANO1 and subsequently activation of LTCCs. This work also identifies a previously under-explored mechanism for constraining K_v7 channel activity, in which pathways that reduce membrane PIP_2, activate PKC, or promote Ca^{2+}-CaM binding can suppress K_v7 currents and thereby enhance LTCC-dependent Ca^{2+} influx (Fig7.1). These mechanisms position K_v7 channels, particularly $K_v7.5$, as key determinants of CCSM excitability and may become dysregulated under disease conditions. Furthermore, these channels have been implicated in both cGMP- and cAMP-pathways (Fig7.2). This thesis postulates that the effect of PKA is partially mediated by the enhancement of K_v7 currents, likely the $K_v7.5$ isoform, supported by reports of strong cAMP-sensitivity. Given the robust effects of K_v7-modulators on phasic contractions, $K_v7.5$ emerges as a plausible therapeutic target in ED, especially in cases with impaired cGMP signalling, like that of PDE5I non-responders. Specifically, strategies aimed at restoring membrane PIP_2 levels, enhancing $K_v7.5$ activity via PKA or enhancing the EPAC-mediated inhibition of SR Ca^{2+} release may offer complementary avenues to induce CCSM relaxation in tissues with cGMP-dysregulation.

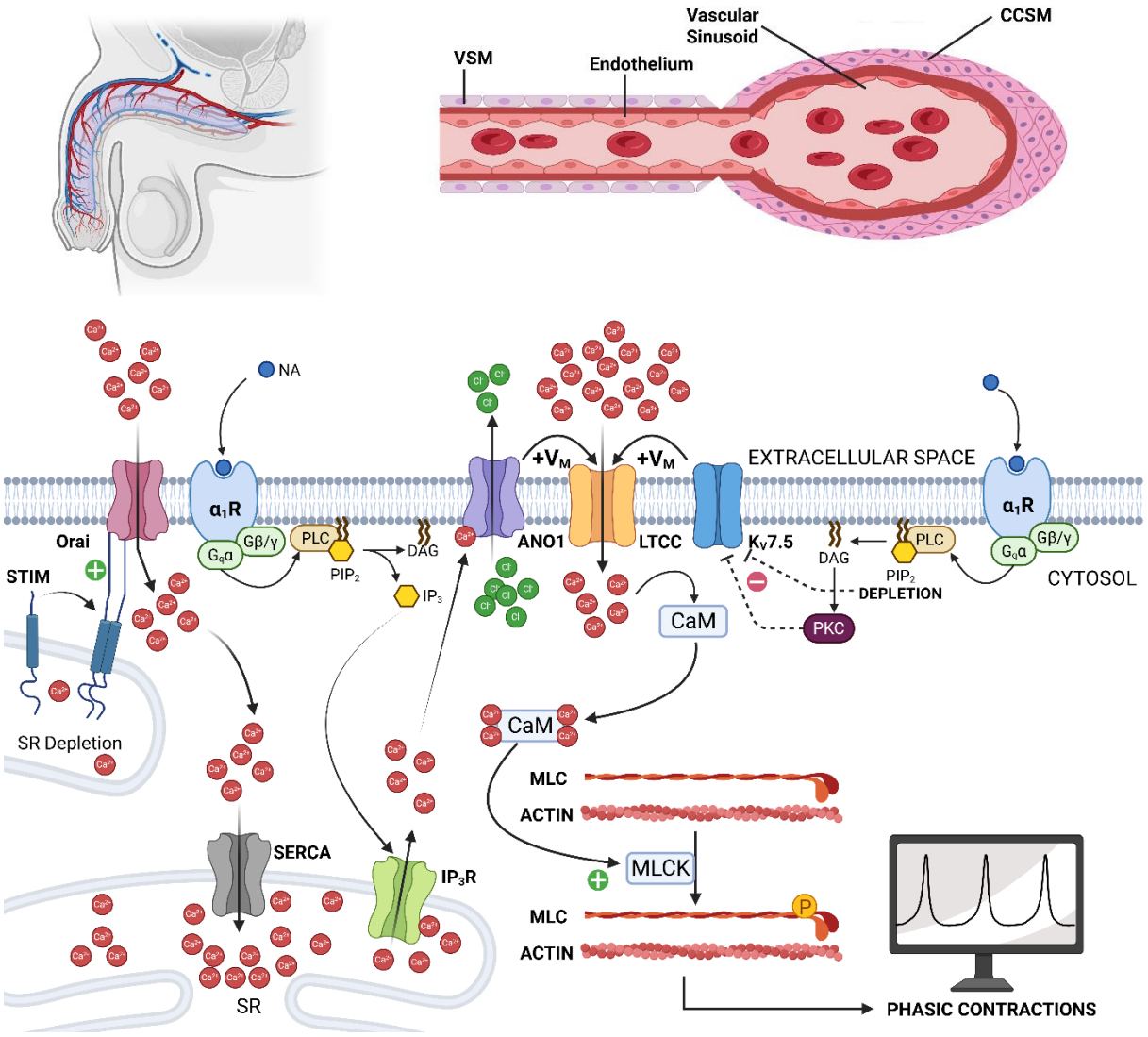


Figure 7.1. Proposed mechanism mediating adrenergic phasic contractions in the mouse CCSM. The flaccid penile state, in which corpus cavernosum smooth muscle (CCSM) contraction collapses the vascular sinusoids and limits penile filling, is maintained via noradrenaline (NA) release from adrenergic nerves. NA binds to α_1-adrenoceptors (α_1R) at the plasma membrane, activating coupled G-proteins ($G_q\alpha$ and $G\beta/\gamma$), which stimulates phospholipase C (PLC)-mediated hydrolysis of phosphatidylinositol 4,5-bisphosphate (PIP_2), generating inositol trisphosphate (IP_3) and diacylglycerol (DAG). IP_3 binds to IP_3 receptors (IP_3R) on the sarcoplasmic reticulum (SR), triggering Ca^{2+} release into the cytosol and activating the calcium-activated chloride channel ANO1, promoting membrane depolarisation ($+V_M$). SR Ca^{2+} depletion activates stromal interaction molecules (STIM) on the SR membrane, which oligomerise and translocate to the plasma membrane to gate Orai channels, permitting Ca^{2+} influx that can replenish SR stores via the sarco/endoplasmic reticulum Ca^{2+}-ATPase (SERCA). In parallel, PIP_2 depletion and DAG-dependent activation of protein kinase C (PKC) inhibit $K_V7.5$ channels, further amplifying depolarisation ($+V_M$). This depolarisation activates L-type Ca^{2+} channels (LTCC), permitting additional Ca^{2+} influx into the cytosol. Collectively, elevated cytosolic Ca^{2+} binds calmodulin (CaM) to form a Ca^{2+}-CaM complex, which activates myosin light chain kinase (MLCK) to phosphorylate myosin light chain (MLC), enabling actin-myosin cross-bridge cycling and generating phasic contractions. (Made using Biorender).

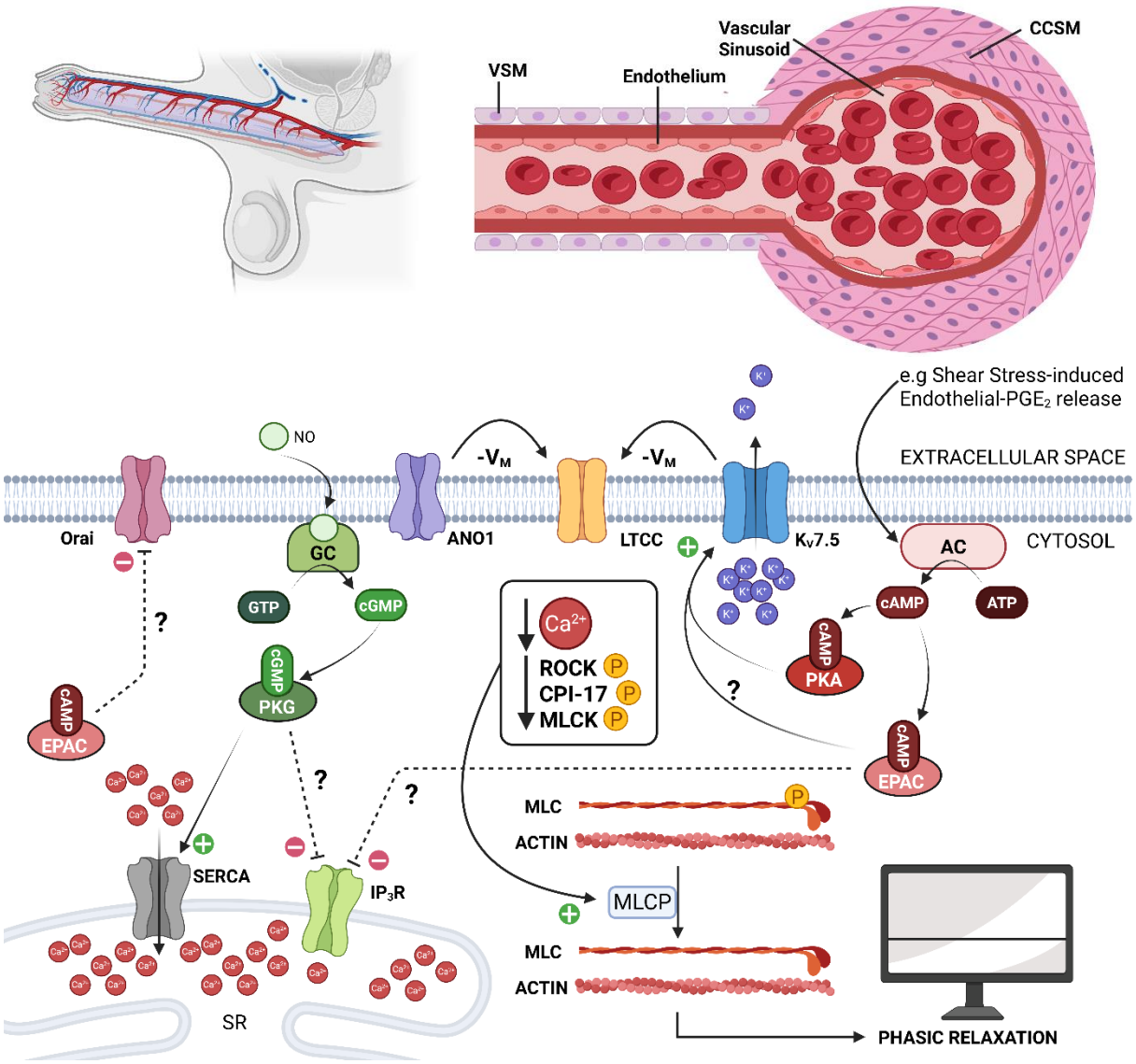


Figure 7.2. Proposed mechanism mediating phasic relaxations in the mouse CCSM. The penile erection requires relaxation of the CCSM, mediated by a reduction in cytosolic Ca^{2+} and decreased myosin light chain (MLC) phosphorylation, to permit blood filling into the vascular sinusoids. Nitric oxide (NO), released from non-adrenergic non-cholinergic (NANC) nerves and endothelia, activates guanylyl cyclase (GC), catalysing the conversion of GTP to cyclic GMP (cGMP), which activates protein kinase G (PKG). PKG promotes sarcoplasmic reticulum (SR) Ca^{2+} sequestration via phospholamban-induced disinhibition of the sarco/endoplasmic reticulum Ca^{2+}-ATPase (SERCA), and may additionally inhibit IP_3 receptor (IP_3R)-mediated Ca^{2+} release, reducing cytosolic Ca^{2+} levels. Suppression of IP_3R-mediated Ca^{2+} release would consequently deactivate ANO1 and promote membrane hyperpolarisation ($-V_M$). In parallel, stimuli such as shear stress-induced endothelial prostaglandin E_2 (PGE_2) release may activate adenylyl cyclase (AC), catalysing the conversion of ATP to cyclic AMP (cAMP), which activates protein kinase A (PKA) and exchange protein directly activated by cAMP (EPAC). PKA and EPAC may promote membrane hyperpolarisation ($-V_M$) via activation of $K_V7.5$ channels, thereby deactivating L-type Ca^{2+} channels (LTCC) and limiting Ca^{2+} influx. EPAC may additionally reduce SR Ca^{2+} release via IP_3R inhibition, or attenuate store-operated Ca^{2+} entry (SOCE) through inhibition of Orai channels. Collectively, reduced cytosolic Ca^{2+} decreases the activity of Rho-associated kinase (ROCK), CPI-17, and myosin light chain kinase (MLCK), shifting the balance towards myosin light chain phosphatase (MLCP)-mediated dephosphorylation of MLC, inhibiting actin-myosin cross-bridge cycling and resulting in phasic relaxation. Question marks (?) denote pathways that remain to be fully elucidated in the CCSM. (Made using Biorender).

8. References

Abbott, G. W. (2016). KCNE4 and KCNE5: K(+) channel regulation and cardiac arrhythmogenesis. *Gene*, 593(2), pp.249–260.

Abbott, G. W., and Goldstein, S. A. (1998). A superfamily of small potassium channel subunits: form and function of the MinK-related peptides (MiRPs). *Quarterly reviews of biophysics*, 31(4), pp.357–398.

Abbracchio, M. P., Boeynaems, J. M., Barnard, E. A., Boyer, J. L., Kennedy, C., Miras-Portugal, M. T., King, B. F., Gachet, C., Jacobson, K. A., Weisman, G. A., and Burnstock, G. (2003). Characterization of the UDP-glucose receptor (re-named here the P2Y14 receptor) adds diversity to the P2Y receptor family. *Trends in pharmacological sciences*, 24(2), pp.52–55.

Abdi, S., Shenouda, P., Patel, N., Saini, B., Bharat, Y., and Calvillo, O. (2004). A novel technique for pudendal nerve block. *Pain physician*, 7(3), pp.319–322.

Adams, M. A., Banting, J. D., Maurice, D. H., Morales, A., and Heaton, J. P. (1997). Vascular control mechanisms in penile erection: phylogeny and the inevitability of multiple and overlapping systems. *International journal of impotence research*, 9(2), pp.85–91.

Afeli, S. A., Malysz, J., and Petkov, G. V. (2013). Molecular expression and pharmacological evidence for a functional role of Kv7 channel subtypes in guinea pig urinary bladder smooth muscle. *PLOS ONE*, 8(9), e75875

Ahmed, W. S., Geethakumari, A. M., and Biswas, K. H. (2021). Phosphodiesterase 5 (PDE5): Structure-function regulation and therapeutic applications of inhibitors. *Biomedicine & pharmacotherapy*, 134, 111128.

Akin, E. J., Aoun, J., Jimenez, C., Mayne, K., Baeck, J., Young, M. D., Sullivan, B., Sanders, K. M., Ward, S. M., Bulley, S., Jaggar, J. H., Earley, S., Greenwood, I. A., and Leblanc, N. (2023). ANO1, CaV1.2, and IP_3R form a localized unit of excitation–contraction coupling in mouse pulmonary arterial smooth muscle. *The Journal of General Physiology*, 155(11), e202213217.

Akinaga, J., García-Sáinz, J. A., and Pupo, A. S. (2019). Updates in the function and regulation of α1-adrenoceptors. *British Journal of Pharmacology*, 176(14), pp.2343–2357.

Al Kawadri, Y., McClafferty, H., Dudem, S., Rabab, K. E., Thornbury, K. D., Sergeant, G. P., Hollywood, M. A., and Shipston, M. J. (2025). Distinct domains of LINGO1 control surface expression and biophysical properties of large conductance Ca2+- and voltage-activated potassium (BK) channels. Journal of biological chemistry, 301(9), p.110550.

Alshihabi, S. N., Chang, Y. S., Frangos, J. A., and Tarbell, J. M. (1996). Shear stress-induced release of PGE_2 and PGI_2 by vascular smooth muscle cells. *Biochemical and Biophysical Research Communications*, 224(3), pp.808–814.

Amberg, G. C., Navedo, M. F., Nieves-Cintrón, M., Molkentin, J. D., and Santana, L. F. (2007). Calcium sparklets regulate local and global calcium in murine arterial smooth muscle. *The Journal of Physiology*, 579(Pt 1), pp.187–201.

Ammendola, A., Geiselhöringer, A., Hofmann, F., and Schlossmann, J. (2001). Molecular determinants of the interaction between the inositol 1,4,5-trisphosphate receptor-associated cGMP kinase substrate (IRAG) and cGMP kinase Iβ. Journal of biological chemistry, 276, pp.24153–24159.

Anastassiadis, T., Deacon, S. W., Devarajan, K., Ma, H., and Peterson, J. R. (2011). Comprehensive assay of kinase catalytic activity reveals features of kinase inhibitor selectivity. *Nature Biotechnology*, 29(11), pp.1039–1045.

Andersson, K. E., and Wagner, G. (1995). Physiology of penile erection. *Physiological reviews*, 75(1), pp.191–236.

Andersson, K. E. (2011). Mechanisms of penile erection and basis for pharmacological treatment of erectile dysfunction. *Pharmacological reviews*, 63(4), pp.811–859.

Andrikopoulos, P., Fraser, S. P., Patterson, L., Ahmad, Z., Burcu, H., Ottaviani, D., Diss, J. K., Box, C., Eccles, S. A., and Djamgoz, M. B. (2011). Angiogenic functions of voltage-gated Na+ channels in human endothelial cells: modulation of vascular endothelial growth factor (VEGF) signaling. *Journal of biological chemistry*, 286(19), pp.16846–16860.

Aoki, T., Nishimura, M., Matsuoka, T., Yamamoto, K., Furuyashiki, T., Kataoka, H., Kitaoka, S., Ishibashi, R., Ishibazawa, A., Miyamoto, S., Morishita, R., Ando, J., Hashimoto, N., Nozaki, K., and Narumiya, S. (2011). PGE_2–EP_2 signalling in endothelium is activated by haemodynamic stress and induces cerebral aneurysm through an amplifying loop via NF-κB. *British Journal of Pharmacology*, 163(6), pp.1237–1249.

Apkon, M., and Nerbonne, J. M. (1988). α_1-Adrenergic agonists selectively suppress voltage-dependent K^+ current in rat ventricular myocytes. *Proceedings of the National Academy of Sciences of the United States of America*, 85, pp.8756–8760.

Arrighi, I., Bloch-Faure, M., Grahammer, F., Bleich, M., Warth, R., Mengual, R., Drici, M. D., Barhanin, J., and Meneton, P. (2001). Altered potassium balance and aldosterone secretion in a mouse model of human congenital long QT syndrome. *Proceedings of the National Academy of Sciences of the United States of America*, 98(15), pp.8792–8797.

Aslam, M., Härtel, F. V., Arshad, M., Gündüz, D., Abdallah, Y., Sauer, H., Piper, H. M., and Noll, T. (2010). cAMP/PKA antagonizes thrombin-induced inactivation of endothelial myosin light chain phosphatase: role of CPI-17. *Cardiovascular research*, 87(2), pp.375–384.

Ayta, I. A., McKinlay, J. B. & Krane, R. J. (1999). The likely worldwide increase in erectile dysfunction between 1995 and 2025 and some possible policy consequences. *BJU International*, 84(1), pp.50–56.

Azevedo, M. F., Faucz, F. R., Bimpaki, E., Horvath, A., Levy, I., de Alexandre, R. B., Ahmad, F., Manganiello, V., and Stratakis, C. A. (2014). Clinical and molecular genetics of the phosphodiesterases (PDEs). *Endocrine reviews*, 35(2), pp.195–233.

Babenko, A. P., Aguilar-Bryan, L., and Bryan, J. (1998). A view of Sur/KIR6.X, KATP channels. *Annual review of physiology*, 60, pp.667–687.

Bai, Y., and Sanderson, M. J. (2006). Airway smooth muscle relaxation results from a reduction in the frequency of Ca^{2+} oscillations induced by a cAMP-mediated inhibition of the IP_3 receptor. *Respiratory Research*, 7, 34.

Bai, Y., Edelmann, M., and Sanderson, M. J. (2009). The contribution of inositol 1,4,5-trisphosphate and ryanodine receptors to agonist-induced Ca^{2+} signalling of airway smooth muscle cells. *American Journal of Physiology: Lung Cellular and Molecular Physiology*, 297(2), pp.L347–L361.

Baldi, L., Hacker, D. L., Adam, M., & Wurm, F. M. (2007). Recombinant protein production by large-scale transient gene expression in mammalian cells: state of the art and future perspectives. *Biotechnology Letters*, 29(5), pp.677–684.

Balla, T. (2013). Phosphoinositides: tiny lipids with giant impact on cell regulation. *Physiological Reviews*, 93(3), pp.1019–1137.

Barbosa, M. L. de C., Fumian, M. M., Miranda, A. L. P. de, Barreiro, E. J., and Lima, L. M. (2011). Therapeutic approaches for tumor necrosis factor inhibition. *Brazilian Journal of Pharmaceutical Sciences*, 47(3), pp.427–446.

Barhanin, J., Lesage, F., Guillemare, E., Fink, M., Lazdunski, M., and Romey, G. (1996). K(V)LQT1 and IsK (minK) proteins associate to form the I(Ks) cardiac potassium current. *Nature*, 384(6604), pp.78–80.

Barrese, V., Stott, J. B., and Greenwood, I. A. (2018). *KCNQ*-encoded potassium channels as therapeutic targets. *Annual review of pharmacology and toxicology*, 58, pp.625–648.

Barros, F., Domínguez, P., and de la Peña, P. (2012). Cytoplasmic domains and voltage-dependent potassium channel gating. *Frontiers in pharmacology*, 3, 49.

Bearelly, P., Phillips, E. A., Pan, S., O'Brien, K., Asher, K., Martinez, D., and Munarriz, R. (2020). Long-term intracavernosal injection therapy: treatment efficacy and patient satisfaction. *International journal of impotence research*, 32(3), pp.345–351.

Becker, A. J., Uckert, S., Stief, C. G., Truss, M. C., Machtens, S., Scheller, F., Knapp, W. H., Hartmann, U., and Jonas, U. (2000). Plasma levels of cavernous and systemic norepinephrine and epinephrine in men during different phases of penile erection. *The Journal of Urology*, 164(2), pp.573–577.

Becker, A. J., Uckert, S., Stief, C. G., Scheller, F., Knapp, W. H., Hartmann, U., and Jonas, U. (2002). Cavernous and systemic plasma levels of norepinephrine and epinephrine during different penile conditions in healthy men and patients with erectile dysfunction. *Urology*, 59(2), pp.281–286.

Behr-Roussel, D., Chamiot-Clerc, P., Bernabe, J., Mevel, K., Alexandre, L., Safar, M. E., and Giuliano, F. (2003). Erectile dysfunction in spontaneously hypertensive rats: pathophysiological mechanisms. *American Journal of Physiology–Regulatory, Integrative and Comparative Physiology*, 284, pp.R682–R688.

Bender, K., Wellner-Kienitz, M. C., and Pott, L. (2002). Transfection of a phosphatidyl-4-phosphate 5-kinase gene into rat atrial myocytes removes inhibition of GIRK current by endothelin and alpha-adrenergic agonists. *FEBS Letters*, 529(2–3), pp.356–360.

Bender, A. T., and Beavo, J. A. (2006). Cyclic nucleotide phosphodiesterases: molecular regulation to clinical use. *Pharmacological reviews*, 58(3), pp.488–520.

Berridge, M. J. (1993). Inositol trisphosphate and calcium signalling. *Nature*, 361(6410), pp.315–325.

Berridge, M. J. (2016). The inositol trisphosphate/calcium signaling pathway in health and disease. *Physiological Reviews*, 96, pp.1261–1296.

Bitsch, M., Kromann-Andersen, B., Schou, J., and Sjøntoft, E. (1990). The elasticity and the tensile strength of tunica albuginea of the corpora cavernosa. *The Journal of urology*, 143(3), pp.642–645.

Bindewald, K., Gündüz, D., Härtel, F., Peters, S. C., Rodewald, C., Nau, S., Schäfer, M., Neumann, J., Piper, H. M., and Noll, T. (2004). Opposite effect of cAMP signaling in endothelial barriers of different origin. *American journal of physiology. Cell physiology*, 287(5), pp.C1246–C1255.

Bivalacqua, T. J., Champion, H. C., Usta, M. F., Cellek, S., Chitaley, K., Webb, R. C., Lewis, R. L., Mills, T. M., and Hellstrom, W. J. G. (2000). Gene transfer of the large-conductance Ca^{2+}-activated K^{+} channel (hSlo) restores erectile function in aged rats. American Journal of Physiology – Heart and Circulatory Physiology, 278, pp.H1401–H1407.

Bivalacqua, T. J., Usta, M. F., Kendirci, M., Pradhan, L., Alvarez, X., Champion, H. C., Kadowitz, P. J., and Hellstrom, W. J. G. (2005). Superoxide anion production in the rat penis impairs erectile function in diabetes: Influence of in vivo extracellular superoxide dismutase gene therapy. The Journal of Sexual Medicine, 2(2), pp.187–197.

Bivalacqua, T. J., Liu, T., Musicki, B., Champion, H. C., and Burnett, A. L. (2007). Endothelial nitric oxide synthase keeps erection regulatory function balance in the penis. European urology, 51(6), pp.1732–1740.

Blaschko, S. D., Mahawong, P., Ferretti, M., Cunha, T. J., Sinclair, A., Wang, H., Schlomer, B. J., Risbridger, G., Baskin, L. S., and Cunha, G. R. (2013). Analysis of the effect of estrogen/androgen perturbation on penile development in transgenic and diethylstilbestrol-treated mice. *Anatomical record (Hoboken)*, 296(7), pp.1127–1141.

Bogeski, I., Kummerow, C., Al-Ansary, D., Schwarz, E. C., Koehler, R., Kozai, D., Takahashi, N., Peinelt, C., Griesemer, D., Bozem, M., Mori, Y., Hoth, M., and Niemeyer, B. A. (2010). Differential redox regulation of ORAI ion channels: a mechanism to tune cellular calcium signaling. Science signaling, 3(115), p.ra24.

Boittin, F. X., Macrez, N., Halet, G., and Mironneau, J. (1999). Norepinephrine-induced Ca^{2+} waves depend on $InsP_3$ and ryanodine receptor activation in vascular myocytes. *American Journal of Physiology: Cell Physiology*, 277(1), pp.C139–C151.

Bolton, T. B. (2006). Calcium events in smooth muscles and their interstitial cells; physiological roles of sparks. *The Journal of Physiology*, 570(Pt 1), pp.5–11.

Boularan, C., and Gales, C. (2015). Cardiac cAMP: production, hydrolysis, modulation and detection. *Frontiers in pharmacology*, 6, 203.

Brackenbury, W. J. (2012). Voltage-gated sodium channels and metastatic disease. *Channels*, 6(5), pp.352–361.

Brackett, N. L., Lynne, C. M., Ibrahim, E., Ohl, D. A., and Sønksen, J. (2010). Treatment of infertility in men with spinal cord injury. *Nature reviews. Urology*, 7(3), pp.162–172.

Bradley, E., Webb, T. I., Hollywood, M. A., Sergeant, G. P., McHale, N. G., and Thornbury, K. D. (2013). The cardiac sodium current Na(v)1.5 is functionally expressed in rabbit bronchial smooth muscle cells. *American journal of physiology. Cell physiology*, 305(4), pp.C427–C435.

Braun, A. P., Fedida, D., and Giles, W. R. (1992). Activation of alpha 1-adrenoceptors modulates the inwardly rectifying potassium currents of mammalian atrial myocytes. *Pflügers Archiv – European Journal of Physiology*, 421(5), pp.431–439.

Brown, D. A., and Adams, P. R. (1980). Muscarinic suppression of a novel voltage-sensitive K+ current in a vertebrate neurone. *Nature*, 283(5748), pp.673–676.

Brueggemann, L. I., Mackie, A. R., Martin, J. L., Cribbs, L. L., and Byron, K. L. (2011). Diclofenac distinguishes among homomeric and heteromeric potassium channels composed of *KCNQ*4 and *KCNQ*5 subunits. *Molecular pharmacology*, 79(1), pp.10–23.

Brueggemann, L. I., Haick, J. M., Cribbs, L. L., and Byron, K. L. (2014a). Differential activation of vascular smooth muscle Kv7.4, Kv7.5, and Kv7.4/7.5 channels by ML213 and ICA-069673. *Molecular Pharmacology*, 86(3), pp.330–341.

Brueggemann, L. I., Mackie, A. R., Cribbs, L. L., Freda, J., Tripathi, A., Majetschak, M., and Byron, K. L. (2014b). Differential protein kinase C-dependent modulation of Kv7.4 and Kv7.5 subunits of vascular Kv7 channels. *The Journal of biological chemistry*, 289(4), pp.2099–2111.

Brueggemann, L. I., Cribbs, L. L., Schwartz, J., Wang, M., Kouta, A., and Byron, K. L. (2018). Mechanisms of PKA-dependent potentiation of Kv7.5 channel activity in human airway smooth muscle cells. *International journal of molecular sciences*, 19(8), 2223.

Brueggemann, L. I., Cribbs, L. L., and Byron, K. L. (2020). Structural determinants of Kv7.5 potassium channels that confer changes in phosphatidylinositol 4,5-bisphosphate (PIP2) affinity and signaling sensitivities in smooth muscle cells. *Molecular pharmacology*, 97(3), pp.145–158.

Burns, L. L., Canaves, J. M., Pennypacker, J. K., Blumenthal, D. K., and Taylor, S. S. (2003). Isoform specific differences in binding of a dual-specificity A-kinase anchoring protein to type I and type II regulatory subunits of PKA. *Biochemistry*, 42(19), pp.5754–5763.

Burnstock, G. (2007). Purine and pyrimidine receptors. *Cellular and molecular life sciences*, 64(12), pp.1471–1483.

Campos de Carvalho, A. C., Roy, C., Moreno, A. P., Melman, A., Hertzberg, E. L., Christ, G. J., and Spray, D. C. (1993). Gap junctions formed of connexin43 are found between smooth muscle cells of human corpus cavernosum. *The Journal of urology*, 149(6), pp.1568–1575.

Caputo, A., Caci, E., Ferrera, L., Pedemonte, N., Barsanti, C., Sondo, E., Pfeffer, U., Ravazzolo, R., Zegarra-Moran, O., and Galietta, L. J. (2008). TMEM16A, a membrane protein associated with calcium-dependent chloride channel activity. Science, 322(5901), pp.590–594.

Carmeliet, E. (1992). Voltage- and time-dependent block of the delayed K+ current in cardiac myocytes by dofetilide. *The Journal of pharmacology and experimental therapeutics*, 262(2), pp.809–817.

Cartledge, J. J., Eardley, I., and Morrison, J. F. (2001). Advanced glycation end-products are responsible for the impairment of corpus cavernosal smooth muscle relaxation seen in diabetes. BJU International, 87(4), pp.402–407.

Casteel, D. E., Smith-Nguyen, E. V., Sankaran, B., Roh, S. H., Pilz, R. B., and Kim, C. (2010). A crystal structure of the cyclic GMP-dependent protein kinase Iβ dimerization/docking domain reveals molecular details of isoform-specific anchoring. *The Journal of biological chemistry*, 285(43), pp.32684–32688.

Catterall, W. A. (2000). Structure and regulation of voltage-gated Ca^{2+} channels. *Annual Review of Cell and Developmental Biology*, 16, pp.521–555.

Catterall, W. A., Goldin, A. L., and Waxman, S. G. (2005). International Union of Pharmacology. XLVII. Nomenclature and structure-function relationships of voltage-gated sodium channels. *Pharmacological reviews*, 57(4), pp.397–409.

Cavaretta, J. P., Sherer, K. R., Lee, K. Y., Kim, E. H., Issema, R. S., and Chung, H. J. (2014). Polarized axonal surface expression of neuronal *KCNQ* potassium channels is regulated by calmodulin interaction with the *KCNQ*2 subunit. *PLOS ONE*, 9(7), e103655.

Chadha, P. S., Zunke, F., Zhu, H. L., Davis, A. J., Jepps, T. A., Olesen, S. P., Cole, W. C., Moffatt, J. D., and Greenwood, I. A. (2012). Reduced *KCNQ*4-encoded voltage-dependent potassium channel activity underlies impaired β-adrenoceptor-mediated relaxation of renal arteries in hypertension. *Hypertension*, 59(4), pp.877–884.

Chadha, P. S., Jepps, T. A., Carr, G., Stott, J. B., Zhu, H. L., Cole, W. C., and Greenwood, I. A. (2014). Contribution of Kv7.4/Kv7.5 heteromers to intrinsic and calcitonin gene-related peptide-induced cerebral reactivity. *Arteriosclerosis, Thrombosis, and Vascular Biology*, 34(4), pp.887–893.

Chan, S. L., Lee, M. C., Tan, K. O., Yang, L. K., Lee, A. S., Flotow, H., Fu, N. Y., Butler, M. S., Soejarto, D. D., Buss, A. D., and Yu, V. C. (2003). Identification of chelerythrine as an inhibitor of Bcl-XL function. *Journal of Biological Chemistry*, 278(23), pp.20453–20456.

Chang, A., Abderemane-Ali, F., Hura, G. L., Rossen, N. D., Gate, R. E., and Minor, D. L. Jr. (2018). A calmodulin C-lobe Ca^{2+}-dependent switch governs Kv7 channel function. *Neuron*, 97(4), pp.836–852.e6.

Chatelier, A., Mercier, A., Tremblier, B., Thériault, O., Moubarak, M., Benamer, N., Corbi, P., Bois, P., Chahine, M., and Faivre, J. F. (2012). A distinct de novo expression of NaV1.5 sodium channels in human atrial fibroblasts differentiated into myofibroblasts. *The Journal of physiology*, 590(17), pp.4307–4319.

Chaytor, A. T., Bakker, L. M., Edwards, D. H., and Griffith, T. M. (2005). Connexin-mimetic peptides dissociate electrotonic EDHF-type signalling via myoendothelial and smooth muscle gap junctions in the rabbit iliac artery. British journal of pharmacology, 144(1), pp.108–114.

Chen, L., Staubli, S. E., Schneider, M. P., Kessels, A. G., Ivic, S., Bachmann, L. M., and Kessler, T. M. (2015). Phosphodiesterase 5 inhibitors for the treatment of erectile dysfunction: a trade-off network meta-analysis. *European urology*, 68(4), pp.674–680.

Chen, J., and Sanderson, M. J. (2017). Store-operated calcium entry is required for sustained contraction and Ca2+ oscillations of airway smooth muscle. Journal of physiology, 595(10), pp.3203–3218.

Chen, Y. F., Huang, G., Wang, Y. M., Cheng, M., Zhu, F. F., Zhong, J. N., and Gao, Y. D. (2019). Exchange protein directly activated by cAMP (Epac) protects against airway inflammation and airway remodeling in asthmatic mice. *Respiratory Research*, 20(1), 285.

Cheng, E. (2007). Real-life safety and efficacy of vardenafil in the treatment of erectile dysfunction—results from 30,010 U.S. patients. *The journal of sexual medicine*, 4(2), pp.432–439.

Cheng, X., Ji, Z., Tsalkova, T., and Mei, F. (2008). Epac and PKA: a tale of two intracellular cAMP receptors. *Acta biochimica et biophysica Sinica*, 40(7), pp.651–662.

Chien, E. K., Saunders, T., and Phillippe, M. (1996). The mechanisms underlying Bay K 8644-stimulated phasic myometrial contractions. *Journal of the Society for Gynecologic Investigation*, 3(3), pp.106–112

Chipperfield, A. R., and Harper, A. A. (2000). Chloride in smooth muscle. *Progress in biophysics and molecular biology*, 74(3–5), pp.175–221.

Cho, H., Nam, G.-B., Lee, S. H., Earm, Y. E., and Ho, W.-K. (2001). Phosphatidylinositol 4,5-bisphosphate acts as a signal molecule in the α1-adrenergic pathway via modulation of acetylcholine-activated K^+ channels in mouse atrial myocytes. *Journal of Biological Chemistry*, 276(1), pp.159–164.

Cho, H., Kim, Y. A., Yoon, J. Y., Lee, D., Kim, J. H., Lee, S. H., and Ho, W. K. (2005). Low mobility of phosphatidylinositol 4,5-bisphosphate underlies receptor specificity of Gq-mediated ion channel regulation in atrial myocytes. *Proceedings of the National Academy of Sciences of the United States of America*, 102, pp.15241–15246.

Chotani, M. A., Mitra, S., Eid, A. H., Han, S. A., and Flavahan, N. A. (2005). Distinct cAMP signaling pathways differentially regulate alpha2C-adrenoceptor expression: role in serum induction in human arteriolar smooth muscle cells. *American journal of physiology. Heart and circulatory physiology*, 288(1), pp.H69–H76.

Christ, G. J., Maayani, S., Valcic, M., and Melman, A. (1990). Pharmacological studies of human erectile tissue: characteristics of spontaneous contractions and alterations in alpha-adrenoceptor responsiveness with age and disease in isolated tissues. *British Journal of Pharmacology*, 101(2), pp.375–381.

Christ, G. J., Stone, B., and Melman, A. (1991). Age-dependent alterations in the efficacy of phenylephrine-induced contractions in vascular smooth muscle isolated from the corpus cavernosum of impotent men. *Canadian Journal of Physiology and Pharmacology*, 69(7), pp.909–913.

Christ, G. J., Schwartz, C. B., Stone, B. A., Parker, M., Janis, M., Gondre, M., Valcic, M., and Melman, A. (1992). Kinetic characteristics of alpha 1-adrenergic contractions in human corpus cavernosum smooth muscle. *American Journal of Physiology*, 263(1 Pt 2), pp.H15–H19.

Christ, G. J. (1995). The penis as a vascular organ. The importance of corporal smooth muscle tone in the control of erection. *Urologic Clinics of North America*, 22(4), pp.727–745.

Christ, G. J., Richards, S., and Winkler, A. (1997). Integrative erectile biology: the role of signal transduction and cell-to-cell communication in coordinating corporal smooth muscle tone and penile erection. *International journal of impotence research*, 9(2), pp.69–84.

Christ, G. J., Brink, P. R., Melman, A., and Spray, D. C. (1998). The Maxi-K (KCa1.1) potassium channel: A novel target for gene therapy of erectile dysfunction. International Journal of Impotence Research, 10, pp.125–132.

Christ, G. J., Day, N. S., Day, M., Zhao, W., Persson, K., Pandita, R. K., Andersson, K. E., and Melman, A. (2001). Corporal gene therapy using the hSlo cDNA in atherosclerotic cynomolgus monkeys with erectile dysfunction. Urology, 57, pp.190–197.

Chu, L. L., and Adaikan, P. G. (2008). Role of chloride channels in the regulation of corpus cavernosum tone: a potential therapeutic target for erectile dysfunction. *The journal of sexual medicine*, 5(4), pp.813–821.

Chung, S. D., Kuo, Y. C., Liu, S. P., Chang, H. C., Yu, H. J., and Hsieh, J. T. (2009). The role of chloride channels in rat corpus cavernosum: in vivo study. *The journal of sexual medicine*, 6(3), pp.708–716.

Cobine, C. A., Hannigan, K. I., McMahon, M., Ni Bhraonain, E. P., Baker, S. A., and Keef, K. D. (2020). Rhythmic calcium transients in smooth muscle cells of the mouse internal anal sphincter. Neurogastroenterology and motility, 32(3), p.e13746.

Collins, E. M., Walsh, M. P. & Morgan, K. G. (1992). Contraction of single vascular smooth muscle cells by phenylephrine at constant [Ca^{2+}]i. *American Journal of Physiology – Heart and Circulatory Physiology*, 262(3 Pt 2), pp.H754–H762.

Comerma-Steffensen, S., Kun, A., Hedegaard, E. R., Mogensen, S., Aalkjaer, C., Köhler, R., Mønster Christensen, B., and Simonsen, U. (2017). Down-regulation of KCa2.3 channels causes erectile dysfunction in mice. *Scientific reports*, 7(1), 3839.

Comerma-Steffensen, S., Prat-Duran, J., Mogensen, S., Fais, R., Pinilla, E., and Simonsen, U. (2022). Erectile dysfunction and altered contribution of KCa1.1 and KCa2.3 channels in the penile tissue of type-2 diabetic db/db mice. *The journal of sexual medicine*, 19(5), pp.697–710.

Conti, M., Mika, D., and Richter, W. (2014). Cyclic AMP compartments and signaling specificity: role of cyclic nucleotide phosphodiesterases. *Journal of General Physiology*, 143(1), pp.29–38.

Corona, G., Lee, D. M., Forti, G., O'Connor, D. B., Maggi, M., O'Neill, T. W., Pendleton, N., Bartfai, G., Boonen, S., Casanueva, F. F., Finn, J. D., Giwercman, A., Han, T. S., Huhtaniemi, I. T., Kula, K., Lean, M. E., Punab, M., Silman, A. J., Vanderschueren, D., Wu, F. C., … EMAS Study Group (2010). Age-related changes in general and sexual health in middle-aged and older men: results from the European Male Ageing Study (EMAS). *The journal of sexual medicine*, 7(4 Pt 1), pp.1362–1380.

Corona, G., Mondaini, N., Ungar, A., Razzoli, E., Rossi, A., and Fusco, F. (2011). Phosphodiesterase type 5 (PDE5) inhibitors in erectile dysfunction: the proper drug for the proper patient. *The journal of sexual medicine*, 8(12), pp.3418–3432.

Costa, W., Carrerete, F., Horta, W., and Sampaio, F. (2006). Comparative analysis of the penis corpora cavernosa in controls and patients with erectile dysfunction. *BJU International*, 97(3), pp.567–569.

Cotecchia, S. (2010). The α1-adrenergic receptors: diversity of signaling networks and regulation. *Journal of Receptor and Signal Transduction Research*, 30(6), pp.410–419.

Craven, M., Sergeant, G. P., Hollywood, M. A., McHale, N. G., and Thornbury, K. D. (2004). Modulation of spontaneous Ca2+-activated Cl– currents in the rabbit corpus cavernosum by the nitric oxide–cGMP pathway. *The Journal of physiology*, 556(2), pp.495–506.

Cruzblanca, H., Koh, D. S., and Hille, B. (1998). Bradykinin inhibits M current via phospholipase C and Ca^{2+} release from intracellular stores. *Proceedings of the National Academy of Sciences of the United States of America*, 95, pp.7151–7156.

Cuíñas, A., García-Morales, V., Viña, D., Gil-Longo, J., and Campos-Toimil, M. (2016). Activation of PKA and Epac proteins by cyclic AMP depletes intracellular calcium stores and reduces calcium availability for vasoconstriction. *Life sciences*, 155, pp.102–109.

Cullere, X., Shaw, S. K., Andersson, L., Hirahashi, J., Luscinskas, F. W., and Mayadas, T. N. (2005). Regulation of vascular endothelial barrier function by Epac, a cAMP-activated exchange factor for Rap GTPase. Blood, 105(5), pp.1950–1955.

Cunha, G. R., Sinclair, A., Ricke, W. A., Robboy, S. J., Cao, M., and Baskin, L. S. (2019). Reproductive tract biology: of mice and men. *Differentiation*, 110, pp.49–63.

Dalaklioglu, S., and Ozbey, G. (2014). Role of different types of potassium channels in the relaxation of corpus cavernosum induced by resveratrol. *Pharmacognosy magazine*, 10(37), pp.47–52.

Dao, K. K., Teigen, K., Kopperud, R., Hodneland, E., Schwede, F., Christensen, A. E., Martinez, A., and Døskeland, S. O. (2006). Epac1 and cAMP-dependent protein kinase holoenzyme have similar cAMP affinity, but their cAMP domains have distinct structural features and cyclic nucleotide recognition. *Journal of Biological Chemistry*, 281(30), pp.21500–21511.

Dausse, J. P., Leriche, A., and Yablonsky, F. (1998). Patterns of messenger RNA expression for alpha1-adrenoceptor subtypes in human corpus cavernosum. *The Journal of Urology*, 160(2), pp.597–600.

Davare, M. A., Horne, M. C., and Hell, J. W. (2000). Protein phosphatase 2A is associated with class C L-type calcium channels (CaV1.2). *Journal of Biological Chemistry*, 275(50), pp.39710–39717.

Davies, S. P., Reddy, H., Caivano, M., and Cohen, P. (2000). Specificity and mechanism of action of some commonly used protein kinase inhibitors. *The Biochemical journal*, 351(Pt 1), pp.95–105.

De Moudt, S., Van Hove, C., Behets, G. J., Vervaet, B. A., and Van den Bergh, A. (2021). Store-operated Ca2+ entry is not required for refilling of sarcoplasmic reticulum Ca2+ stores in mouse aortic smooth muscle. *Frontiers in physiology*, 12, 690525.

de Rooij, J., Zwartkruis, F. J., Verheijen, M. H., Cool, R. H., Nijman, S. M., Wittinghofer, A., and Bos, J. L. (1998). Epac is a Rap1 guanine-nucleotide-exchange factor directly activated by cyclic AMP. *Nature*, 396(6710), pp.474–477.

De Tejada, I. S. (2004). Therapeutic strategies for optimising PDE-5 inhibitor therapy in patients with erectile dysfunction considered difficult or challenging to treat. *International journal of impotence research*, 16(1), pp.S40–S42.

De Young, G. W., and Keizer, J. (1992). A single-pool inositol 1,4,5-trisphosphate-receptor-based model for agonist-stimulated oscillations in Ca^{2+} concentration. *Proceedings of the National Academy of Sciences of the United States of America*, 89(20), pp.9895–9899.

Dean, R., and Lue, T. (2005). Physiology of penile erection and pathophysiology of erectile dysfunction. *Urologic clinics of North America*, 32(4), pp.379–395.

DeFeo, T. T., and Morgan, K. G. (1985). Calcium–force relationships as detected with aequorin in two different vascular smooth muscles of the ferret. *The Journal of physiology*, 369(1), pp.269–282.

Delmas, P., and Brown, D. A. (2005). Pathways modulating neural *KCNQ*/M (Kv7) potassium channels. *Nature Reviews Neuroscience*, 6(11), pp.850–862.

Derler, I., Schindl, R., Fritsch, R., Heftberger, P., Riedl, M. C., Begg, M., House, D., and Romanin, C. (2013). The action of selective CRAC channel blockers is affected by the Orai pore geometry. *Cell calcium*, 53(2), pp.139–151.

Dessauer, C. W. (2002). Kinetic analysis of the action of P-site analogs. *Methods in enzymology*, 345, pp.112–126.

Díaz-Flores, L., Gutiérrez, R., Madrid, J. F., Varela, H., Valladares, F., Acosta, E., Martín-Vasallo, P., and Díaz-Flores, L., Jr. (2009). Pericytes: morphofunction, interactions and pathology in a quiescent and activated mesenchymal cell niche. *Histology and histopathology*, 24(7), pp.909–969.

Diederichs, W., Stief, C. G., Benard, F., Bosch, R., Lue, T. F., and Tanagho, E. A. (1991a). The sympathetic role as an antagonist of erection. *Urological research*, 19(2), pp.123–126.

Diederichs, W., Stief, C. G., Lue, T. F., and Tanagho, E. A. (1991b). Sympathetic inhibition of papaverine induced erection. *The Journal of urology*, 146(1), pp.195–198.

DiSanto, M. E., Wang, Z., Menon, C., Zheng, Y., Chacko, T., Hypolite, J., Broderick, G., Wein, A. J., and Chacko, S. (1998). Expression of myosin isoforms in smooth muscle cells in the corpus cavernosum penis. *American journal of physiology. Cell physiology*, 275(4), pp.C976–C987.

Docherty, J. R. (2010). Subtypes of functional alpha1-adrenoceptor. *Cellular and Molecular Life Sciences*, 67(3), pp.405–417.

Doe, C., Bentley, R., Behm, D. J., Lafferty, R., Stavenger, R., Bamford, M., Panchal, T., Grygielko, E., Wright, L. L., Smith, G. K., Chen, Z., Webb, C., Khandekar, S., Yi, T., Kirkpatrick, R., Dul, E., Jolivette, L., Marino, J. P., Willette, R., Lee, D., and Hu, E. (2007). Novel Rho kinase inhibitors with anti-inflammatory and vasodilatory activities. The Journal of Pharmacology and Experimental Therapeutics, 320(1), pp.89–98.

Doyle, C., Sergeant, G. P., Hollywood, M. A., McHale, N. G., and Thornbury, K. D. (2012). Effects of phenylephrine on spontaneous activity and L-type Ca2+ current in isolated corpus cavernosum myocytes. *The journal of sexual medicine*, 9(11), pp.2795–2805.

Doyle, C., Sergeant, G. P., Hollywood, M. A., McHale, N. G., and Thornbury, K. D. (2014). ATP evokes inward currents in corpus cavernosum myocytes. *The journal of sexual medicine*, 11(1), pp.64–74.

Drake, R., Gray, H., Mitchell, A., and Vogl, W. (2015). *Gray's anatomy for students* (4th ed.). Philadelphia, Pa.: Churchill Livingstone Elsevier, pp.281, 425–428, 516–518.

Drumm, B. T., Large, R. J., Hollywood, M. A., Thornbury, K. D., Baker, S. A., Harvey, B. J., McHale, N. G., and Sergeant, G. P. (2015). The role of Ca2+ influx in spontaneous Ca2+ wave propagation in interstitial cells of Cajal from the rabbit urethra. Journal of physiology, 593(15), pp.3333–3350.

Drumm, B. T., Rembetski, B. E., Baker, S. A., and Sanders, K. M. (2019). Tonic inhibition of murine proximal colon is due to nitrergic suppression of Ca2+ signaling in interstitial cells of Cajal. Scientific reports, 9(1), p.4402.

Drumm, B. T., Rembetski, B. E., Cobine, C. A., Baker, S. A., Sergeant, G. P., Hollywood, M. A., Thornbury, K. D., and Sanders, K. M. (2018). Ca2+ signalling in mouse urethral smooth muscle in situ: role of Ca2+ stores and Ca2+ influx mechanisms. *The Journal of physiology*, 596(8), pp.1433–1466.

Dubsky, M., Veleba, J., Sojakova, D., Marhefkova, N., Fejfarova, V., and Jude, E. B. (2023). Endothelial dysfunction in diabetes mellitus: new insights. *International journal of molecular sciences*, 24(13), 10705.

Dudem, S., Large, R. J., Kulkarni, S., McClafferty, H., Tikhonova, I. G., Sergeant, G. P., Thornbury, K. D., Shipston, M. J., Perrino, B. A., and Hollywood, M. A. (2020). LINGO1 is a regulatory subunit of large conductance, Ca2+-activated potassium channels. Proceedings of the National Academy of Sciences of the United States of America, 117(4), pp.2194–2200.

Dudem, S., Sergeant, G. P., Thornbury, K. D., and Hollywood, M. A. (2021). Calcium-activated K+ channels (KCa) and therapeutic implications. *Handbook of experimental pharmacology*, 267, pp.379–416.

Dudem, S., Boon, P. X., Mullins, N., McClafferty, H., Shipston, M. J., Wilkinson, R. D. A., Lobb, I., Sergeant, G. P., Thornbury, K. D., Tikhonova, I. G., and Hollywood, M. A. (2023). Oxidation modulates LINGO2-induced inactivation of large conductance, Ca2+-activated potassium channels. Journal of biological chemistry, 299(3), p.102975.

Duncan, C., Omran, G. J., Teh, J., Davis, N. F., Bolton, D. M., and Lawrentschuk, N. (2019). Erectile dysfunction: a global review of intracavernosal injectables. *World journal of urology*, 37(6), pp.1007–1014.

Dwivedi, R., Drumm, B. T., Griffin, C. S., Dudem, S., Bradley, E., Alkawadri, T., Martin, S. L., Sergeant, G. P., Hollywood, M. A., and Thornbury, K. D. (2023). Excitatory cholinergic responses in mouse primary bronchial smooth muscle require both Ca^{2+} entry via L-type Ca^{2+} channels and store-operated Ca^{2+} entry via Orai channels. *Cell Calcium*, 112, 102721.

Dzhura, I., Chepurny, O. G., Kelley, G. G., Leech, C. A., Roe, M. W., Dzhura, E., Afshari, P., Malik, S., Rindler, M. J., Xu, X., Lu, Y., Smrcka, A. V., and Holz, G. G. (2010). Epac2-dependent mobilization of intracellular Ca^{2+} by glucagon-like peptide-1 receptor agonist exendin-4 is disrupted in β-cells of phospholipase C-ε knockout mice. *The Journal of Physiology*, 588(Pt 24), pp.4871–4889.

Eid, A. H., Chotani, M. A., Mitra, S., Miller, T. J., and Flavahan, N. A. (2008). Cyclic AMP acts through Rap1 and JNK signaling to increase expression of cutaneous smooth muscle alpha2C-adrenoceptors. *American journal of physiology. Heart and circulatory physiology*, 295(1), pp.H266–H272.

Eid, A. H., El-Yazbi, A. F., Zouein, F., Arredouani, A., Ouhtit, A., Rahman, M. M., Zayed, H., Pintus, G., and Abou-Saleh, H. (2018). Inositol 1,4,5-trisphosphate receptors in hypertension. *Frontiers in Physiology*, 9, 1018.

el Karib, A. O., Sheng, J., Betz, A. L., and Malvin, R. L. (1993). The central effects of a nitric oxide synthase inhibitor (N omega-nitro-L-arginine) on blood pressure and plasma renin. *Clinical and experimental hypertension*, 15(5), pp.819–832.

Emrich, S. M., Yoast, R. E., Xin, P., Arige, V., Wagner, L. E., Hempel, N., Gill, D. L., Sneyd, J., Yule, D. I., and Trebak, M. (2021). Omnitemporal choreographies of all five STIM/Orai and IP3Rs underlie the complexity of mammalian Ca2+ signaling. Cell reports, 34(9), p.108760.

Ergün, M., and Akyüz, O. (2022). Is Li-ESWT effective in diabetic patients with severe erectile dysfunction? Asian Journal of Andrology, 24(5), pp.521–524.

Essler, M., Staddon, J. M., Weber, P. C., and Aepfelbacher, M. (2000). Cyclic AMP blocks bacterial lipopolysaccharide-induced myosin light chain phosphorylation in endothelial cells through inhibition of Rho/Rho kinase signaling. *Journal of immunology*, 164(12), pp.6543–6549.

Evellin, S., Nolte, J, Tysack, K., vom Dorp, F., Thiel, M., Weernink, P. A., Jakobs, K. H., Webb, E. J., Lomasney, J. W., and Schmidt, M. (2002). Stimulation of phospholipase C-epsilon by the M3 muscarinic acetylcholine receptor mediated by cyclic AMP and the GTPase Rap2B. *The Journal of biological chemistry*, 277(19), pp.16805–16813.

Fabiani, M. E., and Story, D. F. (1996). Inhibition of sympathetic noradrenergic transmission by guanabenz and in rat isolated mesenteric artery: involvement of neuronal potassium channels. Pharmacological research, 33(3), pp.171–180.

Falkenburger, B. H., Jensen, J. B., and Hille, B. (2010). Kinetics of PIP_2 metabolism and *KCNQ*2/3 channel regulation studied with a voltage-sensitive phosphatase in living cells. *The Journal of General Physiology*, 135(2), pp.99–114.

Fang, D., Tan, X. H., Song, W. P., Gu, Y. Y., Pan, J. C., Yang, X. Q., Song, W. D., Yuan, Y. M., Peng, J., Zhang, Z. C., Xin, Z. C., Li, X. S., and Guan, R. L. (2022). Single-cell RNA sequencing of human corpus cavernosum reveals cellular heterogeneity landscapes in erectile dysfunction. *Frontiers in endocrinology*, 13, 874915.

Fedida, D., Braun, A. P., and Giles, W. R. (1991). α_1-Adrenoceptors reduce background K^+ current in rabbit ventricular myocytes. *The Journal of Physiology*, 441, pp.673–684.

Fedida, D., and Shimoni, Y. (1990). α-Adrenergic modulation of the transient outward current in rabbit atrial myocytes. *The Journal of Physiology*, 423, pp.257–277.

Feldman, H. A., Goldstein, I., Hatzichristou, D. G., Krane, R. J., and McKinlay, J. B. (1994). Impotence and its medical and psychosocial correlates: results of the Massachusetts Male Aging Study. *The Journal of urology*, 151(1), pp.54–61.

Filippov, A. K., and Brown, D. A. (2013). A mechanism for nerve cell excitation by norepinephrine via α1-adrenoceptors: inhibition of potassium M-current. *Cellular and Molecular Neurobiology*, 33(1), pp.1–4.

Filippi, S., Amerini, S., Maggi, M., Natali, A., and Ledda, F. (1999). Studies on the mechanisms involved in the ATP-induced relaxation in human and rabbit corpus cavernosum. *The Journal of urology*, 161(1), pp.326–331.

Fischmeister, R., Castro, L. R., Abi-Gerges, A., Rochais, F., Jurevicius, J., Leroy, J., and Vandecasteele, G. (2006). Compartmentation of cyclic nucleotide signaling in the heart: the role of cyclic nucleotide phosphodiesterases. *Circulation research*, 99(8), pp.816–828.

Fong, Z., Griffin, C. S., Large, R. J., Hollywood, M. A., Thornbury, K. D., and Sergeant, G. P. (2021). Regulation of P2X1 receptors by modulators of the cAMP effectors PKA and EPAC. Proceedings of the National Academy of Sciences of the United States of America, 118(37), p.e2108094118.

Fonseca, V., Seftel, A., Denne, J., and Fredlund, P. (2004). Impact of diabetes mellitus on the severity of erectile dysfunction and response to treatment: analysis of data from tadalafil clinical trials. *Diabetologia*, 47(11), pp.1914–1923.

Förstermann, U., Mülsch, A., Böhme, E., and Busse, R. (1986). Stimulation of soluble guanylate cyclase by an acetylcholine-induced endothelium-derived factor from rabbit and canine arteries. *Circulation research*, 58(4), pp.531–538.

Foster, M. N., and Coetzee, W. A. (2016). KATP channels in the cardiovascular system. *Physiological reviews*, 96(1), pp.177–252.

Fovaeus, M., Andersson, K. E., and Hedlund, H. (1987). Effects of some calcium channel blockers on isolated human penile erectile tissues. *The Journal of Urology*, 138(5), pp.1267–1272.

Francis, S. H., Morris, G. Z., and Corbin, J. D. (2008). Molecular mechanisms that could contribute to prolonged effectiveness of PDE5 inhibitors to improve erectile function. *International journal of impotence research*, 20(4), pp.333–342.

Fransen, P., Van Hove, C. E., van Langen, J., Schrijvers, D. M., Martinet, W., De Meyer, G. R., and Bult, H. (2012). Contribution of transient and sustained calcium influx, and sensitization to depolarization-induced contractions of the intact mouse aorta. *BMC Physiology*, 12, 9.

Fransen, P., Van Hove, C. E., Leloup, A. J., Martinet, W., De Meyer, G. R., Lemmens, K., Bult, H., and Schrijvers, D. M. (2015). Dissecting out the complex Ca2+-mediated phenylephrine-induced contractions of mouse aortic segments. *PLOS ONE*, 10(3), e0121634.

Frey, U., Huang, Y. Y., and Kandel, E. R. (1993). Effects of cAMP simulate a late stage of LTP in hippocampal CA1 neurons. *Science*, 260(5114), pp.1661–1664.

Fritsch, R. M., Saur, D., Kurjak, M., Oesterle, D., Schlossmann, J., Geiselhöringer, A., Hofmann, F., and Allescher, H. D. (2004). InsP3R-associated cGMP kinase substrate (IRAG) is essential for nitric oxide-induced inhibition of calcium signaling in human colonic smooth muscle. Journal of biological chemistry, 279(13), pp.12551–12559.

Fu, W., Song, B., Li, W., Shen, W., Ji, H., Wang, Y., Zhen, J., Zhou, Z., and Yan, J. (2011). Ultrastructural features and possible functional role of kit-positive interstitial cells in the guinea pig corpus cavernosum. International journal of impotence research, 23(4), pp.173–179.

Fujita, T., Umemura, M., Yokoyama, U., Okumura, S, and Ishikawa, Y. (2017). The role of Epac in the heart. *Cellular and molecular life sciences*, 74(4), pp.591–606.

Gairhe, S., Bauer, N. N., Gebb, S. A., and McMurtry, I. F. (2011). Myoendothelial gap junctional signaling induces differentiation of pulmonary arterial smooth muscle cells. American journal of physiology. Lung cellular and molecular physiology, 301(4), pp.L527–L535.

Gamper, N., and Shapiro, M. S. (2003). Calmodulin mediates Ca^{2+}-dependent modulation of M-type K^+ channels. *The Journal of General Physiology*, 122(1), pp.17–31.

García-Morales, V., Cuíñas, A., Elíes, J., and Campos-Toimil, M. (2014). PKA and Epac activation mediates cAMP-induced vasorelaxation by increasing endothelial NO production. *Vascular pharmacology*, 60(3), pp.95–101.

García-Morales, V., Luaces-Regueira, M., and Campos-Toimil, M. (2017). The cAMP effectors PKA and Epac activate endothelial NO synthase through PI3K/Akt pathway in human endothelial cells. *Biochemical pharmacology*, 145, pp.94–101.

Garland, C. J., and Dora, K. A. (2017). EDH: endothelium-dependent hyperpolarization and microvascular signalling. *Acta Physiologica*, 219(1), pp.152–161.

Gekel, I., and Neher, E. (2008). Application of an Epac activator enhances neurotransmitter release at excitatory central synapses. Journal of neuroscience, 28(32), pp.7991–8002

Ghigo, A., and Mika, D. (2019). cAMP/PKA signaling compartmentalization in cardiomyocytes: lessons from FRET-based biosensors. *Journal of molecular and cellular cardiology*, 131, pp.112–121.

Gloerich, M., and Bos, J. L. (2010). Epac: defining a new mechanism for cAMP action. *Annual Review of Pharmacology and Toxicology*, 50, pp.355–375.

Goeckeler, Z. M., and Wysolmerski, R. B. (2005). Myosin phosphatase and cofilin mediate cAMP/cAMP-dependent protein kinase-induced decline in endothelial cell isometric tension and myosin II regulatory light chain phosphorylation. *The Journal of biological chemistry*, 280(38), pp.33083–33095.

Gold, M. G., Lygren, B., Dokurno, P., Hoshi, N., McConnachie, G., Taskén, K., Carlson, C. R., Scott, J. D., and Barford, D. (2006). Molecular basis of AKAP specificity for PKA regulatory subunits. *Molecular cell*, 24(3), pp.383–395.

Goldstein, A., and Padma-Nathan, H. (1990). The microarchitecture of the intracavernosal smooth muscle and the cavernosal fibrous skeleton. *The Journal of urology*, 144(5), pp.1144–1146.

Gordon, J. L. (1986). Extracellular ATP: effects, sources and fate. *The Biochemical journal*, 233(2), pp.309–319.

Greenwood, I. A., and Ohya, S. (2009). New tricks for old dogs: *KCNQ* expression and role in smooth muscle. *British journal of pharmacology*, 156(8), pp.1196–1203.

Greenwood, I. A., and Stott, J. B. (2020). The Gβ1 and Gβ3 subunits differentially regulate rat vascular Kv7 channels. *Frontiers in Physiology*, 10.

Grewal, S. S., Horgan, A. M., York, R. D., Withers, G. S., Banker, G. A., and Stork, P. J. (2000). Neuronal calcium activates a Rap1 and B-Raf signaling pathway via the cyclic adenosine monophosphate-dependent protein kinase. *The Journal of biological chemistry*, 275(5), pp.3722–3728.

Gu, C., and Cooper, D. M. F. (1999). Calmodulin-binding sites on adenylyl cyclase type VIII. *The Journal of biological chemistry*, 274(12), pp.8012–8021.

Gudi, T., Hong, G. K., Vaandrager, A. B., Lohmann, S. M., and Pilz, R. B. (1999). Nitric oxide and cGMP regulate gene expression in neuronal and glial cells by activating type II cGMP-dependent protein kinase. *FASEB journal*, 13(15), pp.2143–2152.

Guo, C., Jiang, J., Cheng, B., Xie, L., Lin, H., and Jiang, R. (2020). Low androgen status inhibits erectile function by up-regulating the expression of P2X receptors in rat corpus cavernosum. *Andrologia*, 52(7), e13627.

Gur, S., Kadowitz, P. J., Abdel-Mageed, A. B., Kendirci, M., Sikka, S. C., Burnstock, G., and Hellstrom, W. J. (2009). Management of erectile function by penile purinergic P2 receptors in the diabetic rat. *The Journal of urology*, 181(5), pp.2375–2382.

Gur, S., Kadowitz, P.J., Hellstrom, W.J.G. and Abdel-Mageed, A.B. (2020). Ivabradine, a hyperpolarization-activated cyclic nucleotide-gated channel blocker, attenuates human corpus cavernosum contraction in vitro via interference with calcium and potassium transfer. Journal of Sexual Medicine, 17(2), 247–256.

Gutman, G. A., Chandy, K. G., Grissmer, S., Lazdunski, M., McKinnon, D., Pardo, L. A., Robertson, G. A., Rudy, B., Sanguinetti, M. C., Stühmer, W., and Wang, X. (2005). International Union of Pharmacology. LIII. Nomenclature and molecular relationships of voltage-gated potassium channels. *Pharmacological reviews*, 57(4), pp.473–508.

Gwack, Y., Feske, S., Srikanth, S., Hogan, P. G., and Rao, A. (2007). Signalling to transcription: store-operated Ca2+ entry and NFAT activation in lymphocytes. Cell calcium, 42(2), pp.145–156.

Haick, J. M., Brueggemann, L. I., Cribbs, L. L., Denning, M. F., Schwartz, J., and Byron, K. L. (2017). PKC-dependent regulation of Kv7.5 channels by the bronchoconstrictor histamine in human airway smooth muscle cells. *American Journal of Physiology: Lung Cellular and Molecular Physiology*, 312(6), pp.L822–L834.

Hall, D. D., Davare, M. A., Shi, M., Allen, M. L., Weisenhaus, M., Nieves-Cintrón, M., McKnight, G. S., Hell, J. W., and Santana, L. F. (2006). Binding of protein phosphatase 2A to the L-type calcium channel CaV1.2. *Biochemistry*, 45(31), pp.9656–9663.

Hall, C. N., Reynell, C., Gesslein, B., Hamilton, N. B., Mishra, A., Sutherland, B. A., O'Farrell, F. M., Buchan, A. M., Lauritzen, M., and Attwell, D. (2014). Capillary pericytes regulate cerebral blood flow in health and disease. *Nature*, 508(7494), pp.55–60.

Halls, M. L., and Cooper, D. M. F. (2017). Adenylyl cyclase signalling complexes – pharmacological challenges and opportunities. *Pharmacology & therapeutics*, 172, pp.171–180.

Hannan, J. L., Blaser, M. C., Oldfield, L., Pang, J. J., Adams, S. M., Pang, S. C., and Adams, M. A. (2010). Morphological and functional evidence for the contribution of the pudendal artery in aging-induced erectile dysfunction. The Journal of Sexual Medicine, 7(10), pp.3373–3384.

Hannan, J. L., Cheung, G. L., Blaser, M. C., Pang, J. J., Pang, S. C., Webb, R. C., and Adams, M. A. (2012). Characterization of the vasculature supplying the genital tissues in female rats. The Journal of Sexual Medicine, 9(1), pp.136–147.

Hannigan, K. I., Griffin, C. S., Large, R. J., Sergeant, G. P., Hollywood, M. A., McHale, N. G., and Thornbury, K. D. (2017). The role of Ca2+-activated Cl– current in tone generation in the rabbit corpus cavernosum. *American journal of physiology. Cell physiology*, 313(5), pp.C475–C486.

Hannigan, K. I., Large, R. J., Bradley, E., Hollywood, M. A., Sergeant, G. P., McHale, N. G., and Thornbury, K. D. (2016). Effect of a novel BKCa opener on BKCa currents and contractility of the rabbit corpus cavernosum. *American journal of physiology. Cell physiology*, 310(4), pp.C284–C292.

Harmati, G., Papp, F., Szentandrássy, N., Bárándi, L., Ruzsnavszky, F., Horváth, B., Bányász, T., Magyar, J., Panyi, G., Krasznai, Z., and Nánási, P. P. (2011). Effects of the PKC inhibitors chelerythrine and bisindolylmaleimide I (GF 109203X) on delayed rectifier K^+ currents. *Naunyn-Schmiedeberg's Archives of Pharmacology*, 383(2), pp.141–148.

Hart, I. K., Maddison, P., Newsom-Davis, J., Vincent, A., and Mills, K. R. (2002). Phenotypic variants of autoimmune peripheral nerve hyperexcitability. *Brain*, 125(Pt 8), pp.1887–1895.

Hashimoto, D., Hirashima, T., Yamamura, H., Kataoka, T., Fujimoto, K., Hyuga, T., Yoshiki, A., Kimura, K., Kuroki, S., Tachibana, M., Suzuki, K., Yamamoto, N., Morioka, S., Sasaki, T., and Yamada, G. (2021). Dynamic erectile responses of a novel penile organ model utilizing TPEM. *Biology of reproduction*, 104(4), pp.875–886.

Hashitani, H., Fukuta, H., Dickens, E. J., and Suzuki, H. (2002). Cellular mechanisms of nitric oxide-induced relaxation of corporeal smooth muscle in the guinea-pig. *The Journal of Physiology*, 538(Pt 2), pp.573–581.

Hashitani, H., Yanai, Y., Shirasawa, N., Soji, T., Tomita, A., Kohri, K., and Suzuki, H. (2005). Interaction between spontaneous and neurally mediated regulation of smooth muscle tone in the rabbit corpus cavernosum. *The Journal of physiology*, 569(3), pp.723–735.

Hayase, M., Hashitani, H., Kohri, K., and Suzuki, H. (2009). Role of K+ channels in regulating spontaneous activity in detrusor smooth muscle in situ in the mouse bladder. *The Journal of urology*, 181(5), pp.2355–2365.

Hayashi, M., Kajioka, S., Itsumi, M., Takahashi, R., Shahab, N., Ishigami, T., Takeda, M., Masuda, N., Yamaguchi, A., and Naito, S. (2016). Actions of cAMP on calcium sensitization in human detrusor smooth muscle contraction. *BJU International*, 117(1), pp.179–191.

Hedlund, P., Aszodi, A., Pfeifer, A., Alm, P., Hofmann, F., Ahmad, M., Fassler, R., and Andersson, K. E. (2000). Erectile dysfunction in cyclic GMP-dependent kinase I-deficient mice. *Proceedings of the National Academy of Sciences of the United States of America*, 97(5), pp.2349–2354.

Hernandez, C. C., Falkenburger, B., and Shapiro, M. S. (2009). Affinity for phosphatidylinositol 4,5-bisphosphate determines muscarinic agonist sensitivity of Kv7 K^+ channels. *Journal of General Physiology*, 134(5), pp.437–448.

Hertting, G., Axelrod, J., and Patrick, R. W. (1962). Actions of bretylium and guanethidine on the uptake and release of [3H]-noradrenaline. British journal of pharmacology and chemotherapy, 18(1), pp.161–166.

Hewer, R. C., Sala-Newby, G. B., Wu, Y. J., Newby, A. C., and Bond, M. (2011). PKA and Epac synergistically inhibit smooth muscle cell proliferation. *Journal of molecular and cellular cardiology*, 50(1), pp.87–98.

Higashida, H., Hoshi, N., Zhang, J. S., Yokoyama, S., Hashii, M., Jin, D., Noda, M., and Robbins, J. (2005). Protein kinase C bound with A-kinase anchoring protein is involved in muscarinic receptor-activated modulation of M-type *KCNQ* potassium channels. *Neuroscience research*, 51(3), pp.231–234.

Higgins, A., Nash, M., and Lynch, A. M. (2010). Antidepressant-associated sexual dysfunction: impact, effects, and treatment. *Drug, healthcare and patient safety*, 2, pp.141–150.

Hill, M. A., Yang, Y., Ella, S. R., Davis, M. J., and Braun, A. P. (2010). Large conductance, Ca2+-activated K+ channels (BKCa) and arteriolar myogenic signaling. *FEBS letters*, 584(10), pp.2033–2042.

Hogan, P. G., Lewis, R. S., and Rao, A. (2010). Molecular basis of calcium signaling in lymphocytes: STIM and ORAI. *Annual review of immunology*, 28, pp.491–533.

Hollywood, M. A., Cotton, K. D., Thornbury, K. D., and McHale, N. G. (1997). Tetrodotoxin-sensitive sodium current in sheep lymphatic smooth muscle. *The Journal of physiology*, 503(Pt 1), pp.13–20.

Holm, A. N., Rich, A., Miller, S. M., Strege, P., Ou, Y., Gibbons, S. J., Sarr, M. G., Szurszewski, J. H., Rae, J. L., and Farrugia, G. (2002). Sodium current in human jejunal circular smooth muscle cells. *Gastroenterology*, 122(1), pp.178–187.

Hölscher, C., and Rose, S. P. (1992). An inhibitor of nitric oxide synthesis prevents memory formation in the chick. *Neuroscience letters*, 145(2), pp.165–167.

Höppner, C. K., Stief, C. G., Jonas, U., Mandrek, K., Noack, T., and Golenhofen, K. (1996). Electrical and chemical control of smooth muscle activity of rabbit corpus cavernosum in vitro. *Urology*, 48(3), pp.512–518.

Horie, K., Itoh, H., and Tsujimoto, G. (1995). Hamster α1B-adrenergic receptor directly activates Gs in transfected Chinese hamster ovary cells. *Molecular Pharmacology*, 48(3), pp.392–400.

Hoshi, N., Langeberg, L. K., and Scott, J. D. (2005). Distinct enzyme combinations in AKAP signalling complexes permit functional diversity. *Nature cell biology*, 7(11), pp.1066–1073.

Hoshi, N., Zhang, J. S., Omaki, M., Takeuchi, T., Yokoyama, S., Wanaverbecq, N., Langeberg, L. K., Yoneda, Y., Scott, J. D., Brown, D. A., and Higashida, H. (2003). AKAP150 signaling complex promotes suppression of the M-current by muscarinic agonists. *Nature neuroscience*, 6(6), pp.564–571.

Hoyland, K., Vasdev, N., and Adshead, J. (2013). The use of vacuum erection devices in erectile dysfunction after radical prostatectomy. *Reviews in urology*, 15(2), pp.67–71.

Hsu, G., Hsieh, C., Wen, H., Chen, Y., Chen, S., and Mok, M. (2003). Penile venous anatomy: an additional description and its clinical implication. *Journal of andrology*, 24(6), pp.921–927.

Huang, L. J., Durick, K., Weiner, J. A., Chun, J., and Taylor, S. S. (1997). Identification of a novel protein kinase A anchoring protein that binds both type I and type II regulatory subunits. *The Journal of biological chemistry*, 272(12), pp.8057–8064.

Humphries, E. S. A., Kamishima, T., Quayle, J. M., and Dart, C. (2017). Calcium/calmodulin-dependent kinase 2 mediates Epac-induced spontaneous transient outward currents in rat vascular smooth muscle. *The Journal of physiology*, 595(18), pp.6147–6164.

Iacono, F., Barra, S., and Lotti, T. (1995). Elastic fibre concentration in the tunica albuginea of corpora cavernosa and nocturnal tumescence monitoring. *International journal of impotence research*, 7(2), pp.63–70.

Iannotti, F. A., Panza, E., Barrese, V., Viggiano, D., Soldovieri, M. V., and Taglialatela, M. (2010). Expression, localization, and pharmacological role of Kv7 potassium channels in skeletal muscle proliferation, differentiation, and survival after myotoxic insults. *The Journal of pharmacology and experimental therapeutics*, 332(3), pp.811–820.

Ichishima, K., Yamamoto, S., Iwamoto, T., and Ehara, T. (2010). α-Adrenoceptor-mediated depletion of phosphatidylinositol 4,5-bisphosphate inhibits activation of volume-regulated anion channels in mouse ventricular myocytes. *British Journal of Pharmacology*, 161(1), pp.193–206.

Iino, M., Kasai, H., and Yamazawa, T. (1994). Visualization of neural control of intracellular Ca^{2+} concentration in single vascular smooth muscle cells *in situ*. *The EMBO Journal*, 13, pp.5026–5031.

Iino, S., Horiguchi, K., and Nojyo, Y. (2008). Interstitial cells of Cajal are innervated by nitrergic nerves and express nitric oxide-sensitive guanylate cyclase in the guinea-pig gastrointestinal tract. Neuroscience, 152(2), pp.437–448.

Iino, S., Horiguchi, K., Nojyo, Y., Ward, S. M., and Sanders, K. M. (2009). Interstitial cells of Cajal contain signalling molecules for transduction of nitrergic stimulation in guinea pig caecum. Neurogastroenterology and motility, 21(5), pp.542–e13.

Insuk, S. O., Chae, M. R., Choi, J. W., Yang, D. K., Sim, J. H., and Lee, S. W. (2003). Molecular basis and characteristics of KATP channel in human corporal smooth muscle cells. *International journal of impotence research*, 15(4), pp.258–266.

Ivanova, A. D., Filatova, T. S., Abramochkin, D. V., Atkinson, A., Dobrzynski, H., Kokaeva, Z. G., Merzlyak, E. M., Pustovit, K. B., and Kuzmin, V. S. (2021). Attenuation of inward rectifier potassium current contributes to the α_1-adrenergic receptor-induced proarrhythmicity in the caval vein myocardium. *Acta Physiologica*, 231, e13597.

Jackson, W. F. (2022). Endothelial Ion Channels and Cell-Cell Communication in the Microcirculation. *Frontiers in physiology*, *13*, 805149.

Jaggar, J. H., Wellman, G. C., Heppner, T. J., Porter, V. A., Perez, G. J., Gollasch, M., Kleppisch, T., Rubart, M., Stevenson, A. S., Lederer, W. J., Knot, H. J., Bonev, A. D., and Nelson, M. T. (1998). Ca2+ channels, ryanodine receptors and Ca2+-activated K+ channels: a functional unit for regulating arterial tone. *Acta physiologica Scandinavica*, 164(4), pp.577–587.

Jaggar, J. H., Porter, V. A., Lederer, W. J., and Nelson, M. T. (2000). Calcium sparks in smooth muscle. *American journal of physiology. Cell physiology*, 278(2), pp.C235–C246.

Jentsch, T. J. (2000). Neuronal *KCNQ* potassium channels: physiology and role in disease. *Nature reviews. Neuroscience*, 1(1), pp.21–30.

Jepps, T. A., Bentzen, B. H., Stott, J. B., Povstyan, O. V., Sivaloganathan, K., Dalby-Brown, W., and Greenwood, I. A. (2014). Vasorelaxant effects of novel Kv7.4 channel enhancers ML213 and NS15370. *British Journal of Pharmacology*, 171(19), pp.4413–4424.

Jepps, T. A., Carr, G., Lundegaard, P. R., Olesen, S. P., and Greenwood, I. A. (2015). Fundamental role for the KCNE4 ancillary subunit in Kv7.4 regulation of arterial tone. *The Journal of physiology*, 593(24), pp.5325–5340.

Jepps, T. A., Olesen, S. P., Greenwood, I. A., and Dalsgaard, T. (2016). Molecular and functional characterization of Kv7 channels in penile arteries and corpus cavernosum of healthy and metabolic syndrome rats. *British journal of pharmacology*, 173(9), pp.1478–1490.

Jepps, T. A. (2017). Unravelling the complexities of vascular smooth muscle ion channels: fine tuning of activity by ancillary subunits. *Pharmacology & therapeutics*, 178, pp.57–66.

Jeyaraj, S. C., Unger, N. T., Eid, A. H., Mitra, S., Paul El-Dahdah, N., Quilliam, L. A., Flavahan, N. A., and Chotani, M. A. (2012). Cyclic AMP-Rap1A signaling activates RhoA to induce α2C-adrenoceptor translocation to the cell surface of microvascular smooth muscle cells. *American journal of physiology. Cell physiology*, 303(5), pp.C499–C511.

Jezior, J. R., Brady, J. D., Rosenstein, D. I., McCammon, K. A., Miner, A. S., and Ratz, P. H. (2001). Dependency of detrusor contractions on calcium sensitization and calcium entry through LOE-908-sensitive channels. *British Journal of Pharmacology*, 134(1), pp.78–87.

Johnson, M. T., Xin, P., Benson, J. C., Pathak, T., Walter, V., Emrich, S. M., Yoast, R. E., Zhang, X., Cao, G., Panettieri, R. A., and Trebak, M. (2022). STIM1 is a core trigger of airway smooth muscle remodeling and hyperresponsiveness in asthma. Proceedings of the National Academy of Sciences of the United States of America, 119(1), p.e2114557118.

Jones, A. W., Bylund, D. B., and Forte, L. R. (1984). cAMP-dependent reduction in membrane fluxes during relaxation of arterial smooth muscle. *American Journal of Physiology*, 246(2 Pt 2), pp.H306–H311.

Joshi, S., Nelson, M. T., and Werner, M. E. (2012). Amplified NO/cGMP-mediated relaxation and ryanodine receptor-to-BKCa channel signalling in corpus cavernosum smooth muscle from phospholamban knockout mice. *British journal of pharmacology*, 165(2), pp.455–466.

Jung, J., Jo, H. W., Kwon, H., and Jeong, N. Y. (2014). Clinical neuroanatomy and neurotransmitter-mediated regulation of penile erection. *International Neurourology Journal*, 18(2), pp.58–62.

Juskiewenski, S., Vaysse, P., Moscovici, J., Hammoudi, S., and Bouissou, E. (1982). A study of the arterial blood supply to the penis. *Anatomia Clinica*, 4(2), pp.101–107.

Kang, G., Chepurny, O. G., and Holz, G. G. (2001). cAMP-regulated guanine nucleotide exchange factor II (Epac2) mediates Ca2+-induced Ca2+ release in INS-1 pancreatic beta-cells. Journal of physiology, 536(Pt 2), pp.375–385.

Kang, G., Chepurny, O. G., Malester, B., Rindler, M. J., Rehmann, H., Bos, J. L., Schwede, F., Coetzee, W. A., and Holz, G. G. (2006). cAMP sensor Epac as a determinant of ATP-sensitive potassium channel activity in human pancreatic beta cells and rat INS-1 cells. *The Journal of physiology*, 573(Pt 3), pp.595–609.

Karaki, H., Ozaki, H., Hori, M., Mitsui-Saito, M., Amano, K. I., Harada, K. I., Miyamoto, S., Nakazawa, H., Won, K. J., and Sato, K. (1997). Calcium movements, distribution, and functions in smooth muscle. *Pharmacological reviews*, 49(2), pp.157–230.

Karkanis, T., DeYoung, L., Brock, G. B., and Sims, S. M. (2003). Ca2+-activated Cl– channels in corpus cavernosum smooth muscle: a novel mechanism for control of penile erection. *Journal of applied physiology*, 94(1), pp.301–313.

Karna, K. K., Choi, B. R., Kim, C. Y., Kim, H. K., and Park, J. K. (2022). *Rubus occidentalis* and ellagic acid affect the contractility of penile corpus cavernosum smooth muscle through the nitric oxide–cyclic guanosine monophosphate and cyclic adenosine 3′,5′-monophosphate signaling pathway. *Journal of clinical medicine*, 11(10), 2947.

Kato, Y., Yokoyama, U., Yanai, C., Ishige, R., Kurotaki, D., Umemura, M., Fujita, T., Kubota, T., Okumura, S., Sata, M., Tamura, T., and Ishikawa, Y. (2015). Epac1 deficiency attenuated vascular smooth muscle cell migration and neointimal formation. *Arteriosclerosis, Thrombosis, and Vascular Biology*, 35(12), pp.2617–2625.

Kaupp, U. B., and Seifert, R. (2002). Cyclic nucleotide-gated ion channels. *Physiological reviews*, 82(3), pp.769–824.

Kawasaki, H., Springett, G. M., Mochizuki, N., Toki, S., Nakaya, M., Matsuda, M., Housman, D. E., and Graybiel, A. M. (1998). A family of cAMP-binding proteins that directly activate Rap1. *Science*, 282(5397), pp.2275–2279.

Khan, B. V., Harrison, D. G., Olbrych, M. T., Alexander, R. W., and Medford, R. M. (1996). Nitric oxide regulates vascular cell adhesion molecule 1 gene expression and redox-sensitive transcriptional events in human vascular endothelial cells. *Proceedings of the National Academy of Sciences of the United States of America*, 93(17), pp.9114–9119.

Kharkovets, T., Dedek, K., Maier, H, Schweizer, M., Khimich, D., Nouvian, R., Vardanyan, V., Leuwer, R., Moser, T., and Jentsch, T. J. (2006). Mice with altered *KCNQ*4 K+ channels implicate sensory outer hair cells in human progressive deafness. *The EMBO journal*, 25(3), pp.642–652.

Kim, S. C., and Oh, M. M. (1992). Norepinephrine involvement in response to intracorporeal injection of papaverine in psychogenic impotence. *The Journal of urology*, 147(6), pp.1530–1532.

Kim, N. N., Huang, Y., Moreland, R. B., Kwak, S. S., Goldstein, I., and Traish, A. (2000). Cross-regulation of intracellular cGMP and cAMP in cultured human corpus cavernosum smooth muscle cells. *Molecular cell biology research communications*, 4(1), pp.10–14.

Kim, H. R., Xu, J., Maeda, S., Duc, N. M., Ahn, D., Du, Y., and Chung, K. Y. (2020). Structural mechanism underlying primary and secondary coupling between GPCRs and the Gi/o family. *Nature Communications*, 11, p.3160.

Kimura, K., Ito, M., Amano, M., Chihara, K., Fukata, Y., Nakafuku, M., Yamamori, B., Feng, J., Nakano, T., Okawa, K., Iwamatsu, A., and Kaibuchi, K. (1996). Regulation of myosin phosphatase by Rho and Rho-associated kinase (Rho-kinase). *Science*, 273(5272), pp.245–248.

Kinderman, F. S., Kim, C., von Daake, S., Ma, Y., Pham, B. Q., Spraggon, G., Xuong, N. H., Jennings, P. A., and Taylor, S. S. (2006). A dynamic mechanism for AKAP binding to RII isoforms of cAMP-dependent protein kinase. *Molecular cell*, 24(3), pp.397–408.

Kirschner, L. S., Yin, Z., Jones, G. N., and Mahoney, E. (2009). Mouse models of altered protein kinase A signaling. *Endocrine-related cancer*, 16(3), pp.773–793.

Kloner, R. A., Mullin, S. H., Shook, T., Matthews, R., Mayeda, G., Burstein, S., Peled, H., Pollick, C., Choudhary, R., Rosen, R., and Padma-Nathan, H. (2003). Erectile dysfunction in the cardiac patient: how common and should we treat? The Journal of Urology, 170(2 Pt 2), pp.S46–S50.

Klotz, T., Bloch, W., Zimmermann, J., Ruth, P., Engelmann, U., and Addicks, K. (2000). Soluble guanylate cyclase and cGMP-dependent protein kinase I expression in the human corpus cavernosum. International journal of impotence research, 12(3), pp.157–164.

Komalavilas, P., and Lincoln, T. M. (1994). Phosphorylation of the inositol 1,4,5-trisphosphate receptor by cyclic GMP-dependent protein kinase. Journal of biological chemistry, 269(12), pp.8701–8707.

Kubisch, C., Schroeder, B. C., Friedrich, T., Lütjohann, B., El-Amraoui, A., Marlin, S., Petit, C., and Jentsch, T. J. (1999). *KCNQ*4, a novel potassium channel expressed in sensory outer hair cells, is mutated in dominant deafness. *Cell*, 96(3), pp.437–446.

Kuo, I. Y., Wölfle, S. E., and Hill, C. E. (2011). T-type calcium channels and vascular function: the new kid on the block? *The Journal of physiology*, 589(Pt 4), pp.783–795.

Kurokawa, J., Motoike, H. K., Rao, J., and Kass, R. S. (2004). Regulatory actions of the A-kinase anchoring protein Yotiao on a heart potassium channel downstream of PKA phosphorylation. *Proceedings of the National Academy of Sciences of the United States of America*, 101(46), pp.16374–16378.

Lakshmikanthan, S., Zieba, B. J., Ge, Z. D., Momotani, K., Zheng, X., Lund, H., Artamonov, M. V., Maas, J. E., Szabo, A., Zhang, D. X., Auchampach, J. A., Mattson, D. L., Somlyo, A. V., and Chrzanowska-Wodnicka, M. (2014). Rap1b in smooth muscle and endothelium is required for maintenance of vascular tone and normal blood pressure. *Arteriosclerosis, thrombosis, and vascular biology*, 34(7), pp.1486–1494.

Lampe, P. D., and Lau, A. F. (2004). The effects of connexin phosphorylation on gap junctional communication. International journal of biochemistry and cell biology, 36(7), pp.1171–1186.

Large, R. J., Kshatri, A., Webb, T. I., Roy, S., Akande, A., Bradley, E., Sergeant, G. P., Thornbury, K. D., McHale, N. G., and Hollywood, M. A. (2015). Effects of the novel BK (KCa1.1) channel opener GoSlo-SR-5-130 are dependent on the presence of BK β subunits. *British journal of pharmacology*, 172(10), pp.2544–2556.

Large, W. A., and Wang, Q. (1996). Characteristics and physiological role of the Ca2+-activated Cl− conductance in smooth muscle. *American journal of physiology. Cell physiology*, 271(2), pp.C435–C454.

Larsson, H. P. (2010). How is the heart rate regulated in the sinoatrial node? Another piece to the puzzle. *The Journal of general physiology*, 136(3), pp.237–241.

Lasker, G. F., Pankey, E. A., Allain, A. V., Murthy, S. N., Stasch, J. P., and Kadowitz, P. J. (2013). The selective Rho-kinase inhibitor azaindole-1 has long-lasting erectile activity in the rat. *Urology*, 81(2), pp.465.e7–465.e14.

Lavis, L. D., Chao, T. Y., and Raines, R. T. (2011). Synthesis and utility of fluorogenic acetoxymethyl ethers. *Chemical science*, 2(3), pp.521–530.

Lea, A. P., Bryson, H. M., and Balfour, J. A. (1996). Intracavernous alprostadil: A review of its pharmacodynamic and pharmacokinetic properties and therapeutic potential in erectile dysfunction. Drugs & Aging, 8(1), pp.56–74.

Leblanc, N., Ledoux, J., Saleh, S., Sanguinetti, A., Angermann, J., O'Driscoll, K., Britton, F., Perrino, B. A., and Greenwood, I. A. (2005). Regulation of calcium-activated

chloride channels in smooth muscle cells: a complex picture is emerging. *Canadian Journal of Physiology and Pharmacology*, 83(7), pp.541–556.

Lee, S. W., Wang, H. Z., and Christ, G. J. (1999). Characterization of ATP-sensitive potassium channels in human corporal smooth muscle cells. *International journal of impotence research*, 11(4), pp.179–188.

Lee, H. Y., Bardini, M., and Burnstock, G. (2000). P2X receptor immunoreactivity in the male genital organs of the rat. *Cell and tissue research*, 300(2), pp.321–330.

Lee, M. Y., Ha, S. E., Park, C., Park, P. J., Fuchs, R., Wei, L., Jorgensen, B. G., Redelman, D., Ward, S. M., Sanders, K. M., and Ro, S. (2017). Transcriptome of interstitial cells of Cajal reveals unique and selective gene signatures. PLoS one, 12, p.e0176031.

Lee, J. H., Chae, M. R., Kang, S. J., Sung, H. H., Han, D. H., So, I., Park, J. K., and Lee, S. W. (2020a). Characterization and functional roles of *KCNQ*-encoded voltage-gated potassium (Kv7) channels in human corpus cavernosum smooth muscle. *Pflügers Archiv – European journal of physiology*, 472(1), pp.89–102.

Lee, J. E., Park, C. H., Kang, H., Ko, J, Cho, S., Woo, J., Chae, M. R., Lee, S. W., Kim, S. J., Kim, J., and So, I. (2020b). The agonistic action of URO-K10 on Kv7.4 and 7.5 channels is attenuated by co-expression of KCNE4 ancillary subunit. *The Korean journal of physiology & pharmacology*, 24(6), pp.503–516.

Leonard, M. P., Nickel, C. J., and Morales, A. (1989). Hyperprolactinemia and impotence: why, when and how to investigate. *The Journal of urology*, 142(4), pp.992–994.

Lerche, C., Scherer, C. R., Seebohm, G., Derst, C., Wei, A. D., Busch, A. E., and Steinmeyer, K. (2000). Molecular cloning and functional expression of *KCNQ*5, a potassium channel subunit that may contribute to neuronal M-current diversity. *The Journal of biological chemistry*, 275(29), pp.22395–22400.

Lim, X. R., Bradley, E., Griffin, C. S., Hollywood, M. A., Sergeant, G. P., and Thornbury, K. D. (2022b). Fast voltage-dependent sodium (NaV) currents are functionally expressed in mouse corpus cavernosum smooth muscle cells. *British journal of pharmacology*, 179(5), pp.1082–1101.

Lim, X. R., Drumm, B. T., Sergeant, G. P., Hollywood, M. A., and Thornbury, K. D. (2022a). Ca2+-activated Cl– channels (TMEM16A) underlie spontaneous electrical activity in isolated mouse corpus cavernosum smooth muscle cells. *Physiological reports*, 10(22), e15504.

Lin, C. S. (2004). Tissue expression, distribution, and regulation of PDE5. *International journal of impotence research*, 16(Suppl 1), pp.S8–S10.

Lin, Q., Zhao, G., Fang, X., Peng, X., Tang, H., Wang, H., Jing, R., Liu, J., Lederer, W. J., Chen, J., and Ouyang, K. (2016). IP_3 receptors regulate vascular smooth muscle contractility and hypertension. *JCI Insight*, 1(17), e89402.

Lin, X., Long, H., Liu, J., Xiong, W., and Jiang, R. (2023). A low androgen state impairs erectile function by suppressing EPAC1 in rat penile corpus cavernosum. *Translational Andrology and Urology*, 12(10), pp.1528–1539.

Lindemann, J. P., Jones, L. R., Hathaway, D. R., Henry, B. G., and Watanabe, A. M. (1983). β-Adrenergic stimulation of phospholamban phosphorylation and Ca^{2+}-ATPase activity in guinea pig ventricles. The Journal of Biological Chemistry, 258(1), pp.464–471.

Lindman, J., Khammy, M. M., Lundegaard, P. R., Aalkjær, C., and Jepps, T. A. (2018). Microtubule regulation of Kv7 channels orchestrates cAMP-mediated vasorelaxations in rat arterial smooth muscle. *Hypertension*, 71(2), pp.336–345.

Liou, J., Kim, M. L., Heo, W. D., Jones, J. T., Myers, J. W., Ferrell, J. E., Jr, and Meyer, T. (2005). STIM is a Ca2+ sensor essential for Ca2+-store-depletion-triggered Ca2+ influx. *Current biology*, 15(13), pp.1235–1241.

Liu, X. B., Hill, P., and Haile, D. J. (2002). Role of the ferroportin iron-responsive element in iron and nitric oxide dependent gene regulation. *Blood cells, molecules & diseases*, 29(3), pp.315–326.

Lizza, E. F., and Rosen, R. C. (1999). Definition and classification of erectile dysfunction: report of the Nomenclature Committee of the International Society of Impotence Research. *International journal of impotence research*, 11(3), pp.141–143.

Lohse, M. J., Benovic, J. L., Codina, J., Caron, M. G., and Lefkowitz, R. J. (1990). β-Arrestin: a protein that regulates β-adrenergic receptor function. *Science*, 248(4962), pp.1547–1550.

Loussouarn, G., Park, K. H., Bellocq, C., Baró, I., Charpentier, F., and Escande, D. (2003). Phosphatidylinositol-4,5-bisphosphate, PIP2, controls *KCNQ*1/KCNE1 voltage-gated potassium channels: a functional homology between voltage-gated and inward rectifier K+ channels. *The EMBO journal*, 22(20), pp.5412–5421.

Luangkhot, R., Rutchik, S., Agarwal, V., Puglia, K., Bhargava, G., and Melman, A. (1992). Collagen alterations in the corpus cavernosum of men with sexual dysfunction. *The Journal of urology*, 148(2), pp.467–471.

Ludwig, A., Zong, X., Jeglitsch, M., Hofmann, F., and Biel, M. (1998). A family of hyperpolarization-activated mammalian cation channels. *Nature*, 393(6685), pp.587–591.

Lue, T. (2000). Erectile dysfunction. *The New England journal of medicine*, 342(24), pp.1802–1813.

Lue, T. F., Takamura, T., Schmidt, R. A., Palubinskas, A. J., and Tanagho, E. A. (1983). Hemodynamics of erection in the monkey. The Journal of Urology, 130(6), pp.1237–1241.

Lue, T. F., and Dahiya, R. (1997). Molecular biology of erectile function and dysfunction. *Molecular urology*, 1, pp.55–64.

Lugnier, C. (2006). Cyclic nucleotide phosphodiesterase (PDE) superfamily: a new target for the development of specific therapeutic agents. *Pharmacology & therapeutics*, 109(3), pp.366–398.

Maiorino, M. I., Bellastella, G., and Esposito, K. (2014). Diabetes and sexual dysfunction: current perspectives. Diabetes, Metabolic Syndrome and Obesity: Targets and Therapy, 7, pp.95–105.

Maljevic, S., Wuttke, T. V., Seebohm, G., and Lerche, H. (2010). KV7 channelopathies. *Pflügers Archiv – European journal of physiology*, 460(2), pp.277–288.

Malysz, J., Farrugia, G., Ou, Y., Szurszewski, J. H., Nehra, A., and Gibbons, S. J. (2002). The Kv2.2 alpha subunit contributes to delayed rectifier K+ currents in myocytes from rabbit corpus cavernosum. *Journal of andrology*, 23(6), pp.899–910.

Malysz, J., Gibbons, S. J., Miller, S. M., Gettman, M., Nehra, A., Szurszewski, J. H., and Farrugia, G. (2001). Potassium outward currents in freshly dissociated rabbit corpus cavernosum myocytes. *The Journal of urology*, 166(3), pp.1167–1177.

Mandala, V. S., and MacKinnon, R. (2023). The membrane electric field regulates the PIP2-binding site to gate the *KCNQ*1 channel. *Proceedings of the National Academy of Sciences of the United States of America*, 120(21), e2301985120.

Mani, B. K., Robakowski, C., Brueggemann, L. I., Cribbs, L. L., Tripathi, A., Majetschak, M., and Byron, K. L. (2016). Kv7.5 potassium channel subunits are the primary targets for PKA-dependent enhancement of vascular smooth muscle Kv7 currents. *Molecular pharmacology*, 89(3), pp.323–334.

Manoury, B., Tamuleviciute, A. & Tammaro, P. (2010). TMEM16A/anoctamin 1 protein mediates calcium-activated chloride currents in pulmonary arterial smooth muscle cells. *Journal of Physiology*, 588(Pt 13), pp.2305–2314.

Marrion, N. V. (1997). Control of M-current. *Annual review of physiology*, 59, pp.483–504.

Martin, G. M., Chen, P. C., Devaraneni, P., and Shyng, S. L. (2013). Pharmacological rescue of trafficking-impaired ATP-sensitive potassium channels. *Frontiers in physiology*, 4, 386.

Marx, S. O., Kurokawa, J., Reiken, S., Motoike, H., D'Armiento, J., Marks, A. R., and Kass, R. S. (2002). Requirement of a macromolecular signaling complex for beta adrenergic receptor modulation of the *KCNQ*1-KCNE1 potassium channel. *Science*, 295(5554), pp.496–499.

Mason, M. M., Pai, R. K., Masterson, J. M., Lokeshwar, S. D., Chu, K. Y., and Ramasamy, R. (2023). Low-intensity extracorporeal shockwave therapy for diabetic men with erectile dysfunction: A systematic scoping review. Andrology, 11, pp.270–281.

Masterson, L. R., Yu, T., Shi, L., Wang, Y., Gustavsson, M., Mueller, M. M., and Veglia, G. (2011). cAMP-dependent protein kinase A selects the excited state of the membrane substrate phospholamban. *Journal of molecular biology*, 412(2), pp.155–164.

Masuda, H., Yano, M., Sakai, Y., Kihara, K., Yamauchi, Y., and Azuma, H. (2004). Modulation of intrinsic cavernous tone and nitric oxide production by arginase in rabbit corpus cavernosum. Journal of urology, 171(1), pp.490–494.

Masumoto, A., Mohri, M., Shimokawa, H., Urakami, L., Usui, M., & Takeshita, A. (2002). Suppression of coronary artery spasm by the Rho-kinase inhibitor fasudil in patients with vasospastic angina. Circulation, 105(13), pp.1545–1547.

Matchkov, V. V., Larsen, P., Bouzinova, E. V., Rojek, A., Boedtkjer, D. M., Golubinskaya, V., Pedersen, F. S., Aalkjaer, C., and Nilsson, H. (2008). Bestrophin-3 (vitelliform macular dystrophy 2-like 3 protein) is essential for the cGMP-dependent calcium-activated chloride conductance in vascular smooth muscle cells. Circulation Research, 103(8), pp.864–872.

Matchkov, V. V., Aalkjaer, C., and Nilsson, H. (2004). A cyclic GMP-dependent calcium-activated chloride current in smooth-muscle cells from rat mesenteric resistance arteries. The Journal of General Physiology, 123(2), pp.121–134.

Matthews, R. M., Bradley, E., Hollywood, M. A., Lundy, F. T., McGarvey, L. P., Sergeant, G. P., and Thornbury, K. D. (2024). Modulation of fast sodium current in airway smooth muscle cells by exchange protein directly activated by cAMP. American journal of physiology. Cell physiology, 326(1), pp.C1–C9.

McCallum, L. A., Greenwood, I. A., and Tribe, R. M. (2009). Expression and function of Kv7 channels in murine myometrium throughout oestrous cycle. Pflügers Archiv – European Journal of Physiology, 457(5), pp.1111–1120.

McCloskey, C., Cagney, V., Large, R., Hollywood, M., Sergeant, G., McHale, N., and Thornbury, K. (2009). Voltage-dependent Ca2+ currents contribute to spontaneous Ca2+ waves in rabbit corpus cavernosum myocytes. *The journal of sexual medicine*, 6(11), pp.3019–3031.

McCrossan, Z. A., and Abbott, G. W. (2004). The MinK-related peptides. *Neuropharmacology*, 47(6), pp.787–821.

Melman, A., Bar-Chama, N., McCullough, A., Davies, K., Christ, G. J., Slotkin, J., and Rosen, R. (2006). The first human trial for gene transfer therapy for the treatment of erectile dysfunction: Intracavernosal transfer of hMaxi-K. Human Gene Therapy, 17, pp.1165–1176.

Mercer, M., Hollywood, M. A., Sergeant, G. P., and Thornbury, K. D. (2025). Kv7 channels modulate tension and calcium signaling in mouse corpus cavernosum. *American Journal of Physiology: Cell Physiology*, 328(3), pp.C729–C742.

Meredith, A. L., Thorneloe, K. S., Werner, M. E., Nelson, M. T., and Aldrich, R. W. (2004). Overactive bladder and incontinence in the absence of the BK large conductance Ca2+-activated K+ channel. Journal of biological chemistry, 279(35), pp.36746–36752.

Métrich, M., Lucas, A., Gastineau, M., Samuel, J. L., Heymes, C., Morel, E., and Lezoualc'h, F. (2008). Epac mediates beta-adrenergic receptor-induced cardiomyocyte hypertrophy. *Circulation research*, 102(8), pp.959–965.

Mignen, O., Thompson, J. L., and Shuttleworth, T. J. (2008). Both Orai1 and Orai3 are essential components of the arachidonate-regulated Ca2+-selective (ARC) channels. Journal of physiology, 586(1), pp.185–195.

Mills, T. M., Stopper, V. S., and Wiedmeier, V. T. (1994). Effects of castration and androgen replacement on the hemodynamics of penile erection in the rat. *Biology of reproduction*, 51(2), pp.234–238.

Mizusawa, H., Hedlund, P., Håkansson, A., Alm, P., and Andersson, K. E. (2001). Morphological and functional in vitro and in vivo characterization of the mouse corpus cavernosum. *British journal of pharmacology*, 132(6), pp.1333–1341.

Mogami, H., Zhang, H., Suzuki, Y., Urano, T., Saito, N., Kojima, I., and Petersen, O. H. (2003). Decoding of short-lived Ca2+ influx signals into long term substrate phosphorylation through activation of two distinct classes of protein kinase C. Journal of biological chemistry, 278(11), pp.9896–9904.

Mongillo, M., McSorley, T., Evellin, S., Sood, A., Lissandron, V., Terrin, A., Huston, E., Hannawacker, A., Lohse, M. J., Pozzan, T., Houslay, M. D., and Zaccolo, M. (2004). Fluorescence resonance energy transfer-based analysis of cAMP dynamics in live neonatal rat cardiac myocytes reveals distinct functions of compartmentalized phosphodiesterases. *Circulation research*, 95(1), pp.67–75.

Montague, D. K., Jarow, J. P., Broderick, G. A., Burnett, A. L., Bivalacqua, T. J., Champion, H. C., and Lue, T. F. (2005). Chapter 1: The management of erectile dysfunction: An AUA update. The Journal of Urology, 174(1), pp.230–239.

Moore, K. L., Dalley, A. F., and Agur, A. M. R. (2014). *Clinically oriented anatomy* (7th ed.). Philadelphia, PA: Lippincott Williams & Wilkins.

Moosmang, S., Schulla, V., Welling, A., Feil, R., Feil, S., Wegener, J. W., Hofmann, F., and Klugbauer, N. (2003). Dominant role of smooth muscle L-type calcium channel Cav1.2 for blood pressure regulation. *The EMBO Journal*, 22(22), pp.6027–6034.

Morales-Cano, D., Moreno, L., Barreira, B., Pandolfi, R., Chamorro, V., Jimenez, R., Villamor, E., Duarte, J., Perez-Vizcaino, F., and Cogolludo, A. (2015). Kv7 channels critically determine coronary artery reactivity: left–right differences and down-regulation by hyperglycaemia. *Cardiovascular Research*, 106(1), pp.98–108.

Moreland, R. B. (1998). Is there a role of hypoxemia in penile fibrosis: a viewpoint presented to the Society for the Study of Impotence. *International journal of impotence research*, 10(2), pp.113–120.

Moreno, A. P., Campos de Carvalho, A. C., Christ, G., Melman, A., and Spray, D. C. (1993). Gap junctions between human corpus cavernosum smooth muscle cells: gating properties and unitary conductance. *The American journal of physiology*, 264(1 Pt 1), pp.C80–C92.

Morgan, L. M., Martin, S. L., Mullins, N. D., Hollywood, M. A., Thornbury, K. D., and Sergeant, G. P. (2022). Modulation of carbachol-induced Ca2+ oscillations in airway smooth muscle cells by PGE2. *Cell calcium*, 103, 102547.

Morita, T., Wheeler, M. A., Miyagawa, I., Kondo, S., and Weiss, R. M. (1986). Effects of forskolin on contractility and cyclic AMP levels in rabbit detrusor muscle. *Tohoku Journal of Experimental Medicine*, 149(3), pp.283–285.

Movsesian, M. A., Nishikawa, M., and Adelstein, R. S. (1984). Phosphorylation of phospholamban by calcium-activated, phospholipid-dependent protein kinase: Stimulation of cardiac sarcoplasmic reticulum calcium uptake. The Journal of Biological Chemistry, 259(13), pp.8029–8032.

Mulhall, J. P., Secin, F. P., and Guillonneau, B. (2008). Artery sparing radical prostatectomy—myth or reality? *The Journal of urology*, 179(3), pp.827–831.

Mulligan, T., and Schmitt, B. (1993). Testosterone for erectile failure. *Journal of general internal medicine*, 8(9), pp.517–521.

Muneer, A., Kalsi, J., Nazareth, I., and Arya, M. (2014). Erectile dysfunction. *BMJ*, 348, g129.

Murthy, K. S., and Zhou, H. (2003). Selective phosphorylation of the IP3R-I in vivo by cGMP-dependent protein kinase in smooth muscle. American journal of physiology. Gastrointestinal and liver physiology, 284(2), pp.G221–G230.

Musicki, B., Bella, A. J., Bivalacqua, T. J., Davies, K. P., DiSanto, M. E., Gonzalez-Cadavid, N. F., Hannan, J. L., Kim, N. N., Podlasek, C. A., Wingard, C. J., and Burnett, A. L. (2015). Basic science evidence for the link between erectile dysfunction and cardiometabolic dysfunction. *The journal of sexual medicine*, 12(12), pp.2233–2255.

Navedo, M. F., Takeda, Y., Nieves-Cintrón, M., Molkentin, J. D., and Santana, L. F. (2010). Elevated Ca^{2+} sparklet activity during acute hyperglycaemia and diabetes in cerebral arterial smooth muscle. *American Journal of Physiology: Cell Physiology*, 298(2), pp.C211–C220.

Nebigil, C., and Malik, K. U. (1993). Alpha-adrenergic receptor subtypes involved in prostaglandin synthesis are coupled to Ca^{2+} channels through a pertussis toxin-sensitive guanine nucleotide-binding protein. *Journal of Pharmacology and Experimental Therapeutics*, 266(2), pp.1113–1124.

Nehra, A., Goldstein, I., Pabby, A., Nugent, M., Huang, Y. H., de las Morenas, A., Krane, R. J., Udelson, D., Saenz de Tejada, I., and Moreland, R. B. (1996). Mechanisms of venous leakage: a prospective clinicopathological correlation of corporeal function and structure. *The Journal of urology*, 156(4), pp.1320–1329.

Nelson, M. T., Patlak, J. B., Worley, J. F., and Standen, N. B. (1990). Calcium channels, potassium channels, and voltage dependence of arterial smooth muscle tone. *The American journal of physiology*, 259(1 Pt 1), pp.C3–C18.

Nelson, M. T., and Quayle, J. M. (1995). Physiological roles and properties of potassium channels in arterial smooth muscle. *American Journal of Physiology*, 268(4 Pt 1), pp.C799–C822.

Neshatian, L., Strege, P. R., Rhee, P. L., Kraichely, R. E., Mazzone, A., Bernard, C. E., Cima, R. R., Larson, D. W., Dozois, E. J., Kline, C. F., and Mohler, P. J. (2015). Ranolazine inhibits voltage-gated mechanosensitive sodium channels in human colon circular smooth muscle cells. *American journal of physiology. Gastrointestinal and liver physiology*, 309(6), pp.G506–G512.

Neves, S. R., Ram, P. T., and Iyengar, R. (2002). G protein pathways. *Science*, 296(5573), pp.1636–1639.

Ng, F. L., Davis, A. J., Jepps, T. A., Harhun, M. I., Yeung, S. Y. M., Wan, A., Reddy, M., Melville, D., Nardi, A., Khong, T. K., and Greenwood, I. A. (2011). Expression and function of the K+ channel *KCNQ* genes in human arteries. *British Journal of Pharmacology*, 162(1), pp.42–53.

Nguyen, H. M. T., Gabrielson, A. T., and Hellstrom, W. J. G. (2017). Erectile dysfunction in young men—A review of the prevalence and risk factors. Sexual Medicine Reviews, 5(4), pp.508–520.

O'Dell, T. J., Hawkins, R. D., Kandel, E. R., and Arancio, O. (1991). Tests of the roles of two diffusible substances in long-term potentiation: evidence for nitric oxide as a possible early retrograde messenger. *Proceedings of the National Academy of Sciences of the United States of America*, 88(24), pp.11285–11289.

Oelhafen, K., Shayota, B. J., Muhleman, M., Klaassen, Z., Tubbs, R. S., and Loukas, M. (2013). Benjamin Alcock (1801–?) and his canal. *Clinical anatomy*, 26(6), pp.662–666.

Oestreich, E. A., Wang, H., Malik, S., Kaproth-Joslin, K. A., Blaxall, B. C., Kelley, G. G., Dirksen, R. T., and Smrcka, A. V. (2007). Epac-mediated activation of phospholipase C-epsilon plays a critical role in beta-adrenergic receptor-dependent enhancement of Ca2+ mobilization in cardiac myocytes. *The Journal of biological chemistry*, 282(8), pp.5488–5495.

Ogden, D. (1994). *Microelectrode techniques: The Plymouth workshop handbook*. The Company of Biologists Ltd.

Okabe, K., Kitamura, K., and Kuriyama, H. (1988). The existence of a highly tetrodotoxin sensitive Na channel in freshly dispersed smooth muscle cells of the rabbit main pulmonary artery. *Pflügers Archiv*, 411(4), pp.423–428.

Oldenburger, A., Timens, W., Bos, S., Smit, M., Smrcka, A. V., Laurent, A. C., Cao, J., Hylkema, M., Meurs, H., Maarsingh, H., Lezoualc'h, F., and Schmidt, M. (2014). Epac1 and Epac2 are differentially involved in inflammatory and remodeling processes induced by cigarette smoke. *The FASEB Journal*, 28(11), pp.4617–4628.

Oldenburger, A., Roscioni, S. S., Jansen, E., Menzen, M. H., Halayko, A. J., Timens, W., Meurs, H., Maarsingh, H., and Schmidt, M. (2012). Anti-inflammatory role of the cAMP effectors Epac and PKA: implications in chronic obstructive pulmonary disease. *PLOS ONE*, 7(2), e31574.

Overend, C. L., Eisner, D. A., and O'Neill, S. C. (1997). The effect of on spontaneous Ca^{2+} release and sarcoplasmic reticulum calcium content in rat ventricular myocytes. *The Journal of Physiology*, 502(Pt 3), pp.471–479.

Pankey, E. A., Byun, R. J., Smith, W. B., 2nd, Bhartiya, M., Bueno, F. R., Badejo, A. M., Stasch, J. P., Murthy, S. N., Nossaman, B. D., and Kadowitz, P. J. (2012). The Rho kinase inhibitor azaindole-1 has long-acting vasodilator activity in the pulmonary vascular bed of the intact chest rat. *Canadian journal of physiology and pharmacology*, 90(7), pp.825–835.

Pantopoulos, K., and Hentze, M. W. (1995). Nitric oxide signaling to iron-regulatory protein: direct control of ferritin mRNA translation and transferrin receptor mRNA stability in transfected fibroblasts. *Proceedings of the National Academy of Sciences of the United States of America*, 92(5), pp.1267–1271.

Park, C. Y., Hoover, P. J., Mullins, F. M., Bachhawat, P., Covington, E. D., Raunser, S., Walz, T., Garcia, K. C., Dolmetsch, R. E., and Lewis, R. S. (2009). STIM1 clusters and activates CRAC channels via direct binding of a cytosolic domain to Orai1. *Cell*, 136(5), pp.876–890.

Parnell, E., Palmer, T. M., and Yarwood, S. J. (2015). The future of EPAC-targeted therapies: agonism versus antagonism. *Trends in Pharmacological Sciences*, 36(4), pp.203–214.

Penson, D. F., Ng, C., Cai, L., Rajfer, J., and González-Cadavid, N. F. (1996). Androgen and pituitary control of penile nitric oxide synthase and erectile function in the rat. *Biology of reproduction*, 55(3), pp.567–574.

Peppiatt, C. M., Howarth, C., Mobbs, P., and Attwell, D. (2006). Bidirectional control of CNS capillary diameter by pericytes. *Nature*, 443(7112), pp.700–704.

Pereira, L., Métrich, M., Fernández-Velasco, M., Lucas, A., Leroy, J., Perrier, R., Morel, E., Fischmeister, R., Richard, S., Bénitah, J. P., Lezoualc'h, F., and Gómez, A. M. (2007). The cAMP binding protein Epac modulates Ca^{2+} sparks by a Ca^{2+}/calmodulin kinase signalling pathway in rat cardiac myocytes. *The Journal of Physiology*, 583(Pt 2), pp.685–694.

Perez-Reyes, E. (2003). Molecular physiology of low-voltage-activated T-type calcium channels. *Physiological reviews*, 83(1), pp.117–161.

Perez, D. M. (2021). Current developments on the role of α1-adrenergic receptors in cognition, cardioprotection, and metabolism. *Frontiers in Cell and Developmental Biology*, 9, 652152.

Peterson, B. Z., DeMaria, C. D., Adelman, J. P., and Yue, D. T. (1999). Calmodulin is the Ca2+ sensor for Ca2+-dependent inactivation of L-type calcium channels. Neuron, 22(3), pp.549–558.

Phillips, T. R., Wright, D. K., Gradie, P. E., Johnston, L. A., and Pask, A. J. (2015). A comprehensive atlas of the adult mouse penis. *Sexual development*, 9(3), pp.162–172.

Pierce, K. L., Premont, R. T., and Lefkowitz, R. J. (2002). Seven-transmembrane receptors. *Nature reviews. Molecular cell biology*, 3(9), pp.639–650.

Pillay, Y., Nagiah, S., Phulukdaree, A., Krishnan, A., and Chuturgoon, A. A. (2020). Patulin suppresses α1-adrenergic receptor expression in HEK-293 cells. *Scientific Reports*, 10(1), 20115.

Porst, H. (1996). The rationale for prostaglandin E1 in erectile failure: a survey of worldwide experience. *The Journal of urology*, 155(3), pp.802–815.

Porter, V. A., Bonev, A. D., Knot, H. J., Heppner, T. J., Stevenson, A. S., Kleppisch, T., Lederer, W. J., and Nelson, M. T. (1998). Frequency modulation of Ca2+ sparks is involved in regulation of arterial diameter by cyclic nucleotides. *The American journal of physiology*, 274(5), pp.C1346–C1355.

Potier, M., Gonzalez, J. C., Motiani, R. K., Abdullaev, I. F., Bisaillon, J. M., Singer, H. A., and Trebak, M. (2009). Evidence for STIM1- and Orai1-dependent store-operated calcium influx through ICRAC in vascular smooth muscle cells: role in proliferation and migration. FASEB journal, 23(8), pp.2425–2437.

Povstyan, O. V., Barrese, V., Stott, J. B., and Greenwood, I. A. (2017). Synergistic interplay of Gβγ and phosphatidylinositol 4,5-bisphosphate dictates Kv7.4 channel activity. *Pflügers Archiv – European Journal of Physiology*, 469(2), pp.213–223.

Potet, F., Scott, J. D., Mohammad-Panah, R., Escande, D., and Baró, I. (2001). AKAP proteins anchor cAMP-dependent protein kinase to KvLQT1/IsK channel complex. *American journal of physiology. Heart and circulatory physiology*, 280(5), pp.H2038–H2045.

Prakriya, M., Feske, S., Gwack, Y., Srikanth, S., Rao, A., and Hogan, P. G. (2006). Orai1 is an essential pore subunit of the CRAC channel. Nature, 443(7108), pp.230–233.

Prakriya, M., and Lewis, R. S. (2015). Store-operated calcium channels. *Physiological Reviews*, 95(4), pp.1383–1436.

Preston, P., Wartosch, L., Günzel, D., Fromm, M., Kongsuphol, P., Ousingsawat, J., Kunzelmann, K., Barhanin, J., Warth, R., and Jentsch, T. J. (2010). Disruption of the K+ channel beta-subunit KCNE3 reveals an important role in intestinal and tracheal Cl– transport. *The Journal of biological chemistry*, 285(10), pp.7165–7175.

Pretorius, E., Siegelman, E., Ramchandani, P., and Banner, M. (2001). MR imaging of the penis. *RadioGraphics*, 21(Suppl 1), pp.S283–S298.

Prieto, D. (2008). Physiological regulation of penile arteries and veins. *International journal of impotence research*, 20(1), pp.17–29.

Priviero, F. B., Toque, H. A., Nunes, K. P., Priolli, D. G., Teixeira, C. E., and Webb, R. C. (2016). Impaired corpus cavernosum relaxation is accompanied by increased oxidative stress and up-regulation of the Rho-kinase pathway in diabetic (Db/Db) mice. PLoS one, 11(5), p.e0156030.

Purves, G. I., Kamishima, T., Davies, L. M., Quayle, J. M., and Dart, C. (2009). Exchange protein activated by cAMP (Epac) mediates cAMP-dependent but protein kinase A-insensitive modulation of vascular ATP-sensitive potassium channels. *The Journal of physiology*, 587(Pt 14), pp.3639–3650.

Qiu, X., Lin, G., Xin, Z., Ferretti, L., Zhang, H., Lue, T. F., and Lin, C. S. (2013). Effects of low-energy shockwave therapy on the erectile function and tissue of a diabetic rat model. The Journal of Sexual Medicine, 10(3), pp.738–746.

Raeymaekers, L., Hofmann, F., and Casteels, R. (1988). Cyclic GMP-dependent protein kinase phosphorylates phospholamban in isolated sarcoplasmic reticulum from cardiac and smooth muscle. The Biochemical Journal, 252(1), pp.269–273.

Rajfer, J., Aronson, W. J., Bush, P. A., Dorey, F. J., and Ignarro, L. J. (1992). Nitric oxide as a mediator of relaxation of the corpus cavernosum in response to nonadrenergic, noncholinergic neurotransmission. *The New England journal of medicine*, 326(2), pp.90–94.

Rajkumar, R. P., and Kumaran, A. K. (2015). Depression and anxiety in men with sexual dysfunction: A retrospective study. Comprehensive Psychiatry, 60, pp.114–118.

Rapoport, R. M., Draznin, M. B., and Murad, F. (1983). Endothelium-dependent relaxation in rat aorta may be mediated through cyclic GMP-dependent protein phosphorylation. *Nature*, 306(5939), pp.174–176.

Regadas, R. P., Moraes, M. E., Mesquita, F. J., Cerqueira, J. B., and Gonzaga-Silva, L. F. (2010). Experimental model of human corpus cavernosum smooth muscle relaxation. *International Brazilian Journal of Urology*, 36(4), pp.490–496.

Rehmann, H. (2013). Epac-inhibitors: facts and artefacts. *Scientific reports*, 3, 3032.

Rice, R. V., Moses, J. A., McManus, G. M., Brady, A. C., and Blasik, L. M. (1970). The organization of contractile filaments in a mammalian smooth muscle. *The Journal of cell biology*, 47(1), pp.183–196.

Robbins, J. (2001). *KCNQ* potassium channels: physiology, pathophysiology, and pharmacology. *Pharmacology & therapeutics*, 90(1), pp.1–19.

Roberts, O. L., Kamishima, T., Barrett-Jolley, R., Quayle, J. M., and Dart, C. (2013). Exchange protein activated by cAMP (Epac) induces vascular relaxation by activating Ca2+-sensitive K+ channels in rat mesenteric artery. *The Journal of physiology*, 591(20), pp.5107–5123.

Robichaux, W. G., 3rd, and Cheng, X. (2018). Intracellular cAMP sensor EPAC: physiology, pathophysiology, and therapeutics development. *Physiological reviews*, 98(2), pp.919–1053.

Roche, J. P., Westenbroek, R., Sorom, A. J., Hille, B., Mackie, K., and Shapiro, M. S. (2002). Antibodies and a cysteine-modifying reagent show correspondence of M current in neurons to *KCNQ*2 and *KCNQ*3 K+ channels. *British journal of pharmacology*, 137(8), pp.1173–1186.

Rodriguez, E., Jr., Weiss, D. A., Yang, J. H., Menshenina, J., Ferretti, M., Cunha, T. J., Barcellos, D., Chan, L. Y., Risbridger, G., Cunha, G. R., and Baskin, L. S. (2011). New insights on the morphology of adult mouse penis. *Biology of reproduction*, 85(6), pp.1216–1221.

Roos, J., DiGregorio, P. J., Yeromin, A. V., Ohlsen, K., Lioudyno, M., Zhang, S., Safrina, O., Kozak, J. A., Wagner, S. L., Cahalan, M. D., Veliçelebi, G., and Stauderman, K. A. (2005). STIM1, an essential and conserved component of store-operated Ca2+ channel function. *The Journal of cell biology*, 169(3), pp.435–445.

Roscioni, S. S., Maarsingh, H., Elzinga, C. R., Schuur, J., Menzen, M., Halayko, A. J., Meurs, H., and Schmidt, M. (2011). Epac as a novel effector of airway smooth muscle relaxation. *Journal of cellular and molecular medicine*, 15(7), pp.1551–1563.

Rubi, L., Kovar, M., Zebedin-Brandl, E., Koenig, X., Dominguez-Rodriguez, M., Todt, H., Kubista, H., Boehm, S., and Hilber, K. (2017). Modulation of the heart's electrical properties by the anticonvulsant drug retigabine. *Toxicology and applied pharmacology*, 329, pp.309–317.

Ryu, J. K., Jin, H. R., Yin, G. N., Kwon, M. H., Song, K. M., Choi, M. J., Park, J. M., Das, N. D., Kwon, K. D., Batbold, D., Lee, T., Gao, Z. L., Kim, K. W., Kim, W. J., and Suh, J. K. (2013). Erectile dysfunction precedes other systemic vascular diseases due to incompetent cavernous endothelial cell-cell junctions. *The Journal of urology*, 190(2), pp.779–789.

Sachyani, D., Dvir, M., Strulovich, R., Tria, G., Tobelaim, W., Peretz, A., Pongs, O., Svergun, D., Attali, B., and Hirsch, J. A. (2014). Structural basis of a Kv7.1 potassium channel gating module: studies of the intracellular C-terminal domain in complex with calmodulin. *Structure*, 22(11), pp.1582–1594.

Sadana, R., and Dessauer, C. W. (2009). Physiological roles for G protein-regulated adenylyl cyclase isoforms: insights from knockout and overexpression studies. *NeuroSignals*, 17(1), pp.5–22.

Saenz de Tejada, I., Kim, N., Lagan, I., Krane, R. J., and Goldstein, I. (1989a). Regulation of adrenergic activity in penile corpus cavernosum. *The Journal of Urology*, 142(4), pp.1117–1121.

Saenz de Tejada, I., Goldstein, I., Azadzoi, K., Krane, R. J., and Cohen, R. A. (1989b). Impaired neurogenic and endothelium-mediated relaxation of penile smooth muscle from diabetic men with impotence. The New England Journal of Medicine, 320(16), pp.1025–1030.

Sakuma, I., Togashi, H., Yoshioka, M., Saito, H., Yanagida, M., Tamura, M., Kobayashi, T., Yasuda, H., Gross, S. S., and Levi, R. (1992). NG-methyl-L-arginine, an inhibitor of L-arginine-derived nitric oxide synthesis, stimulates renal sympathetic nerve activity in vivo. A role for nitric oxide in the central regulation of sympathetic tone? *Circulation research*, 70(3), pp.607–611.

Saleh, S., Yeung, S. Y. M., Prestwich, S., Pucovský, V., and Greenwood, I. (2005). Electrophysiological and molecular identification of voltage-gated sodium channels in mouse vascular myocytes. *The Journal of physiology*, 568(1), pp.155–169.

Salzer, I., Gafar, H., Gindl, V., Mahlknecht, P., Drobny, H., and Boehm, S. (2014). Excitation of rat sympathetic neurons via M1 muscarinic receptors independently of Kv7 channels. *Pflügers Archiv – European Journal of Physiology*, 466(12), pp.2289–2303.

Sam, P., and LaGrange, C. A. (2018). Anatomy, abdomen and pelvis, penis. In *StatPearls*. StatPearls Publishing.

Sanguinetti, M. C., Curran, M. E., Zou, A., Shen, J., Spector, P. S., Atkinson, D. L., and Keating, M. T. (1996). Coassembly of K(V)LQT1 and minK (IsK) proteins to form cardiac I(Ks) potassium channel. *Nature*, 384(6604), pp.80–83.

Santana, L. F., Navedo, M. F., Amberg, G. C., Nieves-Cintrón, M., Votaw, V. S., and Ufret-Vincenty, C. A. (2008). Calcium sparklets in arterial smooth muscle. *Clinical and Experimental Pharmacology and Physiology*, 35(9), pp.1121–1126.

Santoro, B., Liu, D. T., Yao, H., Bartsch, D., Kandel, E. R., Siegelbaum, S. A., and Tibbs, G. R. (1998). Identification of a gene encoding a hyperpolarization-activated pacemaker channel of brain. *Cell*, 93(5), pp.717–729.

Sarma, G. N., Kinderman, F. S., Kim, C., von Daake, S., Chen, L., Wang, B. C., and Taylor, S. S. (2010). Structure of D-AKAP2:PKA RI complex: insights into AKAP specificity and selectivity. *Structure*, 18(2), pp.155–166.

Sathananthan, A. H., Adaikan, P. G., Lau, L. C., Ho, J., and Ratnam, S. S. (1991). Fine structure of the human corpus cavernosum. *Archives of andrology*, 26(2), pp.107–117.

Schlossmann, J., Ammendola, A., Ashman, K., Zong, X., Huber, A., Neubauer, G., Wang, G. X., Allescher, H. D., Korth, M., Wilm, M., Hofmann, F., and Ruth, P. (2000). Regulation of intracellular calcium by a signalling complex of IRAG, IP3 receptor and cGMP kinase Ibeta. Nature, 404(6774), pp.197–201.

Schmidt, M., Evellin, S., Weernink, P. A., von Dorp, F., Rehmann, H., Lomasney, J. W., and Jakobs, K. H. (2001). A new phospholipase-C-calcium signalling pathway mediated by cyclic AMP and a Rap GTPase. *Nature cell biology*, 3(11), pp.1020–1024.

Schroeder, B. C., Hechenberger, M., Weinreich, F., Kubisch, C., and Jentsch, T. J. (2000). *KCNQ*5, a novel potassium channel broadly expressed in brain, mediates M-type currents. *The Journal of biological chemistry*, 275(31), pp.24089–24095.

Schroeder, B. C., Kubisch, C., Stein, V., and Jentsch, T. J. (1998). Moderate loss of function of cyclic-AMP-modulated *KCNQ*2/*KCNQ*3 K+ channels causes epilepsy. *Nature*, 396(6712), pp.687–690.

Schroeder, B. C., Waldegger, S., Fehr, S., Bleich, M., Warth, R., Greger, R., and Jentsch, T. J. (2000). A constitutively open potassium channel formed by *KCNQ*1 and KCNE3. *Nature*, 403(6766), pp.196–199.

Schroeder, B. C., Cheng, T., Jan, Y. N., and Jan, L. Y. (2008). Expression cloning of TMEM16A as a calcium-activated chloride channel subunit. Cell, 134(6), pp.1019–1029.

Schuman, E. M., and Madison, D. V. (1991). A requirement for the intercellular messenger nitric oxide in long-term potentiation. *Science*, 254(5037), pp.1503–1506.

Seda, M., Pinto, F. M., Wray, S., Cintado, C. G., Noheda, P., Buschmann, H., and Candenas, L. (2007). Functional and molecular characterisation of voltage-gated sodium channels in uteri from nonpregnant rats. *Biology of reproduction*, 77(5), pp.855–863.

Seino, S., & Miki, T. (2003). Physiological and pathophysiological roles of ATP-sensitive K+ channels. *Progress in biophysics and molecular biology*, *81*(2), 133–176.

Sergeant, G. P., Craven, M., Hollywood, M. A., McHale, N. G., and Thornbury, K. D. (2009). Spontaneous Ca2+ waves in rabbit corpus cavernosum: modulation by nitric oxide and cGMP. *The journal of sexual medicine*, 6(4), pp.958–966.

Sevilleja-Ortiz, A., El Assar, M., García-Rojo, E., Romero-Otero, J., García-Gómez, B., Fernández, A., Medina-Polo, J., La Fuente, J. M., Rodríguez-Mañas, L., and Angulo, J. (2020). Enhanced contribution of Orai channels to contractility of human penile smooth muscle in erectile dysfunction. *The Journal of Sexual Medicine*, 17(5), pp.881–891.

Sevilleja-Ortiz, A., El Assar, M., García-Rojo, E., García-Gómez, B., Fernández, A., Sánchez-Ferrer, A., La Fuente, J. M., Romero-Otero, J., Rodríguez-Mañas, L., and Angulo, J. (2021). Ageing-induced hypercontractility is related to functional enhancement of STIM/Orai and upregulation of Orai3 in rat and human penile tissue. *Mechanisms of Ageing and Development*, 200, 111590.

Sevilleja-Ortiz, A., El Assar, M., García-Gómez, B., La Fuente, J. M., Alonso-Isa, M., Romero-Otero, J., Martínez-Salamanca, J. I., Fernández, A., Rodríguez-Mañas, L., and Angulo, J. (2022). STIM/Orai inhibition as a strategy for alleviating diabetic erectile dysfunction through modulation of rat and human penile tissue contractility and *in vivo* potentiation of erectile responses. *The Journal of Sexual Medicine*, 19(12), pp.1733–1749.

Shabsigh, R. (1997). The effects of testosterone on the cavernous tissue and erectile function. *World journal of urology*, 15(1), pp.21–26.

Shafik, A. (2007). Study of interstitial cells in the penis: human study. Journal of sexual medicine, 4(1), pp.66–71.

Shah, M., Mistry, M., Marsh, S. J., Brown, D. A., and Delmas, P. (2002). Molecular correlates of the M-current in cultured rat hippocampal neurons. *The Journal of physiology*, 544(Pt 1), pp.29–37.

Shalev, M., Staerman, F., Allain, H., Lobel, B., and Saiag, B. (1999). Stimulation of P2Y purinoceptors induces, via nitric oxide production, endothelium-dependent relaxation of human isolated corpus cavernosum. *The Journal of urology*, 161(3), pp.955–959.

Shendy, W. S., Elsoghier, O. M., El Semary, M. M., Ahmed, A. A., Ali, A. F., and Saber-Khalaf, M. (2021). Effect of low-intensity extracorporeal shock wave therapy on diabetic erectile dysfunction: Randomised control trial. Andrologia, 53(4), p.e13997.

Shibasaki, T., Sunaga, Y., Fujimoto, K., Kashima, Y., and Seino, S. (2004). Interaction of ATP sensor, cAMP sensor, Ca2+ sensor, and voltage-dependent Ca2+ channel in insulin granule exocytosis. Journal of biological chemistry, 279(9), pp.7956–7961.

Shinde, A. V., Motiani, R. K., Zhang, X., Abdullaev, I. F., Adam, A. P., González-Cobos, J. C., Zhang, W., Matrougui, K., Vincent, P. A., and Trebak, M. (2013). STIM1 controls endothelial barrier function independently of Orai1 and Ca2+ entry. Science signaling, 6(267), p.ra18.

Shinoura, H., Shibata, K., Hirasawa, A., Tanoue, A., Hashimoto, K., and Tsujimoto, G. (2002). Key amino acids for differential coupling of alpha1-adrenergic receptor subtypes to Gs. *Biochemical and Biophysical Research Communications*, 299(1), pp.142–147.

Silva, A. J., Kogan, J. H., Frankland, P. W., and Kida, S. (1998). CREB and memory. *Annual review of neuroscience*, 21, pp.127–148.

Silva, L. F., Nascimento, N. R., Fonteles, M. C., de Nucci, G., Moraes, M. E., Vasconcelos, P. R., and Moraes, M. O. (2005). Phentolamine relaxes human corpus cavernosum by a nonadrenergic mechanism activating ATP-sensitive K+ channel. *International journal of impotence research*, 17(1), pp.27–32.

Silva, F. H., Lanaro, C., Leiria, L. O., Rodrigues, R. L., Davel, A. P., Claudino, M. A., Toque, H. A., and Antunes, E. (2014). Oxidative stress associated with middle aging leads to sympathetic hyperactivity and downregulation of soluble guanylyl cyclase in corpus cavernosum. *American Journal of Physiology: Heart and Circulatory Physiology*, 307(10), pp.H1393–H1400.

Singh, I., Knezevic, N., Ahmmed, G. U., Kini, V., Malik, A. B., and Mehta, D. (2007). Galphaq-TRPC6-mediated Ca2+ entry induces RhoA activation and resultant endothelial cell shape change in response to thrombin. Journal of biological chemistry, 282(11), pp.7833–7843.

Smirnov, S. V., and Aaronson, P. I. (1992). Ca2+ currents in single myocytes from human mesenteric arteries: evidence for a physiological role of L-type channels. *The Journal of physiology*, 457, pp.455–475.

Simmons, M. N., and Jones, J. S. (2007). Male genital morphology and function: an evolutionary perspective. *The Journal of urology*, 177(5), pp.1625–1631.

Simonsen, U., Prieto, D., Sáenz de Tejada, I., and García-Sacristán, A. (1995). Involvement of nitric oxide in the non-adrenergic non-cholinergic neurotransmission of horse deep penile arteries: Role of charybdotoxin-sensitive K^+ channels. British Journal of Pharmacology, 116, pp.2582–2590.

Simonsen, U., Prieto, D., Hernández, M., Sáenz de Tejada, I., and García-Sacristán, A. (1997). Prejunctional α_2-adrenoceptors inhibit non-adrenergic non-cholinergic neurogenic relaxation in horse penile resistance arteries. The Journal of Urology, 157, pp.2356–2360.

Simonsen, U., Contreras, J., García-Sacristán, A., and Martínez, A. C. (2001). Effect of sildenafil on non-adrenergic non-cholinergic neurotransmission in bovine penile small arteries. European Journal of Pharmacology, 412, pp.155–169.

Smrcka, A. V. (2008). G protein βγ subunits: central mediators of G protein-coupled receptor signaling. *Cellular and Molecular Life Sciences*, 65(14), pp.2191–2214.

Soboloff, J., Spassova, M. A., Hewavitharana, T., He, L. P., Xu, W., Johnstone, L. S., Dziadek, M. A., and Gill, D. L. (2006). STIM2 is an inhibitor of STIM1-mediated store-operated Ca2+ entry. Current biology, 16(14), pp.1465–1470.

Soderling, S. H., and Beavo, J. A. (2000). Regulation of cAMP and cGMP signaling: new phosphodiesterases and new functions. *Current opinion in cell biology*, 12(2), pp.174–179.

Somlyo, A. P., and Somlyo, A. V. (2003). Ca^{2+} sensitivity of smooth muscle and nonmuscle myosin II: modulated by G proteins, kinases, and myosin phosphatase. *Physiological Reviews*, 83(4), pp.1325–1358.

Sopko, N. A., Hannan, J. L., and Bivalacqua, T. J. (2014). Understanding and targeting the Rho kinase pathway in erectile dysfunction. *Nature reviews urology*, 11(11), pp.622–632.

Sperelakis, N., Inoue, Y., and Ohya, Y. (1992). Fast Na+ channels in smooth muscle from pregnant rat uterus. *Canadian journal of physiology and pharmacology*, 70(4), pp.491–500.

Steers, W. D. (1990). Neural control of penile erection. *Seminars in urology*, 8(2), pp.66–79.

Stott, J. B., Barrese, V., Jepps, T. A., Leighton, E. V., and Greenwood, I. A. (2015a). Contribution of Kv7 channels to natriuretic peptide mediated vasodilation in normal and hypertensive rats. *Hypertension*, 65(3), pp.676–682.

Stott, J. B., Povstyan, O. V., Carr, G., Barrese, V., and Greenwood, I. A. (2015b). G-protein βγ subunits are positive regulators of Kv7.4 and native vascular Kv7 channel activity. *Proceedings of the National Academy of Sciences of the United States of America*, 112(20), pp.6497–6502.

Stott, J. B., Barrese, V., and Greenwood, I. A. (2016). Kv7 channel activation underpins EPAC-dependent relaxations of rat arteries. *Arteriosclerosis, thrombosis, and vascular biology*, 36(12), pp.2404–2411.

Suadicani, S. O., Urban–Maldonado, M., Tar, M. T., Melman, A., and Spray, D. C. (2009). Effects of ageing and streptozotocin–induced diabetes on connexin43 and P2 purinoceptor expression in the rat corpora cavernosa and urinary bladder. *BJU International*, 103(12), pp.1686–1692.

Subedi, K. P., Ong, H. L., Son, G. Y., Liu, X., and Ambudkar, I. S. (2018). STIM2 induces activated conformation of STIM1 to control Orai1 function in ER-PM junctions. Cell reports, 23(2), pp.522–534.

Suh, B. C., and Hille, B. (2002). Recovery from muscarinic modulation of M current channels requires phosphatidylinositol 4,5-bisphosphate synthesis. *Neuron*, 35(3), pp.507–520.

Sun, L., Xiao, L., Nie, J., Liu, F. Y., Ling, G. H., Zhu, X. J., Tang, W. B., Chen, W. C., Xia, Y., and Liu, H. (2011). Epac1-mediated, high glucose–induced renal proximal tubular cell hypertrophy. *Diabetes*, 60(2), pp.327–340.

Sun, H., Jiang, J., Gong, L., Li, X., Yang, Y., Luo, Y., Guo, Z., Lu, R., Li, H., Li, J., and Zhao, J. (2019). Voltage-gated sodium channel inhibitor reduces atherosclerosis by modulating monocyte/macrophage subsets and suppressing macrophage proliferation. *Biomedicine & pharmacotherapy*, 120, 109352.

Sun, J., and MacKinnon, R. (2020). Structural basis of human *KCNQ*1 modulation and gating. *Cell*, 180(2), pp.340–347.

Sung, H. H., Kam, S. C., Lee, J. H., Chae, M. R., Hong, C., Ko, M., Han, D. H., So, I., and Lee, S. W. (2012). Molecular and functional characterization of ORAI and STIM in human corporeal smooth muscle cells and effects of the transfer of their dominant-negative mutant genes into diabetic rats. *The Journal of Urology*, 187(5), pp.1903–1910.

Tada, M., Kirchberger, M. A., Repke, D. I., and Katz, A. M. (1974). The stimulation of calcium transport in cardiac sarcoplasmic reticulum by adenosine 3′:5′-monophosphate-dependent protein kinase. The Journal of Biological Chemistry, 249(19), pp.6174–6180.

Takahasi, R., Nishimura, J., Hirano, K., Naito, S., and Kanaide, H. (2003). Modulation of Ca2+ sensitivity regulates contractility of rabbit corpus cavernosum smooth muscle. *The Journal of urology*, 169(6), pp.2412–2416.

Takahashi, T., Kikuchi, T., Kidokoro, Y., and Shirakawa, H. (2013). Ca^{2+} influx-dependent refilling of intracellular Ca^{2+} stores determines the frequency of Ca^{2+} oscillations in fertilized mouse eggs. *Biochemical and Biophysical Research Communications*, 430(1), pp.60–65.

Tao, R., Chen, J., Wang, D., Li, Y., Xiang, J., Xiong, L., Ji, J., Wu, J., Zhou, S., Jia, C., Lv, J., Yang, J., and Tang, Q. (2022). The efficacy of Li-ESWT combined with VED in diabetic ED patients unresponsive to PDE5is: A single-center, randomized clinical trial. Frontiers in Endocrinology, 13, p.937958

Taylor, S. S., Ilouz, R., Zhang, P., and Kornev, A. P. (2012). Assembly of allosteric macromolecular switches: lessons from PKA. *Nature reviews. Molecular cell biology*, 13(10), pp.646–658.

Taylor, S. S., Zhang, P., Steichen, J. M., Keshwani, M. M., and Kornev, A. P. (2013). PKA: lessons learned after twenty years. *Biochimica et Biophysica Acta*, 1834(7), pp.1271–1290.

Telinius, N., Majgaard, J., Kim, S., Katballe, N., Pahle, E., Nielsen, J., Hjortdal, V., Aalkjaer, C., and Boedtkjer, D. B. (2015). Voltage-gated sodium channels contribute to action potentials and spontaneous contractility in isolated human lymphatic vessels. *The Journal of physiology*, 593(14), pp.3109–3122.

Teramoto, N., Zhu, H. L., Yotsu-Yamashita, M., Inai, T., and Cunnane, T. C. (2012). Resurgent-like currents in mouse vas deferens myocytes are mediated by NaV1.6 voltage-gated sodium channels. *Pflügers Archiv – European journal of physiology*, 464(5), pp.493–502.

Terrin, A., Di Benedetto, G., Pertegato, V., Cheung, Y. F., Baillie, G., Lynch, M. J., Elvassore, N., Prinz, A., Herberg, F. W., Houslay, M. D., and Zaccolo, M. (2006). PGE1 stimulation of HEK-293 cells generates multiple contiguous domains with different [cAMP]: role of compartmentalized phosphodiesterases. *The Journal of cell biology*, 175(3), pp.441–451.

Thompson, E., Eldstrom, J., and Fedida, D. (2021). Hormonal signaling actions on Kv7.1 (*KCNQ*1) channels. *Annual Review of Pharmacology and Toxicology*, 61, pp.381–400.

Thornbury, K. D., Hollywood, M. A., McHale, N. G., and Sergeant, G. P. (2011). Cajal beyond the gut: interstitial cells in the urinary system — towards general regulatory mechanisms of smooth muscle contractility? Acta gastro-enterologica Belgica, 74(4), pp.536–542.

Thornbury, K. D., Hollywood, M. A., and Sergeant, G. P. (2019). Ion channels and intracellular calcium signalling in corpus cavernosum. In *Smooth muscle spontaneous activity*, pp.171–194. Springer, Singapore.

Thul, P. J., Åkesson, L., Wiking, M., Mahdessian, D., Geladaki, A., Ait Blal, H., Alm, T., Asplund, A., Björk, L., Breckels, L. M., Bäckström, A., Danielsson, F., Fagerberg, L., Fall, J., Gatto, L., Gnann, C., Hober, S., Hjelmare, M., Johansson, F., Lee, S., … Lundberg, E. (2017). A subcellular map of the human proteome. *Science*, 356(6340), eaal3321.

Tobelaim, W. S., Dvir, M., Lebel, G., Cui, M., Buki, T., Peretz, A., Marom, M., Haitin, Y., Logothetis, D. E., Hirsch, J. A., and Attali, B. (2017). Competition of calcified calmodulin N-lobe and PIP_2 at an LQT mutation site in Kv7.1. *Proceedings of the National Academy of Sciences of the United States of America*, 114(5), pp.E869–E878.

Toda, N., Ayajiki, K., and Okamura, T. (2009). Control of systemic and pulmonary blood pressure by nitric oxide formed through neuronal nitric oxide synthase. *Journal of hypertension*, 27(10), pp.1929–1940.

Togashi, H., Sakuma, I., Yoshioka, M., Kobayashi, T., Yasuda, H., Kitabatake, A., Saito, H., Gross, S. S., and Levi, R. (1992). A central nervous system action of nitric oxide in blood pressure regulation. *The Journal of pharmacology and experimental therapeutics*, 262(1), pp.343–347.

Tohkin, M., Yagami, T., Katada, T., and Matsubara, T. (1990). Possible interaction of α1-adrenergic receptor with pertussis toxin-sensitive G proteins responsible for phospholipase C activation. *European Journal of Biochemistry*, 194(1), pp.81–87.

Topper, J. N., Cai, J., Falb, D., and Gimbrone, M. A. Jr. (1996). Identification of vascular endothelial genes differentially responsive to fluid mechanical stimuli. *Proceedings of the National Academy of Sciences of the United States of America*, 93(19), pp.10417–10422.

Traish, A. M., Gupta, S., Toselli, P., de Tejada, I. S., Goldstein, I., and Moreland, R. B. (1995). Identification of α1-adrenergic receptor subtypes in human corpus cavernosum tissue and cultured trabecular smooth muscle cells. *Receptor*, 5(3), pp.145–157.

Traish, A. M., Park, K., Dhir, V., Kim, N. N., Moreland, R. B., and Goldstein, I. (1999). Effects of castration and androgen replacement on erectile function in a rabbit model. *Endocrinology*, 140(4), pp.1861–1868.

Trebak, M. (2012). STIM/Orai signalling complexes in vascular smooth muscle. Journal of physiology, 590(17), pp.4201–4208.

Turner, L. A., Althof, S. E., Levine, S. B., Bodner, D. R., Kursh, E. D., and Resnick, M. I. (1991). External vacuum devices in the treatment of erectile dysfunction: a one-year study of sexual and psychosocial impact. *Journal of sex & marital therapy*, 17(2), pp.81–93.

Tzingounis, A. V., Heidenreich, M., Kharkovets, T., Spitzmaul, G., Jensen, H. S., Nicoll, R. A., and Jentsch, T. J. (2010). The *KCNQ*5 potassium channel mediates a component of the afterhyperpolarization current in mouse hippocampus. *Proceedings of the National Academy of Sciences of the United States of America*, 107(22), pp.10232–10237.

Uckert, S., Hedlund, P., Waldkirch, E., Sohn, M., Jonas, U., Andersson, K. E., and Stief, C. G. (2004). Interactions between cGMP- and cAMP-pathways are involved in the regulation of penile smooth muscle tone. *World journal of urology*, 22(4), pp.261–266.

Uckert, S., Kedia, G. T., Satzger, I., Geismar, U., Sohn, M., Kuczyk, M. A., Hedlund, P., and Waldkirch, E. S. (2010). C-kit-positive multipolar cells in human penile erectile tissue: expression of connexin 43 and relation to trabecular smooth muscle cells. Georgian medical news, 180, pp.13–19.

Udelson, D., L'Esperance, J., Morales, A. M., Patel, R., and Goldstein, I. (2000). The mechanics of corporal veno-occlusion in penile erection: A theory on the effect of stretch-associated luminal constrictability on outflow resistance. International Journal of Impotence Research, 12, pp.315–327.

Ushiyama, M., Kuramochi, T., and Katayama, S. (2006). Treatment with hypotensive agents affects impaired relaxation of penile corpus cavernosum in hypertensive rats. *Hypertension Research*, 29(7), pp.523–532.

Vaeth, M., Yang, J., Yamashita, M., et al. (2017). ORAI2 modulates store-operated calcium entry and T cell-mediated immunity. Nature communications, 8, p.14714.

Vallon, V., Grahammer, F., Richter, K., Bleich, M., Lang, F., Barhanin, J., Völkl, H., and Warth, R. (2001). Role of KCNE1-dependent K+ fluxes in mouse proximal tubule. *Journal of the American Society of Nephrology*, 12(10), pp.2003–2011.

Vardi, Y., Appel, B., Jacob, G., Massarwi, O., and Gruenwald, I. (2010). Can low-intensity extracorporeal shockwave therapy improve erectile function? A 6-month follow-up pilot study in patients with organic erectile dysfunction. European Urology, 58(2), pp.243–248.

Vardi, Y., Appel, B., Kilchevsky, A., and Gruenwald, I. (2012). Does low intensity extracorporeal shock wave therapy have a physiological effect on erectile function? Short-term results of a randomized, double-blind, sham controlled study. The Journal of Urology, 187(5), pp.1769–1775.

Vein, C. (2003). Anatomy and physiology of erection: pathophysiology of erectile dysfunction. *International journal of impotence research*, 15(Suppl 7), pp.S5–S8.

Venkateswarlu, K., Giraldi, A., Zhao, W., Wang, H. Z., Melman, A., Spektor, M., and Christ, G. J. (2002). Potassium channels and human corporeal smooth muscle cell tone: diabetes and relaxation of human corpus cavernosum smooth muscle by adenosine triphosphate sensitive potassium channel openers. *The Journal of urology*, 168(1), pp.355–361.

Vig, M., Peinelt, C., Beck, A., Koomoa, D. L., Rabah, D., Koblan-Huberson, M., Kraft, S., Turner, H., Fleig, A., Penner, R., and Kinet, J. P. (2006). CRACM1 is a plasma membrane protein essential for store-operated Ca2+ entry. Science, 312(5777), pp.1220–1223.

Vliem, M. J., Ponsioen, B., Schwede, F., Pannekoek, W. J., Riedl, J., Kooistra, M. R., Jalink, K., Genieser, H. G., Bos, J. L., and Rehmann, H. (2008). 8-pCPT-2′-O-Me-cAMP-AM: an improved Epac-selective cAMP analogue. *ChemBioChem*, 9(13), pp.2052–2054.

Walsh, K. B., and Kass, R. S. (1988). Regulation of a heart potassium channel by protein kinase A and C. *Science*, 242(4875), pp.67–69.

Walsh, K. B., and Kass, R. S. (1991). Distinct voltage-dependent regulation of a heart-delayed IK by protein kinases A and C. *The American journal of physiology*, 261(6 Pt 1), pp.C1081–C1090.

Walsh, M. P., Horowitz, A., Clément-Chomienne, O., Andrea, J. E., Allen, B. G., and Morgan, K. G. (1996). Protein kinase C mediation of Ca2+-independent contractions of vascular smooth muscle. *Biochemistry and cell biology*, 74(4), pp.485–502.

Wang, H. S., Pan, Z., Shi, W., Brown, B. S., Wymore, R. S., Cohen, I. S., Dixon, J. E., and McKinnon, D. (1998). *KCNQ*2 and *KCNQ*3 potassium channel subunits: molecular correlates of the M-channel. *Science*, 282(5395), pp.1890–1893.

Wang, J., Wang, Y., Du, X., and Zhang, H. (2022). Potassium channel conductance is involved in phenylephrine-induced spontaneous firing of serotonergic neurons. *Frontiers in Cellular Neuroscience*, 16, 891912.

Wang, J. Q., and Mao, L. (2019). The ERK pathway: molecular mechanisms and treatment of depression. *Molecular neurobiology*, 56(9), pp.6197–6205.

Wangemann, P. (2002). K+ cycling and the endocochlear potential. *Hearing research*, 165(1–2), pp.1–9.

Warth, R., and Barhanin, J. (2002). The multifaceted phenotype of the knockout mouse for the KCNE1 potassium channel gene. *American journal of physiology. Regulatory, integrative and comparative physiology*, 282(3), pp.R639–R648.

Watkin, N., and Patel, P. (2020). The diagnosis and management of acquired urethral stricture disease. *Surgery (Oxford)*, 38(4), pp.212–223.

Wehbe, N., Slika, H., Mesmar, J., Nasser, S. A., Pintus, G., Baydoun, S., Badran, A., Kobeissy, F., Eid, A. H., and Baydoun, E. (2020). The role of Epac in cancer progression. *International Journal of Molecular Sciences*, 21(18), 6489.

Weisskopf, M. G., Castillo, P. E., Zalutsky, R. A., and Nicoll, R. A. (1994). Mediation of hippocampal mossy fiber long-term potentiation by cyclic AMP. *Science*, 265(5180), pp.1878–1882.

Welch, E. J., Jones, B. W., and Scott, J. D. (2010). Networking with AKAPs: context-dependent regulation of anchored enzymes. *Molecular interventions*, 10(2), pp.86–97.

Wellman, G. C., Santana, L. F., Bonev, A. D., and Nelson, M. T. (2001). Role of phospholamban in the modulation of arterial Ca2+ sparks and Ca2+-activated K+ channels by cAMP. *American journal of physiology. Cell physiology*, 281(3), pp.C1029–C1037.

Werner, M. E., Zvara, P., Meredith, A. L., Aldrich, R. W., and Nelson, M. T. (2005). Erectile dysfunction in mice lacking the large-conductance calcium-activated potassium (BK) channel. *The Journal of physiology*, 567(2), pp.545–556.

Werner, M. E., Meredith, A. L., Aldrich, R. W., and Nelson, M. T. (2008). Hypercontractility and impaired sildenafil relaxations in the BKCa channel deletion model of erectile dysfunction. American journal of physiology. Regulatory, integrative and comparative physiology, 295(1), pp.R181–R188.

Wessells, H., King, S. H., Schmelz, M., Nagle, R. B., and Heimark, R. L. (2004). Immunohistochemical comparison of vascular and sinusoidal adherens junctions in cavernosal endothelium. *Urology*, 63(1), pp.201–206.

Wickenden, A. D., Zou, A., Wagoner, P. K., and Jegla, T. (2001). Characterization of *KCNQ*5/Q3 potassium channels expressed in mammalian cells. *British journal of pharmacology*, 132(2), pp.381–384.

Williams, B. A., and Sims, S. M. (2007). Calcium sparks activate calcium-dependent Cl− current in rat corpus cavernosum smooth muscle cells. *American journal of physiology. Cell physiology*, 293(4), pp.C1239–C1251.

Wingard, C. J., Husain, S., Williams, J., and James, S. (2003). RhoA–Rho kinase mediates synergistic ET-1 and phenylephrine contraction of rat corpus cavernosum. *American Journal of Physiology: Regulatory, Integrative and Comparative Physiology*, 285(5), pp.R1145–R1152.

Wray, S., Prendergast, C., and Arrowsmith, S. (2021). Calcium-activated chloride channels in myometrial and vascular smooth muscle. *Frontiers in Physiology*, 12, 751008.

Wu, H. Y., Broderick, G. A., Suh, J. K., Hypolite, J. A., and Levin, R. M. (1993). Effects of purines on rabbit corpus cavernosum contractile activity. *International journal of impotence research*, 5(3), pp.161–167.

Wuttke, T. V., Jurkat-Rott, K., Paulus, W., Garncarek, M., Lehmann-Horn, F., and Lerche, H. (2007). Peripheral nerve hyperexcitability due to dominant-negative *KCNQ*2 mutations. *Neurology*, 69(22), pp.2045–2053.

Xu, Q., Chang, A., Tolia, A., and Minor, D. L. Jr. (2013). Structure of a Ca^{2+}/CaM:Kv7.4 (*KCNQ*4) B-helix complex provides insight into M current modulation. *Journal of Molecular Biology*, 425(2), pp.378–394.

Yamamoto, S., Seta, K., Morisco, C., Vatner, S. F., and Sadoshima, J. (2001). Chelerythrine rapidly induces apoptosis through generation of reactive oxygen species in cardiac myocytes. *Journal of Molecular and Cellular Cardiology*, 33(10), pp.1829–1848.

Yart, L., Frieden, M., König, S., Cohen, M., and Martinez de Tejada, B. (2022). Dual effect of nifedipine on pregnant human myometrium contractility: implication of TRPC1. *Journal of Cellular Physiology*, 237(3), pp.1980–1991.

Yazawa, K., and Kameyama, M. (1990). Mechanism of receptor-mediated modulation of the delayed outward potassium current in guinea-pig ventricular myocytes. *The Journal of physiology*, 421, pp.135–150.

Verkhratsky, A. (2005). Physiology and pathophysiology of the calcium store in the endoplasmic reticulum of neurons. *Physiological Reviews*, 85(1), pp.201–279.

Yeung, S., Schwake, M., Pucovský, V., and Greenwood, I. A. (2008). Bimodal effects of the Kv7 channel activator retigabine on vascular K^+ currents. *British Journal of Pharmacology*, 155(1), pp.62–72

Yin, G. N., Das, N. D., Choi, M. J., Song, K. M., Kwon, M. H., Ock, J., Limanjaya, A., Ghatak, K., Kim, W. J., Hyun, J. S., Koh, G. Y., Ryu, J. K., and Suh, J. K. (2015). The pericyte as a cellular regulator of penile erection and a novel therapeutic target for erectile dysfunction. *Scientific reports*, 5, 10891.

Yokoyama, U., Minamisawa, S., Quan, H., Akaike, T., Jin, M., Otsu, K., Ulucan, C., Wang, X., Baljinnyam, E., Takaoka, M., Sata, M., and Ishikawa, Y. (2008). Epac1 is upregulated during neointima formation and promotes vascular smooth muscle cell migration. *American Journal of Physiology: Heart and Circulatory Physiology*, 295(4), pp.H1547–H1555.

Yuan, J. P., Zeng, W., Dorwart, M. R., Choi, Y. J., Worley, P. F., and Muallem, S. (2009). SOAR and the polybasic STIM1 domains gate and regulate Orai channels. *Nature cell biology*, 11(3), pp.337–343.

Yus-Najera, E., Santana-Castro, I., and Villarroel, A. (2002). Identification of a noncontinuous calmodulin-binding site in *KCNQ* potassium channels. *Journal of Biological Chemistry*, 277(32), pp.28545–28553.

Zavaritskaya, O., Dudem, S., Ma, D., Rabab, K. E., Albrecht, S., Tsvetkov, D., Kassmann, M., Thornbury, K., Mladenov, M., Kammermeier, C., Sergeant, G., Mullins, N., Wouappi, O., Wurm, H., Kannt, A., Gollasch, M., Hollywood, M. A., and Schubert, R. (2020). Vasodilation of rat skeletal muscle arteries by the novel BK channel opener GoSlo is mediated by the simultaneous activation of BK and Kv7 channels. *British Journal of Pharmacology*, 177(5), pp.1164–1186.

Zawieja, S. D., Pea, G. A., Broyhill, S. E., Patro, A., Bromert, K. H., Li, M., Norton, C. E., Castorena-Gonzalez, J. A., Hancock, E. J., Bertram, C. D., and Davis, M. J. (2023). IP_3R1 underlies diastolic ANO1 activation and pressure-dependent chronotropy in lymphatic collecting vessels. *The Journal of General Physiology*, 155(12), e202313358

Zaydman, M. A., Silva, J. R., Delaloye, K., *et al.* (2013). Kv7.1 ion channels require a lipid to couple voltage sensing to pore opening. *Proceedings of the National Academy of Sciences of the United States of America*, 110(32), pp.13180–13185.

Zhang, H., Craciun, L. C., Mirshahi, T., Rohács, T., Lopes, C. M., Jin, T., and Logothetis, D. E. (2003). PIP_2 activates *KCNQ* channels, and its hydrolysis underlies receptor-mediated inhibition of M currents. *Neuron*, 37(6), pp.963–975.

Zhang, J., and Shapiro, M. S. (2012). Activity-dependent transcriptional regulation of M-type (Kv7) K+ channels by AKAP79/150-mediated NFAT actions. *Neuron*, 76(6), pp.1133–1146.

Zhao, L., Han, S., Su, H., Li, J., Zhi, E., Li, P., Yao, C., Tian, R., Chen, H., Chen, H., Luo, J., Shi, C., Ji, Z., Hu, J., Wu, G., Zhou, W., Tang, Y., Chen, Y., Lin, G., Lue, T. F., … Li, Z. (2022). Single-cell transcriptome atlas of the human corpus cavernosum. *Nature communications*, 13(1), 4302.

Zhong, X. Z., Harhun, M. I., Olesen, S. P., Ohya, S., Moffatt, J. D., Cole, W. C., and Greenwood, I. A. (2010). Participation of *KCNQ* (Kv7) potassium channels in myogenic control of cerebral arterial diameter. *The Journal of Physiology*, 588(Pt 17), pp.3277–3293.

Zhou, X. B., Arntz, C., Kamm, S., Motejlek, K., Sausbier, U., Wang, G. X., Ruth, P., and Korth, M. (2001). A molecular switch for specific stimulation of the BKCa channel by cGMP and cAMP kinase. *The Journal of biological chemistry*, 276(46), pp.43239–43245.

Zhu, M. H., Chae, M., Kim, H. J., Lee, Y. M., Kim, M. J., Jin, N. G., Yang, D. K., So, I., and Kim, K. W. (2005). Desensitization of canonical transient receptor potential channel 5 by protein kinase C. *American Journal of Physiology: Cell Physiology*, 289(3), pp.C591–C600.

Zieba, B. J., Artamonov, M. V., Jin, L., Momotani, K., Ho, R., Franke, A. S., Neppl, R. L., Stevenson, A. S., Khromov, A. S., Chrzanowska-Wodnicka, M., and Somlyo, A. V. (2011). The cAMP-responsive Rap1 guanine nucleotide exchange factor, Epac, induces smooth muscle relaxation by down-regulation of RhoA activity. Journal of biological chemistry, 286(19), pp.16681–16692.